Multicomponent supramolecular systems

Document status and date:
Published: 09/04/2015

Document Version:
Publisher's PDF, also known as Version of Record (includes final page, issue and volume numbers)

Please check the document version of this publication:

• A submitted manuscript is the version of the article upon submission and before peer-review. There can be important differences between the submitted version and the official published version of record. People interested in the research are advised to contact the author for the final version of the publication, or visit the DOI to the publisher's website.
• The final author version and the galley proof are versions of the publication after peer review.
• The final published version features the final layout of the paper including the volume, issue and page numbers.

Link to publication

Download date: 04. Oct. 2023

Multicomponent Supramolecular Systems

PROEFSCHRIFT

ter verkrijging van de graad van doctor aan de
Technische Universiteit Eindhoven, op gezag van de
rector magnificus, prof.dr.ir. C.J. van Duijn,
voor een commissie aangewezen door het College
voor Promoties, in het openbaar te verdedigen op
donderdag 9 april 2015 om 16:00 uur

door

Rob van der Weegen

Geboren te Roosendaal en Nispen

Dit proefschrift is goedgekeurd door de promotoren en de samenstelling van de promotiecommissie is als volgt:

voorzitter:	prof.dr.ir. J.C. Schouten
promotor:	prof.dr. E.W. Meijer
copromotor:	dr.ir. A.R.A. Palmans
leden:	prof.dr. R.J.M. Nolte (Radboud Universiteit Nijmegen)
	prof.dr. S. de Feyter (Katholieke Universiteit Leuven)
	prof.dr. R.P. Sijbesma
	prof.dr. A.P.H.J. Schenning
adviseur:	dr.ir. J.A.J.M. Vekemans

Table of contents

Chapter 6

Nanoscopic phase separated architectures based on hydrogen-bonded

1

Functional supramolecular architectures

Abstract

In this chapter an overview of the formation of one-dimensional supramolecular polymers is given. First, we highlight examples of functional supramolecular systems for a wide variety of applications. For the rational design of such complex supramolecular architectures, precise knowledge on non-covalent interactions, self-assembly mechanisms and pathways is a necessity. An overview is presented on these topics in relation to one-dimensional supramolecular polymerisation of single components. Next, we present examples of the formation of supramolecular stacks by π-stacking of hydrogen-bonded complexes to highlight the more complex and functional architectures obtained in multicomponent systems. Mechanistic knowledge concerning the formation of such systems is much less advanced compared to that of single-component one-dimensional supramolecular polymers. This chapter ends with the aim and outline of the research described in this thesis.

1.1 Introduction

The non-covalent synthesis of functional supramolecular architectures offers great promise for the fabrication of well-defined organic nanostructures for a variety of applications. Nature provides an excellent source of inspiration as living systems make extensive use of non-covalent interactions in the construction of functional architectures. The cell cytoskeleton, for example, consists of long ordered filaments of protein monomers that dynamically polymerise and depolymerise for vital cell functions. Another example is photosystem II, in which extensive arrays of chromophore molecules are precisely organised through extensive non-covalent interactions with proteins, resulting in the efficient funnelling of light energy towards reaction centres.

Inspired by nature, synthetic chemists have over the past decades harnessed the use of non-covalent interactions for the creation of functional supramolecular architectures.[1] The group of Stupp, for example, has published extensively on the formation of rigid nanofibres from peptide amphiphiles and their subsequent application in the field of regenerative medicine.[2-8] Molecules that consist of peptide segments covalently linked to lipid-like hydrophobic segments self-assemble into rigid nanofibres by a combination of β-sheet formation and van der Waals interactions. By displaying specific peptide sequences on the surface of such nanofibres, highly bioactive nanofibres could be generated, which were applied in regeneration of axons in injured spinal cords, the growth of blood vessels and the regeneration of bone and cartilage.

Non-covalent interactions between small molecules can also be applied for the generation of materials with mechanical properties that are indistinguishable from polymeric systems.[9-12] As first demonstrated by our group, self-complementary hydrogen bonding of small telechelic molecules can result in supramolecular polymers (elongated chains of small molecules held together by non-covalent interactions) with similar behaviour in the bulk and solution phases as conventional macromolecules.[9] As shown by the groups of Leibler and Weder, such supramolecular polymeric materials can exhibit self-healing properties trough dynamic rearrangement of the non-covalent interactions, which has paved the way for several appealing applications in material sciences.[11,12]

Another field of application for one-dimensional supramolecular aggregates lies in the formation of semiconducting nanofibres for organic electronics.[13,14] Müllen and Aida, among others, have attracted much attention with π-conjugated molecules that self-assemble into one-dimensional nanowires capable of transporting charge carriers unidirectionally.[15-25] Strategies have been developed to generate architectures active in organic photovoltaics, for example, by generating donor–acceptor–donor supramolecular stacks or donor–acceptor supramolecular block copolymers.[24,25]

As a last example of functional supramolecular architectures, we highlight the generation of artificial photosynthetic systems. The groups of, Wasielewski, Moore and Würthner among others have published extensively on the self-assembly of (multi)chromophoric systems for the generation and cascade transfer of charge carriers.[26-28] These groups demonstrate that precise control over non-covalent interactions resulted in the generation of discrete and non-discrete supramolecular light-harvesting systems. Transfer of the excitonic energy in such systems to catalytic reaction centres may result in photocatalytic generation of hydrogen gas as recently demonstrated by the groups of Wasielewski and Stupp.[29]

From the examples highlighted above it is evident that functional supramolecular systems offer opportunities for the generation of highly functional materials. Detailed understanding of non-covalent interactions and self-assembly processes is a prerequisite in order to control the generation of desired supramolecular architectures at multiple length scales. The use of multicomponent non-covalent systems gives rise to the formation of more complex and functional architectures when compared with single component systems, albeit at the cost of a more complex self-assembly process. In this chapter not only the advances made in understanding the formation of one-dimensional supramolecular polymers based on single components are reviewed, but also those regarding multicomponent one-dimensional supramolecular polymers.

1.2 Supramolecular chemistry

The field of supramolecular chemistry became highly popularised when the 1987 Nobel Prize was awarded to Cram, Lehn and Pedersen for their seminal work on "*the development and use of molecules with structure-specific interactions of high selectivity*". The field began with the selective binding of alkali metal cations by both natural and synthetic macrocyclic and macropolycyclic ligands and evolved into the new domain of molecular recognition within chemical research.[30-34] Since then, non-covalent interactions such as electrostatic, metal coordination, hydrogen bonding, van der Waals and donor–acceptor interactions have been used in the build-up of a plethora of both discrete and non-discrete self-assembled architectures.

1.2.1 Hydrogen bonding

Hydrogen bonding is a particularly useful non-covalent interaction in the build-up of supramolecular architectures as a result of its strength, directionality and selectivity.[35-37] A hydrogen bond is an interaction between a partial positive charge on hydrogen (donor, D) and an electronegative atom (acceptor, A). A single hydrogen bond can range in strength from very weak (1–2 kJ/mol) to very strong (161.5 kJ/mol) but typical strengths lie around 10–30 kJ/mol for hydrogen bonds involving oxygen and nitrogen heteroatoms. A general approach to increase the binding strength in hydrogen-bonded systems is the use of multiple hydrogen bonds in an array.[38, 39] Work by the groups of Jörgensen and Zimmerman on complementary threefold hydrogen-bonding motifs has revealed that the interaction strength furthermore depends on the arrangement in such multiple hydrogen-bonded arrays. The complex of ADA–DAD, for example, shows a remarkably lower dimerisation constant in chloroform ($K = 10^2$ M^{-1}) when compared to complexes of DAA–ADD ($K = 10^4$ M^{-1}) and AAA–DDD ($K > 10^5$ M^{-1}).[40-42] The difference is attributed to attractive and repulsive secondary cross-interactions of donor and acceptor units in the hydrogen-bond duplexes (Figure 1.1). Optimisation of the array by maximising the number of secondary interactions resulted in an association constant that is three orders of magnitude larger than the weakest array. Calculations by the group of Schneider reveal that the free association energy of hydrogen-bonded complexes increases with 2.9 kJ/mol for every additional attractive interaction.[43]
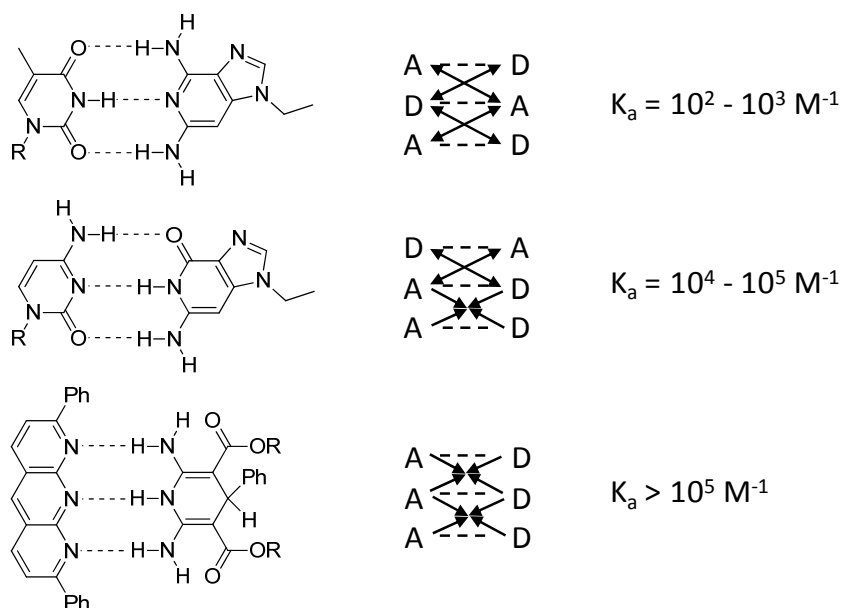
Figure 1.1. Stability of complexes of three-fold hydrogen bonding motifs in chloroform. Image adapted from reference 42.

The quadruple hydrogen-bonding arrays offer the additional possibility of self-complementary hydrogen bonding with both the ADAD and the AADD array. Linear supramolecular polymers based on such self-complementary motifs do not suffer from stoichiometric issues observed in other systems. In our group, quadruple hydrogen-bonding motifs that display the ADAD array have first been reported by Beijer *et al.*[44] Here, acetyl- and ureido-derivatised diaminotriazines are used to form hydrogen-bonded duplexes in chloroform. Preorganisation of the molecules by intramolecular hydrogen bonding into an ADAD array results in a high dimerisation constant of 2×10^5 M^{-1} in chloroform. Sijbesma and Beijer continued this line of research by introducing ureidopyrimidinone (UPy), which contains a preorganised quadruple hydrogen-bonding motif (Figure 1.2).[9,45,46] The 4-keto tautomer with a DDAA motif displays a $K_{dim} = 6 \times 10^7$ M^{-1} while the enol tautomer with a DADA motif displays a $K_{dim} = 9 \times 10^5$ M^{-1}. Which of the tautomers dominates, was shown to depend on the solvent and on the substituent on the isocytosine moiety. A heterocyclic quadruple hydrogen-bonding motif that does not suffer from weakening effects due to tautomerism, has been developed by Corbin and Zimmerman.[48] The different tautomers display the same relative spatial arrangement of donor and acceptor subunits, resulting in the formation of mainly AADD hydrogen-bonding arrays with association constants of $K = 1 \times 10^8$ M^{-1} and 3×10^7 M^{-1} in toluene and chloroform, respectively.
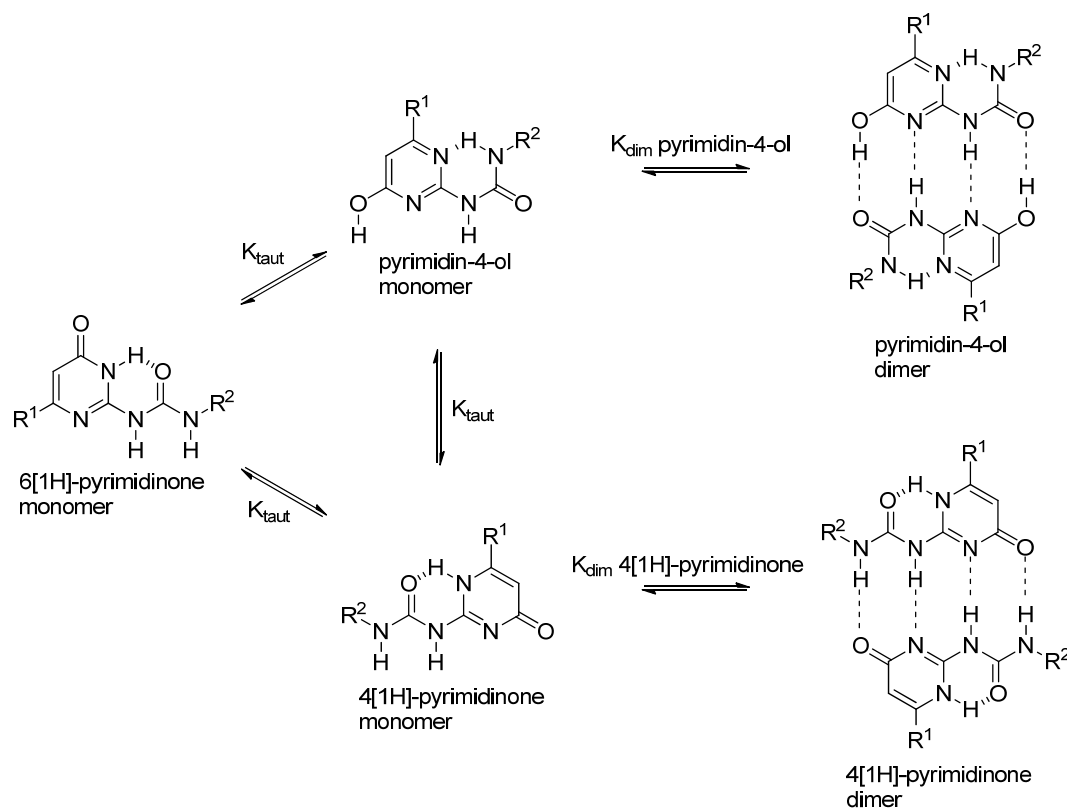
Figure 1.2. Molecular structures of UPy tautomeric forms and their self-complementary hydrogen-bonded dimers. Image adapted from reference 45.

For the formation of hydrogen-bonded complexes, the complementary DAD–ADA motifs have attracted much attention.[49-53] Synthetic chemists have access to a wide variety of diaminotriazine, melamine and diaminopyridine derivatives as DAD arrays and imide, uracil, barbituric acid and cyanuric acid derivatives as ADA arrays. The group of Lehn has for example used bifunctional uracil and diaminopyridine motifs connected by short flexible spacers to obtain linear supramolecular chains that showed liquid crystalline behaviour.[49] The formation of self-assembled bilayer membranes by complementary hydrogen bonding has been observed by Kunitake *et al.*[50-52] They have used hydrophilic cyanuric acid and hydrophobic melamine derivatives to form amphiphilic complementary hydrogen-bond networks in water. Chromophores that bear ADA motifs, such as naphthalene and perylene diimides, can also be used in the formation of hydrogen-bonded complexes. Würthner and co-workers, for example, have demonstrated the formation of perylene-triazine hydrogen-bonded architectures and the subsequent formation of hierarchical mesoscopic superstructures.[53]

Taken together, the use of multiple hydrogen bonds in an array allows the generation of strong and directional supramolecular motifs and opens up opportunities for the self-assembly of complex multicomponent supramolecular architectures.

1.2.2 π-Stacking

Another non-covalent architecture often used in the formation of extended supramolecular aggregates is the association of π-conjugated flat aromatic molecules through dipole–dipole interactions collectively referred to as π-stacking.[49-52] The formation of aggregates by rylenes, porphyrins, phthalocyanines, oligo(phenylene ethylenes), oligothiophenes, merocyanines, hexabenzocoronenes and other π-conjugated molecules has been well documented by multiple research groups.[23,58-64] Herein, the electronic properties of the supramolecular aggregates depend on the intermolecular orientation of the adjacent chromophores. Stacked chromophores can be arranged in a cofacial arrangement (H-type aggregation), resulting in a hypsochromic (blue) shift in UV–Vis spectroscopy or in a parallel or slipped stack arrangement (J-type aggregation), resulting in a bathochromic (red) shift in UV–Vis spectroscopy.

Two appealing and much studied π-conjugated classes of molecules are porphyrins and perylene bisimides, of which the basic molecular structures are depicted in Figure 1.3. Self-assembly based on π-stacking of porphyrins and perylene bisimides has been intensively studied for the generation of supramolecular architectures in both solution and solid state. Among many applications, porphyrin derivatives are particularly useful in the generation of artificial photosynthetic systems as many natural photosynthetic systems are based on porphyrins as well.[65-69] Herein, control over the aggregation and spatial orientation of porphyrins is a key aspect in generating functional architectures. On the other hand perylene bisimides
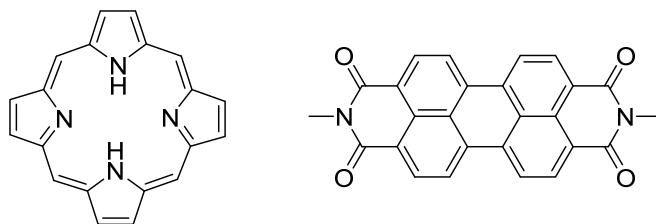
Figure 1.3. Basic molecular architecture of porphyrin (left) and perylene bisimide (right).

are well known for their n-type semiconducting properties, excellent stability and optical properties. As such, perylene bisimides have been extensively applied as coatings and liquid crystals and in organic photovoltaics.[58, 70-74] Both porphyrins and perylenes are easily derivatised at multiple positions, allowing high tunability of the molecular properties. A more detailed introduction to the self-assembly of perylene bisimides and porphyrins will be given in Chapters 2 and 4, respectively.

1.3 Self-assembly mechanisms in one-dimensional supramolecular polymerisation

A relevant aspect in the formation of one-dimensional supramolecular polymers is their formation mechanism because their molecular weight and weight distribution critically depend on the supramolecular polymerisation mechanism. Complementary (A–B) or self-complementary (A–A) supramolecular motifs can form polymeric structures through non-covalent interactions. For supramolecular polymers the degree of polymerisation depends on the association constant, the concentration, the temperature and the supramolecular polymerisation mechanism. For the polymerisation mechanism, two main classes may be identified; the isodesmic and the cooperative (or nucleation–elongation) self-assembly mechanism (Figure 1.4).[75] The isodesmic polymerisation resembles conventional step polymerisation and the resulting aggregate has a dispersity of two and a degree of polymerisation that is strongly dependent on the association constant. The association constant in isodesmic polymerisations is independent of the polymer length.[9]
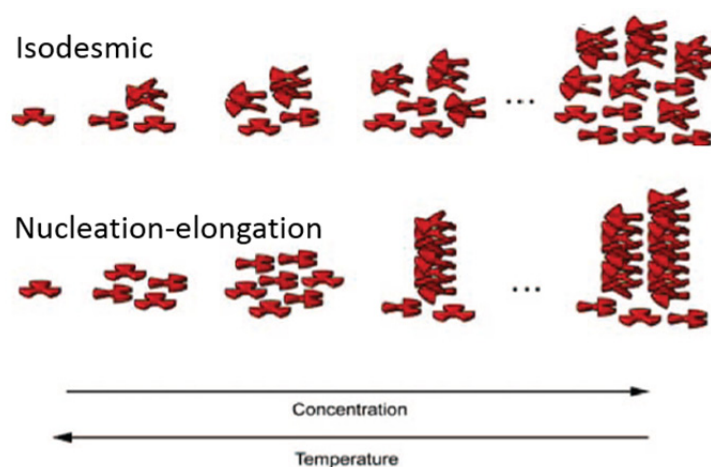
Figure 1.4. Schematic representations of the isodesmic and nucleation–elongation models for supramolecular polymerisation. Image adapted from reference 75.

1.4 Pathway complexity in one-dimensional supramolecular polymerisation

Another important aspect in the controlled formation of functional supramolecular architectures is the selective generation of desired self-assembled structures. Depending on the specific conditions applied, different (metastable) supramolecular structures can be obtained with the same aggregating motif, resulting in different properties of the end product. Therefore, knowledge of and control over the self-assembly pathways of monomers into supramolecular polymers is crucial in the formation of functional supramolecular systems.

Pathway complexity in one-dimensional supramolecular polymerisation has recently been demonstrated by Korevaar *et al*. in the aggregation of π-conjugated *S*-chiral oligo(*p*-phenylenevinylene) (*S*OPV) monomers as a dilute solution in methylcyclohexane (Figure 1.5).[81-82] Here, the formation of a kinetically favoured metastable assembly (*P* helix) is observed, which over time transforms into the thermodynamically favoured aggregate (*M* Helix). With the aid of a chiral auxiliary, the aggregates can change the thermodynamic preference of the self-assembly process. In this way, the aggregation process is forced along the kinetically favoured pathway and metastable assemblies are exclusively obtained.
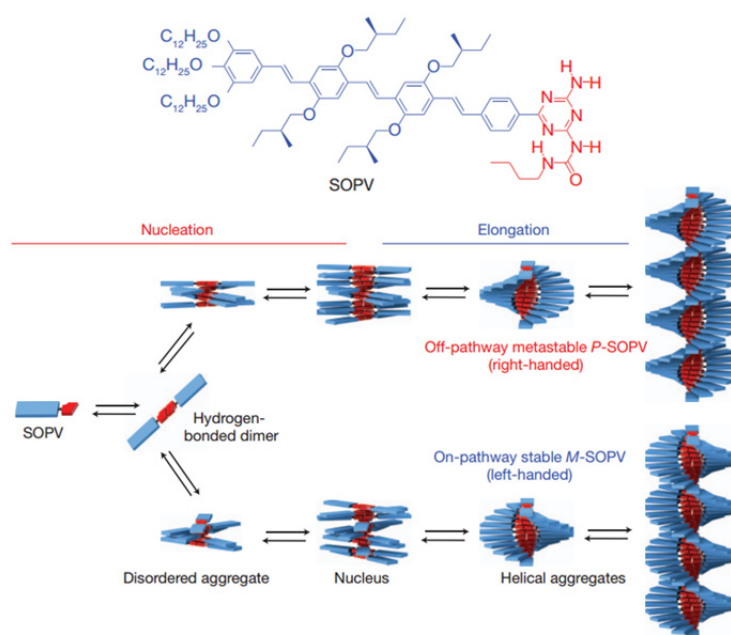
Figure 1.5. Molecular structure of *S*OPV and a schematic representation of its pathway dependent self-assembly. Image adapted from reference 82.

Kinetic control over self-assembly processes of small molecules has also been demonstrated by the group of Rybtchinski.[83] Here, perylene diimide/peptide conjugates are shown to self-assemble into various architectures by careful selection of the self-assembly conditions (Figure 1.6). A variety of metastable self-assembled architectures is generated by self-assembly of the conjugates in water/THF mixtures. The metastable architectures can be trapped by freezing aggregate interconversion kinetics by the addition of water. Conversely, aggregate interconversion can be promoted by the addition of THF co-solvent to weaken the hydrophobic associative interactions. In this way, control is gained over self-assembly pathways of a single supramolecular monomer into a variety of distinct supramolecular architectures.
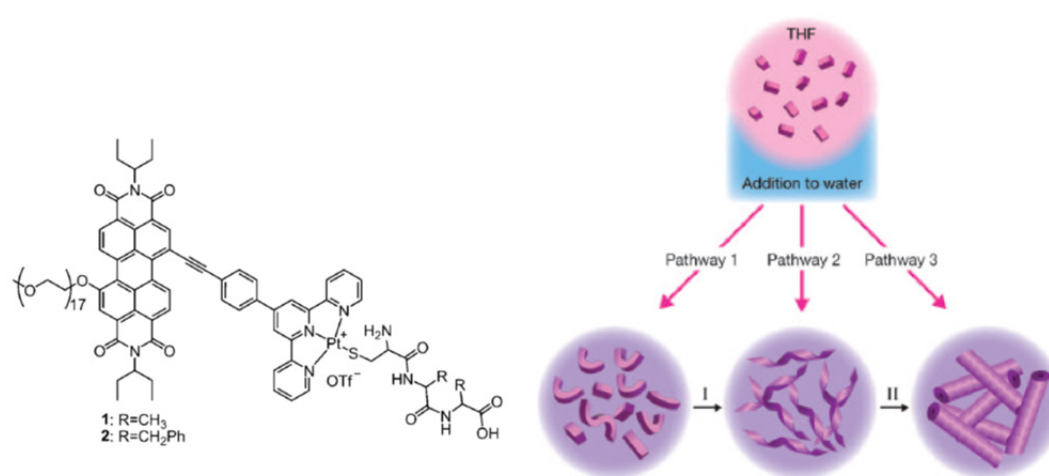
Figure 1.6. Molecular structure of a perylene diimide/peptide conjugate and the schematic representation of its pathway dependent self-assembly. Image adapted from reference 83.

In view of the examples presented above, it is apparent that the outcome of supramolecular polymerisations of single components cannot be predicted with certainty, despite the fact that detailed knowledge about supramolecular interactions and mechanisms that govern the formation of supramolecular polymers is available. Considerations such as the method of aggregate preparation and solvent conditions can greatly influence the outcome of supramolecular polymerisation processes.

1.5 Multicomponent one-dimensional supramolecular polymers

In recent years, multicomponent supramolecular architectures have attracted considerable attention because the structural variability and functionality of the resultant aggregates can be far greater than with their single component counterparts.[84-86] An attractive approach for the generation of multicomponent supramolecular architectures is the formation of one-dimensional supramolecular polymers based on π-stacking of hydrogen-bonded complexes. In this manner, hydrogen bonding can be utilised as a strong, directional interaction to bring together building blocks of two distinct functionalities, while π-stacking interactions of the hydrogen-bonded dimers result in the formation of elongated supramolecular polymers with a hierarchically organised architecture. In this paragraph we highlight a number of impressive examples of the formation of one-dimensional supramolecular polymers of stacked, hydrogen-bonded heterocomplexes.
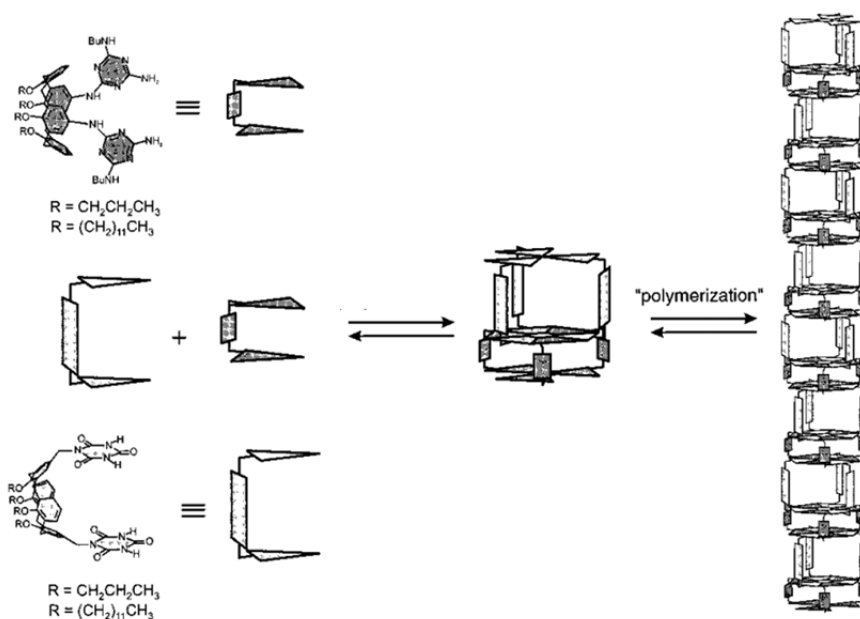
Figure 1.7. Schematic representation of the self-assembly of melamine and barbituric acid appended calix[4]arenes into supramolecular polymers by hydrogen bonding into and stacking of rosettes by the group of Reinhoudt. Image adapted from reference 90.

The groups of Whitesides and Reinhoudt have independently published extensively on the formation of hydrogen-bonded rosettes based on complementary hydrogen bonding between melamine and barbituric acid derivatives.[87-93] It was shown that covalent linkage of the melamine hydrogen-bonding motifs results in spatial preorganisation and the formation of a wide variety of discrete

supramolecular objects in solution. In attempts to form extended polymeric structures, both groups have reported on the heteroaggregation of bismelamine derivatives with bisbarbituric acid derivatives (Figure 1.7).[91,93] Spatial mismatch in the linker lengths of the hydrogen-bonding motifs was found to result in the formation of one-dimensional fibres of stacked hydrogen-bonded rosettes.

A related example has been reported by Hirschberg *et al.* where the covalent connection of two self-complementary ureidotriazine hydrogen-bond motifs with a short spacer was explored (Figure 1.8).[94] The dimers are found to self-assemble into helical polymers by the cooperative π-stacking of the hydrogen-bond pairs. The addition of chiral mono-ureidotriazine results in the formation of supramolecular heteroaggregates with a biased chirality.
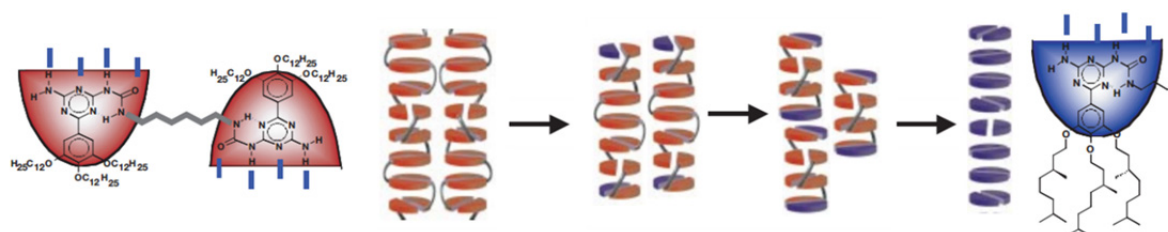
Figure 1.8. Schematic representation of the formation of hydrogen-bonded dimer stacks of bis-ureidotriazines and the formation of heteroaggregates with mono-ureidotriazines. Image adapted from reference 94.

An intriguing example of the formation of supramolecular heteroaggregates by hydrogen bonding and π-stacking has been reported in a collaborative effort by the group of Würthner and our group (Figure 1.9).[84,95,96] Here, a bay-substituted perylene bisimide (PBI) is complexed with diaminotriazine-functionalised oligophenylenevinylene (OPV) by threefold complementary hydrogen bonding. In this way, a supramolecular electron donor–acceptor–donor array is obtained, which self-assembles into one-dimensional aggregates by J-type π-stacking and subsequently further aggregates into chiral rod superstructures. The resulting OPV-PBI supramolecular stacks have successfully been applied in organic photovoltaic devices.
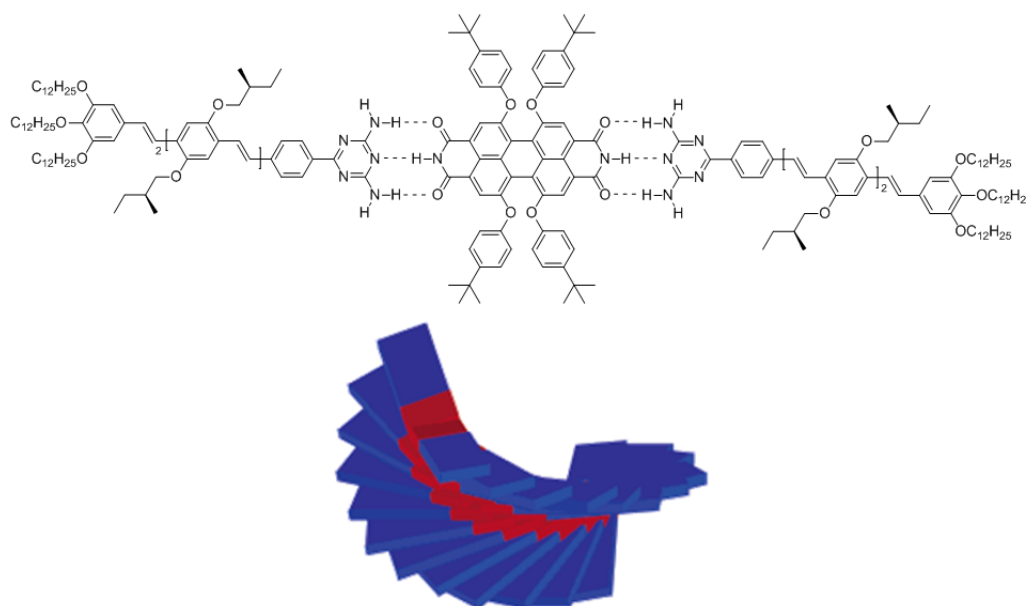
Figure 1.9. A supramolecular stack constructed by threefold hydrogen bonding between PBI and diaminotriazine functionalised OPV. Image adapted from reference 84.

The group of Yagai has reported extensively on the complementary hetero-association and subsequent aggregation of hydrogen-bonding monomers.[97-102] Herein, it is demonstrated that changes in the structure of the self-assembling monomers can result in the formation of diverse supramolecular architectures. An intriguing example is the formation of hexameric rosettes through complementary hydrogen bonding between melamine and cyanurate derivatives that subsequently stack into discotic columns and gelate apolar organic solvents (Figure 1.10). When azobenzene substituted melamines are used, stable columnar aggregates are obtained when the azo-dyes presented an *E* stereochemistry. Photoisomerisation of the azobenzene (*E* to *Z* configuration) results in the formation of sterically more demanding species and the columnar aggregates tend to dissociate. When, however, the melamine motifs are substituted with oligo(phenylene ethynylene) (OPE), the hexameric rosettes form toroidal objects instead of elongated aggregates.

In a different example, the same research group has used monotopic triazines functionalised with two perylene bisimide chromophores via a short alkyl spacer. When mixed with tritopic cyanuric acid, hydrogen-bonded tetramers are obtained that self-assembled in the lateral direction through π-stacking of the perylene chromophores. The use of chiral triazines results in the formation of supramolecular

polymers with a preferred helical sense. Fibrous architectures of the aggregates have been visualised with TEM microscopy.
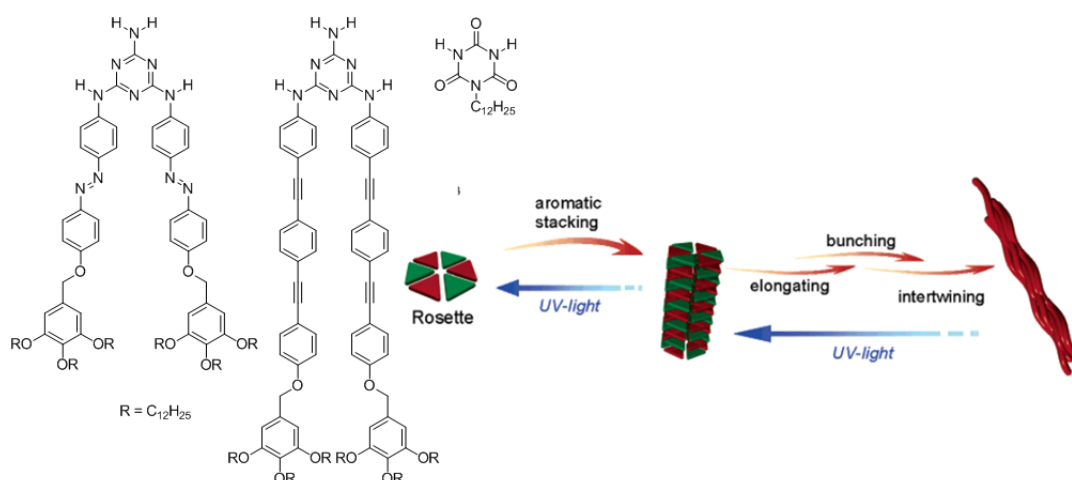
Figure 1.10. Molecular structures of melamine and cyanurate derivatives and a schematic representation of their self-assembly into hexameric rosettes. Image adapted from references 99 and 100.

The melamine–cyanurate complementary hydrogen-bond couple has also been utilised by our group in the formation of π-stacked heterocomplexes.[103] A porphyrin-cyanurate derivative with two available hydrogen-bonding sites forms trimers by complementary hydrogen bonding with diaminotriazine-functionalised oligo(phenylenevinylene) (OPV). The heterotrimers are subsequently found to π-stack into helically ordered fibres that exhibit efficient energy transfer from the OPV units to the porphyrin dye.

While the examples presented above impressively succeed in the formation of supramolecular heteroaggregates, detailed knowledge of their self-assembly mechanisms, competitive pathways and preparation methods is still rather limited in comparison to those of single-component one-dimensional aggregates. The individual components used in the formation of supramolecular heteroaggregates may form self-aggregates that compete with and therefore complicate the formation of the desired supramolecular heteroarchitectures. Detailed knowledge on the formation mechanisms governing the assembly of such architectures would be highly beneficial in the rational design of functional supramolecular systems.

1.6 Aim and outline

As described in this chapter, the self-assembly of molecular building blocks through well-defined non-covalent interactions is a powerful tool to develop complex and functional supramolecular structures. Herein, the formation of one-dimensional elongated supramolecular polymers based on single building blocks has attracted much attention. These structures have been described in great detail concerning the type and strength of their non-covalent interactions, their self-assembly mechanisms and their pathway complexity in self-assembly. Analogous knowledge on the formation of multicomponent one-dimensional supramolecular polymers is less advanced. The formation of homoaggregates by the individual components may complicate the formation of the desired supramolecular architectures. Alternatively, the formation of metastable aggregates might hinder the formation of desired supramolecular architectures. We therefore feel that detailed knowledge of the mechanisms and pathways dealing with the formation of such aggregates would be highly beneficial for the generation of functional supramolecular architectures based on one-dimensional multicomponent stacks.

The focus of this thesis concerns an explorative study into the scope and limitations of the formation and application of multicomponent supramolecular architectures by π-stacking and hydrogen bonding. The aim of this thesis is to provide a detailed study of the preparation and characterisation of these multicomponent supramolecular stacks, to gain a better understanding of the mechanisms, interactions and pathway complexity that govern their self-assembly.

In Chapter 2 the self-assembly of an *N*-monoarylated perylene bisimide is investigated. The perylene bisimide self-assembles into π-stacked aggregates of hydrogen-bonded dimers and displays characteristics of a cooperative growth mechanism. Unexpectedly, only objects of small size are obtained, which is explained with an anti-cooperative mechanism by attenuated growth. In Chapter 3, the co-assembly of a library of triazines with the *N*-monoarylated perylene bisimide by complementary hydrogen bonding and subsequent π-stacking in apolar organic solvents is described. The influence of triazine structure on the competition between homo- and hetero-association is investigated by CD, UV, IR and NMR as techniques. Selective blocking of non-covalent interaction sites on the triazines results in the

more facile formation of preferred aggregates. Furthermore, the use of multivalent triazine architectures results in the selective formation of preferred supramolecular aggregates

In Chapter 4 the self-assembly of a library of porphyrins of structural similarity is described. During investigations on the development of asymmetric triazine-functionalised porphyrins, the delicate self-assembly behaviour of symmetrically functionalised porphyrins was observed. Small changes in the molecular structure of solubilising groups on the periphery of porphyrin tetra-amides results in the formation of diverse supramolecular architectures. Variation in the side-chain architecture remote from the aggregating motif can thus be used as a method to steer the formation of porphyrin supramolecular systems.

In Chapter 5, the use of π-stacked, hydrogen-bonded heterodimers as supra-amphiphiles for the stabilisation of water/oil and all aqueous emulsions is investigated. Triazines and *N*-monoarylated perylene bisimides equipped with hydrophilic groups for aqueous solubility are prepared and investigated for their self-assembly in aqueous solutions. Supra-amphiphiles were prepared by complementary hydrogen bonding between hydrogen-bonding motifs decorated with hydrophilic and hydrophobic solubilising groups. The supra-amphiphiles are shown to be efficient stabilisers of water/oil emulsions. In the second part, the approach is extended towards the stabilisation of all aqueous emulsions.

In Chapter 6, microphase separating materials based on well-defined supramolecular building blocks are described. Triazine derivatives that bear oligodimethylsiloxane chains are complexed with perylene bisimides by complementary hydrogen bonding. The resulting materials exhibit a columnar liquid crystalline phase in the bulk and show microphase separating behaviour in thin films that is reminiscent of block copolymer phase-separation. The presented approach demonstrates the generation of extremely small feature sizes in thin films.

1.7 References

[1]   T. Aida, E.W. Meijer, S.I. Stupp, *Science*, 2012, **335**, 813

[2]   J.D. Hartgerink, E. Beniash, S.I. Stupp, *Science*, 2001, **294**, 1684

[3]   J.D. Hartgerink, E. Beniash, S.I. Stupp, *Proc. Natl. Acad. Sci.*, 2002, **99**, 5133

[4]   V.M. Tysseling-Mattiace, V. Sahni, K.L. Niece, D. Birch, C. Czeisler, M.G. Fehlings, S.I. Stupp, J.A. Kessler, *J. Neurosci.*, 2008, **28**, 3814

[5]   K.R. Rajangam, H.A. Behanna, M.J. Hui, X. Han, J.F. Hulvat, J.W. Lomasney, S.I. Stupp, *Nano. Lett.*, 2006, **6**, 2086

[6]   A. Mata, Y. Geng, K.J. Henrikson, C. Aparicio, S.R. Stock, R.L. Satcher, S.I. Stupp, *Biomaterials*, 2010, **31**, 6004

[7]   R.N. Shah, N.A. Shah, M.M.D. Lim, C. Hsieh, G. Nuber, S.I. Stupp, *Proc. Natl. Acad. Sci.*, 2010, **107**, 3293

[8]   E.D. Spoerke, S.G. Anthony, S.I. Stupp, *Adv. Mater.*, 2009, **21**, 425

[9]   R.P. Sijbesma, F.H. Beijer, L. Brunsveld, B.J.B. Folmer, J.H.K.K. Hirschberg, R.F.M. Lange, J.K.L. Lowe, E.W. Meijer, *Science*, 1997, **278**, 1601

[10]   H. Kautz, D.J.M. van Beek, R.P. Sijbesma, E.W. Meijer, *Macromolecules*, 2006, **39**, 4265

[11]   M. Burnworth, L.M. Tang, J.R. Kumpfer, A.J. Duncan, F.L. Beyer, G.L. Fiore, S.J. Rowan, C. Weder, *Nature*, 2011, **472**, 334

[12]   P. Cordie, F. Tournilhac, C. Soulié-Ziakovic, L. Leibler, *Nature*, 2008, 451, 977

[13]   A.P.H.J. Schenning, E.W. Meijer, *Chem. Commun.*, 2005, 3245

[14]   L.C. Palmer, S.I. Stupp, *Acc. Chem. Res.*, 2008, **41**, 1674

[15]   F.S. Schoonbeek, J.H. van Esch, B. Wegewijs, D.B.A. Rep, M.P. de Haas, T.M. Klapwijk, R.M. Kellogg, B.L. Feringa, *Angew. Chem. Int. Ed.*, 1999, **38**, 1993

[16]   A. El-ghayoury, E. Peeters, A.P.H.J. Schenning, E.W. Meijer, *Chem. Commun.*, 2000, 1969

[17]   A. Ajayaghos, S.J. George, *J. Am. Chem. Soc.*, 2001, **123**, 5148

[18]   E.R. Zubarev, M.U. Pralle, E.D. Sone, S.I. Stupp, *J. Am. Chem. Soc.*, 2001, **123**, 4105

[19]   B.W. Messmore, J.F. Hulvat, E.D. Sone, S.I. Stupp, *J. Am. Chem. Soc.*, 2004, **126**, 14452

[20]   S. Xiao, J. Tang, T. Beetz, X. Guo, N. Tremblay, T. Siegrist, Y. Zhu, M. Steigerwald, C. Nuckolls, *J. Am. Chem. Soc.*, 2006, **128**, 10700

[21]   B. El Hamaoui, L. Zhi, W. Pisula, U. Kolb, J. Wu, K. Müllen, *Chem. Commun.*, 2007, 2384

[22]   J.S. Wu, W. Pisula, K. Müllen, *Chem. Rev.*, 2007, **107**, 718

[23]   J.P. Hill, W. Jin, A. Kosaka, T. Fukushima, H. Ichihara, T. Shimomura, K. Ito, T. Hashizume, N. Ishii, T. Aida, *Science*, 2004, **304**, 1481

[24]   Y. Yamamoto, T. Fukushima, Y. Suna, N. Ishii, A. Saeki, S. Seki, S. Tagawa, M. Taniguchi, T. Kawai, T. Aida, *Science*, 2006, **314**, 1761

[25]   W. Zhang, W. Jin, T. Fukushima, A. Saeki, S. Seki, T. Aida, *Science*, 2011, **334**, 340

[26]   P.D. Frischmann, K. Mahata, F. Würthner, *Chem. Soc. Rev.*, 2013, **42**, 1847

[27]   M.R. Wasielewski, *Acc. Chem. Res.*, 2009, **42**, 1910

[28]   G. Steinberg-Yfrach, P.A. Liddell, S.C. Hung, A.L Moore, D. Gust, T.A. Moore, *Nature*, 1997, **385**, 239

[29]   A.S. Weingarten, R.V. Kazantsev, L.C. Palmer, M. McClendon, A.R. Koltonow, A.P.S. Samuel, D.J. Kiebala, M.R. Wasielewski, S.I. Stupp, *Nat. Chem.*, 2014, **6**, 964

[30]   J.M. Lehn, *Science*, 1985, **227**, 849

[31]   J.M. Lehn, Angew. *Chem. Int. Ed.*, 1990, **29**, 1304

[32]   D.J. Cram, Angew. *Chem. Int. Ed.*, 1986, **25**, 1039

[33]   J.M. Lehn, *Science*, 1993, **260**, 1782

[34]   C.J. Pedersen, *Angew. Chem. Int. Ed.*, 1988, **27**, 1021

[35]   L.J. Prins, D.N. Reinhoudt, P. Timmerman, *Angew. Chem. Int. Ed.*, 2001, **40**, 2382

[36]   G.A. Jeffrey, An Introduction to Hydrogen Bonding, Oxford press, New York, 1997

[37]   P.K. Baruah, S. Khan, *RSC Adv.*, 2013, **3**, 21202

[38]   D.C. Sherrington, K.A. Tashkinen, *Chem. Soc. Rev.*, 2001, **30**, 38

[39]   R.P. Sijbesma, E.W. Meijer, *Chem. Commun.*, 2003, 5

[40]   W.L. Jorgenson, J. Pranata*, J. Am. Chem. Soc.*, 1990, **112**, 2008

[41]   J. Pranata, S.G. Wierschke, W.L. Jorgenson, *J. Am. Chem. Soc.*, 1991, **113**, 2810

[42]   T.J. Murray, S.C. Zimmerman, *J. Am. Chem. Soc.*, 1992, **114**, 4010

[43]   J. Sartorius, H.-J. Schneider, *Chem. Eur. J.*, 1996, **2**, 1446

[44]   F.H. Beijer, H. Kooijman, A.L. Spek, R.P. Sijbesma, E.W. Meijer, *Angew. Chem. Int. Ed.*, 1998, **37**, 75

[45]   F.H. Beijer, R.P. Sijbesma, H. Kooijman, A.L. Spek, E.W. Meijer, *J. Am. Chem. Soc.*, 1998, **120**, 6761

[46]   S.H.M. Söntjens, R.P. Sijbesma, M.H.P. van Genderen, E.W. Meijer, *J. Am. Chem. Soc.*, 2000, **122**, 7487

[47]   T.F.A. de Greef, G. Ercolani, G.B.W.L. Ligthart, E.W. Meijer, R.P. Sijbesma, *J. Am. Chem. Soc.*, 2008, **130**, 13755

[48]   P.S. Corbin, S.C. Zimmerman, *J. Am. Chem. Soc.*, 1998, **120**, 9710

[49]   C. Fouquey, J.-M. Lehn, A.-M. Levelut, *Adv. Mater.*, 1990, **2**, 254

[50]   N. Kimizuka, T. Kawasaki, K. Hirata, T. Kunitake, *J. Am. Chem. Soc.*, 1998, **120**, 4094

[51]   T. Kawasaki, M. Tokuhiro, N. Kimizuka, T. Kunitake, *J. Am. Chem. Soc.*, 2001, **123**, 6793

[52]   N. Kimizuka, T. Kawasaki, T. Kunitake, *J. Am. Chem. Soc.,* 1993, **115**, 4387

[53]   F. Würthner, C. Thalacker, A. Sautter, *Adv. Mater.*, 1999, **11**, 754

[54]   D. González-Rodríguez, A.P.H.J. Schenning, *Chem. Mater.*, 2011, **23**, 310

[55]   Y. Yamamoto, *Sci. Technol. Adv. Mater.*, 2012, **13**, 033001

[56]   F.J.M. Hoeben, P. Jonkheim, E.W. Meijer, A.P.H.J. Schenning, *Chem. Rev.*, 2005, **105**, 1491

[57]   S.S. Babu, V.K. Praveen, A. Ajayaghosh, *Chem. Rev.*, 2014, **114**, 1973

[58]   F. Würthner, *Chem. Commun.*, 2004, 1564

[59]   Y. Li, T. Liu, H. Liu, M-Z. Tian, Y. Li, *Acc. Chem. Res.*, 2014, **47**, 1186

[60]   A. Ajayaghosh, S.J. George, A.P.H.J. Schenning, *Top. Curr. Chem.*, 2005, **258**, 83

[61]   F. Würthner, S. Yao, U. Beginn, *Angew. Chem. Int. Ed.*, 2003, **42**, 3247

[62]   M.M. Bouman, E.W. Meijer, *Adv. Mater.*, 1995, **7**, 385

[63]   I.D. Tevis, L.C. Palmer, D.J. Herman, I.P. Murray, D.A. Stone, S.I. Stupp, *J. Am. Chem. Soc.*, 2011, **133**, 16486

[64]   P. Jonkheijm, P. van der Schoot, A.P.H.J. Schenning, E.W. Meijer, *Science*, 2006, **313**, 80

[65]   T.S. Balaban, H. Tamiaki, A.R. Holzwarth, *Top. Curr. Chem.*, 2005, **258**, 1

[66]   S. Ganapathy, S. Sengupta, P.K. Wawrzyniak, V. Huber, F. Buda, U. Baumeister, F. Würthner, H.J.M. de Groot, M.R. Wasielewski, *PNAS*, 2009, **106**, 11472

[67]   G. Steinberg-Yfrach, P.A. Liddell, S.C. Hung, A.L Moore, D. Gust, T.A. Moore, *Nature*, 1997, **385**, 239

[68]   T. van der Boom, R.T. Hayes, Y.Y. Zhao, P.J. Bushard, E.A. Wiess, M.R. Wasielewski, *J. Am. Chem. Soc.*, 2002, **124**, 9582

[69]   M.R. Wasielewski, *Chem. Rev.*, 1992, **92**, 435

[70]   W. Herbst, K. Hunger, *Industrial Organic Pigments: Production, Properties, Applications*, 2nd edn. WILEY-VCH, Weinheim, 1997

[71]   C.W. Struijk, A.B. Sieval, J.E.J. Dakhors, M. van Dijk, P. Kimkes, R.B.M. Koehorst, H. Donker, T.J. Schaafsma, S.J. Picken, A.M. van de Craats, J.M. Warman, H. Zuilhof, E.J.R. Sudhölter, *J. Am. Chem. Soc.*, 2000, **122**, 11057

[72]   C.D. Dimitrakopoulos, P.R.L. Malenfant, *Adv. Mater.*, 2002, **14**, 99

[73]   K.-Y. Law, *Chem. Rev.*, 1993, **93**, 449

[74]   L. Schmidt-Mende, A. Fechtenkötter, K. Müllen, E. Moons, R.H. Friend, J.D. MacKenzie, *Science*, 2001, **293**, 1119

[75]   T.F.A. de Greef, M.M.J. Smulders, M. Wolffs, A.P.H.J. Schenning, R.P. Sijbesma, E.W. Meijer, *Chem. Rev.*, 2009, **109**, 5687

[76]   A. Ciferri, J. Macromol. *Sci-Pol. R.*, 2003, **43**, 271

[77]   F. Oosawa, *Biophys. Chem.*, 1993, **47**, 101

[78]   L. Brunsveld, E.W. Meijer, R.B. Prince, J.S. Moore, *J. Am. Chem. Soc.*, 2001, **123**, 7978

[79]   C. Nuckolls, T.J. Katz, P.J. Collings, L. Castellanos, *J. Am. Chem. Soc.*, 1999, **121**, 79

[80]   D. Zhao, J.S. Moore, *Org. Biomol. Chem.*, 2003, **1**, 3471

[81]   P.A. Korevaar, S.J. George, A.J. Markvoort, M.M.J. Smulders, P.A.J. Hilbers, A.P.H.J. Schenning, T.F.A. de Greef, E.W. Meijer, *Nature*, 2012, **481**, 7382

[82]   P.A. Korevaar *Pathway complexity in π-conjugated materials* PhD thesis, Eindhoven University of Technology, Eindhoven, the Netherlands, 2014

[83]   Y. Tidhar, H. Weissman, S.G. Wolf, A. Gulina, B. Rybtchinski, *Chem. Eur. J.*, 2011, **22**, 6068

[84]   F. Würthner, Z.J. Chen, F.J.M. Hoeben, P. Osswald, C.C. You, P. Jonkheim, J. von Herrikhuyzen, A.P.H.J. Schenning, P.P.A.M. van der Schoot, E.W. Meijer, E.H.A. Becker, S.C.J. Meskers, R.A.J. Janssen, *J. Am. Chem. Soc.*, 2004, **126**, 10611

[85]   Z. Wang, W.S. Jin, T. Fukushima, A. Saeki, S. Seki, T. Aida, *Science*, 2011, **334**, 340

[86]   D. González-Rodríguez, A.P.H.J. Schenning, *Chem. Mater.*, 2011, **23**, 310

[87]   R.H. Vreekamp, J.P.M. van Duynhoven, M. Hubert, W. Verboom, D.N. Reinhoudt, *Angew. Chem. Int. Ed.*, 1996, **35**, 1215

[88] P. Timmerman, R.H. Vreekamp, R. Hulst, W. Verboom, D.N. Reinhoudt, K. Rissanen, K.A. Udachin, J. Ripmeester, *Chem. Eur. J.*, 1997, **3**, 1832

[89] L.J. Prins, J. Huskens, F. de Jong, P. Timmerman, D.N. Reinhoudt, *Nature*, 1999, **398**, 498

[90] H.-A. Klok, K.A. Jolliffe, C.L. Schauer, L.J. Prins, J.P. Spatz, M. Möller, P. Timmerman, D.N. Reindhoudt, *J. Am. Chem. Soc.*, 1999, **121**, 7154

[91] K.A. Jolliffe, P. Timmerman, D.N. Reinhoudt, *Angew. Chem. Int. Ed.*, 1999, **38**, 933

[92] G.M. Whitesides, E.E. Simanek, J.P. Mathias, G.T. Seto D.N. Chin, M. Mammen, D.M. Gordon, *Acc. Chem. Res.*, 1995, **28**, 37

[93] I.S. Choi, X. Li, E.E. Simanek. R. Akaba, G.M. Whitesides, *Chem. Mater.*, 1999, **11**, 684

[94] J.H.K.K. Hirschberg, L. Brunsveld, A. Ramzi, J.A.J.M. Vekemans, R.P. Sijbesma, E.W. Meijer, *Nature*, 2000, **407**, 167

[95] A.P.H.J. Schenning, J. van Herrikhuyzen, P. Jonkheijm, Z. Chen, F. Würthner, E.W. Meijer, *J. Am. Chem. Soc.*, 2002, **124**, 10252

[96] E.H.A. Beckers, Z. Chen, S.C.J. Meskers, P. Jonkheim, A.P.H.J. Schenning, X.-Q. Li, P. Osswald, F. Würthner, R.A.J. Janssen, *J. Phys. Chem. B.*, 2006, **110**, 16967

[97] S. Yagai, S. Kubota, K. Unoike, T. Karatsu, A. Kitamura, *Chem. Commun.*, 2008, 4466

[98] S. Yagai, T. Nakajima, T. Karatsu, K.-i. Saitow, A. Kitamura, *J. Am. Chem. Soc.*, 2004, **125**, 11500

[99] S. Yagai, T. Nakajima, K. Kishikawa. S. Kohmoto, T. Karatsu, A. Kitamura, *J. Am. Chem. Soc.*, 2005, **127**, 11134

[100] S. Yagai, S. Mahesh, Y. Kikkawa, K. Unoike, T. Karatsu, A. Kitamura, A. Ajayahosh, *Angew. Chem. Int. Ed.*, 2008, **47**, 4691

[101] S. Yagai, M. Higashi, T. Karatsu, A. Kitamura, *Chem. Commun.*, 2006, 1500

[102] T. Tazawa, S. Yagai, Y. Kikkawa, T. Karatsu, A. Kitamura, A. Ajayaghosh, *Chem. Commun.*, 2010, **46**, 1076

[103] F.J.M. Hoeben, M.J. Pouderoijen, A.P.H.J. Schenning, E.W. Meijer, *Org. Biomol. Chem.*, 2006, **4**, 4460

2

Small-sized perylene bisimide assemblies controlled by both cooperative and anti-cooperative assembly processes

Abstract

Cooperative aggregation of monomers into one-dimensional nanostructures typically results in elongated objects. We have analysed the self-assembly of an *N*-monoarylated perylene bisimide, which shows characteristics of a cooperative growth mechanism but unexpectedly yields objects of small size induced by anti-cooperativity with attenuated growth. The *N*-monoarylated perylene bisimide self-assembles into stacks of hydrogen-bonded dimers via a cooperative self-assembly mechanism as determined by UV–Vis and FT-IR spectroscopy. SAXS and DLS experiments were used to determine the aggregate size, which was found to be unexpectedly small for a cooperative growth mechanism. A model including anti-cooperativity by attenuated growth was found to correctly describe the UV–Vis assembly curves and simultaneously results in the formation of small aggregates. Our observations serve as a warning that typical hallmarks of cooperative growth of self-assembled nanostructures do not per se imply the formation of large objects and additional experiments should be performed to characterise the self-assembled structures in solution.

2.1 Introduction

Cooperative self-assembly processes frequently result in the formation of long one-dimensional aggregates, fibres or tube-like architectures, which find applications in supramolecular electronics, self-healing materials or systems with biomedical relevance.[1-4] A key factor in the formation of these supramolecular architectures with high aspect ratio is their cooperative growth mechanism, which characteristically has an increased propensity for monomer addition as a function of chain length. Although the equilibrium constant for monomer addition can explicitly depend on the chain length, it is often assumed that the aggregation process can be divided into a nucleation phase, described by the equilibrium constant K_2 for dimerisation, and an elongation phase, described by the equilibrium constant K ($K_2 \neq K_3 = K_4... = K_i = K$). Typically, cooperative aggregations are characterised by a critical point (e.g., temperature, concentration or solvent composition), which separates regimes where the system is either mainly composed of monomers or present as large aggregates.[5-7] In the absence of cooperative effects, monomer addition occurs with an equilibrium constant independent of the length of the aggregate. This isodesmic assembly process results in the formation of smaller aggregates compared to a cooperative process if the association constants are similar.

There are, however, notable exceptions in which supramolecular polymerisation does not yield elongated objects but results in the formation of small or discretely sized objects, even at high concentrations.[8-14] Rather than following an isodesmic self-assembly pathway, increasing repulsive interactions diminish the association constant and halt the polymerisation at the stage of small aggregates. In most cases, the self-assembly process is anticooperative ($K_2/K > 1$) and therefore no critical temperature or concentration is observed.[15,16] Notable examples were reported by the group of Wasielewski, where π-stacking of covalent perylene-porphyrin and perylene-phthalocyanine conjugates resulted in the formation of monodisperse aggregates as evidenced by multiple analytical techniques. Herein, a balance between steric repulsive interactions and associative π-stacking interactions was suggested to limit the aggregate size. Alternatively, electrostatic repulsive interactions were used to limit aggregate sizes by our group in the self-assembly of discotic amphiphiles.[12] The accumulation of charged groups upon self-assembly was rationalised to counteract

associative interactions and thereby limit the formation of extensive supramolecular aggregates.[13,14]

An appealing class of molecules in (supramolecular) organic chemistry contains perylene bisimides (PBIs). PBIs offer excellent chemical and thermal stability combined with favourable optical properties for application as pigments, n-type semiconductors or liquid crystals in areas such as coatings, electrophotography and photovoltaics.[17-21] Recently, the use of controlled supramolecular interactions in PBI molecules showed great promise in the build-up of complex, functional multi-chromophoric objects.[22,23] Würthner and co-workers first showed the interaction of a variety of supramolecular complexes of receptor-functionalised perylene bisimides with complementary binders based on hydrogen bonding and metal-ligand interactions.[24-28] Later, the formation of π-stacked aggregates of PBIs was reported and subsequently extended to supramolecular architectures based on multiple orthogonal non-covalent interactions.[29-33] An appealing example is the formation of supramolecular nanoribbons and nanoropes by melamine-appended PBIs through complementary hydrogen bonding with barbituric acid derivatives as reported by Yagai and co-workers.[29,34] Würthner and co-workers reported the formation of twisted nanoribbons of perylene dyes by a combination of π-stacking and hydrogen bonding between perylene bisimide cores.[30,31] To date PBI self-assembled architectures constructed by multiple orthogonal interactions mainly incorporated symmetrically substituted perylenes, though some notable exceptions have been reported by the group of Yagai.[34-36]

Our aim is to expand the library of supramolecular architectures based on asymmetric perylene bisimides by combining π-stacking and hydrogen bonding of the perylene cores as non-covalent interactions in order to gain a deeper understanding of the self-assembly mechanisms governing the aggregation of asymmetric π-conjugated chromophores. In this chapter, the synthesis and self-assembly behaviour of an asymmetric perylene bisimide (PBI) are discussed. With temperature dependent ultraviolet-visible (UV–Vis) spectroscopy, the self-assembly mechanism of the supramolecular polymer is deduced and subsequently modelled for conventional one-dimensional supramolecular polymerisation. Estimates for the sizes of the aggregates in solution are then compared to the sizes obtained by small angle X-ray

scattering (SAXS) and dynamic light scattering (DLS) measurements. Finally, alternative models for the self-assembly of the perylene bisimide under study are investigated to rationalise the discrepancy between the predicted and measured aggregate sizes.

2.2 Molecular design and synthesis

The system under investigation is based on asymmetric PBI **1** bearing a solubilising wedge at one imide *N*-position and an unsubstituted nitrogen at the other (Scheme 2.1). The solubilising wedge renders bay-unsubstituted perylenes highly soluble in organic solvents without affecting the optical properties of the perylene core.[37] The unsubstituted imide side of **1** allows twofold complementary hydrogen bonding between perylenes and presents an ADA hydrogen-bonding motif that can be adopted for the formation of PBI based homo- and heteroaggregates.[24,30,38,39]

Asymmetric PBI **1** was synthesised according to Scheme 2.1. Mono-imide **3** and aniline **4** were prepared as reported in literature.[37,40,41] Using standard conditions, **3** and **4** were condensed in quinoline in the presence of water free zinc acetate to yield asymmetric perylene bisimide **1** in 69% yield as a dark red solid after purification by column chromatography. Furthermore, *N*-methylated PBI **2** was prepared as a model compound by treating **1** with methyl iodide in DMF. Both perylene bisimides were fully characterised using NMR and MALDI-ToF MS, indicating that **1** and **2** were obtained as highly pure compounds.
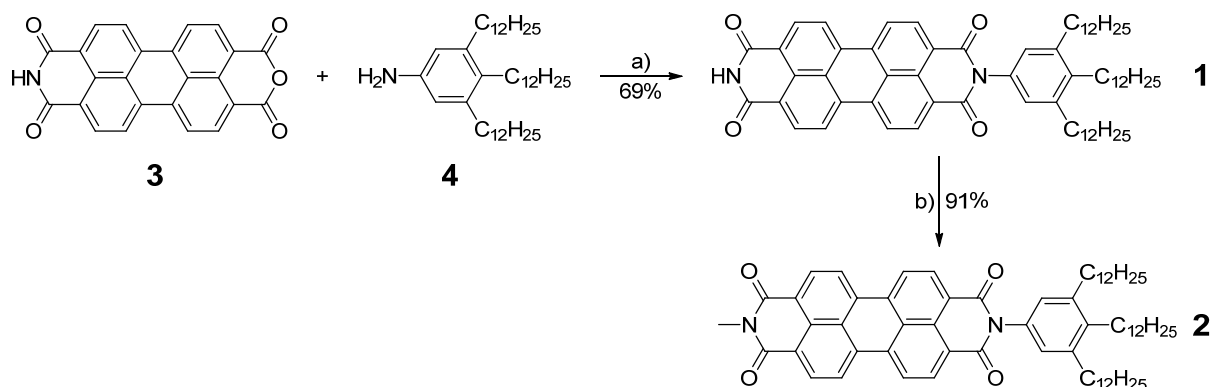
Scheme 2.1. Synthesis of asymmetric perylene bisimides **1** and **2**. Reagents and conditions: a) Zn(OAc)$_2$, Quinoline, 180 °C; b) MeI, K$_2$CO$_3$, DMF, RT.

2.3 Self-assembly in PBI 1 in solution

The self-assembly behaviour of **1** as a dilute solution in methylcyclohexane (MCH) was investigated by employing variable temperature UV–Vis spectroscopy. At elevated temperatures the spectra display characteristic features of PBIs in the molecularly dissolved state (Figure 2.1 A). Upon lowering the temperature, the absorption maximum of **1** shows a hypsochromic shift from λ = 510 to 501 nm and the development of a bathochromic shoulder at λ = 542 nm. These spectral features strongly correspond to previously reported PBIs of structural similarity and are indicative of the formation of face-to-face stacked PBI aggregates with a rotational offset.[37] The unsubstituted imide side of **1** allows self-complementary twofold hydrogen bonding and thus solutions of **1** in MCH are also investigated using FT-IR spectroscopy. The imide NH stretching vibration is observed at 3174 cm^{-1}, which indicates the presence of hydrogen bonding (Figure 2.1 B).[30,42] In contrast, the NH stretching vibration of **1** in chloroform solution is observed at 3377 cm^{-1}, indicating the predominance of non-hydrogen-bonded species under those conditions (Figure 2.1 B). The combined UV–Vis and IR observations strongly suggest that PBI **1** self-assembles in MCH into H-type columnar aggregates consisting of cofacially stacked, hydrogen-bonded dimers as schematically depicted in Figure 2.1 C.

To elucidate the self-assembly mechanism of PBI **1** into supramolecular polymers we probe the absorbance of the aggregate band (λ = 542 nm) as a function of temperature for various concentrations. Much to our surprise, the resultant cooling curves are characterised by a non-sigmoidal shape and a critical temperature at which aggregate growth commences, suggesting a cooperative growth mechanism (Figure 2.1 C). Standard analysis of the data using the K_2-K model for cooperative self-assembly suggests that at intermediate concentrations (c = 2×10^{-5} M) long one-dimensional aggregates consisting of more than thousand monomers should be present in solution at room temperature. The obtained thermodynamic parameters (K_n = 7.4×10^1, K_e = 1.1×10^7, σ = 6.8×10^{-6} at T = 273.15 K, see supplementary information reference 44) suggest a highly cooperative supramolecular polymerisation process.
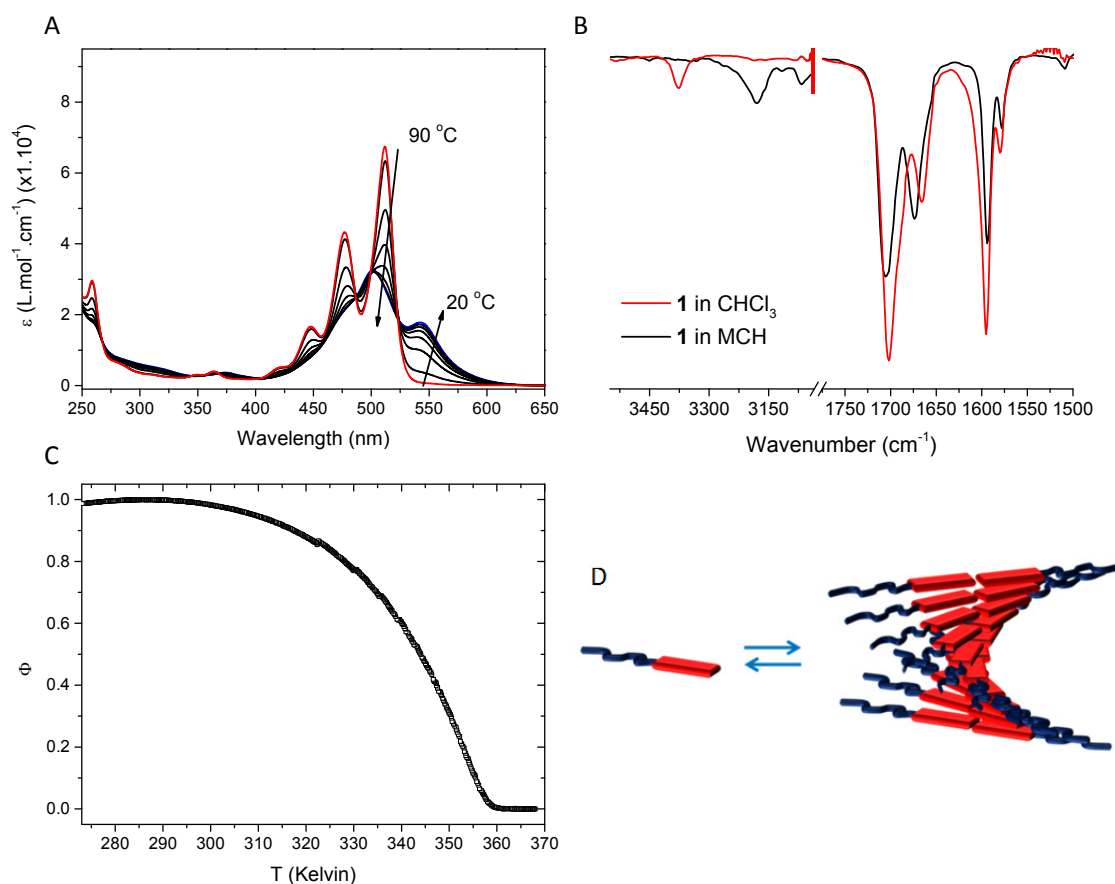
Figure 2.1. Variable temperature UV–Vis spectra of **1** in MCH at c = 2×10⁻⁵ M (A). Infrared spectra of **1** in MCH and CHCl$_3$ at c = 1×10⁻³ M (B). Schematic representation of the self-assembly of **1** into stacks of hydrogen-bonded dimers (C). Cooling curves measured at λ = 542 nm at various concentrations (D).

Small angle X-ray scattering (SAXS) experiments of solutions of PBI **1** in MCH (c = 1.10⁻³ M) (Figure 2.2 A) were performed to verify the validity of the thermodynamic analysis of the UV–Vis melting curves. We use a Guinier approximation and cylindrical form factor analysis to determine the radius of gyration, R$_g$, via two independent routes and obtain a value of R$_g$ ≈ 1.9 nm (Table 2.1). Assuming a typical π-π distance of 0.35 nm between stacked PBI dimers, the number of PBI molecules in an aggregate, amounts to approximately 20 to 30.

Surprisingly, this value is much smaller than expected based on the analysis of the UV–Vis cooling curves with the K_2-K model, especially since the concentration at which the SAXS experiments are performed is fifty times higher (c = 1×10⁻³ M) than
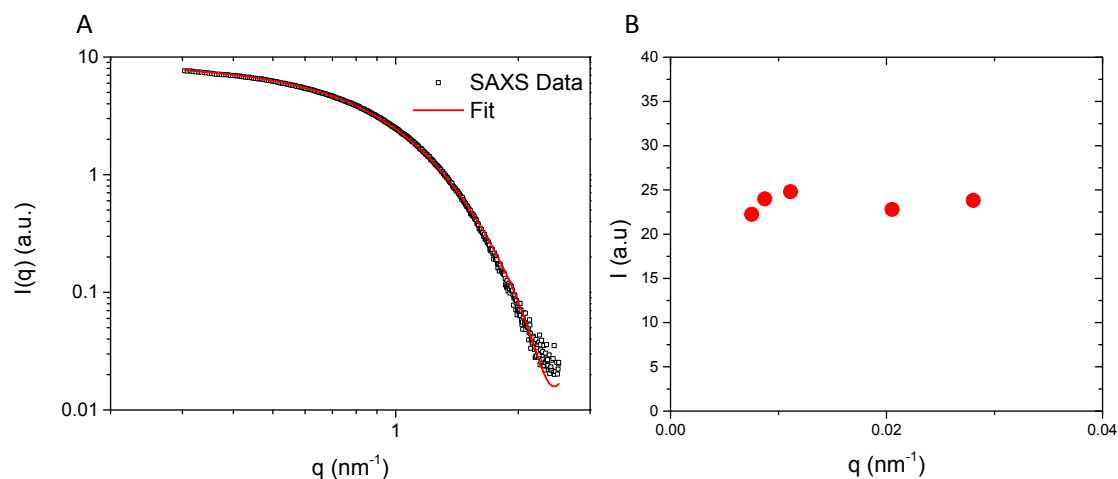
Figure 2.2. SAXS data curve of PBI **1** and a fit using a cylindrical form factor (c = 1×10^{-3} M, MCH) (A). SLS data for PBI **1** in MCH (c = 1×10^{-3} M) (B).

the concentration at which the UV–Vis data are acquired.[43] The SAXS data support the formation of more spherical aggregates instead of the expected elongated cylindrical aggregates. In addition, the absence of a measurable q-dependence of the scattering intensity in static light scattering (SLS) measurements on solutions of **1** further corroborated the absence of elongated one-dimensional objects in dilute MCH solution (Figure 2.2 B), as elongated, large objects generally show an angular dependence of the scattering signal. In accordance with these results, highly concentrated solutions of **1** in MCH (c = 2×10^{-2} M) do not form viscous solutions or gels as commonly observed for molecules that self-assemble into long one-dimensional structures. In summary, the scattering results are in contradiction with the conventional analysis of non-sigmoidal melting curves employing the K_2-K model as only small objects are experimentally observed in MCH solution whereas long self-assembled fibres are expected.[5,31,44]

Table 2.1. Overview of the SAXS results of compound **1**.

R_g (nm)[a]	L (nm)[b]	N_p[b]	R_{cs} (nm)[b]	$L/2R_{cs}$[b]	R_g (nm)[b]
1.94±0.03	5.2	30	1.7	1.5	1.9

Radius of gyration, R_g, cylinder length, L, cylinder cross sectional radius, R_{cs}, and the number of perylene bisimide dimers in a stack N_P. Obtained from a [a]Guinier approximation and [b]modelling with a form factor for rigid cylinders[45,46]

2.4 Modelling the self-assembly mechanism

To gain mechanistic insight into this unusual type of self-assembly behaviour, several self-assembly equilibrium models were analysed in collaboration with Peter Korevaar and Tom de Greef. For detailed discussions on these models, the reader is referred to references 47 and 48. First, an attenuated equilibrium model is considered in which each subsequent monomer addition step proceeds with a diminished equilibrium constant (i.e. anti-cooperative growth).[49] Although this model predicts the formation of small aggregates, no critical point can be observed in the temperature- and concentration-dependent assembly curves. Hence, the model does not describe the experimental observations. However, after modifying the model such that the attenuated assembly starts off with an energetically unfavourable nucleation of two hydrogen-bonded dimers via π-stacking, the formation of small assemblies is observed only beyond a critical concentration and temperature.

As an alternative molecular explanation for cooperative behaviour we hypothesise the formation of a hydrogen-bonded dimer as an unfavourable species via weak twofold hydrogen bonding of two PBI molecules. Subsequent π-stacking of these dimers is likely energetically more favourable than the initial formation of the hydrogen-bonded dimer and results in cooperative growth of the supramolecular polymer. However, upon polymerisation, increased steric crowding may result in a diminished aggregation tendency with increasing polymer length. This may lead to the formation of small self-assembled objects instead of elongated fibres. We model this scenario by assuming that the formation of a hydrogen-bonded dimer occurs with equilibrium constant K_h and the subsequent elongation is described with equilibrium constant K_i, which depends on the chain length i via $K_i = K/i$ (Figure 2.3 A). To demonstrate the behaviour of the system in general, the degree of aggregation as well as DP_n and DP_w are analysed as a function of the dimensionless concentration x_{tot} = $K \times c_{tot}$. Typically, x_{tot} can be increased upon increasing the total concentration c_{tot} or, as the equilibrium constant K increases upon cooling, by decreasing the temperature. Gratifyingly, calculations as a function of x_{tot} capture the experimental results: a critical point is obtained, whereas DP_n and DP_w are low, even at very high values of x_{tot} (Figure 2.3 B). An unfavourable association event (i.e., nucleation, formation of hydrogen-bonded dimer) is in general required to obtain a critical point. However, we note that in order to obtain assemblies of limited size, alternative relations between

the association constant and chain length can be selected to limit the length of the stacks.[50]
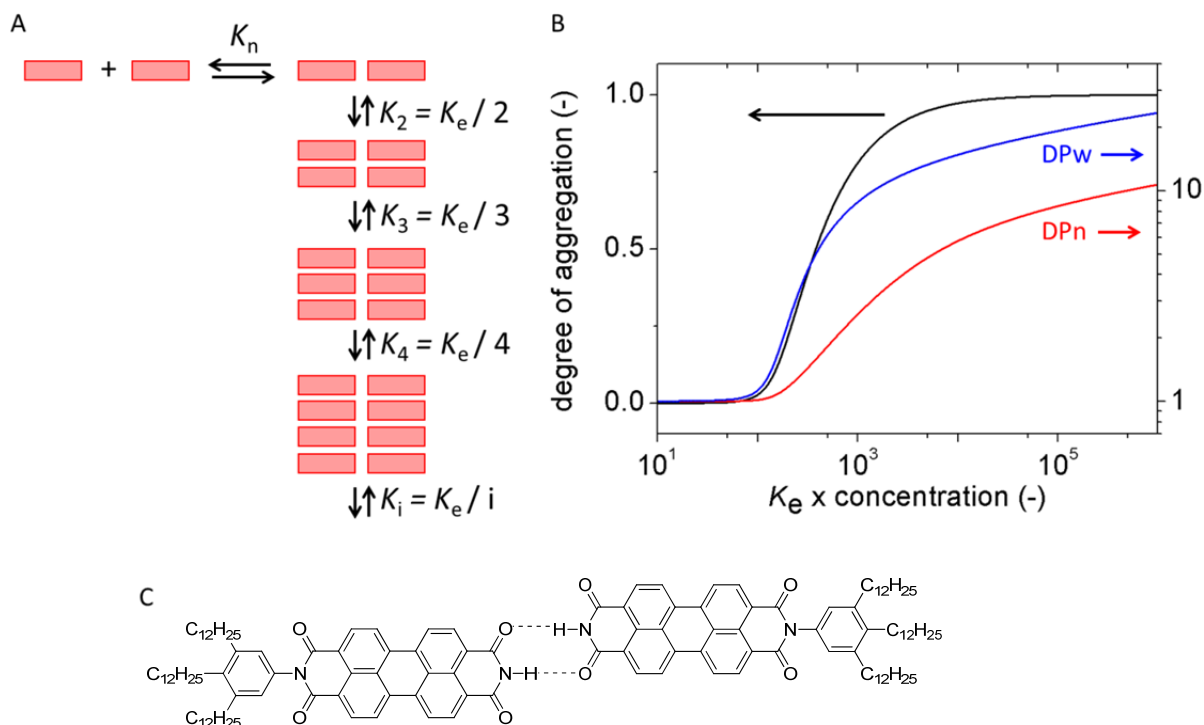
Figure 2.3. Schematic representation of the attenuated equilibrium model for supramolecular polymerisation of PBI **1** with dimerisation as the unfavourable nucleation step (A). Plot of the degree of aggregation and degrees of polymerisation as a function of x_{tot} using the modified attenuated equilibrium model (B). Molecular structure of a hydrogen-bonded dimer of PBI **1** (C).

2.5 The influence of hydrogen bonding

To corroborate the relevance of hydrogen bonding in the cooperative self-assembly of PBI **1**, this interaction was selectively removed by *N*-methylation of the imide to yield PBI **2**.[51] Variable temperature UV–Vis measurements of PBI **2** at c = 2×10^{-5} M reveal the formation of H-aggregated PBIs similar to the aggregates obtained for **1** (Figure 2.4 A). Cooling curves measured for PBI **2** (λ = 540 nm) however, are sigmoidal in shape and lack a critical temperature, indicating an isodesmic growth mechanism (Figure 2.4 B) which is in contrast to the non-sigmoidal cooling curves recorded for **1**. Furthermore, aggregates of PBI **2** are less stable compared to aggregates containing PBI **1** as reflected by the lower temperature for the onset of aggregation for **2** (Figure 2.4 B). As expected, these results indicate that the cooperative self-assembly mechanism observed for PBI **1** is probably related to the interplay of hydrogen-bond dimerisation and concomitant π-stacking of these

29

dimers. Additionally, the hydrogen-bonding interactions further stabilise the self-assembled PBI aggregates.
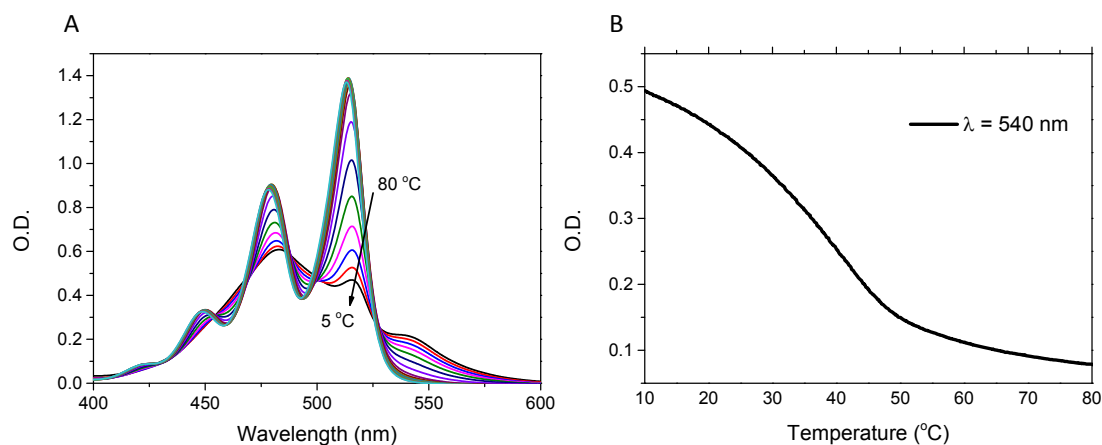
Figure 2.4. Variable temperature UV–Vis spectra of **2** in MCH (c = 2×10^{-5} M, T = 20 °C, l = 1 cm) (A). Cooling curve of **2** measured at λ = 540 nm (c = 4×10^{-5} M, l = 1 cm, rate = 0.1 K/min) (B).

2.6 Conclusion

We have successfully synthesised an asymmetric perylene bisimide bearing a solubilising group on one side and a twofold self-complementary hydrogen-bond motif on the other side. This perylene bisimide self-assembles into aggregates via hydrogen-bond dimerisation and concomitant π-stacking of these dimers. Variable temperature UV–Vis spectroscopy indicated a cooperative supramolecular polymerisation process, which was modelled using the K_2-K model for such processes. SAXS and SLS measurements were used to verify the results of the thermodynamic analysis and surprisingly indicated a discrepancy between the measured and predicted sizes of the aggregates. The self-assembly model was adjusted by allowing the association constant of the elongation phase to decrease upon stack growth. Gratifyingly, calculations using this model captured the experimental observations; a critical point was observed in the assembly curve while the aggregates remained small.

The self-assembly behaviour of the PBI may be rationalised in the following way: hydrogen-bond dimerisation is weak but subsequent π-stacking of these dimers is energetically more favourable. In this way the dimerisation is the nucleation phase in the self-assembly process. Increased steric hindrance upon π-stacking of the dimers can result in a diminished association constant and limited stack length. Our

observations serve as a warning that typical hallmarks of cooperative growth of self-assembled nanostructures do not per se imply the formation of large objects and additional experiments should be performed to characterise the self-assembled structures in solution. Furthermore, the formation of defined supramolecular nano-objects by π-stacking of chromophores may be relevant in the design of artificial photosynthetic systems for which precise control over chromophore packing architecture is required.[52-54] To this end, the steric bulk of solubilising side-chains on the periphery of molecules that show cooperative supramolecular polymerisation can be used as a means to control the size of supramolecular aggregates, as shown for PBI **1**. This approach bears similarities to the use of incremental generations of dendrons to limit the π-stacking of chromophores in solution.[55,56] Having established the self-assembly behaviour of asymmetric PBI **1** into small stacks of hydrogen-bonded dimers, we will proceed in Chapter 3 of this thesis by addressing the supramolecular heteroaggregation of asymmetric PBIs with complementary hydrogen-bonding molecules for the build-up of multicomponent supramolecular systems based on perylene bisimides.

2.7 Experimental section

Instrumentation, materials and methods

Unless specifically mentioned, reagents and solvents were obtained from commercial suppliers and used without further purification. All solvents were of AR quality. Deuterated chloroform for NMR analyses was provided with TMS as the 0 ppm reference. The methylcyclohexane used in all spectroscopic experiments was of spectroscopic grade. Column chromatography was performed on a Biotage Isolera One using SNAP KP-sil columns and solvent gradients.

^{1}H-NMR and ^{13}C-NMR spectra were recorded on a Varian Mercury Vx 400 MHz instrument (100 MHz for ^{13}C) and all chemical shifts are reported in parts per million relative to tetramethylsilane (TMS). MALDI-ToF MS analyses were performed in reflector mode on a PerSeptive Biosystems Voyager-DE Pro using α-cyano-4-hydroxycinnamic acid (CHCA) and 2-[(2E)-3-(4-tert-butylphenyl)-2-methylprop-2-enylidene]malononitrile (DCTB) as matrices. Ultraviolet-visible (UV–Vis) absorbance spectra were recorded on a Jasco V-650 UV–Vis spectrometer with a Jasco ETCR-762 temperature controller. Solid state infrared (IR) spectra were recorded on a Perkin

Elmer Spectrum One spectrometer equipped with an ATR universal sampler accessory and in dilute solution using 1 mm NaCl cells.

The small-angle X-ray scattering (SAXS) experiments were performed by Ilja Voets at the cSAXS beamline at the Swiss Light Source (SLS) at the Paul Scherrer Institute. The samples were filled in 1 mm diameter quartz capillaries with a wall thickness of 0.01 mm (Hilgenberg) and maintained at a temperature of 20±1°C. An X-ray energy of 12.4 keV corresponding to a wavelength, λ, of 0.1 nm and one sample-to-detector distance of 2.17 m were used, to cover a range of 0.3 nm^{-1} ≤ q ≤ 2.5 nm^{-1} with the magnitude of the scattering wave vector, q, given by q = (4π/λ)×sin(θ/2) and the scattering angle, θ. The scattering patterns were recorded on a PSI-developed Pilatus 2 M detector operating in single-photon counting mode. The 2D images were azimuthally integrated and corrected for background scattering according to established procedures provided by the PSI. The q-scale was calibrated by a measurement of silver behenate. The SASfit software package was used for data analysis with a form factor for monodisperse rigid cylinders.[57] The monomer concentration of 1 mM was low enough to safely neglect interactions between the supramolecular self-assemblies, such that the structure factor S(q) ~ 1.

Static light scattering (SLS) was measured by Panayiotis Voudouris and was used to characterise particles in solution. Avoidance of laser induced motions of the particles, such as induced flow which would disturb the measured signal, required special precautions Care was taken to minimise the induced thermal effects, in particular to suppress the thermal lensing as observed through the projection of the transmitted beam. To control the effectiveness of the method, measurements were conducted at different laser wavelengths (740 nm, 633 nm and 532 nm) and powers and the invariance of the relaxation functions to power increase was checked. Scattered intensity was normalised to the toluene intensity. Static and dynamic light scattering experiments were conducted on FORTH/IESL Greece using an ALV-5000 commercial set-up allowing polarised scattering measurements. A He-Ne 633 nm and 20 mW power was used as the light source. The dispersions were contained in dust-free 10 mm tubes. Static light scattering measurements were obtained by averaging the intensity at each angle, over 5 to 10s and the scattering wave vector, q =

(4πn/λ)sin(ϑ/2)) with *n* being the refractive index of the medium and *ϑ* the scattering angle, was varied in a broad range between 0.007-0.028 nm^{-1}.

All fits of the cooling curves with various self-assembly equilibrium models were performed according to reference 44.

Perylenetetracarboxylic acid-3,4-anhydride-9,10-imide (**3**) and tridodecylaniline (**4**) were prepared according to references 37, 40 and 41.

Synthesis

N-3,4,5-Tridodecylphenyl-perylene-3,4:9,10-tetracarboxylic acid bisimide (**1**)

Perylenetetracarboxylic acid-3,4-anhydride-9,10-imide (130 mg, 0.33 mmol), 3,4,5-tridodecylaniline (300 mg, 0.46 mmol), and Zn(OAc)$_2$ (73 mg, 0.33 mmol) were mixed in quinoline (15 mL). The mixture was stirred at 180 °C for 2 hours under an argon atmosphere, resulting in a dark red/brown mixture. After cooling to room temperature the solution was poured into methanol (100 mL), resulting in a dark red precipitate. Remaining quinoline solvent was removed by repetitive precipitations from chloroform in methanol. The crude product was purified by silica gel column chromatography using first chloroform as eluent to remove the bis-tridodecylphenyl side-product and then 5% acetic acid in chloroform (R$_f$ = 0.55). Remaining acetic acid was removed by basic extraction of the chloroform solution with 1 M NaOH. The organic phase was dried over MgSO$_4$, filtered and evaporated in vacuo to yield the product as a red solid. Yield = 90 mg. η = 35%. ^{1}H-NMR (CDCl$_3$) δ = 8.73 (d, 2H), 8.67 (d, 2H), 8.63 (d, 2H), 8.61 (d, 2H), 8.57 (b, 1H, NH), 6.98 (s, 2H, Ar-H), 2.66 (t, 6H, CH$_2$), 1.7-1.2 (mm, 60H, aliphatic), 0.92-0.82 (m, 9H, CH$_3$). ^{13}C-NMR (CDCl$_3$) δ = 163.5, 162.9, 142.2, 139.4, 135.3, 134.4, 132.1, 131.7, 131.2, 130.6, 129.6, 126.8, 126.4, 126.2, 123.9, 123.4, 123.1, 123.0, 33.2, 32.0, 31.9, 31.3, 30.8, 30.5, 30.0, 29.8, 29.7, 29.7, 29.6, 29.5, 29.4, 29.4, 29.4, 28.8, 22.7, 22.7, 14.1, 14.1. MALDI-ToF-MS (m/z) calc for C$_{66}$H$_{86}$N$_2$O$_4$ 970.66 found 971.69 (M+H)$^+$ 993.71 (M+Na)$^+$.

N-3,4,5-Tridodecylphenyl-N'-methyl-perylene-3,4:9,10-tetracarboxylic acid bisimide (**2**)

N-3,4,5-Tridodecylphenyl-perylene-3,4:9,10-tetracarboxylic acid bisimide (23 mg, 0.024 mmol), finely grinded K$_2$CO$_3$ (98 mg, 0.71 mmol) and MeI (100.2 mg, 0.71 mmol) were charged in dry DMF (3 mL) and stirred overnight at room temperature under an argon atmosphere. The resulting red solution was concentrated in vacuo

and the residue was subjected to column chromatography with $CHCl_3$:n-C_7H_{16}:CH_3OH:CH_3COOH/57:48:4:1 as an eluent (R_f = 0.22). Remaining acetic acid was removed by basic extraction of the chloroform solution with 1 M NaOH. The organic phase was dried over $MgSO_4$, filtered and evaporated in vacuo to yield the product as a red solid. Yield = 21 mg. η = 91%. ^{1}H-NMR ($CDCl_3$) δ = 8.61 (d, 2H), 8.46 (d, 2H), 8.39 (d, 2H), 8.31 (d, 2H), 7.07 (s, 2H, Ar-H), 2.66 (t, 6H, CH_2), 1.7-1.2 (mm, 60H, aliphatic), 0.92-0.82 (m, 9H, CH_3). ^{13}C-NMR ($CDCl_3$) δ = 163.2, 163.0, 142.1, 139.2, 133.8, 133.8, 132.2, 131.0, 130.6, 129.2, 128.4, 126.3, 125.7, 125.6, 123.6, 122.8, 122.7, 33.2, 31.9, 31.9, 31.2, 30.8, 30.5, 30.0, 29.8, 29.8, 29.7, 29.7, 29.5, 29.5, 29.4, 29.4, 28.8, 27.1, 22.7, 22.7, 14.1, 14.1. MALDI-ToF-MS (m/z) calc for $C_{67}H_{88}N_2O_4$ 984.67 found 984.67 (M·)[+] 1007.66 (M+Na)[+].

2.8 References

[1]   T. Aida, E.W. Meijer, S.I. Stupp, *Science*, 2012, **335**, 813

[2]   T.F.A. de Greef, M.M.J. Smulders, M. Wolffs, A.P.H.J. Schenning, R.P. Sijbesma, E.W. Meijer, *Chem. Rev.,* 2009, **109**, 5687

[3]   P.Y.W. Dankers, E.W. Meijer, *Bull. Chem. Soc. Jpn.*, 2007, **11**, 2047

[4]   X. Yu, L. Chen, M. Zhang, T. Yi, *Chem. Soc. Rev.*, 2014, **43**, 5346

[5]   P. Jonkheijm, P. van der Schoot, A.P.H.J. Schenning, E.W. Meijer, *Science*, 2006, **313**, 80

[6]   M.M.J. Smulders, M.M.L. Nieuwenhuizen, T.F.A. de Greef, P. van der Schoot, A.P.H.J. Schenning, E.W. Meijer, *Chem. Eur. J.*, 2010, **16**, 362

[7]   P.A. Korevaar, C. Schaefer, T.F.A. de Greef, E.W. Meijer, *J. Am. Chem. Soc.*, 2012, **32**, 13482

[8]   M.J. Ahrens, L.E. Sinks, B. Rybtchinski, L. Wenhau, B.A. Jones, J.M. Giaimo, A.V. Gusev, A.J. Goshe, D.M. Tiede, M.R. Wasielewski, *J. Am. Chem. Soc.*, 2004, **126**, 8284

[9]   X. Li, L.E. Sinks, B. Rybtchinski, M.R. Wasielewski, *J. Am. Chem. Soc.*, 2004, **126**, 10810

[10]   M.J. Ahrens, R.F. Kelly, Z.E.X. Dance, M.R. Wasielewski, *Phys. Chem. Chem. Phys.*, 2007, **9**, 1469

[11]   A. Arnoud, J. Belleney, F. Boué, L. Bouteiller, G. Carrot, V. Wintgens, *Angew. Chem. Int. Ed.*, 2004, **43**, 1718

[12]   P. Besenius, G. Portale, P.H.H. Bomans, H.M. Janssen, A.R.A. Palmans, E.W. Meijer, *PNAS*, 2010, **107**, 17888

[13]   I. de Feijter, P. Besenius, L. Albertazzi, E.W. Meijer, A.R.A. Palmans, I.K. Voets, *Soft Matter*, 2013, **9**, 10025

[14]   M. von Gröning, I. de Feijter, M.C.A. Stuart, I.K. Voets, *J. Mater. Chem. B.*, 2013, **1**, 2008

[15]   D. Zhao, J.S. Moore, *J. Org. Chem.*, 2002, **67**, 3548

[16]   S.I. Stupp, V. LeBonheur, K. Walker, L.S. Li, K.E. Huggins, M. Keser, A. Amstutz, *Science*, 1997, **276**, 384

[17]   W. Herbst, K. Hunger, *Industrial Organic Pigments: Production, Properties, Applications*, 2nd edn. WILEY-VCH, Weinheim, 1997

[18]   C.W. Struijk, A.B. Sieval, J.E.J. Dakhors, M. van Dijk, P. Kimkes, R.B.M. Koehorst, H. Donker, T.J. Schaafsma, S.J. Picken, A.M. van de Craats, J.M. Warman, H. Zuilhof, E.J.R. Sudhölter, *J. Am. Chem. Soc.*, 2000, **122**, 11057

[19]   C.D. Dimitrakopoulos, P.R.L. Malenfant, *Adv. Mater.*, 2002, **14**, 99

[20]   K.-Y. Law, *Chem. Rev.*, 1993, **93**, 449

[21]   L. Schmidt-Mende, A. Fechtenkötter, K. Müllen, E. Moons, R.H. Friend, J.D. MacKenzie, *Science*, 2001, **293**, 1119

[22]   F. Würthner, *Chem. Commun.*, 2004, 1564

[23]   T. van der Boom, R.T. Hayes, Y. Zhao, P.J. Bushard, E.A. Weiss, M.R. Wasielewski, *J. Am. Chem. Soc.*, 2002, **124**, 9582

[24]   F. Würthner, C. Thalacker, A. Sautter, *Adv. Mater*, 1999, **11**, 754

[25]   F. Würthner, C. Thalacker, A. Sautter, W. Schärtl, W. Ibach, O. Hollricher, *Chem. Eur. J.*, 2000, **6**, 3871

[26]   R. Dobrawa, D.G. Kurth, F. Würthner, *Polymer Preprints*, 2004, **45**, 378

[27]   R. Dobrawa, F. Würthner, *Chem. Commun.*, 2002, 1878

[28]   F. Würthner, A. Sautter, D. Schmid, P.J.A. Weber, *Chem. Eur. J.*, 2001, **7**, 894

[29]   S. Yagai, Y. Monma, N. Kawauchi, T. Karatsu, A. Kitamura, *Org. Lett.,* 2007, **9**, 1137

[30]   T.E. Kaiser, H. Wang, V. Stepanenko, F. Würthner, *Angew. Chem. Int. Ed.*, 2007, **46**, 5541

[31]   T.E. Kaiser, V. Stepanenko, F. Würthner, *J. Am. Chem. Soc.*, 2009, **131**, 6719

[32]   V. Percec, M. Peterca, T. Tadjiev, X. Zeng, G. Ungar, P. Leowanawat, E. Aqad, M.R. Imam, B.M. Rosen, U. Akbey, R. Graf, S. Sekharan, D. Sebastiani, H.W. Spiess, P.A. Heiney, S.D. Hudson, *J. Am. Chem. Soc.*, 2011, **133**, 12197

[33]   F. Würthner, C. Thalacker, S. Diele, C. Tschierske, *Chem. Eur. J.*, 2001, **7**, 2245

[34]   T. Seki, S. Yagai, T. Karatsu, A. Kitamura, *J. Org. Chem.*, 2008, **73**, 3328

[35]   T. Seki, Y. Maruya, K. Nakayama, T. Karatsu, A. Kitamura, S. Yagai, *Chem. Commun.*, 2011, **47**, 12447

[36]   S. Yagai, T. Seki, T. Karatsu, A. Kitamura, F. Würthner, *Angew. Chem. Int. Ed.*, 2008, **47**, 3367

[37]   Z. Chen, V. Stepanenko, V. Dehm, P. Prins, L.D.A. Siebbeles, J. Seibt, P. Marquetand, V. Engel, F. Würthner, *Chem. Eur. J.*, 2007, **13**, 436

[38]   C. Ludwig, B. Gompf, J. Petersen, R. Strohmaier, W. Eisenmenger, *Z. Phys. B.*, 1994, **93**, 365

[39]   B. Uder, C. Ludwig, J. Petersen, B. Gompf, W. Eisenmenger, *Z. Phys. B.*, 1995, **97**, 389

[40]   H. Kaiser, J. Lindner, H. Langhals, *Chem. Ber.*, 1991, **124**, 529

[41]   X. Zhang, Z. Chen, F. Würthner, *J. Am. Chem. Soc.,* 2007, **129**, 4886

[42]   H. Langhals, S. Saulich, *Chem. Eur. J.*, 2002, **8**, 5630

[43]   A different self-assembly model may be operative at higher (c = 1×10^{-3} M) concentrations than the concentration (c = 2×10^{-5} M) that was used to fit the *K$_2$-K* model. Thermodynamic data on the self-assembly at high concentrations in MCH is unattainable as the molecules remain aggregated at elevated temperatures. UV–Vis and FT-IR spectra however are very similar for both concentrations, suggesting the presence of similar aggregates. We therefore assume the formation mechanism of the aggregates to be the same at both concentrations.

[44]   M.M.J. Smulders, A.P.H.J. Schenning, E.W. Meijer, *J. Am. Chem. Soc.*, 2008, **130**, 606

[45]   Guinier approximation: I(q) = I$_0$exp((-1/3)×R$_g$^{2}×q^2)) in the range 0.40 ≤ q ≤ 0.67 nm^{-1}

[46]   Form factor form rigid cylinders: R$_g$^{2} = 0.5×R^2 + (1/12)×L^2.

[47]   R. van der Weegen, P.A. Korevaar, P. Voudouris, I.K. Voets, T.F.A. de Greef, J.A.J.M. Vekemans, E.W. Meijer, *Chem. Commun.,* 2013, **49**, 5532

[48]   P.A. Korevaar *Pathway complexity in pi-conjugated materials* PhD thesis, Eindhoven University of Technology, Eindhoven, the Netherlands, 2014

[49]   R. B. Martin, *Chem. Rev.*, 1996, **96**, 3043

[50]   K. F. Freed, *J. Chem. Phys.*, 2012, **137**, 204906

[51]   I.A.W. Filot, A.R.A. Palmans, P.A.J. Hilbers, R.A. van Santen, E.A. Pidko, T.F.A. de Greef, *J. Phys. Chem. B.*, 2010, **114**, 13667

[52]   G. Steinberg-Yfrach, P.A. Liddell, S.C. Hung, A.L Moore, D. Gust, T.A. Moore, *Nature*, 1997, **385**, 239

[53]   S. Bhosale, A.L. Sisson, P. Talukda, A. Fürstenberg, N. Banerji, E. Vauthey, G. Bollot, J. Mareda, C. Röger, F. Würthner, N. Sakai, S. Matile, *Science*, 2006, **313**, 84

[54]   P.D. Frischmann, K. Mahata, F. Würthner, *Chem. Soc. Rev.*, 2013, **42**, 1847

[55]   T. Heek, C. Easting, C. Rest, X. Zhang, F. Würthner, R. Haag, *Chem. Commun.*, 2010, **46**, 1884

[56]   B. Gao, H. Li, H. Liu, L. Zhang, Q. Bai, X. Ba, *Chem. Commun.*, 2011, **47**, 3894

[57]   P. Lindner, T. Zemb, eds., *Neutron, X-rays and Light: Scattering Methods Applied to Soft and Condensed Matter*, Elsevier, Amsterdam, 2002

3

Multicomponent self-assembled systems based on perylene bisimides and triazines

Abstract

The supramolecular heteroaggregation of an asymmetric perylene bisimide with a library of mono- and divalent triazines by complementary hydrogen bonding and subsequent π-stacking was investigated as a dilute solution in methylcyclohexane. For monovalent triazines we observed pathway complexity in the self-assembly by virtue of competition between perylene homoaggregation and perylene-triazine heteroaggregation. By introduction of *N*-phenyl substituents on additional hydrogen-bonding sites of the monotriazines, the composition of the multicomponent supramolecular system could be steered towards the selective formation of supramolecular heteroaggregates. On the other hand, the use of divalent triazines resulted in the selective formation of perylene based supramolecular heteroaggregates, without the interference of pathway complexity. The supramolecular heteroaggregates based on divalent triazines were found to be more stable than heteroaggregates based on their monovalent counterparts as determined by temperature dependent UV–Vis and CD measurements. Additionally, we found that the introduction of a single stereogenic centre on the remote periphery of a divalent triazine results in the formation of chiral perylene bisimide stacks as evidenced by a Cotton effect in the perylene absorption bands in CD spectroscopy.

3.1 Introduction

The formation of defined nanostructures based on a single molecular building block is nowadays reasonably well understood in the field of supramolecular chemistry.[1-3] Synthetic chemists have a wide variety of molecular structures at their disposal in which they can tailor the non-covalent interactions to guide a self-assembly process towards the desired product. However, small variations in molecular architecture may still unexpectedly result in the formation of widely different self-assembled structures.[4-8] Furthermore, kinetically fast pathways towards metastable self-assembled structures have been shown to complicate the formation of desired supramolecular structures.[9-13] Ultimately, this may affect the performance of supramolecular materials designed with specific functionalities. In recent years multicomponent supramolecular architectures have attracted considerable attention because the structural variability and functionality of the final aggregates is far greater than their single component counterparts.[14-16] Similarly, the number of self-assembly pathways leading to undesired self-assembled structures instead of the desired product are also more prevalent. Therefore, it is of utmost importance to control and direct the outcome of multicomponent self-assembly in order to selectively arrive at desired supramolecular architectures.

π-Conjugated building blocks have attracted much attention as supramolecular motifs due to their strong tendency to aggregate into columnar architectures by the formation of π-stacks.[16-19] The perylene bisimides (PBIs) constitute a particularly interesting class of molecules, because a great structural diversity can be achieved by varying either the imide- or the bay-position substituents, which consequently leads to a rich variety in accessible supramolecular architectures.[20] For example, the self-assembly of imide-functionalised bay-unsubstituted PBIs has been investigated in great detail by the group of Würthner and others.[21-25] Here, π-stacked architectures where the PBI chromophores predominantly form H-aggregates could be obtained in both polar and apolar solutions as well as in the solid state. The introduction of bulky substituents at the PBI bay positions resulted in a reduction of the aggregation propensity and changed the aggregation mode from H- to J-type.[22] Conversely, imide N-H substituted bay-functionalised PBIs were found to form one-dimensional double string cable aggregates by a combination of π-stacking and hydrogen bonding (Figure 3.1).[26,27] The PBIs displayed J-type aggregation by virtue of offset π-stacking of the PBI

chromophores in the supramolecular fibre and showed a fluorescence quantum yield of near unity in the aggregated state.
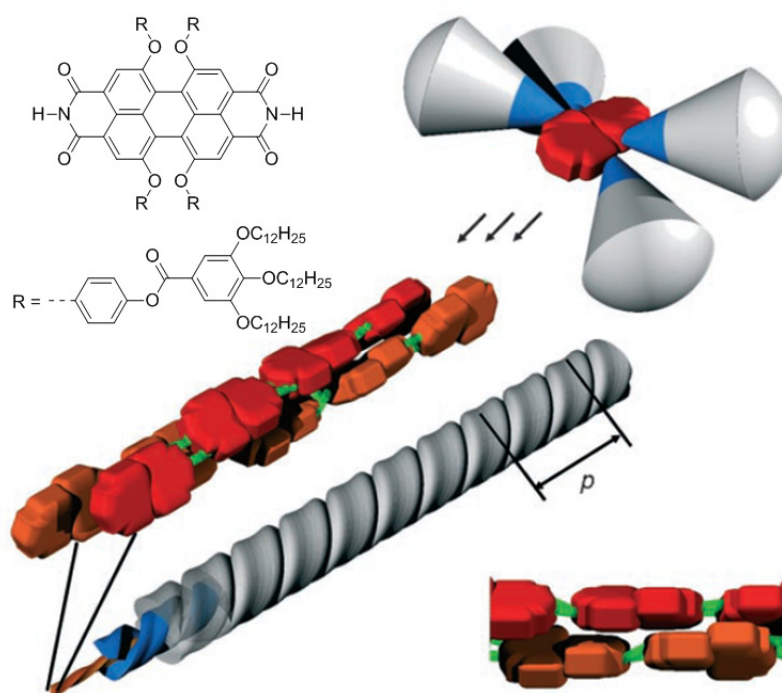
Figure 3.1. Self-assembly of PBI into a double string cable by a combination of twofold hydrogen bonding and π-stacking. Image adapted from reference 27.

Imide N-H substituted PBIs furthermore constitute an acceptor-donor-acceptor (ADA) hydrogen-bonding array that can be complexed by complementary donor-acceptor-donor (DAD) arrays. This triple hydrogen-bonding motif has been widely used in the formation of supramolecular chromophore systems.[14,28-30] An intriguing example is the formation of supramolecular stacks of electron donor and acceptor molecules by the groups of Würthner and Meijer.[14,28,31] Here, a bay-substituted PBI was complexed by threefold hydrogen bonding with diaminotriazine-functionalised oligophenylenevinylene (OPV). The supramolecular trimer subsequently formed one-dimensional aggregates by J-type π-stacking, which coil into larger, chiral rod superstructures as determined by AFM analyses. The resulting OPV-PBI supramolecular stacks could be applied in organic photovoltaic devices.
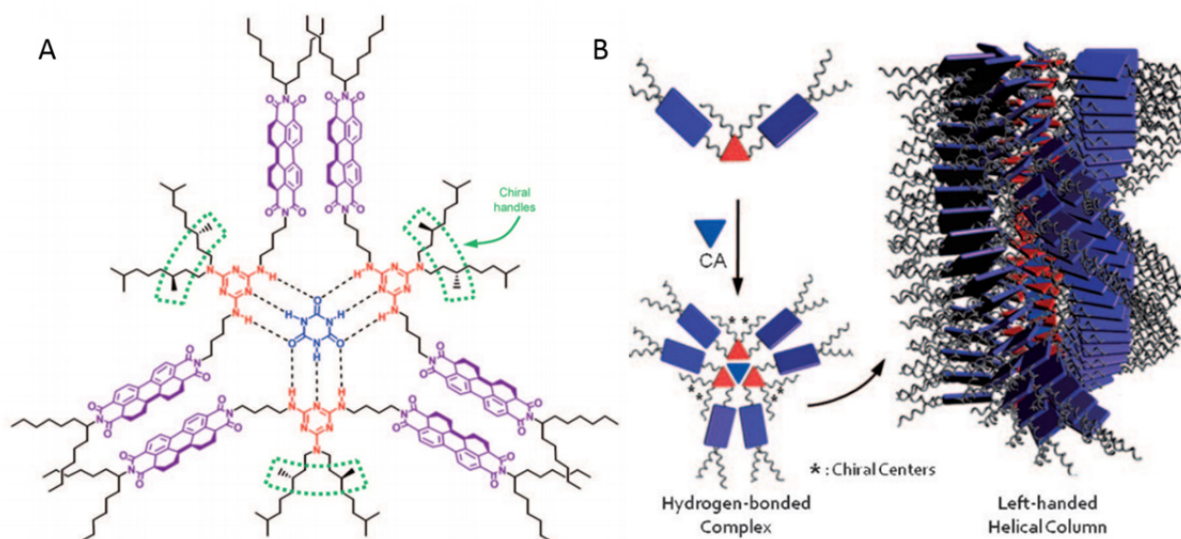
Figure 3.2. Molecular structure of a hydrogen-bonded assembly of PBI-appended melamines with cyanuric acid (A) and a schematic representation of the self-assembly into helical columns (B) Image adapted from reference 35.

Supramolecular stacks of PBIs based on threefold hydrogen bonding have also been investigated by Yagai and co-workers.[32-35] In multiple studies, threefold hydrogen-bonding motifs (e.g., melamine, cyanuric acid) were introduced on the imide positions of the PBI scaffold (Figure 3.2). After complexation by complementary hydrogen-bond moieties and subsequent π-stacking of the complexes, a wide variety of supramolecular architectures such as nanoribbons, nanoropes and multilamellar structures could be generated. From the examples above it is evident that a wide variety of nanoscopic architectures can be generated by the formation of PBI-based supramolecular stacks. Obviously, pathway complexity in self-assembly plays a crucial role in determining the outcome of aggregation processes of such multicomponent supramolecular architectures. Therefore, insights into their self-assembly pathways and mechanisms are valuable in the design of such multicomponent supramolecular architectures.

In Chapter 2, the synthesis and self-assembly of an asymmetric perylene bisimide (PBI) that bears an ADA hydrogen-bonding array were described. In this chapter our aim is to determine guidelines to direct a self-assembling system that shows pathway complexity, along a desired aggregation pathway. A library of mono- and divalent diaminotriazines is synthesised as complementary binders to asymmetric PBI **1a** described in Chapter 2 (Figure 3.3). In the monovalent triazines, phenyl substituents

are introduced to block additional hydrogen-bond interaction sites and limit the formation of off-pathway aggregates. Additionally, the phenyl substituents acidify the N-H protons of the triazines, potentially strengthening the threefold hydrogen bond that is formed with complementary motifs. Furthermore, divalent triazines are designed to have increased π-stacking interactions upon perylene hydrogen bonding and thereby favouring the formation of supramolecular heteroaggregates over homoaggregates. The heteroaggregation of the triazine library with PBI **1a** in dilute solution by hydrogen bonding and subsequent π-stacking is evaluated with NMR, UV–Vis, CD and FT-IR spectroscopy. Spectroscopic titrations and variable temperature measurements are used to reveal the self-assembly pathways of the heteroaggregating supramolecular systems. Furthermore, we investigate the limits of chiral amplification and chiral information transfer by investigating chiral PBI-triazine stacks, where a single chiroptical centre is located on the periphery of the triazine molecule.
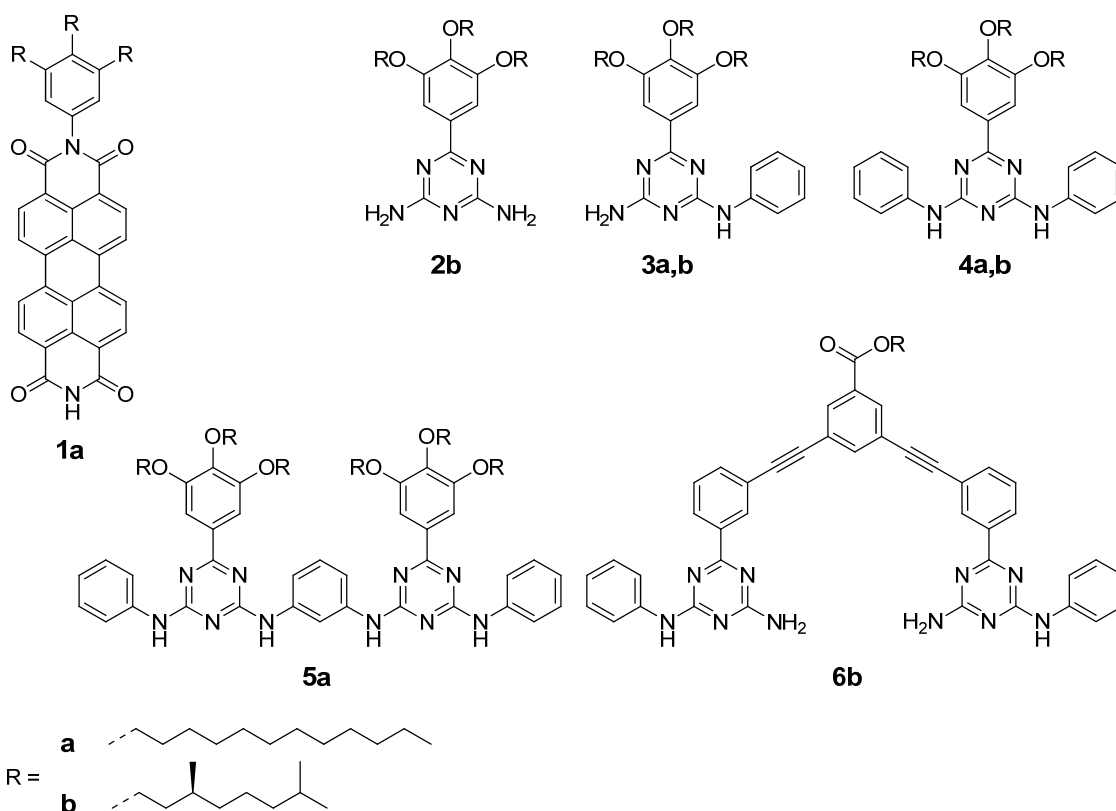
Figure 3.3. Asymmetric perylene bisimide **1a** and a library of mono- and divalent triazines **2-6**.

3.2 Molecular design and synthesis

In Chapter 2 we demonstrated that PBI **1a** self-assembles into stacks of hydrogen-bonded dimers via twofold hydrogen bonding and concomitant π-stacking. The unsubstituted side of the bisimide constitutes a threefold ADA hydrogen bond motif. A common complementary motif to the imide ADA motif is the diaminotriazine hydrogen-bonding array.[14,28-30] Diaminotriazines **2-4** are designed as complementary binders to PBI **1a**, where the introduction of phenyl substituents on the amines results in the blocking of additional hydrogen-bonding interaction sites. Solubilising side-chains with and without stereogenic centres are introduced on the triazine periphery to induce solubility in apolar organic solvents and to allow characterisation of the self-assembly processes with circular dichroism (CD) spectroscopy. Divalent triazines **5a** and **6b** are designed to increase the π-stacking surface upon PBI hydrogen bonding and thereby promote the formation of heteroaggregates. To probe the limits of chiral amplification, triazine **6b** is functionalised with a single stereogenic centre, based on (*S*)-citronellol, on a remote position from the hydrogen-bond moieties.

The synthesis of the library of triazines is shown in Scheme 3.1. Triazines **2a,b** were prepared according to literature procedures, where commercially available dicyandiamide (**7**) was reacted with nitriles **8a,b** to yield triazines **2a,b** after column chromatography in 53-56% yield.[36] As precursors for triazines **3a,b** and **4a,b**, acid chlorides **10a** and **10b** and diphenylbiguanide **11** were prepared as reported in literature, while phenylbiguanide **9** was commercially available.[37-39] The library of triazines was obtained by reacting the biguanide with the corresponding acid chloride under standard amide forming conditions followed by a short period of heating under reflux conditions to facilitate ring closure of the initially formed amides to the triazines. Bisbiguanide **14** was prepared in moderate yield by reacting commercially available phenyldicyandiamide **12** with 1,3-diaminobenzene in a boiling mixture of 1 M HCl and ethanol. Bistriazine **5a** was obtained by reacting **14** with acid chloride **10a** in 42% yield after column chromatography using the same conditions as for the monotriazines. For the synthesis of bistriazine **6b**, alkyne **15** was prepared according to literature procedures and esterified with alcohol **16** in standard conditions.[40] Iodotriazine **19** was synthesised by a condensation between phenylbiguanide **9** and methyl 3-iodobenzoate (**18**). A Sonogashira coupling between alkyne **17** and iodide
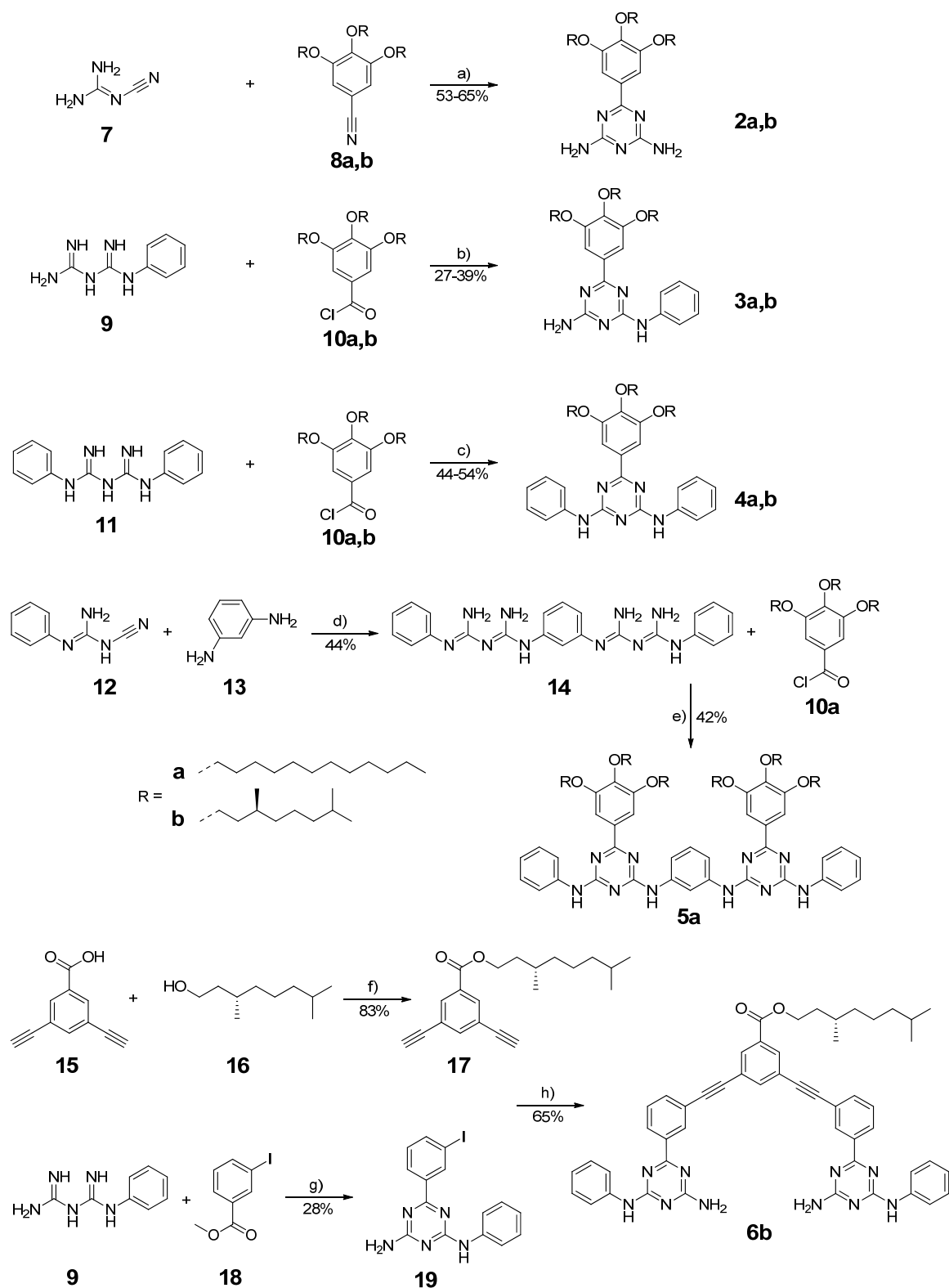
Scheme 3.1. Synthesis of monovalent triazines **2-4** and divalent triazines **5a** and **6b**. Reagents and conditions: a) Zn(OAc)$_2$, isopropanol, 90 °C; b) Et$_3$N, DMA, CHCl$_3$, 0 °C to 70 °C; c) Et$_3$N, DMA, CHCl$_3$, 0 °C to 70 °C; d) 1 M HCl, ethanol, 80 °C; e) Et$_3$N, DMA, CHCl$_3$, 0 °C to 70 °C; f) EDC, DMAP, CHCl$_3$, RT; g) NaOMe, methoxyethanol, 125 °C; h) ACN, THF, toluene, allylpalladium(II) chloride dimer, tri-*tert*-butylphosphine, DABCO, RT.

19 yielded chiral bistriazine **6b** in 65% yield. All the triazine end-products were purified by column chromatography and fully characterised using MALDI-ToF spectrometry and NMR spectroscopy.

3.3 Self-assembly of monovalent triazines with perylene bisimide

In apolar organic solvents, the formation of perylene triazine heteroaggregates is expected to take place by a combination of complementary hydrogen bonding and aggregation by π-stacking. To separately evaluate the strength of the threefold hydrogen bond formed between PBI **1a** and the monovalent triazines **2a**, **3a** and **4a**, respectively, NMR titrations were performed in deuterated chloroform, a solvent wherein aggregation by π-stacking is limited and only hydrogen bond driven dimerisation takes place. Triazine is added incrementally to a solution of PBI **1a**, to study the shift of the perylene N-H proton upon hydrogen bonding. Figure 3.4 shows the shift of the perylene N-H proton as a function of increasing amount of triazines **2a**, **3a** and **4a**, respectively. A gradual downfield shift of the perylene N-H proton is observed, indicating the formation of perylene-triazine complexes by hydrogen bonding. By fitting the data to a one-to-one binding model, the association constants can be extracted. For triazines **2a**, **3a** and **4a**, binding constants of K_a = 592 M^{-1}, 312 M^{-1} and 280 M^{-1} in CDCl$_3$ are obtained, respectively. Interestingly, the complementary hydrogen bonding becomes slightly weaker when phenyl substituents are introduced
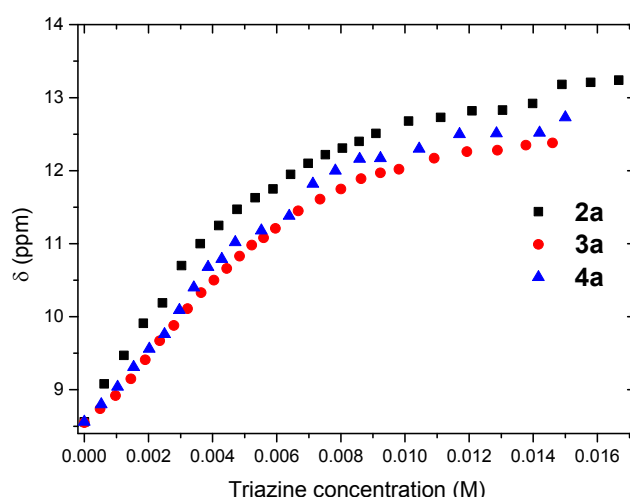
Figure 3.4. Chemical shift of the N-H proton of **1a** in ^{1}H-NMR spectroscopy as a function of concentration of **2a**, **3a** and **4a**. (c_{1a} = 5×10^{-3} M, CDCl$_3$, T = 20 °C).

on the triazine NH_2-positions, which contrasts the higher acidity of the N-H protons that bear phenyl groups. The binding constant values indicate that the specific triazine design does not greatly influence the strength of the threefold hydrogen bond as they are of the same magnitude. Remarkably, for triazines **3a** and **4a**, a slight upfield shift is observed for the aromatic protons of both the perylene and triazine as well as broadening of the aromatic perylene signals. These observations indicate that these perylene-triazine complexes tend to aggregate by π-stacking in $CDCl_3$ at c = $5×10^{-3}$ M. No such observations are made for triazine **2a**.

Next, we have investigated the heteroaggregation of perylene **1a** with monovalent triazines **2-4** in a solvent where π-stacking interactions are prominent. As described in Chapter 2, **1a** in methylcyclohexane (MCH) self-assembles into relatively short stacks of hydrogen-bonded dimers and the aggregation process can be conveniently monitored by UV–Vis and FT-IR spectroscopy. Therefore, we carried out titrations of triazine molecules **2-4** into MCH solutions of PBI **1a** (c = $2×10^{-5}$ M) and monitored the changes in the perylene absorption spectrum as a function of triazine equivalents. It should be noted that in the spectral region of interest (λ = 300 to 650 nm) the PBI absorption is observed exclusively. Typical examples of UV–Vis and CD spectra for a titration of **4b** into PBI **1a** are shown in Figure 3.5. By increasing triazine content, the perylene absorption bands shift to the red and change shape significantly, suggesting the formation of heteroaggregates. The shape and position of the PBI absorption bands, with respect to the molecularly dissolved state, indicate the formation of J-aggregates, probably caused by offset π-stacking of the perylene chromophores in the heteroaggregate. Concomitantly, as triazine **4b** is decorated with side-chains containing stereogenic (*S*-configuration) centres, a Cotton effect ($λ_{max}$ = 570 nm, Δε = 13.6 L×mol^{-1}×cm^{-1}, g_{value} = $8.25×10^{-4}$) is observed with CD spectroscopy, indicating transduction of chiral information from the triazine to the perylene and the formation of chiral aggregates. The presence of a Cotton effect suggests a chiral orientation of adjacent perylenes in the heteroaggregate. The size (Δε and g_{value}) and shape of the observed Cotton effect are comparable to aggregates of structurally similar PBIs studied by the group of Würthner.[5,25] Combined, the observations suggest that perylene-triazine heterodimers form aggregates by offset π-stacking with a rotational (helical) displacement.

Similar observations with regard to UV–Vis spectral changes are made when titrations are performed with triazines **3a** and **3b**, though surprisingly no Cotton effect is observed in the case of chiral triazine **3b** (Figure 3.5 C). This suggests that heteroaggregates of **3** with **1a** also form J-type perylene aggregates albeit without transduction of chiral information in the case of triazine **3b**. This may be related to the non-symmetrical nature of triazine **3,** which in the case of π-stacking of **3:1** heterodimers can adopt multiple spatial configurations, resulting in a more disordered aggregate. Interestingly, n the case of triazine **2a**, we cannot observe the formation of perylene-triazine heteroaggregates in MCH solution, as the perylene absorption spectrum remained similar to the homoaggregated state of **1a**. Diaminotriazine **2a** might form hydrogen-bonded homoaggregates such as rosettes in methylcyclohexane solution instead of forming perylene-triazine heteroaggregates, as self-assembly of diaminotriazines into various architectures such as rosettes and tapes has been reported in both the solid state and in solution.[41-44]
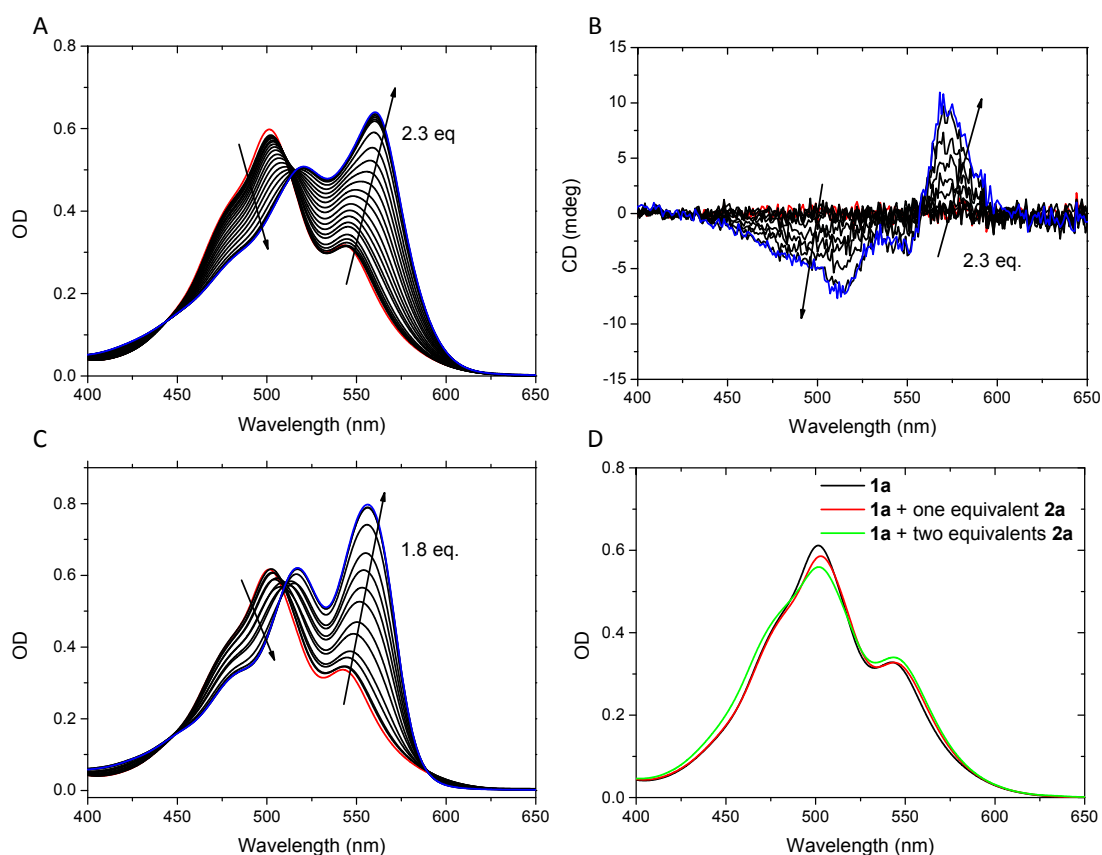
Figure 3.5. UV–Vis spectra of a titration of triazine **4b** into perylene **1a** (A). CD spectra of a titration of triazine **4b** into perylene **1a** (B). UV–Vis spectra of a titration of triazine **3a** into perylene **1a** (C). UV–Vis spectra of **1a** with and without various equivalents of triazine **2a** (D) (c_{1a} = 2×10^{-5} M, l = 1 cm, T = 20 °C, MCH).

The phenyl substituents on the amines of triazines **3** and **4** preclude the formation of hydrogen-bonded networks such as rosettes, thereby probably favouring the formation of heteroaggregates with perylene **1a**. In the titrations with triazines **3** and **4**, more than one equivalent of triazine is required to achieve saturation in the UV–Vis spectral changes and thus convert all perylene homoaggregates to perylene-triazine heteroaggregates. We suggest this is representative of the competition between various self-assembly pathways to homo- and heteroaggregates present in the system, schematically represented in Figure 3.6.
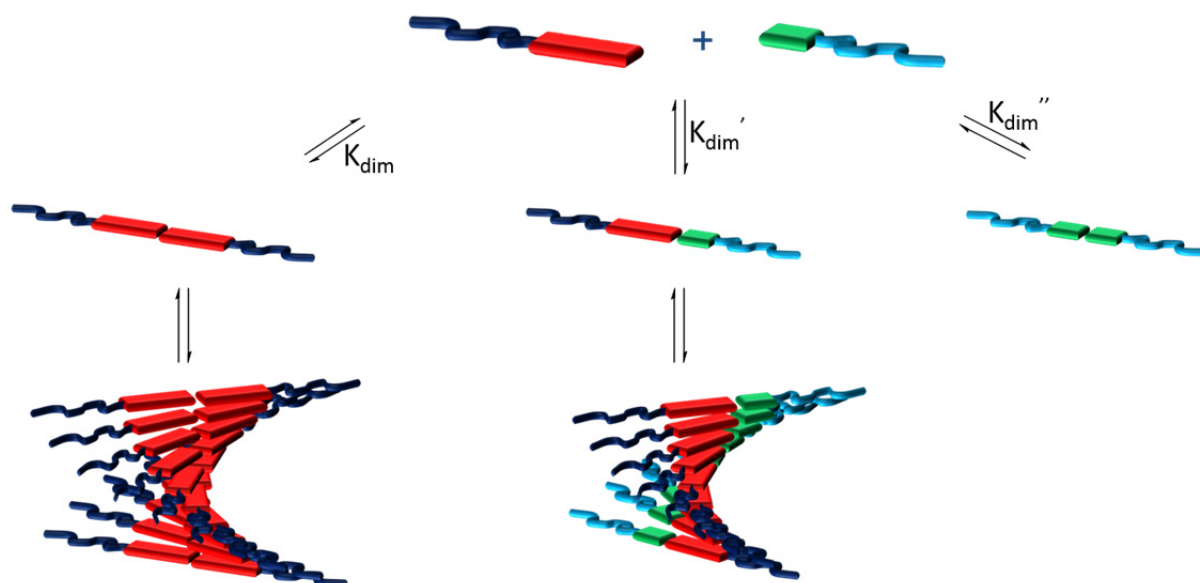
Figure 3.6. Schematic representation of the self-assembly pathways of a mixed perylene bisimide-triazine system.

To gain insight into the self-assembly mechanisms of the heteroaggregates, the resultant solutions of the titrations (c_{1a} = 2×10^{-5} M, two equivalents of triazine) were subjected to variable temperature measurements. We probe the absorbance at the absorption maximum of the heteroaggregates (λ = 556 nm) and the CD at the maximal Cotton effect (λ = 570 nm) as a function of temperature (Figure 3.7). Surprisingly, two transitions are observed in the temperature dependent assembly curve, instead of solely the perylene-triazine heteroaggregation from the molecularly dissolved state. The first transition in the UV–Vis trace (λ = 556 nm) has a critical temperature of T = 85 °C and appears to be a cooperative process. For both **1a:3a** and **1a:4b** mixtures a second transition is observed around T = 45 °C, concomitant with the appearance of a Cotton effect in the CD trace for the mixture **1a:4b**. Temperature dependent measurements on solutions of perylene **1a** in the absence of

any triazine show a remarkable resemblance to the first part of the cooling curves of the heteromixtures. Furthermore when full UV–Vis spectra are recorded at various temperatures between T = 45 and 85 °C, they are similar for solutions with and without triazine, suggesting the preferential formation of pure homoaggregates of PBI **1a** in this temperature regime. Only when the solutions are cooled below T = 45 °C, a transition to perylene-triazine heteroaggregates is observed.
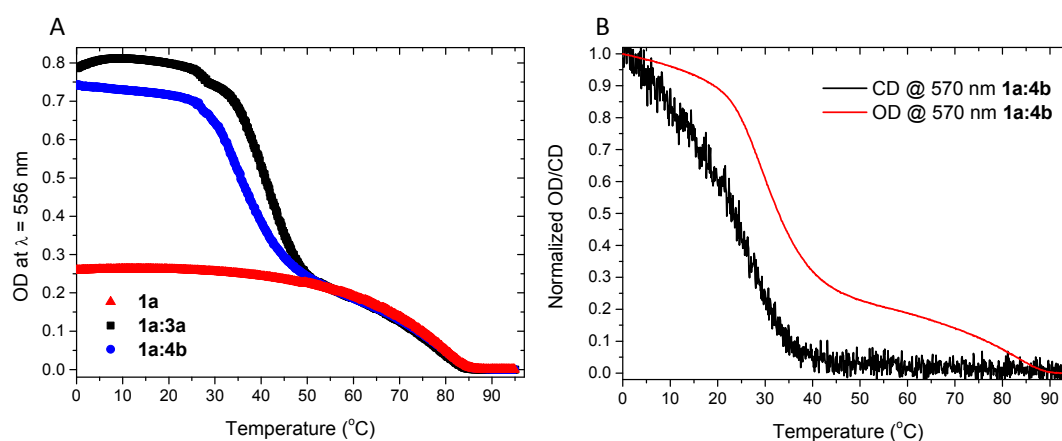
Figure 3.7. UV–Vis cooling curves of solutions of **1a** (▲), **1a** with triazine **3a** (■) and PBI **1a** with triazine **4b** (●) (MCH, c_{1a} = 2×10^{-5} M, $c_{3a\ or\ 4b}$ = 4×10^{-5} M, λ = 556 nm) (A). UV–Vis and CD cooling curves of a solution of PBI **1a** and triazine **4b** (MCH, c_{1a} = 2×10^{-5} M, c_{4b} = 4×10^{-5} M, λ = 570 nm) (B).

These experiments show that the self-assembly of perylene-triazine heteroaggregates from the molecularly dissolved state proceeds via a complex pathway involving multiple aggregated states. At elevated temperatures in MCH solution, both perylene and triazine are in the molecularly dissolved state. After lowering the temperature, **1a** first forms homoaggregates consisting of short stacks of hydrogen-bonded dimers. Upon further temperature decrease, the perylene-triazine heteroaggregates become more stable than the perylene homoaggregates, and heteroaggregates are formed, presumably via depolymerisation of perylene homoaggregates to free **1a** and concomitant heteroaggregation with free triazine. To obtain further insight into the heteroaggregation of PBI **1a** with triazines **2-4**, we performed FT-IR spectroscopy on the heteroaggregates in MCH solution (Figure 3.8). The position of the carbonyl stretching vibration of PBI **1a** is very sensitive to changes in the hydrogen bonds that it is participating in. The measurements were performed at a concentration of c_{1a} = 5×10^{-4} M to cope with the relatively low intensity of
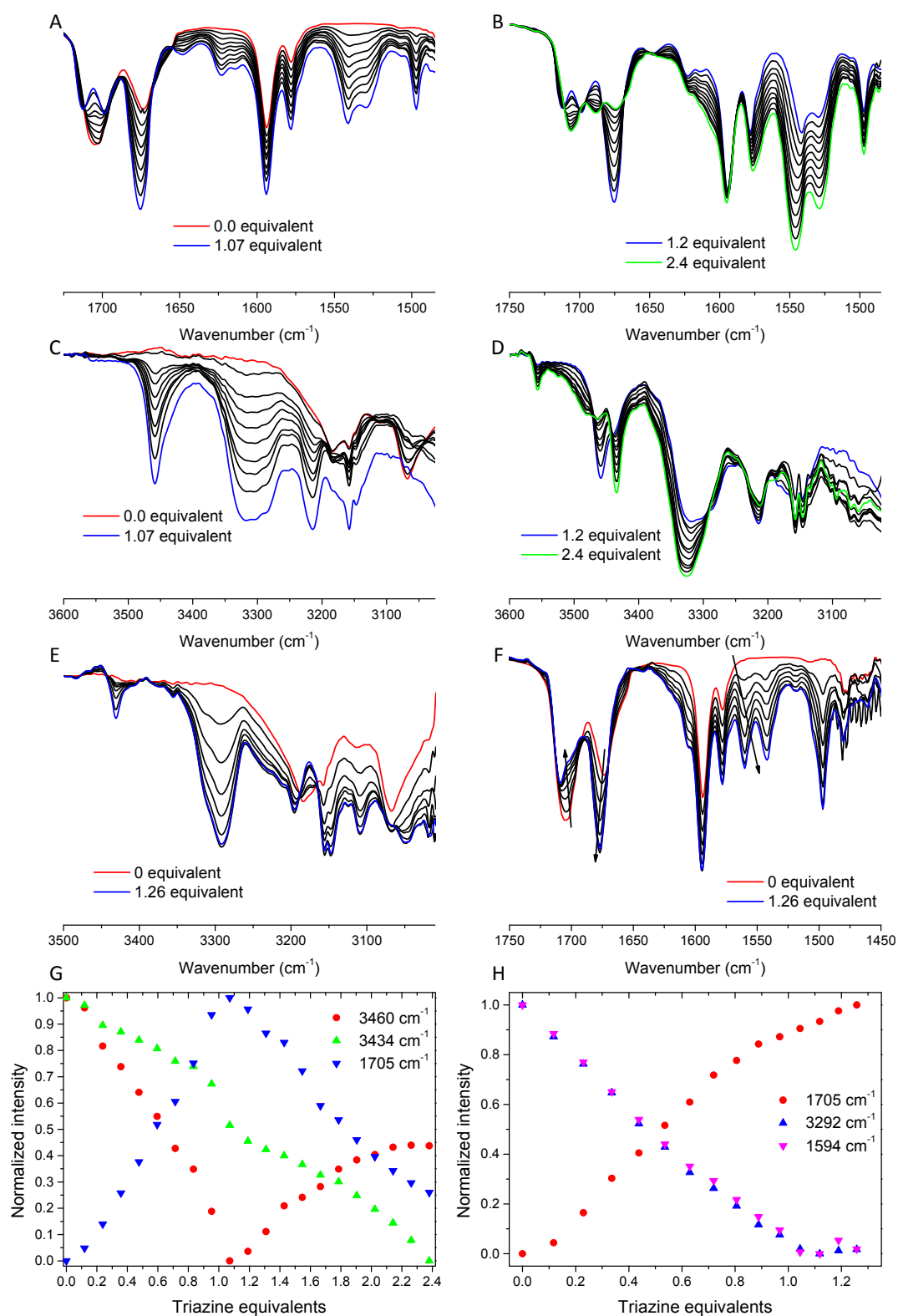
Figure 3.8. FT-IR spectra of a titration of triazine **3a** to a solution of PBI **1a** in MCH (A-D) (c_{1a} = 5×10^{-4} M). FT-IR spectra of a titration of triazine **4a** to a solution of PBI **1a** in MCH (E-F) (c_{1a} = 5×10^{-4} M). Normalised intensity of FT-IR signals of PBI **1a** as a function of added triazine **3a** (G). Normalised intensity of FT-IR signals of PBI **1a** as a function of added triazine **4a** (H).

49

infrared absorption bands with respect to optical transitions in the UV–Vis regime. The results of the titrations of **3a** and **4a** into a solution of **1a** are shown in Figure 3.8. Clear changes are observed in the carbonyl vibration of **1a** upon addition of **4a**, indicating the formation of perylene-triazine heteroaggregates through hydrogen bonds (Figure 3.7 8). The changes level off after the addition of one equivalent of **4a**, suggesting the formation of heteroaggregates with a 1:1 stoichiometry. The titration of **2a** into **1a** did not result in changes in the carbonyl stretching vibration of the perylene, again suggesting the formation of homoaggregates, similar to the UV–Vis experiments, while the titration of **3a** into **1a** showed markedly different behaviour. Upon the gradual addition of one equivalent **3a** to perylene **1a**, we observe changes in the perylene carbonyl region, which indicate the formation of hydrogen-bonded perylene-triazine dimers that subsequently stack to form heteroaggregates. Intriguengly, instead of saturating at one equivalent of **3a**, upon further addition of **3a** a second process is observed, in which again the signals corresponding to carbonyl vibration of **1a** shift significantly. These results seem to suggest further interaction of excess **3a** with heteroaggregates of **1a:3a**.

We have repeated the UV–Vis titrations described above at the same concentration as the FT-IR titrations to gain more insight (Figure 3.9 A and B). Remarkably, also here two different processes are observed for triazine **3a**. In the first process (zero to one equivalent) the formation of heteroaggregates is observed, as the spectra are clearly similar to spectra observed in the initial titrations with triazines **3** and **4**. Upon addition of more than one equivalent of triazine, the UV–Vis spectra gradually convert to a different shape, indicating that the orientation of adjacent perylene bisimides in the aggregate changes and again suggesting the interaction of excess triazine **3a** with the heteroaggregates. Similar observations have not been made for triazines **4a,b**, suggesting that in this case heteroaggregates are exclusively formed by one-to-one hydrogen bonding and subsequent π-stacking of these heterodimers.
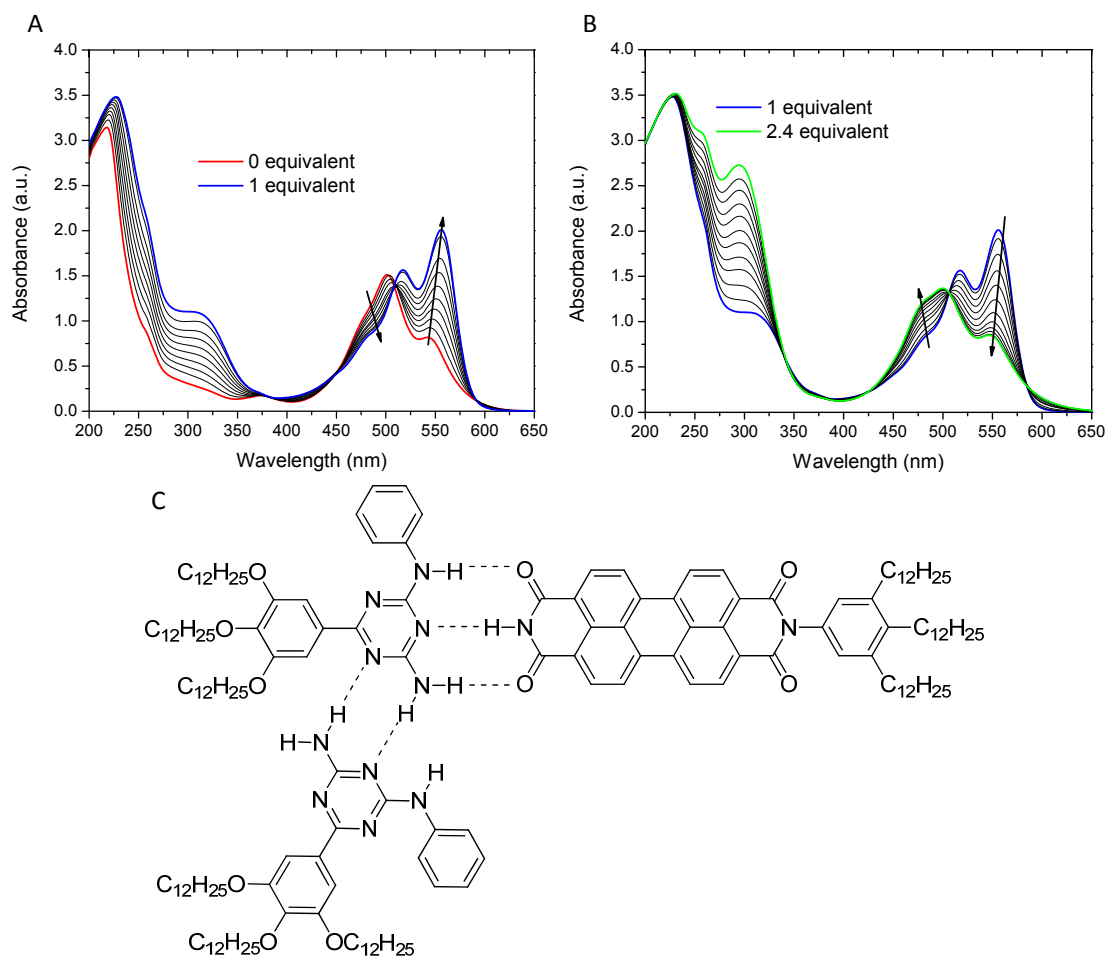
Figure 3.9. UV–Vis titration of triazine **3a** into **1a** (A,B) (MCH, c_{1a} = 5×10^{-4} M, l = 1 mm, T = 20 °C). Hypothetical heterotrimer structure by complexation of excess triazine **3a** to a heterodimer **1a:3a** by additional twofold hydrogen-bonding (C).

Upon inspection of the molecular structure of the **1a:3a** heterodimer, it is clear that the unsubstituted side of the triazine presents a twofold hydrogen-bonding site. Excess triazine that does not take part in threefold hydrogen-bonding to **1a** can instead participate in twofold hydrogen bonding to the **1a:3a** heterodimer in a similar pattern as reported in the homocomplexation of unsubstituted diaminotriazines (Figure 3.9 C).[41-44] By introducing one or two phenyl substituents on the amino groups in triazine **2**, the additional twofold hydrogen-bonding sites on the diaminotriazines are blocked. Blocking of these twofold hydrogen-bonding sites results in markedly different heteroaggregation behaviour with molecules bearing complementary hydrogen-bonding motifs.

Having established the formation of π-stacked heterocomplexes **1a:3** and **1a:4**, we revisit the remarkable behaviour of PBI **1a** described in Chapter 2, which shows cooperative assembly curves yet forms aggregates of small size. Small angle X-ray scattering (SAXS) measurements were performed on solutions of **1a:3a** and **1a:4a** in MCH (c = 1×10^{-3} M) (Figure 3.10). We have used a Guinier approximation and cylindrical form factor analysis to obtain values of $R_g \approx 1.2$ and 2.0 for **1a:3a** and **1a:4a** respectively (Table 3.1). Interestingly, the results suggest that heteroaggregates **1a:3a** and **1a:4a** similarly do not form elongated one-dimensional aggregates but rather form aggregates of small size. Likely, the constraints that limit aggregate growth in PBI **1a** are similarly present in heteroaggregates of **1a** with triazines **3a** and **4a**.
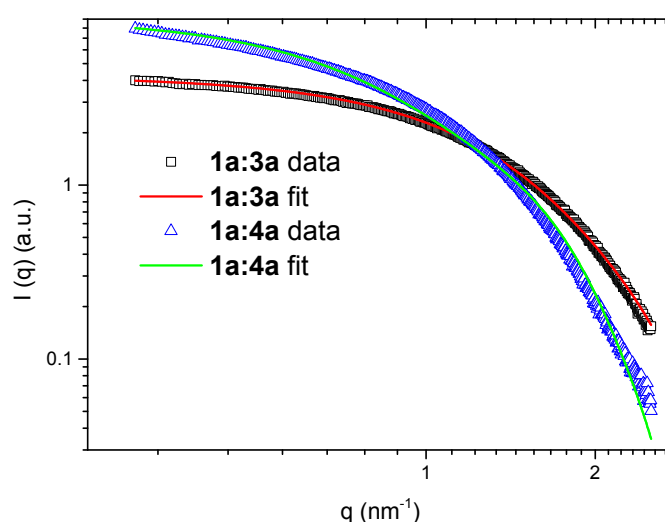
Figure 3.10. SAXS data curves of **1a:3a** and **1a:4a** and fits using cylindrical form factor (c = 1×10^{-3} M, MCH)

Table 3.1. Overview of the SAXS results of heteroaggregates **1a:3a** and **1a:4a**.

Sample	R_g (nm)[a]	L (nm)[b]	N_p[b]	R_{cs} (nm)[b]	$L/2R_{cs}$[b]	R_g (nm)[b]
1a:3a	1.38±0.01	3.9	22	1.1	1.7	1.4
1a:4a	1.88±0.38	6.7	38	1.4	2.4	2.2

Radius of gyration, R_g, cylinder length, L, cylinder cross sectional radius, R_{cs}, and the number of perylene bisimide dimers in a stack N_P. Obtained from a [a]Guinier approximation and [b]modelling with a form factor for rigid cylinders[45,46]

So far we have shown that monovalent triazines **2-4** form heterodimers by threefold complementary hydrogen bonding with PBI **1a**, and that these dimers

subsequently form π-stacked aggregates in dilute MCH solution. The formation of these stacked heterostructures is shown to compete with the formation of perylene and triazine homoaggregates. Blocking of the additional twofold hydrogen-bonding interaction sites on the triazine proves effective in biasing the system towards the facile formation of π-stacked hydrogen-bonded heterodimers. However, also in this case, the formation of heterostructures is found to proceed via the formation of perylene π-stacked homodimers followed by de-assembly of these homoaggregates and the subsequent assembly of hydrogen-bonded heterocomplexes. This may be the result of stronger π-stacking interactions for the perylene dimers with respect to the perylene-triazine dimers as the perylene dimers have a larger flat aromatic surface. In an attempt to further favour the formation of heteroaggregates over homoaggregates we switch to the use of divalent triazines. We hypothesise that hydrogen-bonded structures of PBI **1a** with divalent triazines will display a larger aromatic surface available for π-stacking interactions and thus stabilise the formation of stacked heteroaggregates over homoaggregates.

3.4. Self-assembly of divalent triazines with perylene bisimide

Having described the self-assembly of perylene **1a** with a library of complementary monovalent triazines, we proceed to investigate the heteroaggregation of **1a** with more complex, divalent triazine molecules **5a** and **6b**. For bistriazine **5a** we monitor the assembly process by UV–Vis (Figure 3.11 A and B) and FT-IR (Figure 3.11 C and D) titrations in MCH solution. Upon the gradual addition of bistriazine **5a** to **1a** in MCH (c_{1a} = 5×10^{-4} M) two transitions are observed with both UV–Vis and FT-IR spectroscopy. The first transition occurs between the addition of 0 and 0.5 equivalents of triazine while the second transition occurs between the addition of 0.5 and 1 equivalents, reflecting the divalent nature of triazine **5a**. In the first part (0 to 0.5 eq.) of the titration, addition of **5a** to a solution of **1a** results in the formation of **1a$_2$:5a** trimer heterostructures which are stacked as is evident from the absorption spectra. The addition of more triazine (0.5 to 1 eq.) results in the dissociation of the trimer structures in favour of the formation of **1a:5a** dimer aggregates. Addition of excess of **5a** above one equivalent does not result (as expected) in further changes in UV–Vis and FT-IR spectra. To evaluate the self-assembly mechanism and the stability of the **1a$_2$:5a** heteroaggregates, a cooling curve was recorded with UV–Vis spectroscopy at c_{1a} = 1×10^{-5} M and λ = 565 nm.
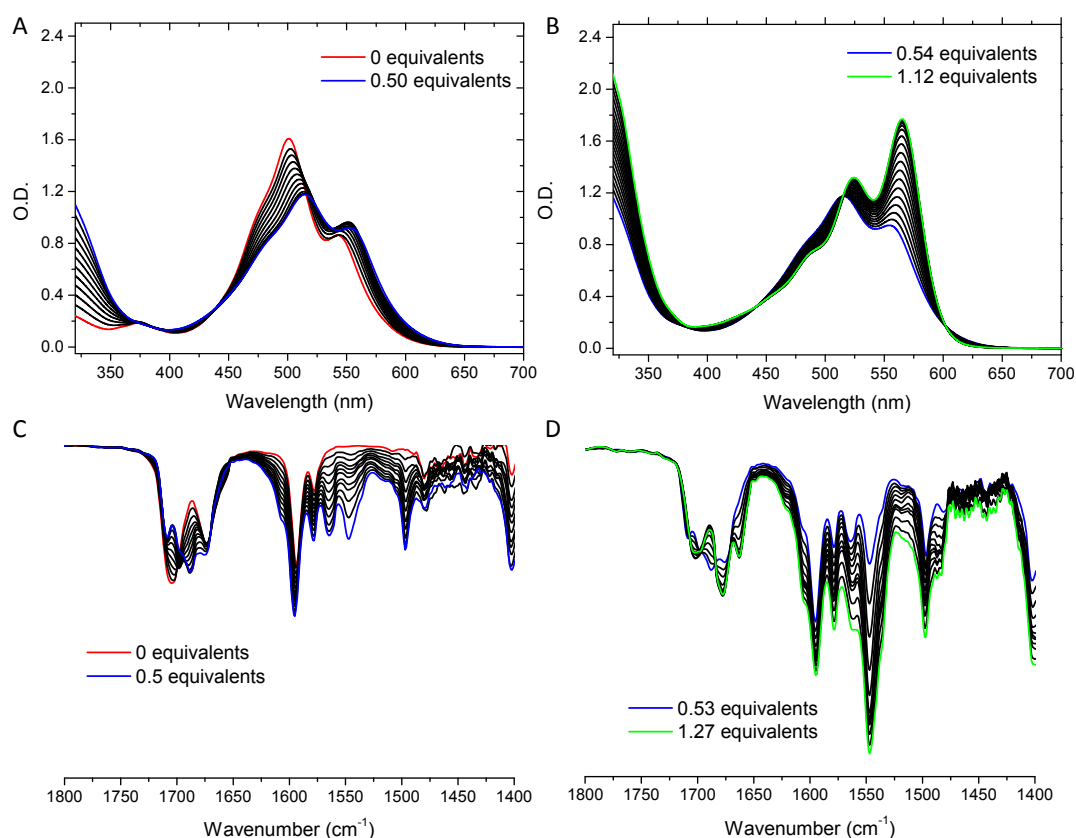
Figure 3.11. UV–Vis (A,B) and FT-IR (C,D) titrations of triazine **5a** into perylene **1a** (MCH, c_{1a} = 5×10^{-4} M, l = 1 mm).

Gratifyingly, a non-sigmoidal curve with a single critical temperature is observed, suggesting a cooperative self-assembly process for the **1a$_2$:5a** heterostructures. The **1a$_2$:5a** heteroaggregates are more stable than the perylene **1a** homoaggregates as evidenced by the higher critical temperature T_e measured in the cooling curves of **1a$_2$:5a** heteroaggregates and **1a** homoaggregates (Figure 3.12). Therefore, unlike in the case of monotriazines **3** and **4** where perylene homoaggregation precedes heteroaggregation and the two aggregation pathways are in competition with each other, the aggregate formation pathway of **1a$_2$:5a** proceeds directly from the free monomers in solution to the heteroaggregate as schematically depicted in Figure 3.13 B.
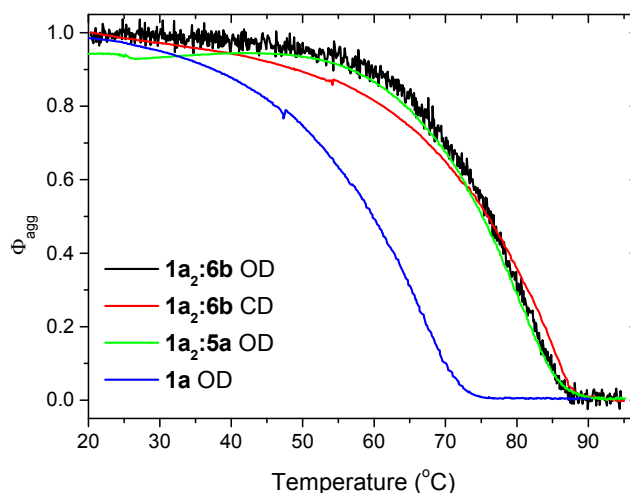
Figure 3.12. UV–Vis cooling curves for heterocomplexes **1a$_2$:5a** (λ = 565 nm), **1a$_2$:6b** (λ = 568 nm, including CD,) and **1a** (λ = 542 nm) (MCH, c_{1a} = 1×10^{-5} M, l = 1 cm, rate = 0.2 °C/min).

In the case of divalent triazine **6b** no titrations can be performed owing to the limited solubility of **6b** in the methylcyclohexane solvent. Instead, solubility of **6b** can be enhanced in the presence of triazine **1a** and thus a solution containing **1a** (c = 1×10^{-5} M) and **6b** (c = 5×10^{-6} M, 0.5 equivalent) was prepared. The UV–Vis spectrum of the mixture is highly similar to the spectra observed for **1a:3** and **1a:4** heteroaggregates and therefore indicative of the formation of **1a$_2$:6b** heteroaggregates (Figure 3.14 A). Remarkably, a Cotton effect (λ_{max} = 568 nm, $\Delta\varepsilon$ = - 45.5 L×mol^{-1}×cm^{-1}, g_{value} = 1.15×10^{-2}) in the absorption region of the PBI chromophore is observed with CD spectroscopy, suggesting a helical arrangement of the PBI chromophores in the **1a$_2$:6b** heteroaggregate (Figure 3.14 B). This observation indicates the transduction of chiral information from the single chiral side-chain on **6b** to the PBI chromophores in the aggregate, which is remarkable considering the remoteness of the perylene chromophores to the single stereogenic centre on **6b**. The Cotton effect for **1a$_2$:6b** is mirror image to the one observed for **1a:4b**, indicating a similar arrangement but of opposite helicity of the PBIs in both aggregates. Very remarkable is the relatively large value of $\Delta\varepsilon$ and the g_{value} of **1a$_2$:6b** in comparison to **1a:4b** as **1a$_2$:6b** has only a single chiroptical centre in comparison to three chiroptical centres in **1a:4b**. Apparently, aggregates of **1a$_2$:6b** possess a higher internal helical order than aggregates of **1a:4b**.

A

1a₂:5a

1a₂:6b

R =

B

C
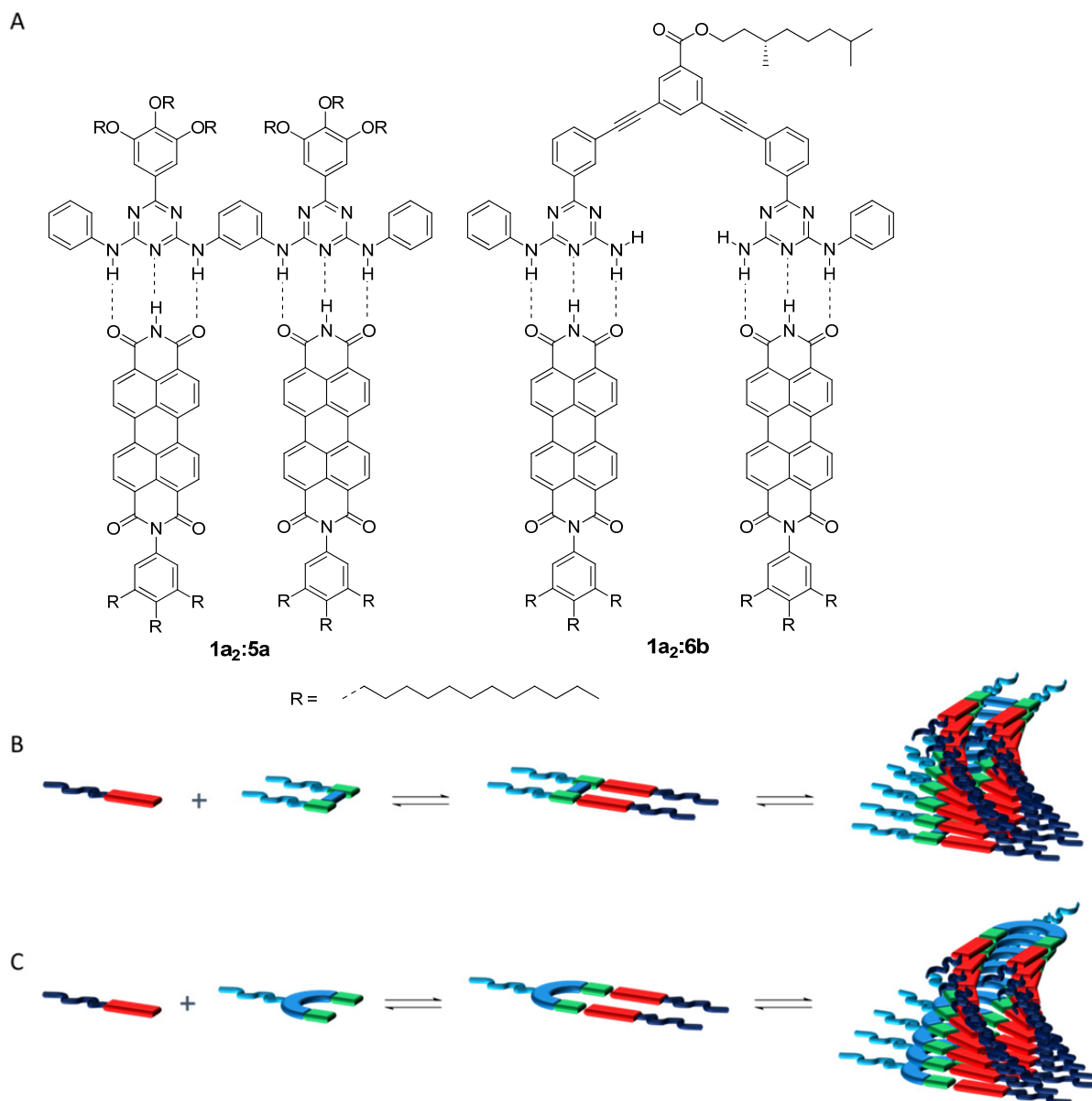
Figure 3.13. Molecular structures of hydrogen-bonded trimers **1a₂:5a** and **1a₂:6b** (A). Schematic representation of the single self-assembly pathways for the formation of **1a₂:5a** (B) and **1a₂:6b** (C) heteroaggregates in dilute solutions of MCH.
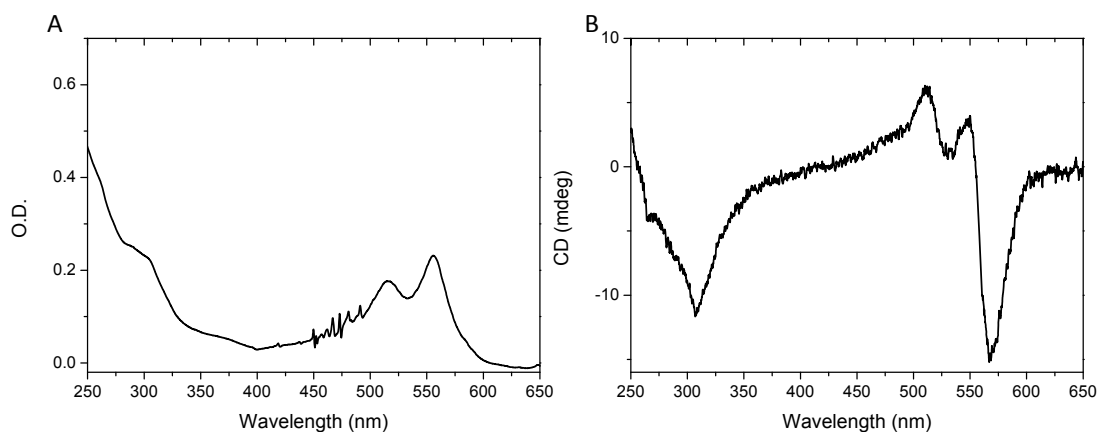
Figure 3.14. UV–Vis (A) and CD (B) spectra of **1a₂:6b** (MCH, c_{1a} = 1×10⁻⁵ M, l = 1 cm).

We probe the self-assembly mechanism of the heteroaggregates with variable temperature UV–Vis and CD spectroscopy (c_{1a} = 1×10⁻⁵ M, λ = 570 nm). Similar as for the **1a₂:5a** heteroaggregates, a non-sigmoidal curve with a single critical temperature is observed in both the UV–Vis and CD signals, indicating a cooperative self-assembly mechanism for the **1a₂:6b** heterostructures (Figure 3.12). Again, gratifyingly, the observed critical temperature for the heteroaggregates is higher than the critical temperature of the self-assembly process of PBI **1a** itself at the same concentration, suggesting a higher stability of the heteroaggregates compared to the perylene homoaggregates. The self-assembly of the **1a₂:6b** heterostructures therefore proceeds directly from the individual monomers, without interfering competition of the other self-assembly pathways as schematically depicted in Figure 3.13 C.

3.5. Conclusion

In conclusion, we have synthesised a library of triazine molecules varying in molecular architecture and studied their behaviour in the heteroaggregation by hydrogen bonding with a mono-arylated perylene bisimide to be able to understand and control the pathways that govern the homo- or heteroaggregation pathways of these molecular components. In a series of monotriazines we selectively blocked additional hydrogen-bonding interaction sites by the introduction of zero, one, or two phenyl substituents. Remarkably, the strength of the threefold hydrogen bond between perylene and triazine was only slightly affected by the phenyl substituents as evaluated by ^{1}H-NMR spectroscopy in chloroform solution. The formation of hydrogen bonded stacks is however hugely affected by the phenyl substituents on

the triazines. Blocking of the additional twofold hydrogen bonding sites on the triazines resulted in the formation of supramolecular perylene-triazine stacks while triazines with unblocked twofold hydrogen bonding sites formed either more complex aggregates or homoaggregates as evidenced by UV–Vis and FT-IR spectroscopy. However, pathway complexity in self-assembly was also observed in the formation of the desired hydrogen bonded stacks, as perylene homoaggregation was shown to precede perylene-triazine heteroaggregation by temperature dependent spectroscopy. Herein, the formation of perylene homoaggregates might buffer and therefore slow down the formation of supramolecular heteroaggregates. Measurements on the self-assembly kinetics of perylene-triazine heteroaggregates in the presence of perylene homoaggregates might reveal additional insights into the observed pathway complexity. Remarkably, in relation to the small aggregates observed for perylene homoaggregates in Chapter 2, perylene-triazine heteroaggregates were also found to be of small size instead of elongated one-dimensional stacks by SAXS measurements.

To further favour the formation of supramolecular heteroaggregates over homoaggregates, we investigated the use of divalent triazines to increase the aromatic π-stacking surface of the hydrogen-bonded heterocomplexes. Both divalent triazines were shown to form supramolecular stacks by hydrogen bonding with perylene and subsequent π-stacking of hydrogen-bonded trimers. Gratifyingly, temperature dependent UV–Vis spectroscopy proved these heteroaggregates to be more stable than perylene homoaggregates or heteroaggregates of perylene with monovalent triazines. No pathway complexity (competition with perylene homoaggregation) was observed in the formation of heteroaggregates with divalent triazines. In the molecular design of supramolecular stacks by hydrogen bonding and subsequent π-stacking, pathway complexity in self-assembly plays a dominant role in determining the outcome of a self-assembly process. The introduction of substituents to block undesired additional interactions can be used to steer aggregation pathways towards the desired heteroaggregate. Furthermore, multivalent architectures can be used to increase the π-surface available for π-stacking interactions and thereby further stabilise the formation of supramolecular heteroaggregates over homoaggregates of the individual components. Additionally, we showed the induction of supramolecular chirality in the PBI chromophore stacks from chiral

triazines. The observed Cotton effect in the PBI chromophores is similar in size and shape as observed for chiral PBIs of structural similarity, but is very remarkable as it is induced by a single stereogenic centre on a remote position in the triazine structure.

3.6. Experimental section

Instrumentation, materials and methods
Unless specifically mentioned, reagents and solvents were obtained from commercial suppliers and used without further purification. All solvents were of AR quality. Deuterated chloroform for NMR analyses was provided with TMS as the 0 ppm reference. The methylcyclohexane used in all spectroscopic experiments was of spectroscopic grade. Column chromatography was performed on a Biotage Isolera One using SNAP KP-SNAP columns and solvent gradients. ^{1}H-NMR and ^{13}C-NMR spectra were recorded on a Varian Mercury Vx 400 MHz instrument (100 MHz for ^{13}C) and all chemical shifts are reported in parts per million relative to tetramethylsilane (TMS). MALDI-ToF MS analyses were performed in reflector mode on a PerSeptive Biosystems Voyager-DE Pro using α-cyano-4-hydroxycinnamic acid (CHCA) and 2-[(2E)-3-(4-tert-butylphenyl)-2-methylprop-2-enylidene]malononitrile (DCTB) as matrices. Ultraviolet-visible (UV–Vis) absorbance spectra were recorded on a Jasco V-650 UV–Vis spectrometer with a Jasco ETCR-762 temperature controller. Circular dichroism (CD) spectra were recorded on a JASCO J-815 CD spectrometer with a JASCO PTC-348 temperature controller. Solid state infrared (IR) spectra were recorded on a Perkin Elmer Spectrum One spectrometer equipped with a ATR universal sampler accessory and in dilute solution using 1 mm NaCl cells.

The small-angle X-ray scattering (SAXS) experiments were performed by Ilja Voets at the cSAXS beamline at the Swiss Light Source (SLS) at the Paul Scherrer Institute. The samples were filled in 1 mm diameter quartz capillaries with a wall thickness of 0.01 mm (Hilgenberg) and maintained at a temperature of 20±1°C. An X-ray energy of 12.4 keV corresponding to a wavelength, λ, of 0.1 nm and one sample-to-detector distance of 2.17 m were used, to cover a range of 0.3 nm^{-1} ≤ q ≤ 2.5 nm^{-1} with the magnitude of the scattering wave vector, q, given by q = $(4\pi/\lambda)\times\sin(\theta/2)$ and the scattering angle, θ. The scattering patterns were recorded on a PSI-developed Pilatus 2 M detector operating in single-photon counting mode. The 2D images were azimuthally integrated and corrected for background scattering according to

established procedures provided by the PSI. The *q*-scale was calibrated by a measurement of silver behenate. The SASfit software package was used for data analysis with a form factor for monodisperse rigid cylinders.[47] The monomer concentration of 1 mM was low enough to safely neglect interactions between the supramolecular self-assemblies, such that the structure factor *S*(q) ~ 1.

The synthesis of triazines **2-5** was performed in close collaboration with Bas de Waal. The synthesis of triazine **6b** was performed by Dr. Matthew Carnes and Dr. Feng Wang. Acid chlorides **10a,b** were synthesised according to reference 37 and 38. Diphenylbiguanide was synthesised according to reference 39. Compound **15** was synthesised according to reference 40.

NMR titrations were fitted according to a one-to-one binding model (equation 3.1) using the non-linear curve fitting procedure included in the Origin 9 software package.[48] $[A]_0$ is the starting PBI **1a** concentration, Δ_δ is the observed chemical shift difference and $[B]$ is the triazine concentration. The fitted parameters are $\Delta_{\delta,AB}$ and $1/K_a$

$$\Delta_\delta = \frac{\Delta_{\delta,AB}}{[A]_0} \cdot \frac{1}{2} \cdot \left(([A]_0 \cdot [B] \cdot \frac{1}{K_a}) - \sqrt{\left(\left([A]_0 + [B] + \frac{1}{K_a} \right) - 4 \cdot [A]_0 \cdot [B] \right)} \right) \qquad \textbf{Equation 3.1}$$

Synthesis

N²-Phenyl-6-[3,4,5-tris(dodecyloxy)phenyl]-1,3,5-triazine-2,4-diamine (**3a**)

Monophenylbiguanide (173 mg, 0.98 mmol) and triethylamine (0.42 mL) were dissolved in dimethylacetamide (4 mL, 3.01 mmol). 3,4,5-Tris(dodecyloxy)benzoyl chloride (**10**) (693 mg, 1 mmol) was dissolved in chloroform (3 mL) and added dropwise to the biguanide solution. The mixture was stirred at room temperature for 20 hours and subsequently heated to 60 °C for 1 hour. The solvents were removed by vacuum evaporation and the crude product was dissolved in chloroform (100 mL). The organic phase was washed with 5% NaHCO$_3$ solution (2 x 80 mL), water (80 mL) and brine (80 mL) and subsequently dried over Na$_2$SO$_4$. The crude product was purified by column chromatography (0% to 10% ethyl acetate in chloroform over 10 column volumes) to give the product as a white solid. Yield: 218 mg. η = 27%. ^{1}H-NMR (400 MHz, CDCl$_3$) δ = 7.66 (d, J = 8.3 Hz, 2H, aromatic), 7.64 (s, 2H, aromatic), 7.35 (t, J

= 7.6 Hz, 2H, aromatic), 7.09 (t, J = 7.2 Hz, 1H aromatic), 7.04 (broad, 1H, N-H), 5.16 (broad, 2H, NH), 4.08 (t, J = 6.4 Hz, 4H, -OCH$_2$-), 4.03 (t, J = 6.4 Hz, 2H, -OCH$_2$-), 1.9-1.7 (m, 6H, alkyl), 1.6-1.2 (m, 54H, alkyl), 0.879 (t, J = 6.8 Hz, 9H, CH$_3$). ^{13}C-NMR (100 MHz, CDCl$_3$) δ = 171.2, 164.5, 152.9, 141.5, 138.4, 131.0, 128.7, 123.5, 120.6, 106.6, 71.6, 67.2, 39.3, 39.2, 37.5, 37.3, 37.3, 36.4, 29.9, 29.6, 28.0, 27.9, 24.7, 24.7, 22.7, 22.6, 22.6, 19.6, 19.5. FT-IR (ATR) (cm^{-1}): 3320.6, 3181.9, 2923, 2853, 603, 1774.2, 1530, 1496, 1468, 1419, 1368, 1317, 1227, 1116. MALDI-ToF MS (m/z) calc for C$_{51}$H$_{85}$N$_5$O$_3$ 815.67 found 816.47 (M+H)$^+$.

N^2-Phenyl-6-{3,4,5-tris[(S)-3,7-dimethyloctyloxy]phenyl}-1,3,5-triazine-2,4-diamine (**3b**)

Monophenylbiguanide (560 mg, 3.16 mmol) and triethylamine (1.4 mL, 10 mmol) were dissolved in dimethylacetamide (25 mL). 3,4,5-Tris[(*S*)-3,7-dimethyloctyloxy]benzoyl chloride (1.84 g, 3.02 mmol) was dissolved in chloroform (25 mL) and added dropwise to the biguanide solution. The mixture was stirred at room temperature for 18 hours and subsequently heated for one hour at 60 °C. The solvents were removed by vacuum evaporation. The residue was dissolved in chloroform (250 mL) and the solution washed with 1N NaOH (100 mL). The aqueous layer was extracted back with chloroform (50 mL). The combined organic layers were washed with water (100 mL) and brine (200 mL) and dried over Na$_2$SO$_4$. The suspension was filtered and the filtrate was concentrated in vacuo. The crude residue was purified by column chromatography (0% to 20% ethyl acetate in chloroform over 10 column volumes) to give the product as a colourless viscous oil. R$_f$ = 0.12 (10% ethyl acetate in chloroform). Yield = 860 mg. η = 38.6%. ^{1}H-NMR (400 MHz, CDCl$_3$) δ = 7.67 (d, 2H, aromatic), 7.65 (s, 2H, aromatic), 7.34 (t, J = 7.6 Hz, 2H, aromatic), 7.09 (t , J = 7.6 Hz, 1H, aromatic), 7.09 (b, 1H, N-H), 5.19 (b, 2H, NH$_2$), 4.2-4.0 (m, 6H, OCH$_2$), 2.0-0.7 (mm, 57H, alkyl). ^{13}C-NMR (100 MHz, CDCl$_3$) δ = 172.0, 167.5, 152.9, 141.3, 131.0, 106.5, 71.6, 67.3, 39.3, 39.2, 37.5, 37.3, 37.3, 36.4, 29.8, 29.6, 27.9, 24.7, 24.7, 22.7, 22.6, 22.5, 19.6, 19.5. FT-IR (ATR) (cm^{-1}): 3328.8, 3194.1, 2955, 2928.9, 2871.8, 1627.2, 1542, 1468, 1412, 1377, 1317, 1223.2, 1116. MALDI-ToF MS (m/z) calc for C$_{45}$H$_{73}$N$_5$O$_3$ 731.57 found 732.56 (M+H)$^+$ 754.54 (M+Na)$^+$.

N²,N⁴-Diphenyl-6-[3,4,5-tris(dodecyloxy)phenyl]-1,3,5-triazine-2,4-diamine (**4a**)

Diphenylbiguanide (288 mg, 1.14 mmol) and triethylamine (0.42 mL, 3 mmol) were dissolved in dimethylacetamide (12 mL). 3,4,5-Tris(dodecyloxy)benzoyl chloride (691 mg, 1.0 mmol) was dissolved in chloroform (7 mL) and added dropwise to the biguanide solution. The mixture was stirred at room temperature for 24 hours and heated afterwards at 50 °C for 1 hour. The solvents were removed by vacuum evaporation and the crude product was dissolved in chloroform (100 mL). The organic phase was washed with saturated $NaHCO_3$ solution (2 x 100 mL), water (100 mL) and brine (100 mL) and subsequently dried over Na_2SO_4. The suspension was filtered and the filtrate was concentrated in vacuo. The crude residue was purified by column chromatography (0% to 10% ethyl acetate in chloroform over 10 column volumes) to give the product as a white solid. R_f = 0.23 (2.5% EtOAc in $CHCl_3$). Yield = 450 mg. η = 44%. ^{1}H-NMR (400 MHz, $CDCl_3$) δ = 7.69 (s, 2H, aromatic), 7.68 (d, 4H, aromatic), 7.36 (t, J = 7.9 Hz, 4H, aromatic), 7.15 (broad, 2H, N-H), 7.12 (t, J = 7.12 Hz, 2H, aromatic), 4.10 (t, 4H, J = 6.5 Hz, OCH_2), 4.05 (t, J = 6.5 Hz, 2H, -OCH_2-), 1.9-1.7 (m, 6H), 1.6-1.1 (54H, alkyl), 0.88 (t, J = 6.7 Hz, 9H, CH_3). ^{13}C- NMR (100 MHz, $CDCl_3$) δ = 171.2, 164.5, 152.9, 141.5, 138.4, 130.9, 128.8, 123.5, 120.6, 106.7, 73.4, 69.0, 31.9, 31.9, 30.3, 29.7, 29.7, 29.7, 29.6, 29.6, 29.6, 29.6, 29.4, 29.4, 29.3, 29.3, 26.1, 26.0, 22.6, 14.1 FT-IR (ATR) (cm^{-1}): 3512.4, 3296.1, 2923, 2853, 1607, 1571, 1537, 1497, 1421, 1355, 1228, 1118. MALDI-ToF MS (m/z) calc for $C_{57}H_{89}N_5O_3$ 891.70 found 892.66 (M+H)$^+$

N²,N⁴-Diphenyl-6-{3,4,5-tris[(S)-3,7-dimethyloctyloxy]phenyl}-1,3,5-triazine-2,4-diamine (**4b**)

Diphenylbiguanide (319 mg, 1.26 mmol) and triethylamine (0.5 mL, 3.59 mmol) were dissolved in dimethylacetamide (10 mL). 3,4,5-tris{(*S*)-3,7-dimethyloctyloxy}benzoyl chloride (680 mg, 1.11 mmol) was dissolved in chloroform (12 mL) and added dropwise to the biguanide solution. The mixture was stirred at room temperature for 18 hours and subsequently heated at 60 °C for 1 hour. The solvents were removed by vacuum evaporation and the crude product was dissolved in chloroform (200 mL). The organic phase was washed with 1N NaOH (100 mL), water (100 mL) and brine (200 mL) and subsequently dried over Na_2SO_4. The suspension was filtered and the filtrate was concentrated in vacuo. The residue was purified by column chromatography (0% to 10% ethyl acetate in chloroform over 10 column volumes) to give the product as a colourless oil. Yield = 550 mg. η = 54%. ^{1}H-NMR (400 MHz,

CDCl$_3$) δ = 7.70 (s, 2H, aromatic), 7.68 (d, J = 8 Hz, 4H, aromatic), 7.36 (t, J = 7.2 Hz, 4H, aromatic), 7.17 (broad, 2H, N-H), 7.11 (t, J = 7.2 Hz, 2H, aromatic), 4.2-4 (m, 6H, -OCH$_2$-), 2-0.8 (mm, 57H, alkyl). ^{13}C-NMR (100 MHz, CDCl$_3$) δ = 171.2, 164.5, 152.9, 141.5, 138.4, 131.0, 128.7, 123.5, 120.6, 106.6, 71.6, 67.2, 39.3, 39.2, 37.5, 37.3, 37.3, 36.4, 29.9, 29.6, 28.0, 27.9, 24.7, 24.7, 22.7, 22.6, 22.6, 19.6, 19.5. FT-IR (ATR) (cm^{-1}): 3394.7, 3268, 2954, 2927, 2870 1601, 1573, 1541, 1509, 1495, 1459, 1442, 1420, 1369, 1320.9, 1114. MALDI-ToF MS (m/z) calc for C$_{51}$H$_{77}$N$_5$O$_3$ 807.60 found 808.61 (M+H)$^+$.

Benzene-1,3-phenylbiguanide (**14**)

1,3-Diaminobenzene (1.53 g, 14.17 mmol) was dissolved in 1 M aqueous HCl (29 mL). Phenyldicyandiamide (4.54 g, 28.34 mmol) was added followed by ethanol (20 mL). The mixture was refluxed for 22 hours and subsequently concentrated by vacuum evaporation. The resulting sticky mass was stirred with acetone (100 mL) for 30 minutes and the residue isolated after decantation and subsequently vacuum dried. The resulting crude product (3.60 g) was dissolved in methanol (65 mL) and cooled to 0 °C, after which NaOH (880 mg, powder) was added. The mixture was stirred at room temperature for one hour and the precipitate was collected by filtration. The residue was washed with water (3 x 10 mL) and methanol (2 x 15 mL), resulting in a white powder. Yield: 1.59 g (44.2%). ^{1}H NMR (400 MHz, DMSO-d6 + bit of 6M HCl in dioxane to protonate, TMS): δ = 10.07 (b, 2H, NH), 9.99 (b, 2H, NH), 7.51 (b, 4H, NH$_2$), (b, 4H, NH$_2$), 7.35-7.1 (mm, 14H, aromatic). ^{13}C-NMR (100 MHz, DMSO-d6 + bit of 4 N HCl in dioxane to protonate, TMS): δ = 156.3, 155.9, 145 (broad), 129.6, 129.3, 122.3, 121.9, 116.4, 115.6. MALDI-ToF MS (m/z) calc for C$_{22}$H$_{24}$N$_{10}$ 428.22 found 429.27 (M+H)$^+$.

N^2,N$^{2'}$-(1,3-Phenylene)bis(N^4-phenyl-6-(3,4,5-tris(dodecyloxy)phenyl)-1,3,5-triazine-2,4-diamine) (**5a**)

Benzene-1,3-phenylbiguanide (427 mg, 1.0 mmol) and triethylamine (0.84 mL, 6 mmol) were dissolved in dimethylacetamide (40 mL). 3,4,5-Tris(dodecyloxy)benzoyl chloride (1.25 g, 1.8 mmol) was dissolved in chloroform (40 mL) and added dropwise to the biguanide solution. The mixture was stirred for 22 hours at room temperature and subsequently heated at 70 °C for 2 hours after which the solvents were removed by rotary evaporation. The residue was redissolved in chloroform (200 mL) and the

solution was washed with 1 N NaOH (100 mL), water (100 mL) and brine (200 mL). The organic layer was dried over Na_2SO_4, filtered and concentrated by vacuum evaporation to yield of crude material (1.37 g). This was purified by column chromatography (0% to 10% ethyl acetate in chloroform over 10 column volumes) to give the product as a yellow viscous oil. R_f = 0.30 (10% ethyl acetate in chloroform). Yield = 710 mg. η = 41.6%. ^{1}H-NMR (400 MHz, $CDCl_3$) δ = 7.69 (s, 4H, aromatic), 7.61 (b, 4H, aromatic), 7.33 (t, J = 8 Hz, 4H, aromatic), 7.15 (b, 8H, NH and aromatic), 7.09 (t, J = 7.2 Hz, 2H, aromatic), 4.2-4.0 (m, 12H, OCH_2-), 1.9-1.7 (m, 12H OCH$_2$$CH_2$-), 1.6-1.2 (mm, 108H, alkyl), 0.88 (m, 18H, CH_3). ^{13}C-NMR (100 MHz, $CDCl_3$) δ = 171.2, 164.4, 152.9, 141.6, 139.0, 130.9, 128.7, 106.7, 73.4, 69.0, 31.9, 30.3, 29.7, 29.7, 29.6, 29.6, 29.4, 29.4, 29.3, 29.3, 26.1, 26.1, 22.6, 14.1. FT-IR (ATR) (cm^{-1}): 3410.4, 3271.6, 2923, 2853, 1602.7, 1542, 1496, 1418, 1370, 1225, 1117. MALDI-ToF MS (m/z) calc for $C_{108}H_{172}N_{10}O_6$ 1706.35 found 1707.31 (M+H)$^+$ 1729.27 (M+Na)$^+$.

(S)-3,7-Dimethyloctyl 3,5-diethynylbenzoate (**17**)

3,5-Diethynylbenzoic acid (0.46 g, 2.7 mmol), EDC (1.2 g, 7.7 mmol) and DMAP (0.75 g, 6.2 mmol) were dissolved in chloroform (40 mL). (*S*)-3,7-Dimethyloctan-1-ol (0.6 g) was added and the resulting mixture was stirred at room temperature for 18 hours. The crude reaction mixture was washed with 1M HCl (3 x 50 mL), 1M NaOH (3 x 50 mL) and brine (50 mL) and the organic phase was subsequently dried over $MgSO_4$. The material was used without further purification in subsequent synthesis. ^{1}H NMR (400 MHz, $CDCl_3$, TMS): δ = 8.1 (s, 2H, aromatic), 7.75 (s, 1H, aromatic), 4.3 (m, 2H, O-CH_2), 3.13 (s, 2H, C≡C-H), 1.8 (m, 2H, aliphatic), 1.6-0.8 (17H, aliphatic). ^{13}C NMR (100 MHz, $CDCl_3$, TMS): δ = 165.0, 139.2, 133.2, 131.2, 122.9, 81.8, 78.4, 64.1, 39.2, 37.1, 35.5, 30.0, 28.0, 24.6, 22.7, 22.6, 19.6.

6-(3-Iodophenyl)-N^2-phenyl-1,3,5-triazine-2,4-diamine (**19**)

Methyl 3-iodobenzoate (2.95 g, 11.2 mmol), phenylbiguanide (3 g, 16.9 mmol) and sodium methoxide (0.91 g, 16.9 mmol) were stirred for 3 hours under reflux conditions in methoxyethanol (25 mL). Water (100 mL) was added to the crude reaction mixture, after which a white precipitate appeared. The precipitate was isolated by filtration and dried under vacuum. The crude material was purified by column chromatography (5% to 15% THF in CH_2Cl_2). Yield = 1.21 g. η = 28%. ^{1}H-NMR (400 MHz, $CDCl_3$) δ = 8.76 (s, 1H, aromatic), 8.36 (d, 1H, aromatic), 7.82 (d, 1H,

aromatic), 7.7 (d, 2H, aromatic), 7.4 (t, 2H, aromatic), 7.24 (t, 1H, aromatic), 7.13 (t, 1H, aromatic), 7.1 (b, 1H, NH), 5.24 (b, 2H, NH$_2$).

(S)-3,7-Dimethyloctyl-3,5-bis{[3-(4-amino-6-phenylamino-1,3,5-triazin-2-yl)phenyl]ethynyl}benzoate (**6b**)

6-(3-Iodophenyl)-N^2-phenyl-1,3,5-triazine-2,4-diamine **19** (430 mg, 1.1 mmol) and allylpalladium chloride dimer (18.5 mg, 0.05 mmol) were charged in a Schlenk tube and subjected to four cycles of vacuum and argon refill. Acetonitrile (15 mL), tetrahydrofuran (10 mL) and toluene (5 mL) were added to the mixture. Tri-*tert*-butylphosphine (0.1 mL, 0.41 mmol) was added upon which the mixture yellow to black. (*S*)-3,7-Dimethyloctyl 3,5-diethynylbenzoate **17** (56 mg, 0.17 mmol) was added, followed by DABCO (270 mg, 2.3 mmol). The resulting mixture was stirred overnight. The progress of the reaction was followed by thin layer chromatography (CHCl$_3$/THF : 5/1) and showed the presence of a large amount of presumably mono-addition compound. Allylpalladium chloride dimer (10 mg, 0.027 mmol), Tri-*tert*-butylphosphine (30 μL, 0.12 mmol) and DABCO (100 mg, 0.85 mmol) were added and the mixture was stirred for an additional 3 days. The reaction mixture was concentrated by vacuum evaporation and the residue extracted with CHCl$_3$. The crude extract was evaporated and the residue purified by column chromatography to yield a yellow solid. Yield = 91 mmol. H = 65%. ^{1}H-NMR (400 MHz, CDCl$_3$): δ = 8.59 (s, 2H, aromatic), 8.37 (d, J = 8 Hz, 2H, aromatic), 8.17 (s, 2H, aromatic), 7.9 (s, 1H, aromatic), 7.7 (d, J = 7.6 Hz, 2H, aromatic), 7.66 (d, J = 8 Hz, 4H, aromatic), 7.49 (t, J = 7.6 Hz, 2H, aromatic), 7.39 (t, J = 7.6 Hz, 4H, aromatic), 7.12 (t, J = 7.2 Hz, 2H, aromatic), 7.1 (b, 2H, N-H), 5.24 (b, 4H, NH$_2$), 4.4 (m, 2H, O-CH$_2$), 1.8-0.8 (19H, aliphatic). ^{13}C-NMR (100 MHz, CDCl$_3$) δ = 167.4, 165.3, 164.9, 138.3, 136.8, 134.6, 132.1, 131.8, 131.2, 128.9, 128.5, 124.0, 123.6, 122.8, 120.4, 92.5, 88.0, 64.1, 39.2, 37.1, 35.5, 30.0, 28.0, 25.3, 24.6, 22.7, 22.6, 19.8. FT-IR (ATR) (cm^{-1}): 3411, 3331, 3172, 2955, 2925, 2865, 1719, 1600, 1530, 1497, 1440, 1399, 1251. MALDI-ToF MS (m/z) calc for C$_{51}$H$_{48}$N$_{10}$O$_2$ 832.40 found 833.40 (M+H)$^+$

3.7 References

[1]   T.F.A. de Greef, M.M.J. Smulders, M. Wolffs, A.P.H.J. Schenning, R.P. Sijbesma, E.W. Meijer, *Chem. Rev.,* 2009, **109**, 5687

[2]   T. Aida, E.W. Meijer, S.I. Stupp, *Science*, 2012, **335**, 813

[3]   Z. Chen, A. Lohr, C.R. Saha-Möller, F. Würthner, *Chem. Soc. Rev.*, 2009, **38**, 564

[4]   M. Takeuchi, S. Tanaka, S. Shinkai, *Chem. Commun.,* 2005, 5539

[5]   S. Ghosh, X-Q. Li, V. Stepanenko, F. Würthner, *Chem. Eur. J.*, 2008, **14**, 11343

[6]   R. Marty, R. Nigon, D. Leite, H. Frauenrath, *J. Am. Chem. Soc.*, 2014, **136**, 3919

[7]   Xu. Lin, M. Hirono, T. Seki, H. Kurata, T. Karatsu, A. Kitamura, D. Kuzuhara, H. Yamada, T. Ohba, A. Saeki, S. Seki, S. Yagai, *Chem. Eur. J.*, 2013, **19**, 6561

[8]   M. Shirakawa, S. Kawano, N. Fujita, K. Sada, S. Shinkai, *J. Org. Chem.*, 2003, **68**, 5037

[9]   P.A. Korevaar, S.J. George, A.J. Markvoort, M.M.J. Smulders, P.A.J. Hilbers, A.P.H.J. Schenning, T.F.A. de Greef, E.W. Meijer, *Nature*, 2012, **481**, 492

[10]   M.M. Bouman, E.W. Meijer, *Adv. Mater.*, 1995, **7**, 385

[11]   F. Würthner, S. Yao, U. Beginn, *Angew. Chem. Int. Ed.*, 2003, **42**, 3247

[12]   A. Lohr, M. Lysetska, F. Würthner, *Angew. Chem. Int. Ed.*, 2005, **44**, 5071

[13]   A. Lohr, F. Würthner, *Angew. Chem. Int. Ed.*, 2008, **47**, 1232

[14]   F. Würthner, Z.J. Chen, F.J.M. Hoeben, P. Osswald, C.C. You, P. Jonkheim, J. von Herrikhuyzen, A.P.H.J. Schenning, P.P.A.M. van der Schoot, E.W. Meijer, E.H.A. Becker, S.C.J. Meskers, R.A.J. Janssen, *J. Am. Chem. Soc.*, 2004, **126**, 10611

[15]   Z. Wang, W.S. Jin, T. Fukushima, A. Saeki, S. Seki, T. Aida, *Science*, 2011, **334**, 340

[16]   D. González-Rodríguez, A.P.H.J. Schenning, *Chem. Mater.*, 2011, **23**, 310

[17]   Y. Yamamoto, *Sci. Technol. Adv. Mater.*, 2012, **13**, 033001

[18]   F.J.M. Hoeben, P. Jonkheim, E.W. Meijer, A.P.H.J. Schenning, *Chem. Rev.*, 2005, **105**, 1491

[19]   S.S. Babu, V.K. Praveen, A. Ajayaghosh, *Chem. Rev.*, 2014, **114**, 1973

[20]   F. Würthner, *Chem. Commun.*, 2004, 1564

[21]   Z. Chen, V. Stepanenko, V. Dehm, P. Prins, L.D.A. Siebbeles, J. Seibt, P. Marquetand, V. Engel, F. Würthner, *Chem. Eur. J.*, 2007, **13**, 436

[22]   F. Würthner, C. Thalacker, S. Diele, C. Tschierske, *Chem. Eur. J.*, 2001, **7**, 2245

[23]   V. Percec, M. Peterca, T. Tadjiev, X. Zeng, G. Ungar, P. Leowanawat, E. Aqad, M.R. Imam, B.M. Rosen, U. Akbey, R. Graf, S. Sekharan, D. Sebastiani, H.W. Spiess, P.A. Heiney, S.D. Hudson, *J. Am. Chem. Soc.*, 2011, **133**, 12197

[24]   X. Zhang, Z. Chen, F. Würthner, *J. Am. Chem. Soc.*, 2007, **129**, 4886

[25]   V. Dehm, Z. Chen, U. Baumeister, P. Prins, L.D.A. Siebbeles, F. Würthner, *Org. Lett.*, 2007, **9**, 1085

[26]   T.E. Kaiser, V. Stepanenko, F. Würthner, *J. Am. Chem. Soc.*, 2009, **131**, 6719

[27]   T.E. Kaiser, H. Wang, V. Stepanenko, F. Würthner, *Angew. Chem. Int. Ed.*, 2007, **46**, 5541

[28]   A.P.H.J. Schenning, J. van Herrikhuyzen, P. Jonkheijm, Z. Chen, F. Würthner, E.W. Meijer, *J. Am. Chem. Soc.*, 2002, **124**, 10252

[29] W. Seitz, A.J. Jimenez, E. Carbonell, B. Grimm, M.S. Rodríguez-Morgade, D.M. Guldi, T. Torres, *Chem. Commun.*, 2010, **46**, 127

[30] S. Yagai, *J. Photochem. Photobiol. C: Photochem. Rev.*, 2006, **7**, 164

[31] E.H.A. Beckers, Z. Chen, S.C.J. Meskers, P. Jonkheim, A.P.H.J. Schenning, X.-Q. Li, P. Osswald, F. Würthner, R.A.J. Janssen, *J. Phys. Chem. B.*, 2006, **110**, 16967

[32] S. Yagai, M. Usui, T. Seki, H. Murayama, Y. Kikkawa, S. Uemura, K. Karatsu, A. Kitamura, A. Asano, S. Seki, *J. Am. Chem. Soc.*, 2012, **134**, 7983

[33] S. Yagai, Y. Monma, N. Kawauchi, T. Karatsu, A. Kitamura, *Org. Lett.*, 2007, **9**, 1137

[34] T. Seki, A. Asana, S. Seki, Y. Kikkawa, H. Murayama, T. Karatsu, A. Kitamura, S. Yagai, *Chem. Eur. J.*, 2011, **17**, 3598

[35] S. Yagai, T. Seki, H. Murayama, Y. Wakikawa, T. Ikoma, Y. Kikkawa, T. Karatsu, A. Kitamura, Y. Honsho, S. Seki, *Small*, 2010, **6**, 2831

[36] J.H.K.K Hirschberg, L. Brunsveld, A. Ramzi, J.A.J.M. Vekemans, R.P. Sijbesma, E.W. Meijer, *Nature*, 2001, **407**, 1

[37] A.R.A. Palmans, J.A.J.M. Vekemans, H. Fischer, A.R. Hikmet, E.W. Meijer, *Chem. Eur. J.*, 1997, **3**, 300

[38] M.H.C.H. van Houtem, R. Martín-Rapún, J.A.J.M. Vekemans, E.W. Meijer, *Chem. Eur. J.*, 2010, **16**, 2258

[39] O. LeBel, T. Maris, H. Duval, J.D. Wuest, *Can. J. Chem.*, 2005, **83**, 615

[40] K. Matsuda, M.T. Stone, J.S. Moore, *J. Am. Chem. Soc.*, 2002, **124**, 11836

[41] F.H. Beijer, R.P. Sijbesma, J.A.J.M. Vekemans, E.W. Meijer, H. Kooijman, A.L. Spek, *J. Org. Chem.*, 1996, **61**, 6371

[42] R. Deans, V.M. Rotello, *J. Org. Chem.*, 1997, **62**, 4528

[43] P. Brunet, M. Simar, J.D. Wuest, *J. Am. Chem. Soc.*, 1997, **119**, 2737

[44] P. Jonkheijm, A. Miura, M. Zdanowska, F.J.M. Hoeben, S. de Feyter, A.P.H.J. Schenning, F.C. de Schrijver, E.W. Meijer, *Angew. Chem., Int. Ed.*, 2004, **43**, 74

[45] Guinier approximation: $I(q) = I_0 exp((-1/3) \times R_g^2 \times q^2))$ in the range $0.40 \leq q \leq 0.67$ nm^{-1}

[46] Form factor form rigid cylinders: $R_g^2 = 0.5 \times R^2 + (1/12) \times L^2$.

[47] P. Lindner, T. Zemb, eds., *Neutron, X-rays and Light: Scattering Methods Applied to Soft and Condensed Matter*, Elsevier, Amsterdam, 2002

[48] A.J. Lowe, F.M. Pfeffer, P. Thodarson, *Supramolecular Chemistry*, 2012, **24**, 585

4

Directing the self-assembly behaviour of porphyrin-based supramolecular systems

Abstract

The self-assembly behaviour of a library of tetra-amidated porphyrin molecules decorated with a variety of solubilising wedges was investigated as dilute solutions in methylcyclohexane. Small changes in the solubilising wedge architecture of the porphyrins result in the formation of different aggregate types as evidenced by UV–Vis and CD spectroscopy. The porphyrins form H- or J-aggregates or a mixture of both. Furthermore, the mechanisms of formation differ for both types of aggregates; the formation of J-aggregates proceeds via an isodesmic mechanism and the formation of H-aggregates proceeds via a cooperative mechanism. Porphyrins that display the formation of both types of aggregates were examined with detailed thermodynamic and kinetic experiments to determine which self-assembly pathway dominates. H- and J-aggregates self-assemble in a parallel pathway in which both compete for the monomer instead of a sequential pathway in which one of the aggregates interconverts into the other. Thermodynamic analysis of H-aggregating porphyrins reveals that the competing self-assembly pathway towards J-aggregates is operational in these systems as well. However, for these porphyrins the final thermodynamically stable self-assembled state is devoid of J-aggregates. Our findings show that porphyrin self-assembly may be directed towards specific aggregated states by remarkably small changes in the architecture of their solubilising wedges.

4.1 Introduction

Porphyrins are heterocyclic aromatic macrocycles that occur ubiquitously in nature and play a crucial role in oxygen transport, enzymes and various photosynthetic systems. In photosystem II and chlorosomes extensive arrays of porphyrins feature in light-harvesting, exciton splitting and funnelling of excitonic energy to reaction centres. Of paramount importance for the functionality of porphyrins in these systems is their mutual geometric orientation which is a result of specific non-covalent interactions between the porphyrins (chlorosomes) or a non-covalent framework of proteins that organises the porphyrins in a specific manner.[1]

Inspired by the functional versatility of porphyrins in nature, chemists have used synthetic porphyrin derivatives for a myriad of applications. These include artificial photosynthetic systems, organic photovoltaics, molecular rotors, supramolecular chemistry, templated non-covalent synthesis, catalysis, artificial enzymes and photodynamic therapy.[2-13] The molecular structure of porphyrins is easily modified on both the core and the periphery giving rise to easily tuneable (supra)molecular properties.[14-18] A key feature is furthermore the metal binding centre which allows a versatile use of porphyrins in catalysis and metal-ligand based supramolecular chemistry.[7,8,12]

In supramolecular chemistry the formation of non-discrete porphyrin aggregates has been studied in great detail taking advantage of combinations of π-stacking, hydrogen bonding, metal–ligand and hydrophobic interactions to create functional multichromophoric aggregates. The group of Wasielewski, for example, reported on the self-assembly of Zn-porphyrins appended with four perylene bisimides into either two-dimensional or one-dimensional aggregates depending on the perylene bay substituents (Figure 4.1 A and B).[5,19] The self-assembly of these donor-acceptor constructs was mainly driven by π-stacking interactions between the perylene chromophores while porphyrin-porphyrin interactions only contributed to a slight extent to the stabilisation of the aggregates. Nolte and co-workers investigated the self-assembly of porphyrin-functionalised benzene-1,3,5-tricarboxamides, in which three non-symmetrical porphyrins were connected by amide linkages to a benzene core (Figure 4.1 C).[20,21] The porphyrin trimers were found to self-assemble cooperatively in columnar stacks by a combination of hydrogen bonding of the
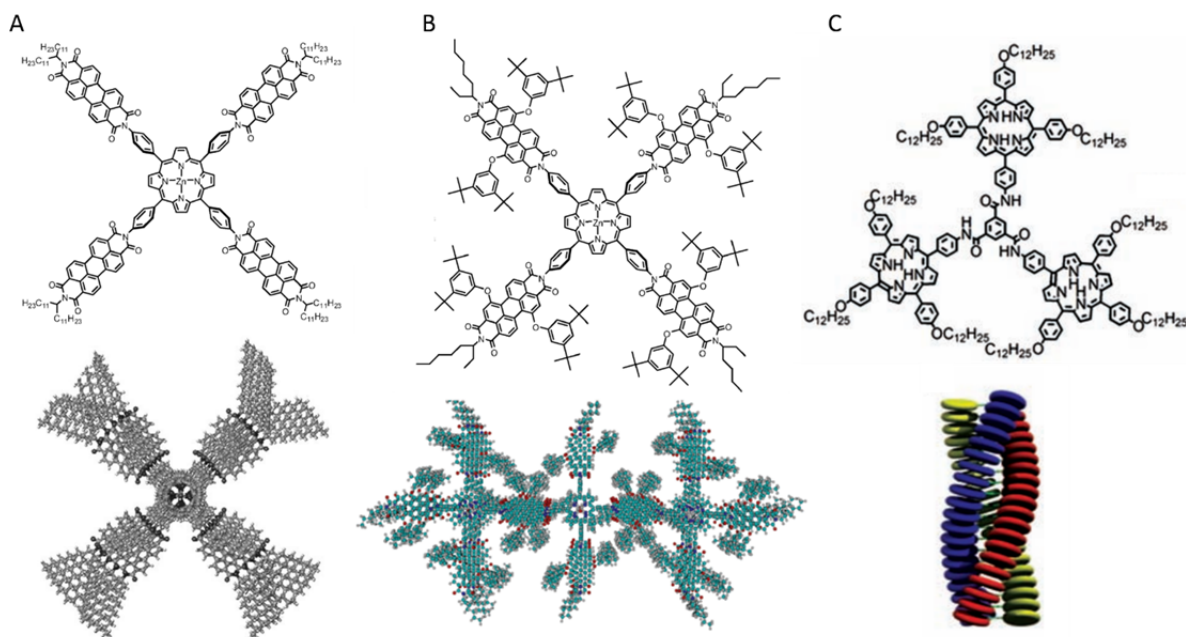
Figure 4.1. Molecular structures of self-assembling porphyrins and schematic representations of their aggregate structures. Images adapted from references 19 (A), 5 (B) and 20 (C).

benzene cores and cofacial H-aggregation of the porphyrin subunits in chloroform and hexane solution. Interestingly, different aggregation behaviour of the porphyrin trimers was found in cyclohexane solution as evidenced by the different excitonic coupling of the porphyrin chromophores, indicating the delicate interplay of hydrogen bonding and π-stacking interactions in the self-assembly of such discotics. The strategy of combining hydrogen bonding and π-stacking interactions has also been pursued by Shinkai and co-workers.[22,23] Here, solubilising chains were appended to either the 3- or 4-positions on the phenyl rings of tetraphenylporphyrins via phenoxyacetamide linkers. The resulting porphyrins were shown to be efficient organogelators. Remarkably, the different connectivity of the amides to the porphyrin gave rise to either H- or J-type aggregates as evidenced by absorbance studies. Furthermore, considerable differences in gelator efficiency and thermal stability of the assemblies were found. The use of metal–ligand interactions for the formation of extended porphyrin aggregates was demonstrated by the group of Kobuke.[24-26] They first showed that *meso*-imidazolyl-substituted Zn-porphyrins form discrete assemblies as a consequence of metal-ligand binding and hydrogen bonding. In a further study it was shown that extensive porphyrin arrays could be prepared by directly linking two mono(imidazolyl)-Zn-porphyrins at the *meso*-position, by

intermolecular self-coordination in which the porphyrin subunits adopt a slipped, cofacial arrangement.

Supramolecular polymers based on porphyrins have also been studied in our group.[27-31] In these studies tetra-amidated porphyrins were appended with solubilising wedges and the dynamics and thermodynamics of their self-assembly in apolar solvents was investigated. The porphyrins were found to self-assemble predominantly into long cofacial H-aggregated stacks, although in specific cases depending on the preparation method of the self-assembled architectures, J-aggregates could also be obtained. These results suggest that minor variations in the porphyrin structure can give rise to the formation of different types of aggregates. Furthermore, careful selection of the preparation method might be adopted as a tool to guide the self-assembly process through the phenomenon of pathway complexity towards the desired aggregated state.[32]

A relevant recent example where pathway complexity in a porphyrin supramolecular polymer was exploited in order to obtain a living supramolecular polymerisation, was reported by the group of Takeuchi.[33] Here, porphyrins bearing hydrogen-bond moieties (amides) and solubilising groups on two of the *meso*-phenyl positions were shown to assemble into J-aggregates via an isodesmic self-assembly mechanism in methylcyclohexane solution (Figure 4.2). These J-aggregates appeared to be metastable because a spontaneous conversion into H-aggregates via a strongly cooperative mechanism was observed over time. The authors exploited this metastablity by seeding solutions of J-aggregates with small aliquots of porphyrin H-aggregates and observed a selective elongation of the existing H-aggregated fibres instead of the nucleation of new stacks. The porphyrins in the J-aggregate depolymerised into monomers which, due to the large nucleation barrier for the H-aggregates, preferentially grow on top of existing stacks. Repetitive seeding experiments resulted in the formation of supramolecular fibres of predetermined and controlled size, which were analysed by atomic force microscopy and dynamic light scattering in a process termed living supramolecular polymerisation.
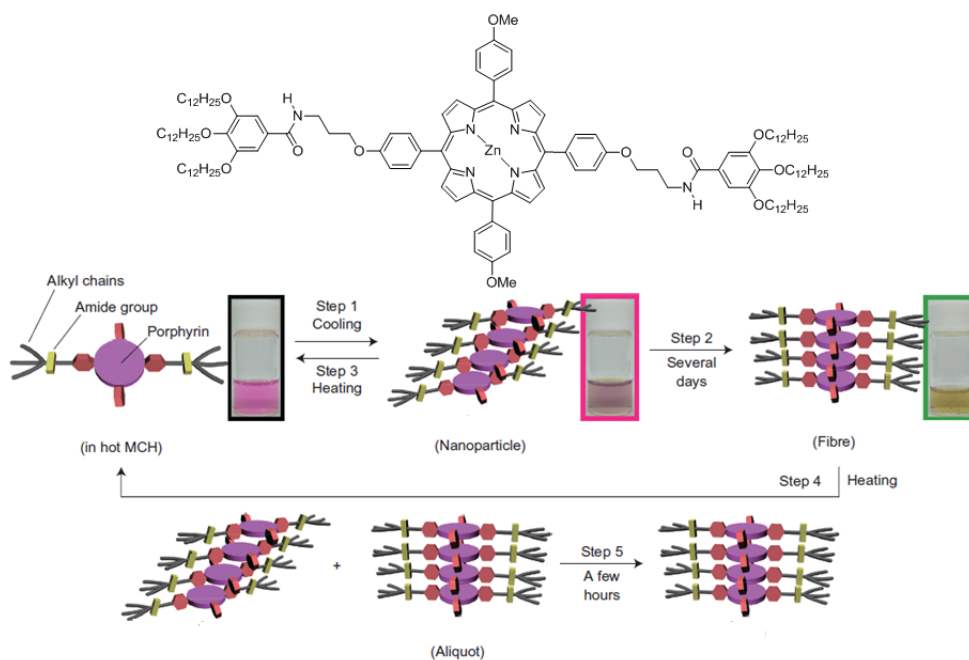
Figure 4.2. Schematic representation of the pathway complexity in the living supramolecular polymerisation of a Zn-porphyrin derivative. Image adapted from reference 33.

From the examples above it becomes clear that porphyrins are highly interesting molecules for the generation of supramolecular architectures. However, pathway complexity in their self-assembly can result in the formation of a variety of self-assembled architectures from the same molecular structure.[32] Furthermore, small changes in the molecular architecture frequently result in the formation of different types of aggregates. While observations on these phenomena have been reported for porphyrin supramolecular systems, systematic studies have rarely been carried out. Based on previous investigations in our group we here investigate a library of tetra-amidated porphyrins that self-assemble by a combination of hydrogen bonding and π-stacking interactions, for their pathway complexity in supramolecular self-assembly (Figure 4.3). Our aim is to get insights into the pathway complexity and sensitivity of porphyrin supramolecular systems towards changes in the molecular architecture of the solubilising periphery. Such insights are useful with respect to the reproducible generation of supramolecular architectures based on porphyrin subunits. The research presented in this chapter was carried out in close collaboration with Bram Teunissen.
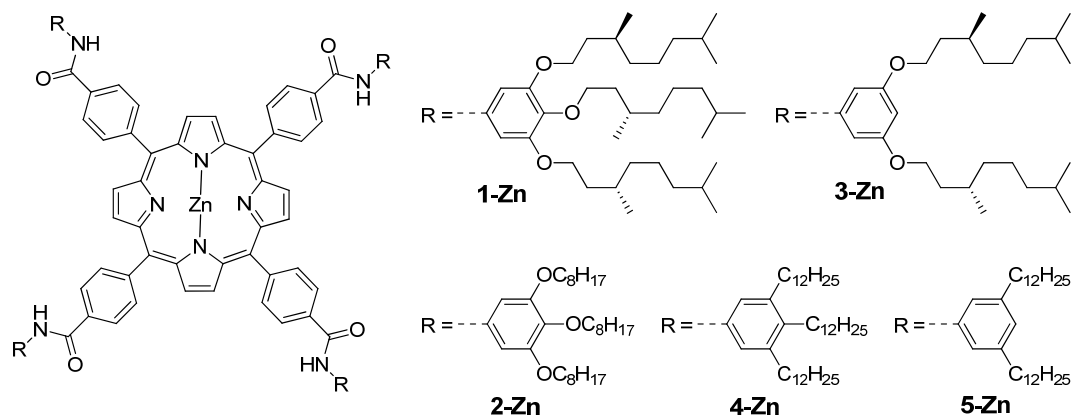
Figure 4.3. Library of porphyrin tetra-amides **1-Zn** - **5-Zn** that bear a variety of solubilising wedges on the periphery.

4.2 Molecular design and synthesis

The self-assembly behaviour of porphyrins **1-Zn** and **2-Zn** has been studied in detail in our group. In the current design, the tetraphenylporphyrin cores are functionalised with solubilising aliphatic wedges via amide linkages to provide solubility in apolar organic solvents and aggregation through four-fold hydrogen bonding between porphyrins. To study the effects of the molecular architecture of the solubilising periphery on the aggregation behaviour of such porphyrins, we designed porphyrins **1-Zn** - **5-Zn**. The solubilising wedge for porphyrin **3-Zn** resembles that of porphyrin **1-Zn** but lacks the *para*-substituent on the phenyl ring. Porphyrins **4-Zn** and **5-Zn** bear alkyl chains directly attached to the phenyl ring instead of an alkoxy linkage as in porphyrins **1-Zn** - **3-Zn**. In comparison with porphyrin **4-Zn**, again the *para*-substituent on the solubilising wedge is omitted in porphyrin **5-Zn**. Porphyrins **1-Zn** - **5-Zn** now constitute a library of porphyrins decorated with aliphatic solubilising wedges that should give supramolecular porphyrin aggregates in apolar solutions.

The syntheses of the porphyrins **1-Zn** - **5-Zn** are shown in Scheme 4.1. The key aniline precursors that were reacted with *meso*-tetra(4-carboxyphenyl)porphyrin in the final step of the synthesis were prepared according to two different routes. Starting from methyl gallate, aniline derivatives **6** and **7** were prepared according to reported procedures.[29-31] For aniline derivative **13**, a similar route was followed as for **6** and **7** starting from methyl 3,5-dihydroxybenzoate (**8**). Double Williamson ether synthesis between **8** and tosylate **9** afforded methyl ester **10** in 92% yield.
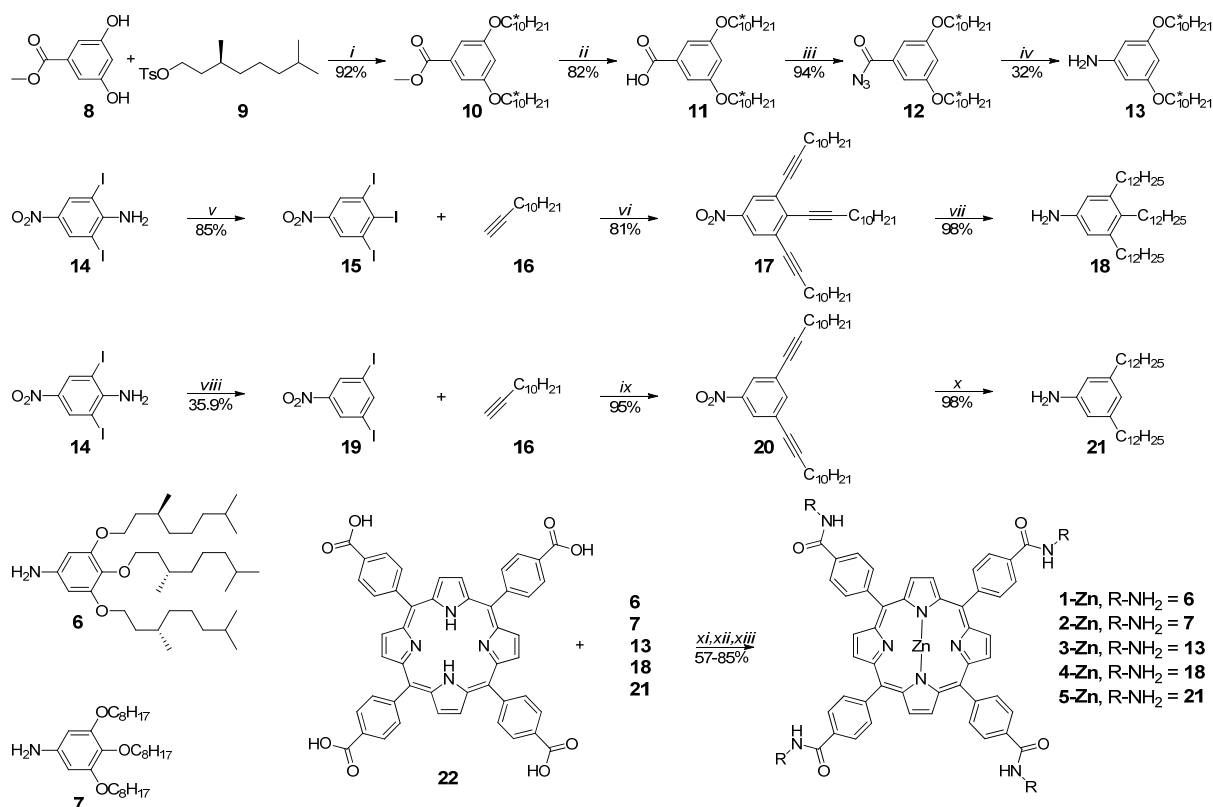
Scheme 4.1. Synthesis of porphyrins **1-Zn** - **5-Zn**. Reagents and conditions: i) K_2CO_3, TBAB, MIBK, reflux; ii) NaOH, EtOH, reflux; iii) ethyl chloroformate, TEA, THF; NaN_3, H_2O, THF, RT; iv) dioxane, 90 °C, tetrabutylammonium hydroxide; v) $NaNO_2$, H_2SO_4, KI, acetic acid, H_2O; vi) $Pd(PPh_3)_2Cl_2$, CuI, Et_3N, 80 °C; vii) Pd/C, H_2, EtOAc, EtOH; viii) $NaNO_2$, H_2SO_4, ethanol, reflux; ix) $Pd(PPh_3)_2Cl_2$, CuI, Et_3N, 60 °C; x) Pd/C, H_2 EtOAc, EtOH; xi) $C_2Cl_2O_2$, DMF, $CHCl_3$; xii) Et_3N, $CHCl_3$, 0 °C; xiii) $Zn(OAc)_2$, DCM, RT.

Subsequently, the methyl ester functionality in **10** was hydrolysed to the free acid **11** with sodium hydroxide in boiling methanol and the latter converted to the acyl azide **12** by subsequent treatment with ethyl chloroformate and sodium azide. A Curtius rearrangement of **12** in hot dioxane afforded the corresponding isocyanate in situ, which was hydrolysed to the amine to afford aniline **13** in 32% yield after column chromatography. For the synthesis of aniline **18** a reported procedure was used.[34-35] For the synthesis of aniline **21**, the same procedure as for **18** was applied but slightly modified. First, a Sandmeyer reaction was performed on 2,6-diiodo-4-nitroaniline **14**, after which the intermediate diazonium salt was treated with potassium iodide affording 1,2,3-triiodo-5-nitrobenzene (**15**). For the synthesis of **19**, the Sandmeyer reaction on **14** was performed in ethanol as a solvent, resulting in protodediazoniation upon thermolysis of the diazonium salt.[36-39] Both **15** and **19** were then reacted with 1-dodecyne (**16**) under Sonogashira conditions to afford alkynes **17**

and **20**. Treatment of alkynes **17** and **20** with molecular hydrogen in the presence of palladium catalyst resulted in the simultaneous reduction of the alkyne and nitro functionalities to yield aniline derivatives **18** and **21** in 98% and 89% yield, respectively. Next, the library of porphyrins **1-Zn - 5-Zn** was generated by reaction of commercially available *meso*-tetra(4-carboxyphenyl)porphyrin with the various anilines described above, under standard conditions for amide bond formation. In the final step, the porphyrins were treated with zinc acetate in dichloromethane to yield zinc metallated porphyrins **1-Zn - 5-Zn**. The end products were thoroughly purified by column chromatography and characterised by NMR spectroscopy and MALDI-ToF spectrometry, which indicated that **1-Zn - 5-Zn** were obtained as highly pure compounds.

4.3 Self-assembly in methylcyclohexane solution

The self-assembly behaviour of zinc porphyrins **1-Zn - 5-Zn** as a dilute solution in methylcyclohexane (MCH) was investigated by UV–Vis spectroscopy (Figure 4.4). Three different methods for aggregate preparation were evaluated: 1) injection of a small aliquot of a concentrated porphyrin solution (c = 1×10^{-3} M) in a non-aggregating solvent (chloroform) into an aggregating solvent (MCH) resulting in a final concentration of c = 2.5×10^{-6} M followed by equilibration of the sample for five hours at room temperature; 2) rapidly cooling (quenching) a porphyrin solution in MCH (c = 2.5×10^{-6} M) from the molecularly dissolved state at high temperature (T = 363 K) to the assembled state at low temperature (T = 293 K); 3) slow cooling (rate = 0.5 K/min) of a porphyrin solution (c = 2.5×10^{-6} M) from the molecularly dissolved state (T = 363 K) to the assembled state (T = 293 K) and equilibration of the sample for 12 hours. The UV–Vis spectra recorded for all sample-preparation methods as well as the molecularly dissolved state at T = 363 K are depicted in Figure 4.4. At elevated temperatures in methylcyclohexane (T = 363 K, c = 2.5×10^{-6} M) all porphyrins show sharp Soret absorption bands indicative of molecularly dissolved species in solution with λ_{max} = 419 nm. As expected, the molecular structure of the wedge architectures does not influence the ground state electronic properties of the porphyrin cores. Upon self-assembly, however, differences in aggregation behaviour are observed in the series of porphyrins **1-Zn - 5-Zn**. Furthermore, the aggregation behaviour varies with the aggregate preparation method. Porphyrin **1-Zn**, has previously been studied in great detail by our group, and shows an aggregation behaviour independent of
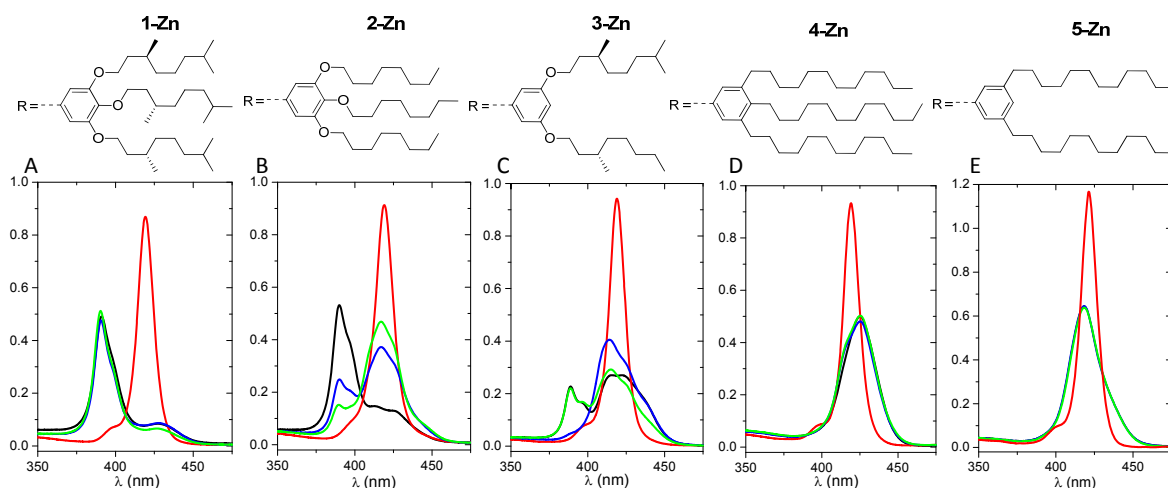
Figure 4.4. UV–Vis spectra recorded for porphyrins **1-Zn - 5-Zn** after different sample preparation methods (red lines: molecularly dissolved, black lines: injection method, blue lines: quenching method, green lines: slow cooling method, MCH, c = 2.5×10^{-6} M, l = 1 cm). From left to right: porphyrins **1-Zn** to **5-Zn**.

the method of aggregate preparation (Figure 4.4 A).[30,31] Porphyrin **1-Zn** forms one-dimensional stacks of cofacially aggregated porphyrins (H-aggregates) as indicated by the hypsochromic shift of the Soret absorption to λ_{max} = 390 nm with respect to the molecularly dissolved state. In contrast, porphyrins **4-Zn** and **5-Zn** also display aggregation behaviour that is independent of aggregate preparation method; but a different type of aggregate is obtained (Figure 4.4 D and E). Here, λ_{max} of the Soret absorption peak remains roughly constant but the Soret band appears broadened and diminishes in intensity. These spectral features conform to a slipped stack arrangement or J-aggregates where the porphyrin central cores are laterally displaced with respect to each other, instead of the cofacial arrangement as observed for porphyrin **1-Zn**. Interstingly, for both porphyrins **2-Zn** and **3-Zn**, spectral features of the Soret band reminiscent to cofacial and slipped-stack aggregation can be observed (Figure 4.4 B and C). Both the hypsochromically shifted band at λ = 390 nm and the diminished band at λ = 419 nm can be observed, indicating the coexistence of both aggregated states in solution. Furthermore, for porphyrins **2-Zn** and **3-Zn** the composition of the self-assembled state strongly depends on the preparation of the aggregate. Summarizing, porphyrins **1-Zn - 5-Zn** can be classified into three different types according to the aggregates they form. Porphyrin **1-Zn** displays cofacial H-aggregation, porphyrins **4-Zn** and **5-Zn** display slipped stack J-aggregation while porphyrins **2-Zn** and **3-Zn** show the coexistence of both these aggregate types.

Next, we compare the self-assembly mechanism of porphyrins **1-Zn - 5-Zn** by monitoring the UV–Vis and CD signals as a function of temperature under thermodynamically controlled conditions by slow cooling (rate = 0.5 K/min). Porphyrin **1-Zn**, which forms cofacial H-aggregates, was previously shown to self-assemble via a cooperative mechanism as dilute solutions in MCH.[30,31] The UV–Vis and CD cooling curves display non-sigmoidal shapes characterised by a critical temperature below which aggregation takes place, typical for a nucleation-elongation mechanism. In contrast, cooling curves measured for porphyrins **4-Zn** and **5-Zn** (Figure 4.5) are sigmoidal in shape and lack a critical temperature. This is indicative of an isodesmic self-assembly mechanism. Apparently, the two different aggregate types formed by porphyrins **1-Zn - 5-Zn** are formed by different self-assembly mechanisms.
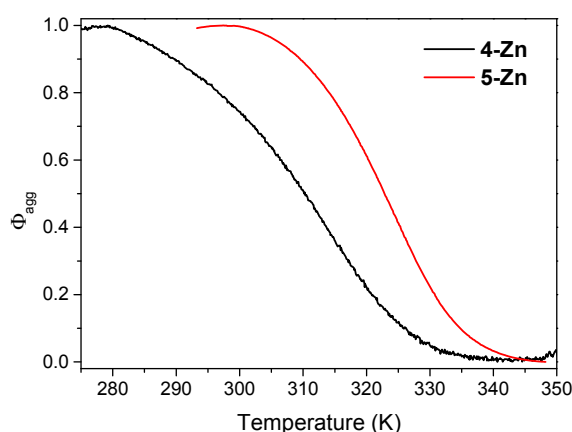
Figure 4.5. UV–Vis cooling curves of porphyrins **4-Zn** and **5-Zn** in MCH solution (λ = 419 nm, c = 2.5×10^{-6} M, l = 1 cm, rate = 0.5 K/min).

In contrast to porphyrins **1-Zn**, **4-Zn** and **5-Zn** which form only one type of aggregate, porphyrins **2-Zn** and **3-Zn** show the coexistence of both aggregate types in solution. As porphyrin **3-Zn** possesses stereogenic centres, H-aggregates formed by porphyrin **3-Zn** are chiral and show a Cotton effect in CD spectroscopy (no Cotton effect is observed for J-aggregated states of **1-Zn** and **3-Zn**). Therefore, the Cotton effect observed for porphyrin **3-Zn** can be used as a selective tool to probe the aggregation mechanism of the H-aggregates formed by **3-Zn**. Thus, variable temperature UV–Vis and CD experiments were carried out to study the formation mechanisms of both aggregate types in porphyrin **3-Zn**. Cooling a dilute solution of **3-Zn** (T = 360 K, c = 2.5×10^{-6} M, MCH) at a rate of 0.5 K/min to T = 305 K results in the

selective formation of porphyrin J-aggregates as evident from UV–Vis and CD spectra. The self-assembly process is monitored at λ = 419 nm and the resulting curve is sigmoidal in shape and no critical temperature is observed, suggesting an isodesmic self-assembly mechanism (Figure 4.6). Further cooling of the solution below T = 305 K results in the formation of cofacial porphyrin H-aggregates as evidenced by the appearance of a hypsochromically shifted absorption and the concomitant appearance of a Cotton effect at λ = 390 nm (Figure 4.7 A). The resulting cooling curve is non-sigmoidal in shape and a clear critical temperature T_e is observed, indicative of a cooperative assembly mechanism. However, the resulting solution appears not to be under thermodynamic equilibrium, as Cotton effect of only -33 mdeg is obtained in the cooling curve instead of the maximal Cotton effect at c = 2.5×10^{-6} M of -145 mdeg that was found in the equilibrium experiment described in Figure 4.4.
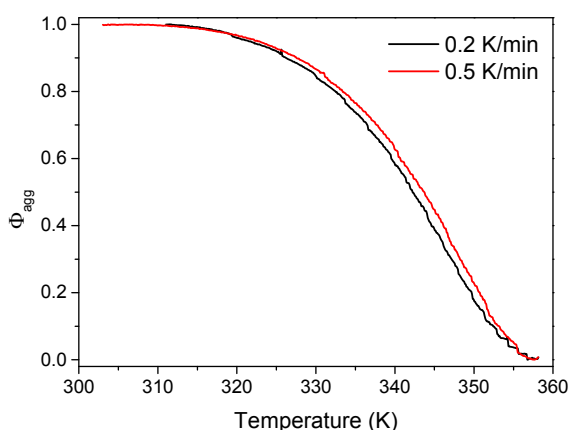
Figure 4.6. UV–Vis cooling curves for **3-Zn** MCH solution (λ = 419 nm, c = 2.5×10^{-6} M, l = 1 cm, rate = 0.5 K/min and 0.2 K/min).

Apparently, the formation of H-aggregates of porphyrin **3-Zn** is kinetically slow with respect to the cooling rate applied. Indeed, after equilibration of the resulting solution at room temperature for 12 hours, the Cotton effect further develops to its maximum value of -145 mdeg, indicating that the assembly curve was not measured at equilibrium conditions. To overcome the kinetic issues observed in the formation of aggregates of porphyrin **3-Zn**, a disassembly curve is measured instead. A solution of porphyrin **3-Zn** (c = 2.5×10^{-6} M, MCH) is equilibrated at room temperature for a period of 72 hours (maximum Cotton effect of -145 mdeg stable after 24 hours). Next, the cofacial porphyrin aggregates are disassembled by heating from room

temperature (Figure 4.7 B). Gratifyingly, they reveal a strongly non-sigmoidal disassembly curve with a sharp transition at a critical temperature T_e = 309 K. These results indicate that the cofacial H-stacks formed by porphyrin **3-Zn** assemble via a highly cooperative self-assembly mechanism. The results suggest that the two different aggregated states present in porphyrin **3-Zn** are formed by the same self-assembly mechanisms that govern the self-assembly of the corresponding porphyrins that form a single aggregate (**1-Zn** and **5-Zn**). Additionally, the results indicate a significant hysteresis effect in the assembly and disassembly of H-aggregates of porphyrin **3-Zn** as the assembly and disassembly curves are strongly dissimilar for the same experimental conditions (Figure 4.7). The observed hysteresis is probably rate-dependent hysteresis, as cooled solutions of **3-Zn** develop a Cotton effect over time upon equilibration at low temperatures.
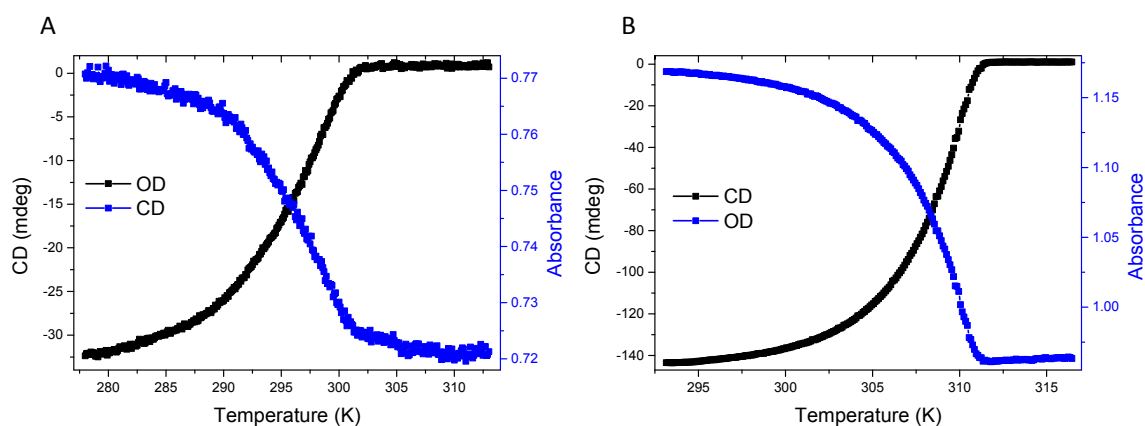
Figure 4.7. UV–Vis and CD cooling (A) and heating (B) curves of porphyrin **3-Zn** (λ = 390 nm, c = 2.5×10^{-6} M, l = 1 cm, rate = 0.1 K/min).

4.4 Sequential versus parallel pathways in self-assembly

In a self-assembling system consisting of a monomer and two different self-assembled species, two principal mechanism can be differentiated; a parallel and a sequential pathway (Figure 4.8). In the parallel pathway, the monomer is in equilibrium with both aggregated states, and both aggregated states do not interconvert directly (Figure 4.8 A). Conversion between the two aggregates occurs via disassembly to the free monomer and subsequent reassembly into the aggregates. In the sequential pathway, monomers first form one type of aggregate which subsequently converts to a second, different type of aggregate (Figure 4.8 B). Here, the first aggregate can be interpreted as an intermediate for forming the

second aggregate. A cooperative or nucleated supramolecular polymerisation can be interpreted as a sequential pathway supramolecular polymerisation, where pre-nucleus aggregates are the intermediate state in the formation of the cooperatively formed supramolecular polymer. In the case of porphyrin **3-Zn**, the presence of two distinct aggregates may therefore be explained by the cooperative self-assembly mechanism of the cofacial H-aggregates instead of being an independent aggregate. In this case, the observed J-aggregate would be the nucleus state in the cooperative supramolecular polymerisation of the H-aggregates.
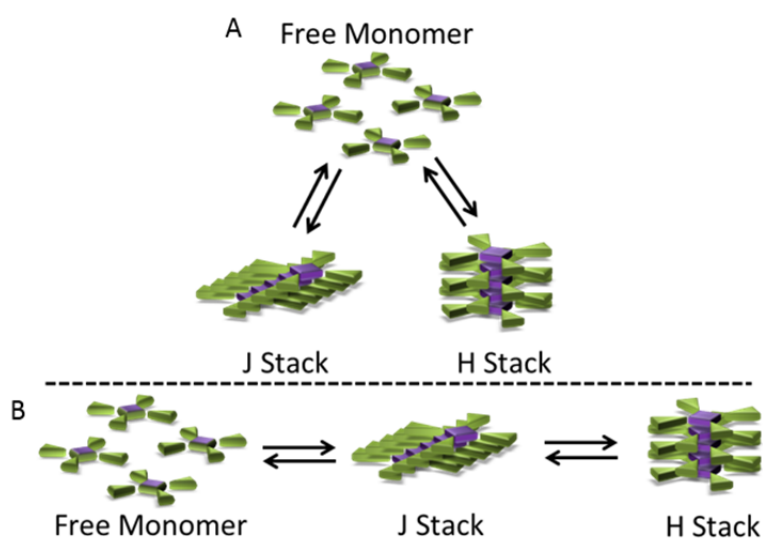
Figure 4.8. Schematic illustration of parallel versus sequential self-assembly pathways of a monomer and two aggregated states.

In order to discern the relation between the two aggregated states observed in porphyrin **3-Zn**, we turn our attention to kinetic experiments on the self-assembly process. Solutions of **3-Zn** in methylcyclohexane (c = 2.5×10^{-6} M) at different temperatures are prepared by injection from a concentrated solution of **3-Zn** in chloroform and allowed to reach equilibrium (Figure 4.9 A). At equilibrium, all porphyrins are aggregated in either H- or J-aggregates, where the magnitude of the Cotton effect at λ = 390 nm corresponds to the amount of H-aggregate present at the various temperatures. The equilibrated solutions are then cooled to T = 293 K and again the Cotton effect at λ = 390 nm is monitored as a function of time. The resulting kinetic curves are compared to the kinetic curves obtained from the experiment where the stock solution is injected into MCH at T = 293 K (Figure 4.9 B). All solutions should over time reach the same equilibrium ratio between H- and J-aggregates and
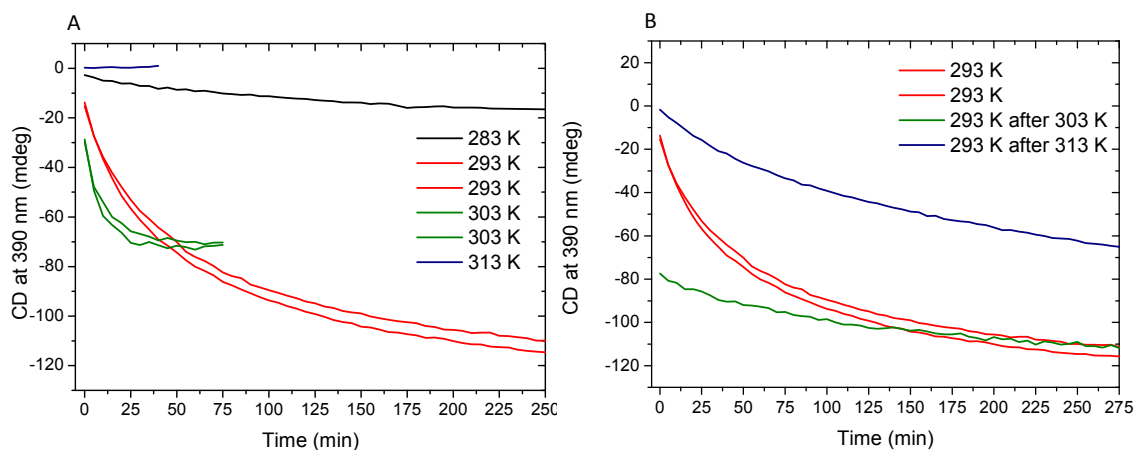
Figure 4.9. Kinetic experiments on aggregate formation of **3-Zn** in MCH (A) (c = 2.5×10^{-3} M, l = 1 cm) by injection from chloroform into MCH at different temperatures. Kinetic experiments on aggregate conversion of **3-Zn** after a temperature step from T = 303 K (green curve) or T = 313 K (blue curve) to T = 293 K, compared to injection form CHCl$_3$ into MCH at T = 293 K (red curve) (B).

thus the same Cotton effect. Interestingly, we observe that the formation of H-aggregates proceeds at a lower rate when J-aggregates are present from the initial equilibration experiment (cool to T = 293 K, Figure 4.9 green and blue curves) than when the self-assembly process is carried out from molecularly dissolved solution (direct injection at T = 293 K, Figure 4.9 red curves). Hence it appears that the presence of J-aggregates of **3-Zn** inhibits the formation of H-aggregates in MCH solution. Furthermore, this inhibition appears stronger when more of the J-aggregate is present in the preaggregated solution (Figure 4.9 B, blue versus green curves). As a result, the H- and J-aggregated states observed in porphyrin **3-Zn** must follow a parallel self-assembly pathway where both aggregated states are in competition for the same monomer (Figure 4.8 A). Re-equilibration from J- to H-aggregates proceeds via disassembly of the J-aggregates to the free monomer and subsequent re-assembly of H-aggregates. This process must be slower than the direct formation of H-aggregates from the molecularly dissolved state. Conversely, the sequential self-assembly pathway would require the preformation of J-aggregates in order to form H-aggregates (Figure 4.8 B). In this case, the H-aggregate formation from the pre-assembled J-stacks should proceed equally fast or faster (not slower) than the self-assembly process from the molecularly dissolved state. Therefore, the sequential self-assembly pathway cannot be operative in porphyrin **3-Zn**. In conclusion, the observation of two different aggregates for porphyrin **3-Zn** cannot be explained by the formation of pre-nucleus aggregates in cooperative supramolecular

polymerisation. Instead, porphyrin **3-Zn** possesses two parallel aggregation pathways that compete for and interconvert through the free porphyrin monomers.

Intrigued by the self-assembly behaviour observed in porphyrin **3-Zn**, we wondered whether the same pathway complexity could also be observed in the other porphyrins. Porphyrin **2-Zn** also shows the coexistence of J- and H-aggregates in MCH solution and a cooling curve measured at the monomer band $\lambda = 419$ nm ($c = 2.5 \times 10^{-5}$ M, rate = 0.5 K/min) shows the occurrence of two aggregation steps (Figure 4.10 A). The first aggregation process starts at T = 360 K, while the second commences around T = 337 K. This observation suggests the occurrence of similar pathway complexity in porphyrin **2-Zn** as in porphyrin **3-Zn**. In porphyrin **2-Zn**, the formation of J-aggregates occurs before the formation of H-aggregates and therefore we also investigated the self-assembly process of exclusively H-aggregating porphyrin **1-Zn**. We recorded assembly curves at specific wavelengths and full UV–Vis and CD spectra for **1-Zn** as a function of temperature (Figure 4.10 B to D). Interestingly, a cooling curve recorded at the monomer absorption band $\lambda = 419$ nm shows the presence of two distinct aggregation processes for **1-Zn** (Figure 4.10 B). The first transition, starting at T = 360 K, appears as an isodesmic self-assembly process in view of the absence of a critical temperature. The second process occurs at T = 335 K and is characteristic of a cooperative supramolecular polymerization. Moreover, when a cooling curve is measured at a wavelength specific for the H-aggregate ($\lambda = 390$ nm), a single cooperative transition is observed in both the optical density and the Cotton effect, which overlaps with the second transition observed in the assembly curve measured at $\lambda = 419$ nm. In the UV–Vis and CD spectra we observed that starting from the molecularly dissolved state (T = 80 °C), the Soret band is diminished in intensity and slightly broadened upon cooling (Figure 4.10 C). These spectral characteristics are similar to the ones observed for porphyrins **3-Zn** and **5-Zn** and suggest the formation of offset-stacked porphyrin J-aggregates. Upon further cooling the solution, the absorption band corresponding to H-aggregates at $\lambda = 390$ nm appears, concomitant with a characteristic Cotton effect (Figure 4.10 D). The above described results indicate that porphyrin **1-Zn** aggregates into two distinct aggregates, though only one type of aggregate is obtained at room temperature in MCH independent of the aggregate preparation method (*vide infra*). Apparently, cofacial H-aggregates of **1-Zn** are more stable than J-aggregates of **1-Zn** and conversion between the two

aggregates via the monomer (Figure 4.8 A) is fast enough to allow the exclusive formation of H-stacks. This is in contrast with the structurally similar porphyrin **3-Zn**, where both aggregate types coexist at room temperature and aggregate conversion via the monomer is much slower. Nevertheless, porphyrin **1-Zn** probably possesses similar pathway complexity as displayed by porphyrin **3-Zn**. The group of Takeuchi has recently reported on the supramolecular assembly of structurally related porphyrins into J- and H-aggregates.[33] Their finding show the J-aggregates to be a metastable state that converts into H-aggregates via the free monomer in a highly cooperative manner. Our results confirm the formation of multiple aggregated states in porphyrin supramolecular polymers that polymerise and depolymerise in a parallel pathway via the free monomer. In contrast, our findings show a coexistence of J- and H-aggregates as relatively stable mixtures of the aggregates are obtained for some of our porphyrins, as opposed to the auto-catalytic aggregate conversion observed by Takeuchi. Combined, the results indicate that both the kinetics and thermodynamics
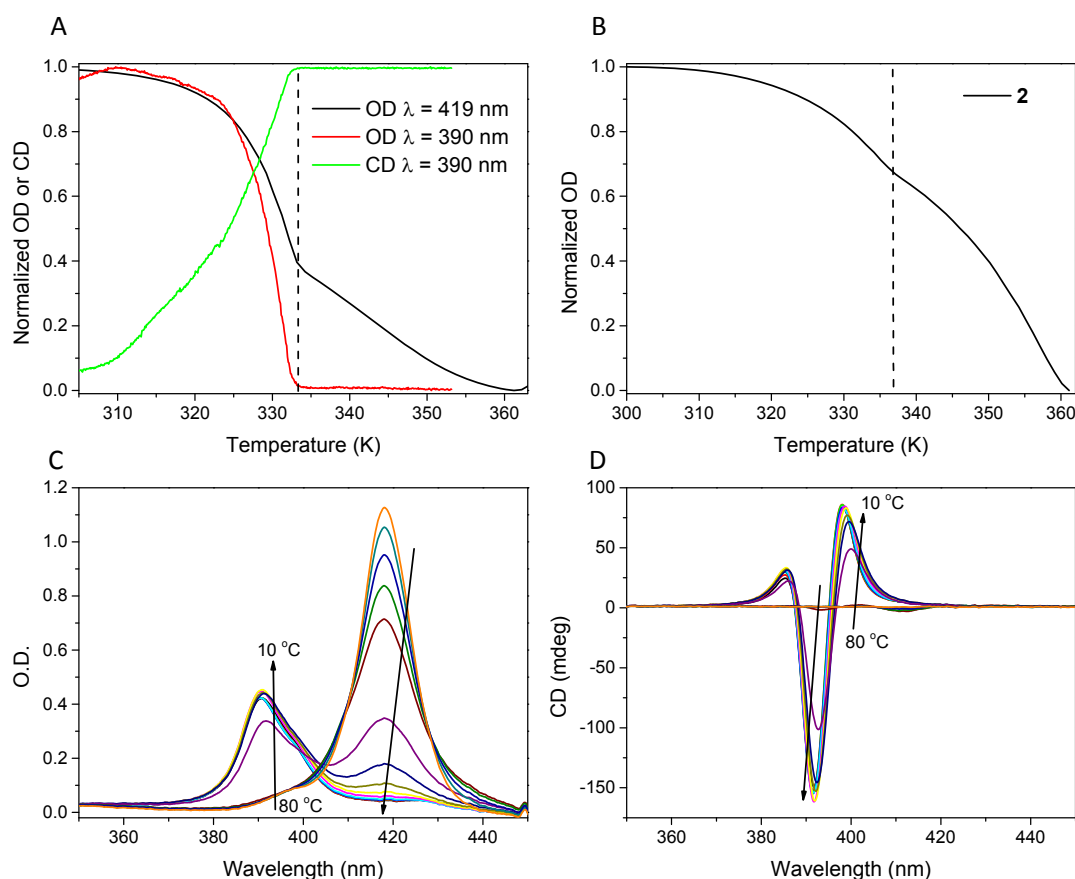
Figure 4.10. Cooling curves of porphyrins **1-Zn** (A) and **2-Zn** (B) (λ = 419 or 390 nm, c = 2.5×10^{-6} M, rate = 0.5 K/min, l = 1 cm) and the corresponding UV–Vis and CD spectra for **2-Zn** as a function of temperature.

of the formation of multiple aggregated states of porphyrins is highly dependent on the peripheral substituents of the porphyrin molecules. For porphyrins **1-Zn** - **5-Zn** presented in this chapter, the alkoxy linkage on the solubilising wedge appears to influence the equilibrium between H- and J-aggregates. Porphyrins **1-Zn** - **3-Zn** (alkoxy linkage) form H-aggregates, while porphyrins **4-Zn** and **5-Zn** exclusively form J-aggregates. The phenyl group of the solubilizing wedge is more electron rich for **1-Zn** - **3-Zn**, possibly resulting in a more acidic amide NH and a stronger hydrogen bond. FT-IR analysis of **1-Zn** - **5-Zn** as solutions in MCH however, proved inconclusive in judging the hydrogen bonds in **1-Zn** - **5-Zn**. Alternatively, the alkoxy linkages may provide additional electrostatic interactions between adjacent porphyrins in the stacked aggregate, thereby favouring cofacial aggregation of the porphyrins over J-aggregation.

4.5 Copper metallated porphyrins

For porphyrin **2-Zn** it was previously found that by changing the porphyrin central metal atom from zinc to copper, the formation of cofacial H-aggregates was promoted with respect to the formation of J-aggregates.[30] To investigate the influence of the central metal atom on our findings of pathway complexity in porphyrin supramolecular systems, we synthesize copper variants of porphyrins **1-Zn** - **5-Zn**. As for the zinc porphyrins, copper porphyrin aggregates were prepared by three different methods and their UV–Vis spectra were recorded (Figure 4.11).
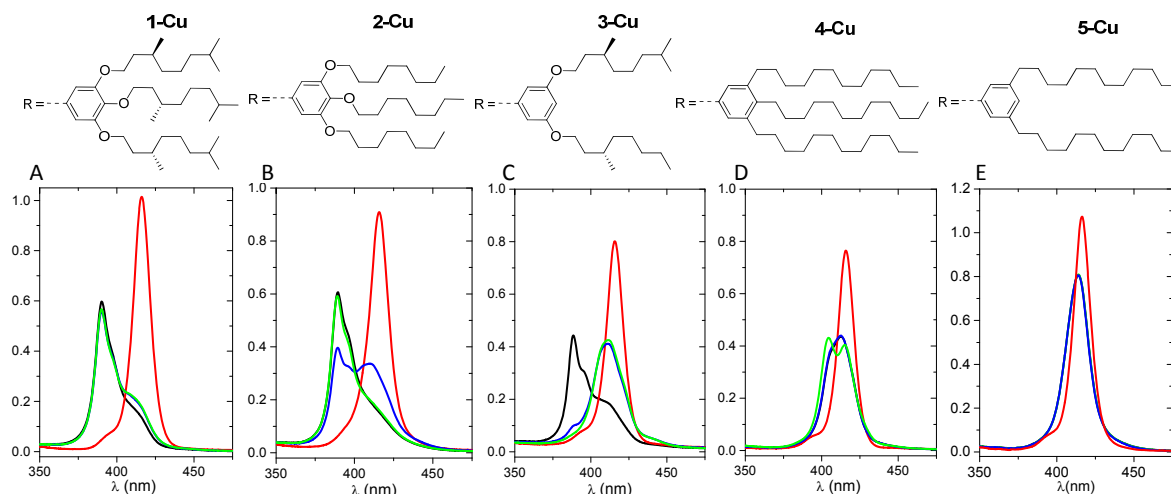
Figure 4.11. UV–Vis spectra recorded for copper metallated variants of porphyrins **1-Cu** - **5-Cu** after different sample preparation (red lines: molecularly dissolved, black lines: injection method, blue lines: quenching method, pink lines: slow cooling method, MCH, c = 2.5×10^{-6} M, l = 1 cm).

Interestingly, copper porphyrins **1-Cu - 5-Cu** show largely similar behaviour when compared to the zinc variants. Porphyrin **1-Cu** forms cofacial H-aggregates and porphyrins **4-Cu** and **5-Cu** form offset stacked J-aggregates, all independent of the aggregate preparation method, similar to the zinc porphyrins. For porphyrin **2-Cu** coexistence of both aggregated states is observed when the aggregates are prepared by quenching a solution from the molecularly dissolved state at elevated temperatures. For porphyrin **3-Cu** both types of aggregates can be obtained in a selective manner by selecting the proper aggregate preparation method.

Similar to our observations for porphyrins **1-Zn** and **2-Zn**, two assembly processes could be identified for porphyrins **1-Cu** and **2-Cu** by slow cooling of solutions from the molecularly dissolved state to the aggregate and measuring their assembly curves (λ = 416 nm, c = 2.5×10^{-6} M) (Figure 4.12). Again, the first assembly process appears isodesmic while the second process appears to be a cooperative aggregation characterised by a critical temperature. For both porphyrins, the H-aggregated state appears thermodynamically more stable and conversion between the two aggregates via the monomer is fast on the time scale of the cooling experiment (rate = 0.5 K/min). The results for porphyrins **1-Cu - 5-Cu** suggest that similar pathway complexity in their aggregation processes exist as in their zinc counterparts and that small changes in the solubilising periphery of the porphyrins have a significant effect on the nature of the self-assembled aggregate formed by these porphyrins.
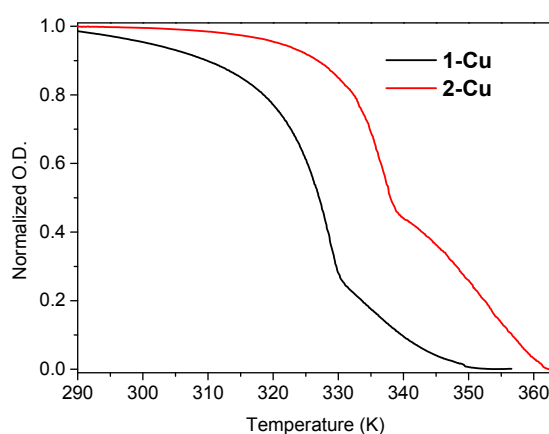
Figure 4.12. UV–Vis cooling curves for porphyrins **1-Cu** and **2-Cu** in methylcyclohexane (c = 2.5×10^{-6} M, l = 1 cm, λ = 416 nm).

4.6 Intermezzo: towards supramolecular porphyrin heteroaggregates and porphyrin systems in water

During our investigations into porphyrin supramolecular systems, an extensive effort was put into the synthesis and characterisation of porphyrins **23-Zn** and **27-Zn** (Figure 4.13). In the case of porphyrin **23-Zn**, elongated one-dimensional porphyrin aggregates in water were targeted with a similar design as used earlier in our group.[30,31] In the case of porphyrin **27-Zn**, the formation of elongated supramolecular heterostacks by complementary hydrogen bonding was envisioned. In both cases the J-aggregation pathway described in this chapter was found to dominate the aggregation processes. SAXS, DLS and DOSY analyses furthermore showed aggregates of **23-Zn** to be small (≈ 5 nm). For porphyrin **27-Zn**, no evidence could be found for the formation of heterostacks with complementary hydrogen-bond motifs by multiple spectroscopic techniques. For both porphyrins various aggregate preparation methodologies were tested to no avail in attempts to selectively prepare cofacial porphyrin H-aggregates. The results are consistent with the observation that the self-assembly of tetra-amidated porphyrins is very sensitive to peripheral modifications.
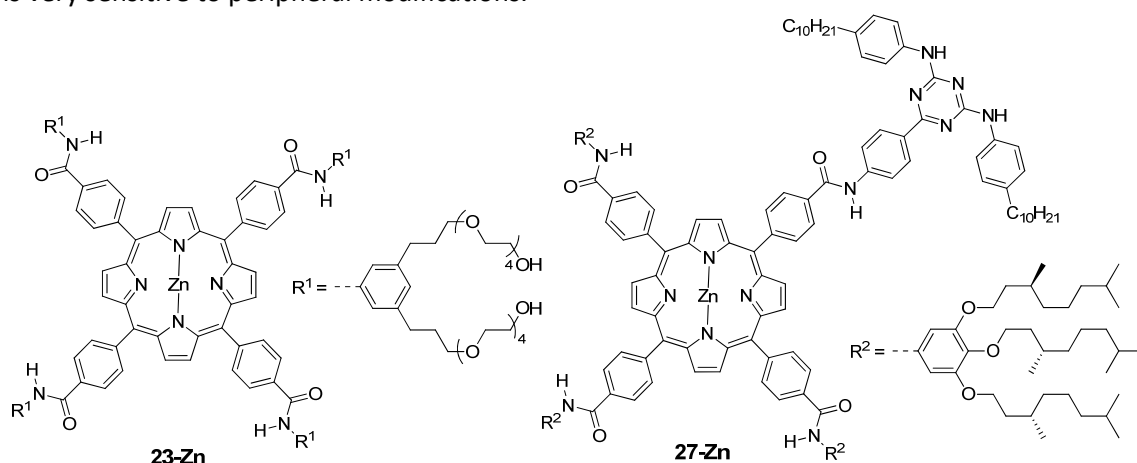
Figure 4.13. Molecular structures of water-soluble porphyrin **23-Zn** and asymmetric, triazine-functionalised porphyrin **27-Zn**.

4.7 Conclusion

The pathway complexity in the self-assembly process of a library of structurally similar tetra-amidated zinc porphyrins has been investigated by spectroscopic techniques. Intriguengly, small changes in the solubilising wedge architecture on the periphery of the porphyrin molecules are shown to have a dramatic effect on the nature of the obtained aggregate. Depending on wedge architecture, either H- or J-aggregates may exclusively occur or coexistence between these species may be observed. Temperature dependent spectroscopy measurements show that the self-assembly mechanisms for H- and J-aggregates are cooperative and isodesmic, respectively. By way of kinetic experiments on the self-assembly process, we

demonstrate that both aggregated states feature parallel self-assembly pathways from the porphyrin monomers and convert via depolymerisation to the free monomer. Furthermore, variable temperature spectroscopy suggests that the competitive pathway of J-type aggregation is also present in porphyrins that ultimately exclusively form H-aggregates at equilibrium conditions. In addition to the molecular architecture, the aggregate preparation method influences the self-assembly process. Depending on the specific self-assembly conditions, different aggregates can be obtained for the same porphyrin. In comparison to recent work by the group of Takeuchi, we similarly find the formation of multiple aggregated states in hydrogen-bonded porphyrin supramolecular systems. In both cases, conversion between aggregate types was found to proceed via depolymerisation to the free monomer. However, our findings show a coexistence of multiple aggregated states instead of one aggregated state being purely metastable as observed by Takeuchi and co-workers.[33] Combined, the results indicate that both the kinetics and thermodynamics of the formation of multiple aggregated states of porphyrins by hydrogen bonding and π-stacking is highly dependent on the peripheral substituents of the porphyrin molecules. For the presented porphyrins, the alkoxy linkages between the phenyl ring and the alkyl chains in the solubilising wedge appear to influence the preference of the system for H- or J-aggregates. To test the generality of the pathway complexity phenomenon in porphyrin supramolecular systems, we have investigated the copper metallated variants of the porphyrin library. Again, the nature of the aggregated state is hugely affected by the porphyrin peripheral architecture. Variable temperature UV–Vis spectroscopy suggests the intermediacy of similar pathway complexity in self-assembly as observed for the zinc porphyrin library.

The results show that porphyrin supramolecular systems are highly sensitive towards variations in the molecular architecture of the solubilising peripheries. A variety of porphyrin based aggregates is accessible by tuning of these peripheral solubilising moieties, leaving the porphyrin core and its optical properties unmodified. The generation of multichromophoric arrays based on porphyrins with control over aggregate size and morphology is relevant with respect to a variety of applications such as artificial photosynthetic systems.[40] Variations in the peripheral porphyrin architecture can thus be used as a tool to control the organisation of

porphyrins in supramolecular architectures without affecting the properties of the individual porphyrin molecules. On the other hand, the pathway complexity that is displayed by the porphyrins described in this chapter also shows limitations to their use as supramolecular motifs. Modular approaches for the creation of functional one-dimensional supramolecular aggregates that depend on the aggregation of mixtures of various symmetrically or asymmetrically substituted monomers into highly reproducible aggregates are limited since structurally similar monomers do not necessarily form structurally similar aggregates.[41, 42]

4.8 Experimental section

Instrumentation, materials and methods

Unless specifically mentioned, reagents and solvents were obtained from commercial suppliers and used without further purification. All solvents were of AR quality. Deuterated chloroform for NMR analyses was provided with TMS as the 0 ppm reference. The methylcyclohexane used in all spectroscopic experiments was of spectroscopic grade. Column chromatography was performed on a Biotage Isolera One using SNAP KP-SNAP columns and solvent gradients. ^{1}H-NMR and ^{13}C-NMR spectra were recorded on a Varian Mercury Vx 400 MHz instrument (100 MHz for ^{13}C) and all chemical shifts are reported in parts per million relative to tetramethylsilane (TMS). MALDI-ToF MS analyses were performed in reflector mode on a PerSeptive Biosystems Voyager-DE Pro using α-cyano-4-hydroxycinnamic acid (CHCA) and 2-[(2E)-3-(4-tert-butylphenyl)-2-methylprop-2-enylidene]malononitrile (DCTB) as matrices. Ultraviolet-visible (UV–Vis) absorbance spectra were recorded on a Jasco V-650 UV–Vis spectrometer with a Jasco ETCR-762 temperature controller. Circular dichroism (CD) spectra were recorded on a JASCO J-815 CD spectrometer with a JASCO PTC-348 temperature controller. Solid state infrared (IR) spectra were recorded on a Perkin Elmer Spectrum One spectrometer equipped with an ATR universal sampler accessory and in dilute solution using 1 mm NaCl cells.

The syntheses of (*S*)-3,7-Dimethyloctyl 4-methylbenzenesulfonate **9** and 3,4,5-tris[(*S*)-3,7-dimethyloctyloxy]aniline **6** were performed according to reference 30.

Synthesis

Methyl 3,5-bis[(S)-3,7-dimethyloctyloxy]benzoate (**10**)

(*S*)-3,7-Dimethyloctyl 4-methylbenzenesulfonate **9** (8.355 g, 26.7 mmol) was dissolved in MIBK (30 mL). To this solution methyl 3,5-dihydroxybenzoate **8** (2.040 g, 12.136 mmol), K_2CO_3 (8.30 g, 60 mmol) and TBAB (0.64 g, 2 mmol) where added and the solution was heated under reflux conditions for 24 hours. MIBK was removed under vacuum and the residue was taken up in DCM (50 mL) and 3 N HCl (50 mL). The product was further extracted from the aqueous layer with DCM (3 x 70 mL) and the combined organic fractions were washed with water (100 mL) and brine (100 mL) and then dried with Na_2SO_4. The suspension was filtered and the filtrate was concentration in vacuo. The residue was purified by column chromatography (gradient of 0% to 10% ethyl acetate in heptane). Yield = 5.03 g. η = 92.3%. ^{1}H-NMR (400 MHz, $CDCl_3$) δ = 7.16 (s, 2H, Ar-H), 6.63 (s, 1H, Ar-H), 3.99 (m, 4H, CH_2-O), 3.90 (s, 3H, O-CH_3), 1.81 (m, 2H, CH_3-*CH*), 1.55 (m, 4H, O-CH_2-*CH₂*), 1.16 (m, 12H, CH_2), 0.95 (d, 6H, CH_3), 0.88, (d, 12H, CH_3). ^{13}C-NMR (100 MHz, $CDCl_3$) δ = 167.1, 160.0, 131.7, 107.6, 106.8, 66.8, 52.3, 39.5, 37.6, 36.0, 29.6, 27.7, 24.5, 22.2, 19.5. MALDI-ToF-MS (m/z) calc. for $C_{28}H_{48}O_4$ 448.36 found 448.40 (M$^-$)$^+$.

3,5-Bis[(S)-3,7-dimethyloctyloxy}benzoic acid (**11**)

Methyl-3,5-bis{(*S*)-3,7-dimethyloctyloxy}benzoate **10** (5.02 g, 11.2 mmol) was dissolved in ethanol (50 mL) and a solution of NaOH (2.24 g, 53.8 mmol) in H_2O (10 mL) was added. The mixture was refluxed for 72 hours. The solvent was evaporated and the residue was partitioned between H_2O and DCM (each 100 mL). The organic layer was neutralized with 1 M HCl (50 mL), washed with H_2O (2 x 50 mL) and brine (50 mL) and then dried with Na_2SO_4. The suspension was filtered and the filtrate was concentration in vacuo to yield a yellow oil. Yield = 3.97 g. η = 81.6%. ^{1}H-NMR (400 MHz, $CDCl_3$) δ = 7.22 (s, 2H, Ar-H), 6.69 (s, 1H, Ar-H), 4.01 (m, 4H, CH_2-O), 1.78 (m, 2H, **CH₃**-*CH*), 1.52 (m, 4H, O-**CH₂**-*CH₂*), 1.19 (m, 12H, CH_2), 0.96 (d, 6H, CH_3), 0.89 (d, 12H, **CH₃**). ^{13}C-NMR (100 MHz, $CDCl_3$) δ = 160.2, 130.9, 108.1, 107.6, 66.6, 39.7, 37.6, 36.3, 29.8, 28.2, 24.5, 22.5, 19.7. MALDI-ToF-MS was inconclusive.

3,5-Bis[(S)-3,7-dimethyloctyloxy]benzoyl azide (**12**)

3,5-Bis[(*S*)-3,7-dimethyloctyloxy]benzoic acid **11** (3.9 g, 8.98 mmol), and triethylamine (1.7 mL) where dissolved in THF (60 mL) and cooled to 0 °C. A solution of ethyl

chloroformate (1.09 mL, 11.4 mmol) in THF (15 mL) was added dropwise. The solution was stirred for 45 minutes at 0 ˚C, the resulting ethyl chloroformate ester was not isolated. A solution of NaN_3 (1.8 g, 27.7 mmol) in water (15 mL) was added; afterwards the solution was stirred for 2 hours while being allowed to warm to room temperature. Water (150 mL) and diethyl ether (150 mL) were added and the layers were separated. The aqueous layer was extracted with diethyl ether (2 x 75 mL) and the combined organic layers were dried with Na_2SO_4. The suspension was filtered and the filtrate was concentration in vacuo to yield a yellow oil. Yield = 4.03 g. η = 94.1%. ^{1}H-NMR (400 MHz, CDCl$_3$) δ = 7.15 (s, 2H, Ar-H), 6.69 (s, 1H, Ar-H), 4.00 (m, 4H, CH$_2$-O), 1.81 (m, 2H, CH$_3$-*CH*), 1.59 (m, 4H, O-CH$_2$-*CH$_2$*), 1.27-1.12 (m, 12H, CH$_2$), 0.92 (d, 6H, CH$_3$), 0.85 (d, 12H, CH$_3$). ^{13}C-NMR (100 MHz, CDCl$_3$) δ = 160.2, 108.1, 107.1, 67.0, 39.5, 37.4, 36.3, 30.1, 28.4, 24.7, 22.7, 20.0.

3,5-Bis[(S)-3,7-dimethyloctyloxy]aniline (**13**)

3,5-Bis[(*S*)-3,7-dimethyloctyloxy]benzoyl azide **12** (4.02 g, 8.75 mmol) was dissolved in dioxane (50 mL) and heated under reflux conditions for 30 minutes. After reflux the solution was cooled to 70 ˚C and slowly added to a solution of tetrabutylammonium hydroxide (40 wt% in water, 8 mL) in dioxane (200 mL) at 90 ˚C via a cannula. The solution was stirred for another 15 minutes at 90 ˚C, allowed to cool to room temperature and dried under vacuum. The residue was partitioned between water (150 mL) and diethyl ether (150 mL) and the layers were separated. The combined organic layers were washed with brine (50 mL), dried using Na_2SO_4, filtered and dried under vacuum. The crude product was purified by column chromatography (gradient of 0% to 15% ethyl acetate in heptane). Yield = 1.14 g. η = 32.0%. ^{1}H-NMR (400 MHz, CDCl$_3$) δ = 5.91 (s, 2H, Ar-H), 5.84 (s, 1H, Ar-H), 3.93 (m, 4H, CH$_2$-O), 1.76 (m, 2H, CH$_3$-*CH*), 1.49 (m, 4H, O-CH$_2$-*CH$_2$*), 1.30-1.17 (m, 12H, CH$_2$), 0.93 (d, 6H, CH$_3$), 0.87 (d, 12H, CH$_3$). ^{13}C-NMR (100 MHz, CDCl$_3$) δ = 161.2, 148.2, 94.3, 92.1, 66.2, 39.2, 37.3, 36.2, 29.9, 28.0, 24.6, 22.7, 22.6, 19.6.

1,2,3-Triiodo-5-nitrobenzene (**15**)

Glacial acetic acid (60 mL) was cooled in an ice bath and 2,6-diiodo-4-nitroaniline (10.3 g, 26.4 mmol) was slowly added. Then a solution of sodium nitrite (3 g, 0.043 mmol) in sulphuric acid (15 mL) was added dropwise and subsequently the mixture was allowed to warm to room temperature. The mixture was stirred until everything

was dissolved (90 minutes) and poured into ice water (200 mL) while stirring. Urea (4.0 g, 66.6 mmol) was added and the mixture was filtered. Potassium iodide (6.0 g, 36.2 mmol) in water (30 mL) was added while stirring. The yellow/brown reaction mixture was then heated to 95 °C for 2 hours. After cooling, sodium bisulphate (5.0 g, 41.6 mmol) was added to quench the excess iodide. The precipitate was filtered of, the crude product was dried under vacuum and purified by column chromatography (gradient of 0% to 30% chloroform in heptane) to afford the product as yellow crystals. Yield = 11.69 g. η = 88.4%. ^{1}H-NMR (400 MHz, CDCl$_3$): δ = 8.62 (s, 2H, Ar-H).

1,2,3-Tri(dodecynyl)-5-nitrobenzene (17)

1,2,3-Triiodo-5-nitrobenzene **15** (3 g, 6 mmol), TEA (100 mL), CuI (112 mg, 0.6 mmol) and bis(triphenylphosphine)-palladium(II) dichloride (256 mg, 0.3 mmol) were charged in a Schlenk tube and the reaction mixture was subjected to five freeze-pump-thaw cycles. The resulting mixture was heated to 80 °C and then 1-dodecyne (3.54 g, 20.9 mmol) was added dropwise under argon counterflow. The resulting mixture was stirred for 4 hours at 80 °C after which the solvent was removed in vacuo. The crude material was purified by column chromatography (gradient of 0% to 10% dichloromethane in heptane). Yield = 3.0 g. η = 82%. ^{1}H-NMR (400 MHz, CDCl$_3$) δ = 8.08 (s, 2H, Ar-H), 2.55 (t, 2H, C≡C-CH$_2$), 2.45 (t, 4H, C≡C-CH$_2$, 1.8-1.0 (m, 48H, aliphatic), 1.90 (t, 9H, CH$_3$).

3,4,5-Triidodecylaniline (18)

1,2,3-Tri(1-dodecynyl)-5-nitrobenzene **17** (3 g, 4.92 mmol) was dissolved in a mixture of ethyl acetate (45 mL) and ethanol (5 mL). Argon was bubbled through the solution for 15 minutes after which Pd/C (300 mg) was carefully added and the mixture was subsequently subjected to H$_2$ in a Parr hydrogenation apparatus. Upon completion of the reaction, the suspension was filtered and the solution was evaporated to dryness. The crude product was purified by column chromatography using heptane as eluent. Yield = 3 g. η = 98%. ^{1}H-NMR (400 MHz, CDCl$_3$) δ = 6.4 (s, 2H, Ar-H), 2.47 (t, 6H, Ar-CH$_2$), 1.6-1.0 (m, 60H, aliphatic), 0.88 (t, 9H, CH$_3$).

1,3-Diiodo-5-nitrobenzene (19)

2,6-Diiodo-4-nitroaniline (10.24 g, 26.67 mmol) was dissolved in ethanol (167 mL) and the solution was cooled to 0 ˚C. Sulphuric acid (14 mL) was added dropwise and the

mixture was heated to 60 ˚C. Sodium nitrite (5.29 g, 77.0 mmol) was slowly added and the mixture was heated under reflux for 3 hours after which the mixture was allowed to cool to room temperature and poured into ice water (200 mL). The resulting solids where filtered of and dried under vacuum. The crude material was recrystallized from iso-propanol to afford greenish needles. Yield = 3.53 g. η = 35.9%. ^{1}H-NMR (400 MHz, CDCl$_3$) δ = 8.52 (s, 2H, Ar-H), 8.37 (s, 1H, Ar-H).

*1,3-Di(1-dodecynyl)-5-nitrobenzene (**20**)*

1,3-Diiodo-5-nitrobenzene **19** (600 mg, 1.6 mmol), TEA (20 mL), CuI (20 mg, 0.11 mmol) and bis(triphenylphosphine)-palladium(II) dichloride (40 mg, 0.057 mmol) were charged in a Schlenk tube and the reaction mixture was subjected to five freeze-pump-thaw cycles. The resulting mixture was heated to 60 °C and 1-dodecyne (532 mg, 3.2 mmol) was added dropwise under argon counterflow. The resulting mixture was stirred for 24 hours at 60 °C after which the solvent was removed in vacuo. The crude material was purified by column chromatography (gradient of 0% to 25% dichloromethane in heptane). Yield = 0.68 g. η = 94.7%. ^{1}H-NMR (400 MHz, CDCl$_3$) δ = 8.08 (s, 2H, Ar-H), 7.66 (s, 1H, Ar-H), 2.41 (t, 4H, J = 7.1 Hz, C≡C-CH$_2$), 1.68 – 1.55 (m, 4H, CH$_2$), 1.50 – 1.39 (m, 4H, CH$_2$), 1.39 – 1.19 (m, 24H, CH$_2$), 0.97 – 0.79 (m, 6H, CH$_3$).

*3,5-Didodecylaniline (**21**)*

1,3-Di(1-dodecynyl)-5-nitrobenzene **20** (0.682 g, 1.51 mmol) was dissolved in a mixture of ethyl acetate (45 mL) and ethanol (5 mL). Argon was bubbled through the solution for 15 minutes after which Pd/C (300 mg) was carefully added and the mixture was subsequently subjected to H$_2$ in a Parr hydrogenation apparatus. Upon completion of the reaction, the suspension was filtered and solution was evaporated to dryness. The crude product was purified by column chromatography using heptane as eluent. Yield = 0.58 g. η = 88.6%. ^{1}H-NMR (200 MHz, CDCl$_3$) δ = 6.42 (s, 1H, Ar-H), 6.35 (s, 2H, Ar-H), 3.5 (b, 2H, NH), 2.47 (s, 4H, Ar-CH$_2$), 1.56 (s, 4H, CH$_2$), 1.40-1.14 (d, 36H, CH$_2$), 0.88 (s, 6H, CH$_3$). ^{13}C-NMR (100 MHz, CDCl$_3$) δ = 144.0, 137.4, 119.3, 112.7, 36.0, 32.1, 31.6, 29.8, 29.6, 29.6, 29.6, 29.5, 29.4, 29.3, 22.5, 14.2. MALDI-ToF-MS (m/z) calc for C$_{30}$H$_{55}$N 429.43 found 429.46 (M$^-$)$^+$.

General procedure for the synthesis of tetra-amide porphyrins

Tetrakis(4-carboxyphenyl)porphyrin **22** was dissolved in chloroform under an argon atmosphere. Oxalyl chloride (30 equivalents) and DMF (2 µL) were added and the mixture was stirred for 3 hours at room temperature. The solvent and all volatiles were removed *in vacuo* and the remaining residue redissolved in chloroform and cooled to 0 °C. A solution of the aniline derivative and DIPEA in chloroform was added dropwise to the acid chloride solution under an argon atmosphere, after which the mixture was stirred for 24 hours at room temperature. Upon completion, the solvent was removed in vacuo and the residue redissolved in chloroform. The organic phase was washed with 1 M HCl (3x), 1 M NaOH (3x) and brine (1x) and dried over sodium sulphate. The crude material was further purified by column chromatography.

*Porphyrin **3***

Tetrakis(4-carboxyphenyl)porphyrin **22** (113 mg, 0.14 mmol) in CHCl$_3$ (15 mL), 3,5-bis[(*S*)-3,7-dimethyloctyloxy]aniline (426 mg, 1.05 mmol) and *N,N*-diisopropylethylamine (0.28 mL) in CHCl$_3$ (15 mL). Column conditions: gradient of 0% to 15% MeOH in CHCl$_3$. Yield = 0.26 g. η = 85.3%. ^{1}H-NMR (400 MHz, CDCl$_3$) δ = 8.84 (s, 8H, ß-pyrrolic protons), 8.32 (d, 8H, Ar-H), 8.24 (d, 8H, Ar-H), 8.08 (s, 4H, NH), 7.04 (s, 8H, Ar-H), 6.37 (s, 4H, Ar-H), 4.08 (m, 16H, CH$_2$-O), 1.85 (m, 2H, CH$_3$-*CH*), 1.59 (m, 16H, O-CH$_2$-CH$_2$), 1.42-1.10 (m, 48H, CH$_2$), 1.01 (d, 24H, CH$_3$), 0.88 (d, 48H, CH$_3$), -2.79 (s, 2H,). ^{13}C-NMR (100 MHz, CDCl$_3$) δ = 165.6, 160.8, 145.6, 139.6, 134.8, 134.6, 125.5, 119.2, 98.9, 66.6, 39.3, 37.3, 36.2, 29.9, 28.0, 24.7, 22.7, 22.6, 19.7. MALDI-ToF-MS (m/z) calc for C$_{152}$H$_{210}$N$_8$O$_{12}$ 2340.61 found 2341.34 (M+H)$^+$.

*Porphyrin **4***

Tetrakis(4-carboxyphenyl)porphyrin **22** (100 mg, 0.13 mmol) in CHCl$_3$ (20 mL, 3,4,5-tridodecylaniline (430 mg, 0.72 mmol) and *N,N*-diisopropylethylamine (218 mg, 1.7 mmol) in CHCl$_3$ (20 mL). Column chromatography conditions: heptane:dichloromethane:ethyl acetate 9:9:1. Yield = 0.30 g. η = 73%. ^{1}H-NMR (400 MHz, CDCl$_3$) δ = 8.87 (s, 8H, ß-pyrrolic protons), 8.35 (d, J = 8.4 Hz, 8H, Ar-H), 8.28 (d, J = 8.4 Hz, 8H, Ar-H), 8.04 (s, 4H, NH), 7.47 (s, 8H, Ar-H), 2.67 (m, 24H), 1.66 (m, 24H), 1.5-1.2 (m, 216H, aliphatic), 0.9 (m, 36H, CH$_3$), -2.81 (s, 2H). ^{13}C-NMR (100 MHz, CDCl$_3$) δ = 165.4, 145.4, 142.1, 135.5, 135.3, 134.9, 134.8, 125.5, 119.1, 118.8, 35.4, 33.4, 31.9, 31.9, 31.8, 31.7, 31.2, 30.3, 30.0, 29.7, 29.7, 29.6, 29.5, 29.4, 29.3, 29.0,

26.4, 26.3, 22.8, 22.7, 22.6, 22.6, 14.1, 14.1. MALDI-ToF MS (m/z) calc for $C_{216}H_{338}N_8O_4$ 3110.66 found 3111.68 (M+H)$^+$.

Porphyrin 5

Tetrakis(4-carboxyphenyl)porphyrin **22** (110 mg, 0.14 mmol) in CHCl$_3$ (20 mL, 3,5-didodecylaniline (343 mg, 0.75 mmol) and *N,N*-diisopropylethylamine (222 mg, 1.7 mmol) in CHCl$_3$ (20 mL). Column chromatography conditions: heptane:chloroform:ethyl acetate 4:3:1. Yield = 0.23 g. η = 56.8%. ^{1}H-NMR (400 MHz, CDCl$_3$) δ = 8.87 (s, 8H, ß-pyrrolic protons) 8.35 (d, 8H, Ar-H), 8.29 (d, 8H, Ar-H), 8.10 (s, 4H, NH), 7.47 (s, 8H, Ar-H), 6.89 (s, 4H, Ar-H), 2.67 (t, 16H Ar-CH$_2$), 1.70 (m, 16H, Ar-CH$_2$-CH$_2$), 1.28 (d, 144H, aliphatic protons), 0.88 (t, 24H, CH$_3$), -2.78 (s, 2H). ^{13}C-NMR (100 MHz, CDCl$_3$) δ = 165.5, 145.3, 144.3, 137.7, 134.7, 127.9, 125.5, 119.1, 117.7, 64.2, 36.3, 31.9, 31.4, 29.6, 22.5, 14.5. MALDI-ToF-MS (m/z) calc. for $C_{168}H_{242}N_8O_4$ 2436.90 found 2437.96 (M+H)$^+$.

General procedure for metal insertion into tetra-amidated porphyrins

For zinc insertion: The free porphyrin base was dissolved in dichloromethane and zinc acetate was added. The mixture was stirred for 24 hours at room temperature and afterwards the solvent was removed in vacuo. The crude mixture was purified using column chromatography.

For copper insertion: The free porphyrin base was dissolved in chloroform and copper(II) acetate was added. The mixture was stirred under reflux conditions for 24 hours and afterwards the solvent was removed in vacuo. The crude mixture was purified using column chromatography.

Porphyrin 3-Zn

Porphyrin **3** (262 mg, 0.11 mmol), zinc acetate (250 mg, 1.34 mmol) and chloroform (10 mL). Column chromatography conditions: gradient of 0% to 15% MeOH in CHCl$_3$. Yield = 243 mg. η = 91%. ^{1}H-NMR (400 MHz, CDCl$_3$) δ = 8.96 (s, 8H, ß-pyrrolic pyrrolic protons), 8.37 (d, 8H, Ar-H), 8.27 (d, 8H, Ar-H), 8.06 (s, 4H, NH), 7.05 (s, 8H, Ar-H), 6.35 (s, 4H, Ar-H), 4.07 (m, 16H, CH$_2$-O), 1.86 (m, 8H, CH$_3$-*CH*), 1.55 (m, 16H, O-CH$_2$-*CH$_2$*), 1.42-1.10 (m, 48H, CH$_2$), 0.99 (d, 24H, CH$_3$), 0.90 (d, 48H, CH$_3$). ^{13}C-NMR (100 MHz, CDCl$_3$) δ = 165.6, 160.7, 149.9, 146.6, 139.5, 134.9, 134.5, 132.2, 125.3, 98.9,

66.6, 39.3, 37.3, 36.2, 29.9, 28.0, 24.7, 22.7, 22.6, 19.7. MALDI-ToF-MS (m/z) calc for $C_{152}H_{210}N_8O_{12}Zn$ 2402.52 found 2403.55 $(M+H)^+$.

Porphyrin *3-Cu*

Porphyrin **3** (191 mg, 0.08 mmol), copper(II) acetate (150 mg, 0.82 mmol) and chloroform (20 mL). Column chromatography conditions: gradient of 0% to 10% MeOH in $CHCl_3$. Yield = 147 mg. η = 75%. MALDI-ToF-MS (m/z) calc. for $C_{152}H_{210}N_8O_{12}Cu$ 2401.52 found 2402.54 $(M+H)^+$.

Porphyrin *4-Zn*

Porphyrin **4** (33 mg, 0.03 mmol), zinc acetate (50 mg, 0.27 mmol) and chloroform (3 mL). Column chromatography conditions: heptane:dichloromethane:ethyl acetate 9:9:1. Yield = 29 mg. η = 86%. ^{1}H-NMR (400 MHz, $CDCl_3$) δ = 8.96 (s, 8H ß-pyrrolic protons), 8.34 (d, J = 8 Hz, 8H, aromatic), 8.23 (d, J = 8 Hz, 8H, aromatic), 8.04 (s, 4H, NH), 7.44 (s, 8H, aromatic), 2.66 (m, 24H), 1.67 (m, 24H), 1.5-1.2 (m, 216H, aliphatic), 0.88 (m, 36H, CH_3). ^{13}C-NMR (100 MHz, $CDCl_3$) δ = 165.4, 145.4, 142.1, 135.5, 135.3, 134.9, 134.8, 125.5, 119.1, 118.8, 35.4, 33.4, 31.9, 31.9, 31.8, 31.7, 31.2, 30.3, 30.0, 29.7, 29.7, 29.6, 29.5, 29.4, 29.3, 29.0, 26.4, 26.3, 22.8, 22.7, 22.6, 22.6, 14.1, 14.1. MALDI-ToF-MS (m/z) calc for $C_{216}H_{336}N_8O_4Zn$ 3172.57 found 3173.61 $(M+H)^+$.

Porphyrin *4-Cu*

Porphyrin **4** (33 mg, 0.03 mmol), copper acetate (50 mg, 0.28 mmol) and chloroform (3 mL). Column chromatography conditions: heptane:dichloromethane:ethyl acetate 9:9:1. Yield = 30 mg. η = 89%. MALDI-ToF-MS (m/z) calc for $C_{216}H_{336}CuN_8O_4$ 3171.57 found 3171.64 $(M^-)^+$.

Porphyrin *5-Zn*

Porphyrin **5** (141 mg, 0.06 mmol), copper acetate (140 mg, 0.76 mmol) and chloroform (15 mL). Column chromatography conditions: heptane:chloroform:ethyl acetate 4:3:1. Yield = 145 mg. η = 99%. ^{1}H-NMR (400 MHz, $CDCl_3$) δ = 8.89 (s, 8H, ß-pyrrolic protons) 8.27 (d, 8H, Ar-H), 8.13 (d, 8H, Ar-H), 8.13 (s, 4H, NH), 7.39 (s, 8H, Ar-H), 6.86 (s, 4H, Ar-H), 2.63 (t, 16H Ar-CH_2), 1.66 (m, 16H, Ar-CH_2-C**H_2**), 1.34-1.28 (d, 144H, aliphatic protons), 0.87 (t, 24H, CH_3). ^{13}C-NMR (100 MHz, $CDCl_3$) δ = 165.6, 149.8, 146.3, 144.0, 137.8, 134.6, 134.3, 132.1, 125.2, 120.0, 117.5, 45.6, 36.1, 31.9,

31.5, 29.7, 29.7, 29.6, 29.6, 29.5, 29.4, 22.7, 14.1. MALDI-ToF-MS (m/z) calc for $C_{168}H_{240}N_8O_4Zn$ 2498.81 found 2498.83 $(M^.)^+$.

*Porphyrin **5-Cu***

Porphyrin 5 (71 mg, 0.03 mmol), copper acetate (80 mg, 0.44 mmol) and chloroform (20 mL). Column chromatography conditions: gradient of 0% to 10% MeOH in $CHCl_3$. Yield = 66 mg. η = 92%. MALDI-ToF-MS (m/z) calc for $C_{168}H_{240}N_8O_4Cu$ 2497.82 found 2498.84 $(M+H)^+$.

Synthesis of porphyrin 23-Zn

3,6,9,12-Tetraoxapentadec-14-yn-1-ol (**24**)

Tetraethyleneglycol (10 g, 51.5 mmol) was dissolved in anhydrous THF (30 mL). Sodium hydride (60%, 1.24 g, 51.5 mmol) was added and the mixture was stirred for 5 minutes. 3-bromoprop-1-yne (80% in toluene, 6.5 g, 50.5 mol) was slowly added and the mixture was stirred for 24 hours at room temperature. The solids were filtered of and the filtrate was concentrated in vacuo. The resulting brown oil was dissolved in water (100 mL). The disubstituted product was extracted with toluene (2 x 50 mL) and the mono-substituted product was subsequently extracted from the aqueous layer with DCM (8 x 50 mL). The combined organic fractions where dried with $MgSO_4$, filtered and concentrated in vacuo to give a yellow oil. Yield = 5.37 g. η = 89.7%. ^{1}H-NMR (400 MHz, $CDCl_3$) δ = 4.21 (s, 2H, CΞC-CH_2), 3.67 (s, 14H, CH_2), 3.61 (s, 2H, CH_2-OH), 2.52 (s, 1H, OH), 2.42 (s, 1H, CΞC-H).

15,15'-(5-nitro-1,3-phenylene)bis(3,6,9,12-tetraoxapentadec-14-yn-1-ol) (**25**)

1,3-Diiodo-5-nitrobenzene (**19**) (2.47 g, 6.86 mmol), 3,6,9,12-tetraoxapentadec-14-yn-1-ol (**23**) (1.99 g, 8.60 mmol), bis(triphenylphosphine)-palladium(II) dichloride (121 mg, 0.17 mmol) and CuI, (60 mg, 0.32 mmol) were dissolved in triethylamine (80 mL) and put under an argon atmosphere. Five freeze-pump-thaw cycles were performed after which the mixture was heated to 35 °C and allowed to stir for 48 hours. The resulting suspension was filtered and the filtrate was concentrated in vacuo. The residue was purified using column chromatography (gradient chloroform to ethanol over 10 column volumes) to result in the title compound. Yield = 0.81 g. η = 63.3%. ^{1}H-NMR (400 MHz, $CDCl_3$) δ= 8.19 (s, 2H, Ar-H), 7.76 (s, 1H, Ar-H), 4.43 (s, 4H, CΞC-CH_2), 3.68-3.62 (m, 28H, O-CH_2-*CH_2*), 3.60 (t, 4H, CH_2-OH) 2.54 (s, 2H, -OH). ^{13}C-NMR

(100 MHz, CDCl$_3$) δ = 105.1, 67.6, 63.7, 39.3, 37.1, 36.2, 31.1, 29.6, 28.1, 24.7, 22.6, 19.6, 13.9. MALDI-ToF-MS (m/z) calc for C$_{28}$H$_{41}$NO$_{12}$ 583.26 found 606.26 (M+Na)$^+$.

15,15'-(5-amino-1,3-phenylene)bis(3,6,9,12-tetraoxapentadecan-1-ol) (**26**)

15,15'-(5-nitro-1,3-phenylene)bis(3,6,9,12-tetraoxapentadec-14-yn-1-ol) (**25**) (810 mg, 1.44 mmol) was dissolved in a mixture of ethyl acetate (36 mL) and ethanol (4 mL) and bubbled with argon for 30 minutes. Pd/C was added and the mixture was subsequently subjected to H$_2$ in a Parr hydrogenation apparatus. After 24 hours, the catalyst was filtered and the solvent removed in vacuo. The residue was purified by column chromatography (gradient chloroform to ethanol over 10 column volumes Yield = 0.75 g. η = 96.5%. ^{1}H-NMR (400 MHz, CDCl$_3$) δ = 6.42 (s, 1H, Ar-H), 6.38 (s, 2H, Ar-H), 3.77-3.59 (m, 28H, O-CH$_2$-CH$_2$), 3.46 (t, 4H, CH$_2$-OH), 2.55 (t, 4H, Ar-CH$_2$), 1.88 (t, 4H, CH$_2$). ^{13}C NMR (100 MHz, CDCl$_3$) δ = 146.4, 143.0, 119.1, 113.0, 76.7, 72.9, 72.6, 70.6, 70.6, 70.6, 70.3, 70.1, 70.0, 61.7, 61.6, 32.1, 31.0. LC-MS (m/z) calc for C$_{28}$H$_{51}$NO$_{10}$ 561.35 found 562.38 (M+H)$^+$.

*Porphyrin **23***

Tetrakis(4-carboxyphenyl)porphyrin (**22**) (113 mg, 0.14 mmol) was dissolved in THF (15 mL) and 15,15'-(5-amino-1,3-phenylene)bis(3,6,9,12-tetraoxapentadecan-1-ol) (**26**) (100 mg, 0.18 mmol) and DMT-MM (42 mg, 15 mmol) were added. The mixture was stirred for 48 hours at room temperature. The solvent were removed in vacuo and the crude residue was purified by column chromatography (gradient methanol 0% to 20% in chloroform over 15 column volumes), followed by preparative LC (50% to 90% acetonitrile in water). Yield = 0.022 g. η = 24.6%. ^{1}H-NMR (400 MHz, CDCl$_3$) δ = 9.15 (s, 4H, NH$_2$), 8.85 (s, 8H, ß-pyrrolic protons), 8.33 (s, 16H, porphyrin-Ar-H), 7.61 (s, 8H, Ar-H), 6.87 (s, 4H, Ar-H), 3.68 (s, 141H, CH$_2$-CH$_2$-O), 3.54 (s, 16H, CH$_2$-OH), 2.77 (s, 16H, Ar-CH2), 2.00 (s, 16H, Ar-CH$_2$-*CH$_2$*), -2.77 (s, 2H, pyrrole N-H). ^{13}C-NMR (100 MHz, CDCl$_3$) δ = 166.4, 145.1, 142.9, 138.6, 135.1, 134.6, 125.8, 124.6, 119.4, 118.1, 76.7, 72.7, 70.6, 70.6, 70.6, 70.5, 70.5, 70.2, 70.1, 61.6, 32.3, 31.2. LC-MS (m/z) calc for C$_{160}$H$_{226}$N$_8$O$_{44}$ 2965.53 found 742.67 (M+4H)$^{4+}$.

*Porphyrin **23-Zn***

Porphyrin **23** (20 mg, 6.7 μmol), zinc acetate (20 mg, 0.11 mmol) and DCM (5 mL). Yield = 20 mg. η = 99.9%. ^{1}H-NMR (400 MHz, CDCl$_3$) δ = 9.18 (s, 4H, NH$_2$), 8.84 (s, 8H,

ß-pyrrolic protons), 8.23 (s, 16H, Ar-H), 7.48 (s, 8H, Ar-H), 6.77 (s, 4H, Ar-H), 3.58 (s, 141H, CH_2-CH_2-O), 3.35 (s, 16H, CH_2-OH), 2.62 (s, 16H, Ar-CH2), 1.85 (s, 16H, Ar-CH_2-CH_2). ^{13}C-NMR (100 MHz, CDCl$_3$) δ = 180.8, 172.6, 166.4, 149.7, 146.6, 142.7, 138.6, 134.5, 131.7, 125.5, 124.6, 119.8, 118.2, 76.7, 72.2, 70.3, 70.2, 70.2, 70.1, 69.8, 69.7, 61.1, 32.2, 30.9, 23.0. LC-MS (m/z) calc for $C_{160}H_{224}N_8O_{44}Zn$ 3026.49 found 758.25 (M+4H)[4+].

Synthesis of porphyrin 27-Zn

4-Decylaniline hydrochloride (28)

4-Decylaniline (1.55 g, 6.64 mmol) was dissolved in chloroform (50 mL) and 4 M HCl in dioxane (2 mL) was added slowly. The mixture was stirred for 15 minutes under argon and subsequently evaporated to dryness. The crude material was used without further purification

Di(4-decylphenyl)biguanide (29)

4-Decylaniline hydrochloride (28) (1.55 g, 5.74 mmol) and $NaN(CN)_2$ (0.24 g, 5.46 mmol) were dissolved in ethanol (100 mL). The mixture was stirred for 18 hours at 85 °C under an argon atmosphere and afterwards concentrated in vacuo. The residue was taken up in ethyl acetate (100 mL) and 1 M NaOH (100 mL). A solid precipitate was formed on the interface of the aqueous and organic layer. The solid was isolated and washed with 1 M NaOH (2 x 10 mL) and water (2 x 10 mL) and subsequently dried under vacuum. Yield = 442 mg. η = 49%. ^{1}H-NMR (400 MHz, CDCl$_3$) δ = 10.1 (b, 2H, C=NH), 7.5 (b, 3H, NH), 7.1 (m, 2H, Ar-H), 2.5 (t, 4H), 1.2 (m, 32H), 0.8 (t, 6H). MALDI-ToF MS (m/z) calc for $C_{34}H_{55}N_5$ 533.45 found 534.48 (M+H)[+], 556.51 (M+Na)[+].

N^2-N^4-Bis(4-decylphenyl)-6-(4-nitrophenyl)-1,3,5-triazine-2,4-diamine (30)

Di(4-decylphenyl)biguanide (29) (247 mg, 0.47 mmol) was dissolved in chloroform (11 mL) and dimethylacetamide (11 mL). The solution was cooled to 0 °C and subsequently a solution of 4-nitrobenzoylchloride (85 mg, 0.46 mmol) in chloroform (12 mL) was added dropwise under an argon atmosphere. The mixture was stirred at room temperature for 15 hours and subsequently heated for 4 hours at 70 °C. The solvents were removed in vacuo and the residue purified by column chromatography (10% ethyl acetate in heptane). Yield = 229 mg. η = 74%. ^{1}H-NMR (400 MHz, CDCl$_3$) δ

= 8.6 (d, J = 9 Hz, 2H), 8.3 (d, J = 9 Hz, 2H), 7.5 (d, J = 8.4 Hz, 4H), 7.2 (d, J = 8.4 Hz, 4H), 7.1 (b, 2H, NH), 2.6 (t, J = 7.2 Hz, 4H), 1.3 (m, 32H), 0.9 (t, 6H). MALDI-ToF MS (m/z) calc for $C_{41}H_{56}N_6O_2$ 654.45 found 665.39 (M+H)$^+$.

6-(4-Aminophenyl)-N^2,N^4-bis(4-decylphenyl)-1,3,5-triazine-2,4-diamine (**31**)

N^2-N^4-Bis(4-decylphenyl)-6-(4-nitrophenyl)-1,3,5-triazine-2,4-diamine (**30**) was dissolved in ethyl acetate (60 mL) and bubbled with argon for 30 minutes. Pd/C was added and the mixture was subsequently subjected to H_2 in a Parr hydrogenation apparatus. After 24 hours, the catalyst was filtered and the solvent removed in vacuo. The crude material was purified by column chromatography (20% ethyl acetate in heptane). Yield = 175 mg, η = 80%. ^{1}H-NMR (400 MHz, CDCl$_3$) δ = 8.2 (d, J = 8.6 Hz, 2H), 7.6 (d, J = 8.4 Hz, 4H), 7.2 (d, J = 8.4 Hz, 4H), 7.0 (b, 2H, NH), 6.7 (d, J = 8.8 Hz, 2H), 4.0 (b, 2H, NH$_2$), 2.6 (t, 4H), 1.3 (m, 32H), 0.9 (m, 6H). ^{13}C-NMR (100 MHz, CDCl$_3$): δ = 164.5, 149.9, 138.0, 136.2, 130.2, 128.7, 120.6, 114.2, 35.4, 31.9, 29.7, 29.5, 29.3, 22.7, 14.1. MALDI-ToF MS (m/z) calc for $C_{41}H_{58}N_6$ 634.47 found 635.41 (M+H)$^+$.

*Porphyrin **32***

Tetrakis(4-carboxyphenyl)porphyrin (**22**) (1.00 g, 1.26 mmol), 3,4,5-tris[(*S*)-3,7-dimethyloctyloxy]aniline (**6**) (2.13 g, 3.79 mmol, 3 eq.), PyBOP (2.9 g, 5.56 mmol, 4.4 eq.) and *N*,*N*-diisopropylethylamine (2.2 mL, 12.65 mmol, 10 eq.) were dissolved in dimethylacetamide (60 mL) and stirred at room temperature for 15 hours under an argon atmosphere with protection from light. The solvent was removed by vacuum evaporation and the residue redissolved in CHCl$_3$ (250 mL). The organic phase was washed with 1 M HCl (3 x 200 mL), 1 M NaOH (3 x 200 mL), H$_2$O (1 x 200 mL) and brine (1 x 200 mL). The organic phase was dried over Na$_2$SO$_4$, filtered and concentrated by vacuum evaporation to yield a dark red solid. The crude product was purified by column chromatography using first chloroform/heptane/ethyl acetate in a 4:4:1 ratio to remove tetra-substituted porphyrin **2** (R$_f$ = 0.8 in 5% ethanol/toluene) followed by a gradient of ethanol (0 − 5%) in toluene over 20 column volumes to give the product (R$_f$ = 0.2 in 5% ethanol/toluene) as a red solid. Yield = 0.42 g. η = 13.7%. ^{1}H-NMR (400 MHz, CDCl$_3$) δ = 8.86 (s, 8H, ß-pyrrolic protons), 8.53 (d, *J* = 8.1 Hz, 2H), 8.36 (d, *J* = 7.0 Hz, 8H), 8.28 (d, *J* = 8.1 Hz, 6H), 8.03 (s, 3H, NH), 7.10 (s, 6H), 4.10 (m, 12H), 4.05 (m, 6H), 2.0-0.9 (m, 171 H), -2.8 (s, 2H). MALDI-ToF MS (m/z) calc for $C_{156}H_{225}N_7O_{14}$ 2421.71, found 2421.77 (M$^-$)$^+$.

Porphyrin 27

Porphyrin **32** (120 mg, 50 µmol) and 6-(4-aminophenyl)-N2,N4-bis(4-decylphenyl)-1,3,5-triazine-2,4-diamine **31** (68 mg, 42 µmol) were dissolved in dimethylacetamide (10 mL) and PyBOP (41 mg, 79 µmol) and *N,N*-diisopropylethylamine (35 µL, 200 µmol) were added. The mixture was stirred at room temperature under an argon atmosphere with protection from light for 20 hours. The solvent was removed in vacuo and the residue taken up in chloroform (50 mL). The organic phase was washed with 1 M HCl (3 x 30 mL), 1 M NaOH (3 x 30 mL) and brine (1 x 30 mL). The organic layer was dried over Na_2SO_4, filtered and concentrated in vacuo. The crude material was purified by column chromatography using chloroform/heptane/ethyl acetate in a 4:4:1 ratio as eluent. A second purification was performed by preparative TLC (5% ethanol in toluene) to yield the target compound. Yield = 30 mg. η = 20%. ^{1}H-NMR (400 MHz, $CDCl_3$) δ = 8.9 (s, 8H, ß-pyrrolic protons), 8.5 (d, J = 9.2 Hz, 2H), 8.4 (m, 16H), 8.1 (3H, NH), 8.1 (d, J = 9.2 Hz, 2H), 7.7 (b, 1H, NH) 7.5 (d, J = 8.8 Hz, 4H), 7.2 (m, 4H), 7.1 (b, 2H, NH) 7.1 (s, 6H), 4.0 (m, 18H), 2.6 (m, 4H), 2.0-0.9 (m, 209 H), -2.8 (s, 2H). MALDI-ToF MS (m/z) calc for $C_{197}H_{281}N_{13}O_{13}$ 3039.18, found 3040.21 (M+H)[+].

Porphyrin 27-Zn

Porphyrin **27** (20 mg, 8.2 µmol), zinc acetate (20 mg, 0.11 mmol) and DCM (5 mL). The crude material was purified by column chromatography using chloroform/heptane/ethyl acetate in a 4:4:1 ratio as eluent. Yield = 11 mg. η = 55%. ^{1}H-NMR (400 MHz, $CDCl_3$) δ = 8.9 (s, 8H, ß-pyrrolic protons), 8.5 (d, J = 9.2 Hz, 2H), 8.4 (m, 16H), 8.1 (3H, NH), 8.1 (d, J = 9.2 Hz, 2H), 7.7 (b, 1H, NH) 7.5 (d, J = 8.8 Hz, 4H), 7.2 (m, 4H), 7.1 (b, 2H, NH) 7.1 (s, 6H), 4.0 (m, 18H), 2.6 (m, 4H), 2.0-0.9 (m, 209 H). ^{13}C-NMR.[43] MALDI-ToF MS (m/z) calc for $C_{197}H_{279}N_{13}O_{13}Zn$ 3101.09, found 3102.11 (M+H)[+].

4.9 References

[1]   S. Ganapathy, S. Sengupta, P.K. Wawrzyniak, V. Huber, F. Buda, U. Baumeister, F. Würthner, H.J.M. de Groot, M.R. Wasielewski, *PNAS*, 2009, **106**, 11472

[2]   P. Thordarson, E.J.A. Bijsterveld, A.E. Rowan, R.J.M Nolte, *Nature*, 2003, **424**, 915

[3]   G. Steinberg-Yfrach, P.A. Liddell, S.C. Hung, A.L Moore, D. Gust, T.A. Moore, *Nature*, 1997, **385**, 239

[4]   M.C. O'Sullivan, J.K. Sprafke, D.V. Kondratuk, C, Rinfray, T.D.W. Claridge, A. Saywell, M.O. Blunt, J.N. O'Shea, P.H. Beton, M. Malfois, H.L. Anderson, *Nature*, 2011, **469**, 72

[5]   T. van der Boom, R.T. Hayes, Y.Y. Zhao, P.J. Bushard, E.A. Wiess, M.R. Wasielewski, *J. Am. Chem. Soc.*, 2002, **124**, 9582

[6]   M.R. Wasielewski, *Chem. Rev.*, 1992, **92**, 435

[7]   V. Schurig, F. Betschinger, *Chem. Rev.*, 1992, **92**, 873

[8]   B. Meunier, *Chem. Rev.*, 1992, **92**, 1411

[9]   Y. Murakami, J. Kikuchi, Y. Hisaeda, O. Hayashida, *Chem. Rev.*, 1996, **96**, 721

[10]   G. S. Kottas, L.I. Clarke, D. Horinek, J. Michi, *Chem. Rev.*, 2005, **105**, 1281

[11]   I. Beletskaya, V.S. Tyurin, A.Y. Tsivadze, R. Guilard, C. Stern, *Chem. Rev.*, 2009, **109**, 1659

[12]   C.M. Drain, A. Varotto, I. Radivojevic, *Chem. Rev.*, 2009, **109**, 1630

[13]   R. Bonnett, *Chem. Soc. Rev.*, 1995, **24**, 19

[14]   P. Rothemund, *J. Am. Chem. Soc.*, 1935, **57**, 2010

[15]   P. Rothemund, *J. Am. Chem. Soc.*, 1936, **58**, 625

[16]   J.S. Lindsey, I.C. Schreiman, H.C. Hsu, P.C. Kearney, A.M. Marguerettaz, *J. Org. Chem.*, 1987, **52**, 827

[17]   J.S. Lindsey, *The Porphyrin Handbook*, 2000, **1**, 45

[18]   M.O. Senge, *Chem. Commun.*, 2011, **47**, 1943

[19]   M.J. Ahrens, R.F. Kelley, Z.E.X. Dance, M.R. Wasielewski, *Phys. Chem. Chem. Phys.*, 2007, **9**, 1469

[20]   R. van Hameren, P. Schon, A.M. van Buul, J. Hoogboom, S.V. Lazarenko, J.W. Gerritsen, H. Engelkamp, P.C.M. Christianen, H.A. Heuts, J.C. Maan, T. Rasing, S. Speller, A.E. Rowan, J. Elemans, R.J.M. Nolte, *Science*, 2006, **314**, 1433

[21]   R. van Hameren, A.M. van Buul, M.A. Castriciano, V. Villari, N. Micali, P. Schon, S. Speller, L.M. Scolaro, A.E. Rowan, J. Elemans, R.J.M. Nolte, *Nano Lett.*, 2008, **8**, 253

[22]   M. Shirakawa, S. Kawano, N. Fujita, K. Sada, S. Shinkai, *J. Org. Chem.*, 2003, **68**, 5037

[23]   M. Shirakawa, N. Fujita, S Shinkai, *J. Am. Chem. Soc.*, 2005, **127**, 4164

[24]   N. Nagata, S. Kugimiya, W. Fujiwara, Y. Kobuke, *New. J. Chem.*, 2003, **27**, 743

[25]   R. Takahashi, Y. Kobuke, *J. Am. Chem. Soc.*, 2003, **125**, 2372

[26]   K. Ogawa, Y. Kobuke, *Angew. Chem. Int. Ed.*, 2000, **39**, 4070

[27]   F.J.M. Hoeben, M. Wolffs, J. Zhang, S. de Feyer, P. Leclère, A.P.H.J. Schenning, E.W. Meijer, *J. Am. Chem. Soc.*, 2007, **129**, 9819

[28]   M. Wolffs, F.J.M. Hoeben, E.H.A. Beckers. A.P.H.J. Schenning, E.W. Meijer, *J. Am. Chem. Soc.*, 2005, **127**, 13484

[29]   F. Helmich, C.C. Lee, A.P.H.J. Schenning, E.W. Meijer, *J. Am. Chem. Soc.*, 2010, **132**, 16753

[30]   F. Helmich, *PhD thesis*, 2012, Eindhoven University of Technology

[31]   F. Helmich, C.C. Lee, M.M.L. Nieuwenhuizen, J.C. Gielen, P.C.M. Christianen, A. Larsen, G. Fytas, P.E.L.G. Leclere, A.P.H.J. Schenning, E.W. Meijer, *Angew. Chem. Int. Ed.*, 2010, **49**, 3939

[32]   P.A. Korevaar, S.J. George, A.J. Markvoort, M.M.J. Smulders, P.A.J. Hilbers, A.P.H.J. Schenning, T.F.A. de Greef, E.W. Meijer, *Nature*, 2012, **481**, 492

[33]   S. Ogi, K. Sugiyasu, S. Manna, S. Samitsu, M. Takeuchi, *Nature Chemistry*, 2014, **6**, 188

[34] X. Zhang, Z. Chen, F. Würthner, *J. Am. Chem. Soc.*, 2007, **129**, 4886

[35] Z. Chen, V. Stepanenko, V. Dehm, P. Prins, L.D.A. Siebbeles, J. Seibt, P. Marquetand, V. Engel, F. Würthner, *Chem. Eur. J.*, 2007, **13**, 436

[36] P. Griefs, *Liebigs Ann. Chem.*, 1860, **113**, 201

[37] D.F. DeTar, T. Kosuge, *J. Am. Chem. Soc.*, 1958, **80**, 6072

[38] T.J. Broxton, J.F. Bunnett, C.H. Paik, *J. Org. Chem.*, 1977, **42** 643

[39] C. Görl, N. Beck, K. Kleiber, H.G. Alt, *J. Mol. Cat. A: Chem.,* 2012, **352**, 110

[40] C. Röger, Y. Miloslavina, D. Brunner, A.R. Holzwarth, F. Würthner, *J. Am. Chem. Soc.*, 2008, **130**, 5929

[41] L. Albertazzi, D. van der Zwaag, C.M.A. Leenders, R. Fitzner, R.W. van der Hofstad, E.W. Meijer, *Science*, 2014, **344**, 491

[42] W. Zhang, W.S. Jin, T. Fukushima, A. Saeki, S. Seki, T. Aida, *Science,* 2011, **334**, 340

[43] The low amount of material rendered ^{13}C-NMR inconclusive.

5

Supra-amphiphiles by hydrogen bonding between perylene bisimides and triazines

Abstract

The formation of supra-amphiphiles by complementary hydrogen bonding between perylene bisimides and triazines is investigated. A perylene bisimide is functionalised with tetra(ethyleneoxy) or dodecyl side-chains and a triazine with tetra(ethylene)oxy or dodecyloxy side-chains to introduce solubility in polar and apolar media. The self-assembly of the perylene moieties into aggregates and with triazine moieties into heteroaggregates by hydrogen bonding and π-stacking is investigated and we find it to be very similar in water and methylcyclohexane. Mixed systems of hydrophilic and hydrophobic subunits in binary solvent mixtures are found to stabilise emulsions by the formation of supra-amphiphiles. The resulting emulsion phases are stabilised by supramolecular interactions and are stable over prolonged periods of time. In a next step, we extend the approach towards supra-amphiphiles for the stabilisation of water-in-water emulsions. To this end, the triazine subunit is decorated with sugar side-groups to induce solubility in dextran-rich aqueous solutions. Unfortunately, PEG-solutions containing the perylene subunit prove unstable and formed perylene precipitates both over time and in contact with the triazine-containing dextran-solution. Nevertheless, the presented approach shows that supra-amphiphiles by hydrogen bonding are applicable as efficient stabilisers for water/oil emulsions and show great promise to be extended to the stabilisation of all-aqueous emulsions and to be applied for the generation of complex supramolecular architectures on liquid/liquid interfaces.

5.1 Introduction

Amphiphiles belong to an important class of molecules in the field of supramolecular self-assembly and feature in a wide array of applications ranging from drug delivery[1-4], nano/microreactors, and artificial enzyme mimicking[5-9] to templates for the processing of well-defined materials[10-12] and stabilisers for emulsions.[13-14] Conventional amphiphilic molecules contain covalently linked hydrophilic and hydrophobic moieties which provide aqueous solubility and a driving force for self-assembly respectively. Supramolecular amphiphiles, or supra-amphiphiles, are a new class of amphiphiles, differing from conventional amphiphiles by the replacement of the covalent bond between the hydrophilic and hydrophobic moieties by a non-covalent or dynamic covalent linkage.[15-18] Supra-amphiphiles provide opportunities for modular synthesis of components, stimuli responsive behaviour and the facile formation of functional self-assembled systems by hierarchical self-assembly.

The use of supra-amphiphiles by hydrogen bonding for the formation of bilayer membranes in aqueous solutions was first reported by Kunitake *et al.*[19-21] They showed that a melamine substituted with aliphatic side-chains and a cyanuric acid derivative bearing a quaternary ammonium head group resulted in the formation of hydrogen-bond mediated bilayer membranes. Our group has reported on the use of hydrogen-bond interactions to perform the non-covalent synthesis of supramolecular dendritic architectures in water. Here, hydrophobic dendrimers were non-covalently functionalised with hydrophilic solubilising groups to induce solubility in aqueous media and the complex can be termed a supra-amphiphile. Subsequently, a variety of other non-covalent interactions such as host-guest complexation[22-24], metal-ligand coordination[25-26], electrostatic attraction[27], charge transfer interaction[28,29], π-π interaction[30] and coiled-coil peptide interaction[29] have been utilised in the formation of supra-amphiphiles and their subsequent assembly into complex architectures in aqueous solutions. Notable examples of the formation of supra-amphiphiles have been reported by Zhang and co-workers (Figure 5.1). Based on previous work by Jeon and co-workers, a supramolecular glycolipid was for example constructed through the complexation of an alkyl viologen with a sugar-appended naphthalene inside cucurbit[8]uril (Figure 5.1 A).[23,24] The supramolecular glycolipids formed vesicle-like aggregates where the sugar moieties decorated the outer surface. In another

example, bola-form supra-amphiphiles were prepared by mixing bola-form amphiphiles functionalised with electron-poor and electron-rich moieties (Figure 5.1 B). Upon the formation of a charge-transfer complex, bola-form supra-amphiphiles were obtained, which subsequently self-assembled into 1D or 2D nanostructures depending on the directionality of the charge transfer interaction and the connectivity of the naphthalene subunits.
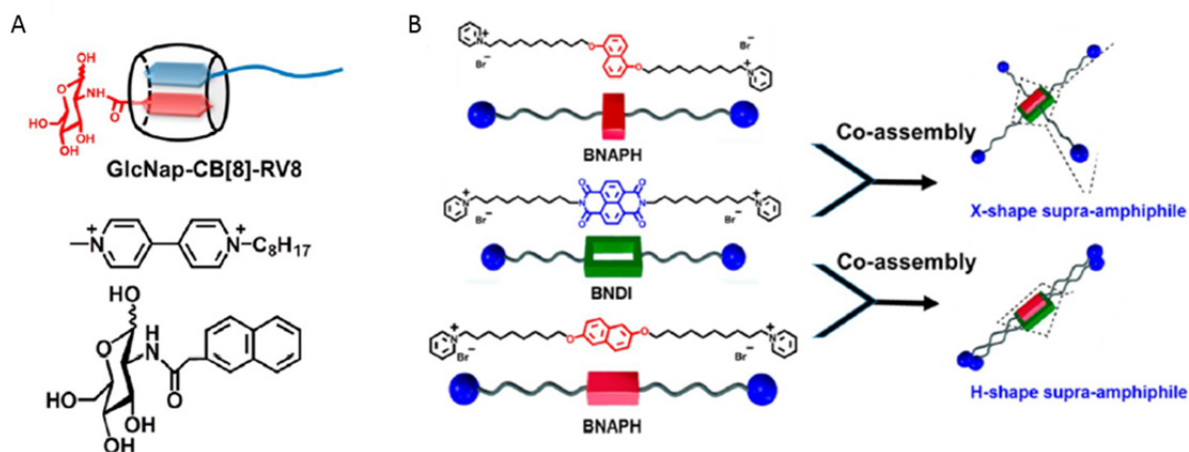
Figure 5.1. A) The formation of a supra-amphiphile by cucurbit[8]uril complexation of viologen and naphthalene derivatives. B) The formation of bola-form supra-amphiphiles by the formation of charge-transfer complexes between naphthalene diimide and naphthalene diimide and other naphthalene derivatives. Images adapted from reference 17.

To date, supra-amphiphiles have been investigated in the context of their self-assembly in aqueous solutions and aqueous solvent mixtures but rarely in binary solvent systems. Controlled self-assembly of (functional) supra-amphiphiles on the interface of immiscible solvents potentially may be valuable for the stabilisation of microemulsions, eventually leading to a variety of applications such as artificial photosynthetic systems.[32,33] In the first part of this chapter we describe the formation of supra-amphiphiles based on hydrogen bonded architectures for self-assembly at the oil/water interface. The hydrogen-bond motifs used for this study are the perylene bisimide and triazine compounds described in Chapters 2 and 3 which are equipped with either hydrophilic or hydrophobic side-chains, respectively (Figure 5.2). In the second part of this chapter we attempt to extend this approach to water-in-water or all aqueous emulsions in collaboration with the group of Dr. A.H.C. Shum (University of Hong Kong).
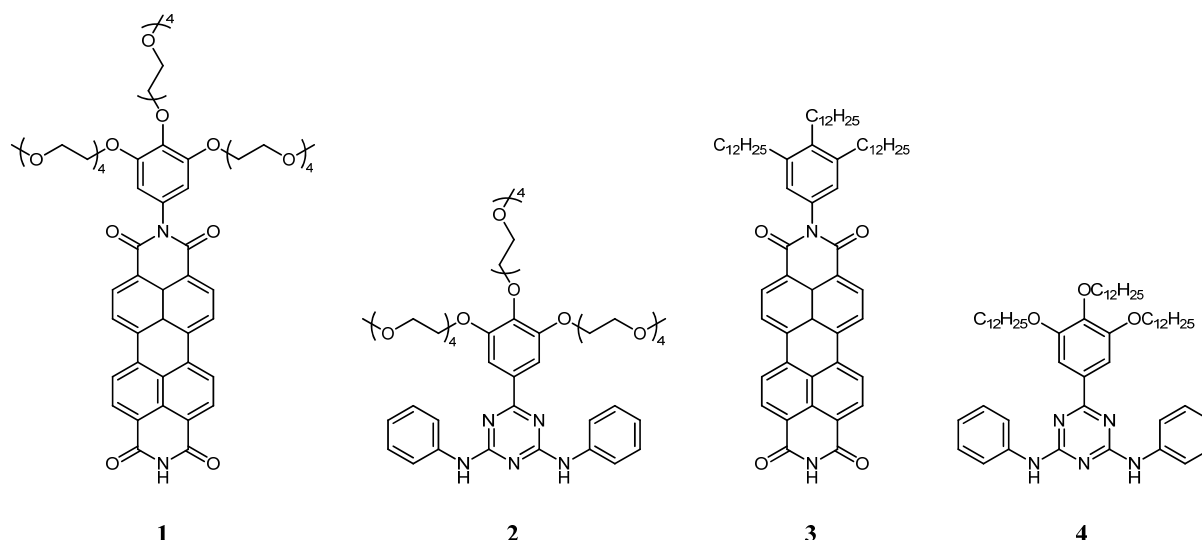
Figure 5.2. Perylene bisimides **1** and **3** and triazines **2** and **4** bearing tetra(ethyleneoxy) and dodecyl or dodecyloxy side-chains respectively, for the formation of supra-amphiphiles.

5.2 Molecular design and synthesis

Perylene bisimide self-assembly has been studied in great detail in both polar[34,35] and apolar solvents[36] and has been found to produce highly similar aggregates in both solvent types.[37] Therefore, we choose to use the complementary hydrogen-bond couple of asymmetric perylene bisimides and triazines described in Chapter 3 for the formation of supra-amphiphiles by hydrogen bonding. The hydrophobic moieties in this study are perylene **3** decorated with dodecyl and triazine **4** decorated with dodecyloxy side-chains. To induce water solubility to these hydrogen-bond moieties we replaced the dodecyl(oxy) side-chains with tetra(ethyleneoxy) side-chains, a strategy that has previously been applied successfully for solubilising perylene bisimides as well as other self-assembling molecules in aqueous solutions.[30,38-40]

The synthesis of tetra(ethyleneoxy)-substituted perylene bisimide **1** and triazine **2** is outlined in Scheme 5.1. Gallic acid derivative **5**, kindly provided by Jolanda Spiering, was subsequently treated with ethyl chloroformate and sodium azide to form acyl azide **6** in good yield. Next, the acyl azide (**6**) was converted into its isocyanate analogue by a Curtius rearrangement and the latter was subsequently hydrolysed to obtain aniline derivative **7** in 84% yield after column chromatography. Next, aniline **7** was reacted with perylene mono-anhydride **8** in imidazole using zinc acetate as a

catalyst to yield asymmetric perylene bisimide **1** in a decent yield of 55% after column chromatography. For the synthesis of triazine **2**, gallic acid derivative **5** was converted to acid chloride **9** by treatment with oxalyl chloride in THF. Acid chloride **9** was then reacted with diphenylbiguanide (**10**) in a mixture of chloroform and dimethylacetamide in a two-step reaction (amide formation and ring closure) to yield triazine **2** in 60% yield after column chromatography. Perylene **1** and triazine **2** were fully characterized by NMR spectroscopy and MALDI-ToF spectrometry, proving that **1** and **2** were isolated as highly pure compounds.
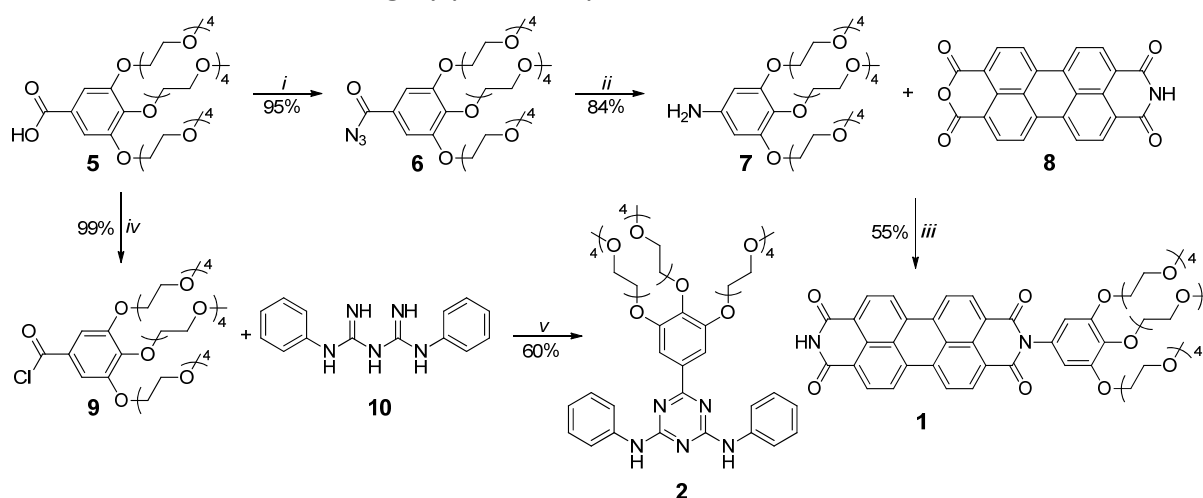
Scheme 5.1. Synthetic scheme towards water-soluble perylene bisimide **1** and triazine **2**. Reagents and conditions: i) ethyl chloroformate, TEA, THF; NaN$_3$, H$_2$O, THF, RT; ii) dioxane, 100 °C; tetrabutylammonium hydroxide; iii) Zn(OAc)$_2$, imidazole, 140 °C; iv) C$_2$Cl$_2$O$_2$, DMF, THF, RT; v) Et$_3$N, DMA, CHCl$_3$, 0 °C to 70 °C.

5.3 Self-assembly of in aqueous solution

Before investigating the interfacial self-assembly of supra-amphiphiles based on **1 - 4**, we first evaluate the self-assembly of water-soluble perylene **1** and triazine **2** in aqueous solutions by UV–Vis spectroscopy to verify whether their self-assembly behaviour is similar to that of **3** and **4** in apolar solvents. The absorption spectrum of PBI **1** in water (c = 5×10^{-5} M) shows similar spectral characteristics as aliphatic PBI **3** in methylcyclohexane (MCH) as described in Chapter 2 (Figure 5.3 A). For perylene **1**, the absorption maximum in the molecularly dissolved state (λ = 512 nm in CHCl$_3$) displays a hypsochromic shift (λ = 483 nm) and the development of a bathochromically shifted shoulder (λ = 556 nm) upon aggregation in H$_2$O. Gratifyingly, the observed spectral features for **1** are consistent with cofacial H-aggregates of PBIs

in aqueous solution and are very similar to the spectral features observed for PBI **3** in MCH, suggesting the formation of similar aggregates in both solvents.[28]
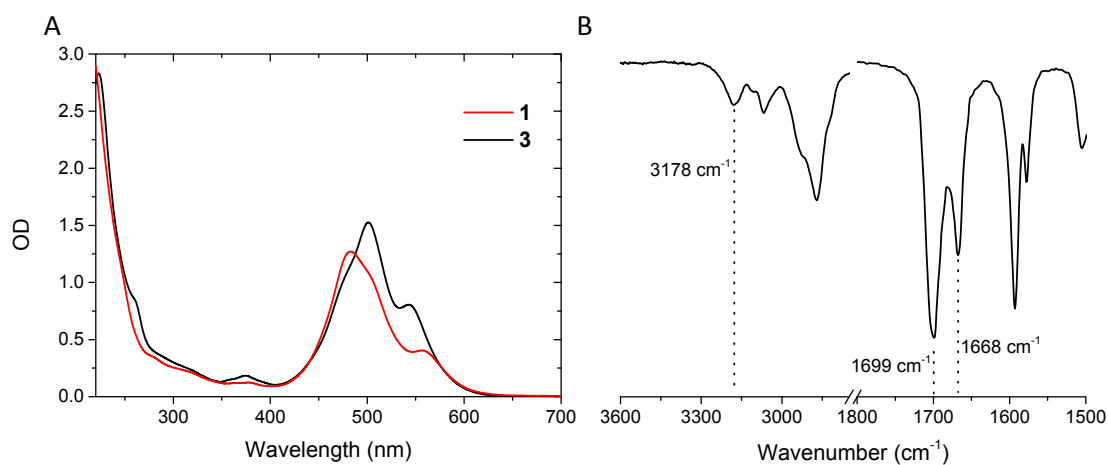
Figure 5.3. UV–Vis spectra of **1** and **3** in H_2O and MCH respectively (A) (c = 5×10^{-5} M, l = 1 cm, T = 20 °C). FT-IR spectrum of **1** drop cast from THF (B).

In Chapter 2, we showed that PBI **3** in MCH forms aggregates consisting of stacked, hydrogen-bonded dimers and that the shape of the carbonyl vibration in infrared spectroscopy was sensitive to hydrogen bonding. Therefore, infrared spectroscopy was measured on aqueous solutions (H_2O and D_2O) of **1** (c = 1×10^{-4} M, CaF_2 cell, l = 1 mm). Unfortunately the absorption of water in the region of interest interferes with the determination of hydrogen bonding in aqueous solution. However, a drop-cast film of PBI **1** from THF displays the NH stretching vibration at 3178 cm^{-1} and the carbonyl vibrations at 1699 cm^{-1} and 1668 cm^{-1}, which are similar in position and shape as measured for PBI **1** in the solid state and in MCH solution (Figure 5.3 B). We can therefore conclude that in the solid state the tetra(ethyleneoxy)-chains present in **1** do not interfere with hydrogen bonding of **1** and that **1** forms aggregates consisting of hydrogen-bonded, π-stacked dimers. Possibly, PBI **1** also forms aggregates of stacked dimers in aqueous environment, though direct measurement of the twofold hydrogen bond in water remains elusive. Elucidation of the self-assembly mechanism from cooling curves for **1** proved impractical owing to typical lower critical solution temperature behaviour of the methoxy-terminated tetra(ethyleneoxy) side-chains.

Next, we have turned our attention to the heterocomplexation and subsequent π-stacking of triazine **2** with PBI **1**. Upon addition of aliquots of triazine **2** to a solution

of PBI **1** in water (c = 5×10^{-5} M), the perylene absorption spectrum changes significantly (Figure 5.4). The absorption maximum is red-shifted from λ = 483 nm to λ = 518 nm and a shoulder is developed at λ = 560 nm; as observed for perylene **3** and triazine **4** (Chapter 3) and characteristic for the formation of stacked perylene-triazine heterodimers. After the addition of two equivalents of triazine **2**, no further significant changes in the perylene absorption spectrum are observed. Similar to our observations for their alkylated counterparts (**3** and **4**, Chapter 3), the non-stoichiometric amounts of **2** needed for the formation of pure heteroaggregates **1:2** most likely stem from the competition between homo- and heteroaggregates of PBI **1** with itself or triazine **2**, respectively.
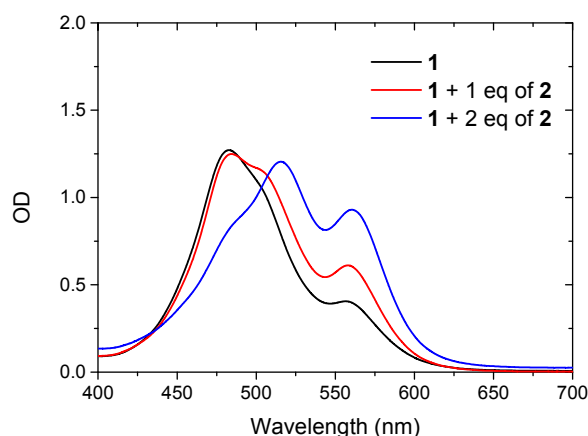
Figure 5.4. UV–Vis spectra for PBI **1** with increasing amounts of triazine **2** in water (c = 5×10^{-5} M, l = 1 cm, T = 20 °C).

The similarity in spectroscopic behaviour of **1** and **2** compared to hydrophobic counterparts **3** and **4** suggests that the self-assembly behaviour of mixtures of **1** and **2** in aqueous solutions is similar compared to mixtures of hydrophobic compounds **3** and **4** in MCH. Perylene **1** forms aggregates consisting of stacked dimers by itself and stacked heterodimers in combination with triazine **2**.

5.4 Self-assembly at the oil-water interface

To investigate the heterocomplexation of compounds **1 - 4** into supra-amphiphiles by hydrogen bonding, we prepared separate solutions of **1** and **2** in water and **3** and **4** in MCH (c = 5×10^{-5} M). In the next step, we mixed the water and MCH solutions (0.5 mL each) to obtain mixed systems with equimolar amounts of

water- and MCH-soluble hydrogen-bonding motifs. The resulting binary systems were thoroughly mixed for 60 seconds with a vortex mixer, after which emulsions were obtained (Figure 5.5). For both perylene-triazine mixtures (**1:4** and **2:3**) as well as for the perylene-perylene mixture (**1:3**) creaming of the emulsions is observed, resulting in a dense layer of droplets of the dispersed phase in the continuous phase on top of a clear layer of continuous phase. The triazine-triazine (**2:4**) combination proved unsuccessful in the stabilisation of water/MCH emulsions. For all emulsions after creaming, the droplets of the dispersed phase are localised at the top of the vial, suggesting a lower density for the dispersed phase. Therefore, the dispersed phase is likely MCH (ρ = 0.77 g/cm^3), while the continuous phase is water (ρ = 1 g/cm^3). The creamed emulsions are found to be remarkably stable over time (months) at ambient conditions as no visible demixing was observed.
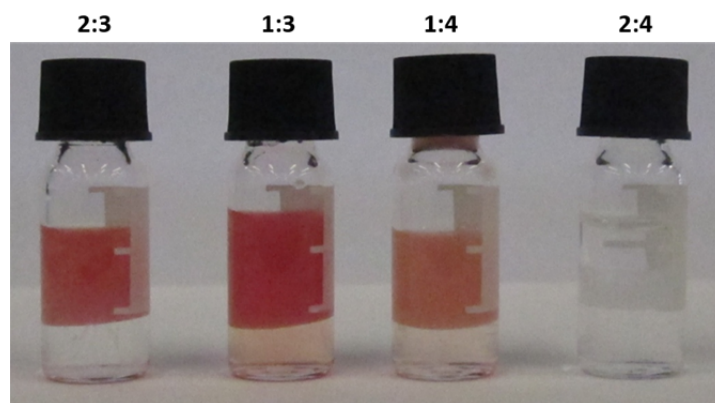
Figure 5.5. Photographs of vials containing emulsions of a binary mixture of water (0.5 mL) and MCH (0.5 mL) and 5×10^{-5} M of supra-amphiphile after vortex mixing.

Control experiments were performed where compounds **1 - 4** were individually applied to the binary solvent mixture. No stable emulsions were obtained, indicating that compounds **1 - 4** lack the amphiphilic character to stabilise water/MCH emulsions. The stabilisation observed for the mixtures must therefore be related to the formation of supra-amphiphiles by hydrogen bonding (Figure 5.6). Furthermore, the colour of the emulsion phases suggests the presence of stacked perylene-perylene or perylene-triazine aggregates as the emulsion phases are similar in colour to solutions of stacked aggregates in single solvents. The hydrogen-bonded supra-amphiphiles thus aggregate further through π-stacking interactions, which stabilises the water/MCH emulsions.
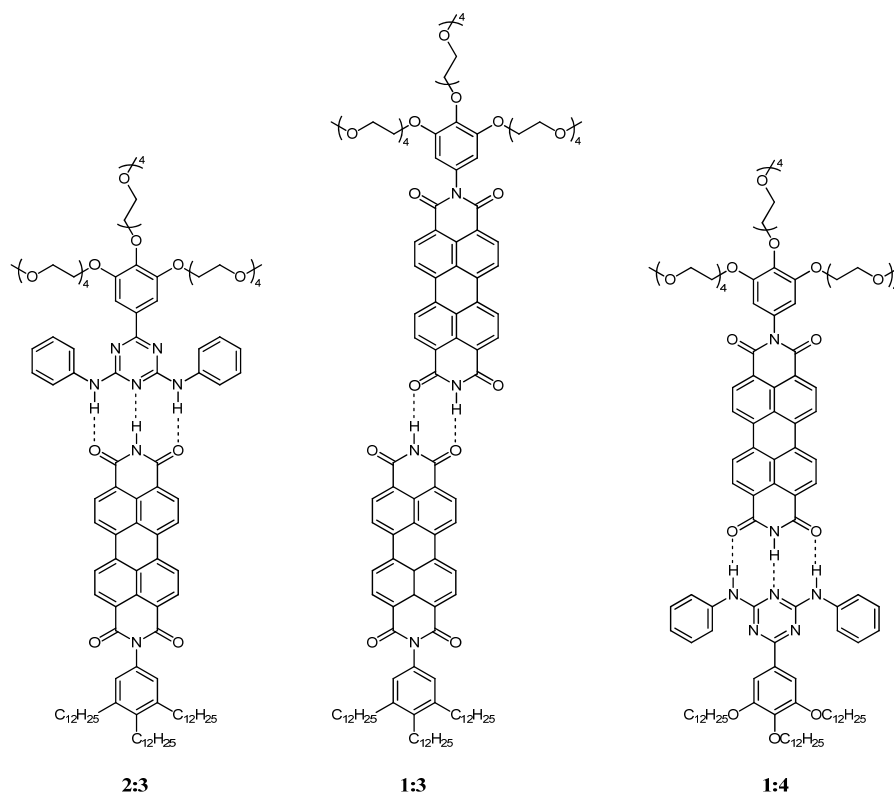
Figure 5.6. Molecular structure of supra-amphiphiles **2:3**, **1:3** and **1:4** formed by complementary hydrogen bonding.

We further characterised the water/MCH emulsions formed by supra-amphiphiles **2:3**, **1:3** and **1:4**, by optical microscopy (Figure 5.7). A droplet of the above described creamed emulsion was transferred to a glass substrate and imaged. For all emulsions, polydisperse droplets are observed with sizes ranging from 10 to 200 μm. The results indicate that the supra-amphiphiles efficiently stabilise droplets of the dispersed phase in the continuous phase.
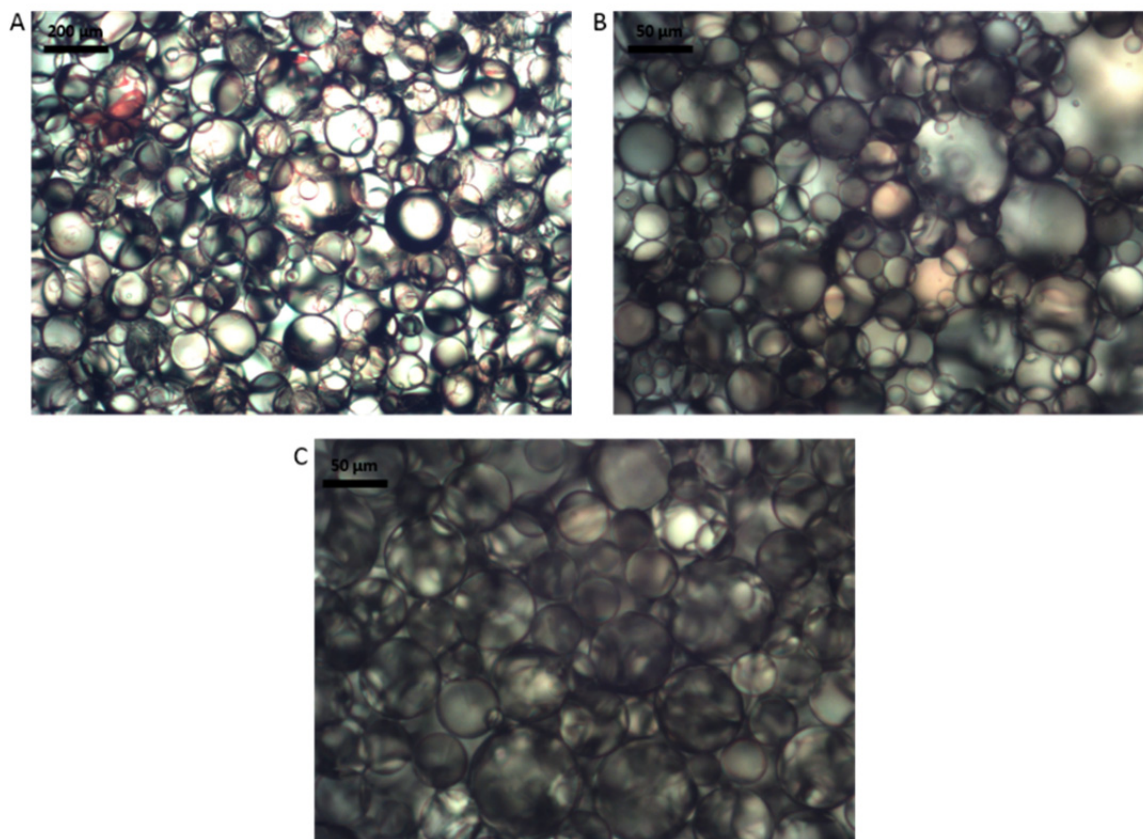
Figure 5.7. Optical microscopy images of water/MCH emulsions formed by complementary hydrogen-bonded supra-amphiphiles **1:3** (A), **2:3** (B) and **1:4** (C). c = 5×10^{-5} M, 0.5 mL MCH, 0.5 mL H$_2$O, vortex mix.

The creamed emulsion of **1:3** was further investigated with confocal fluorescence microscopy. Perylene **3** is highly fluorescent in both the molecularly dissolved and the aggregated state. Perylene **3** shows mirror image fluorescence to the UV–Vis spectrum with a small Stokes shift ($\lambda_{max,abs}$ = 510 nm, $\lambda_{max,fl}$ = 518 nm) and a broad red-shifted fluorescence from λ = 600 to 750 nm. On the other hand, the fluorescence of PBI **1** is completely quenched. Similar behaviour has previously been observed in the groups of Würthner and Langhals, where bay-unsubstituted PBIs decorated with benzo-ether substituents on the *N*-positions showed a completely quenched fluorescence, which was attributed to intramolecular charge-transfer.[39,40] Furthermore, heterocomplexation of PBI **3** with triazine **2** also results in a completely quenched fluorescence. Therefore, the confocal fluorescence experiments are limited to the fluorescent emulsion of **1:3**. A droplet of the creamed water/MCH emulsion of **1:3** (c = 5×10^{-5} M was investigated with confocal fluorescence microscopy (Figure 5.8). The monomeric and aggregated states of the PBIs were simultaneously excited
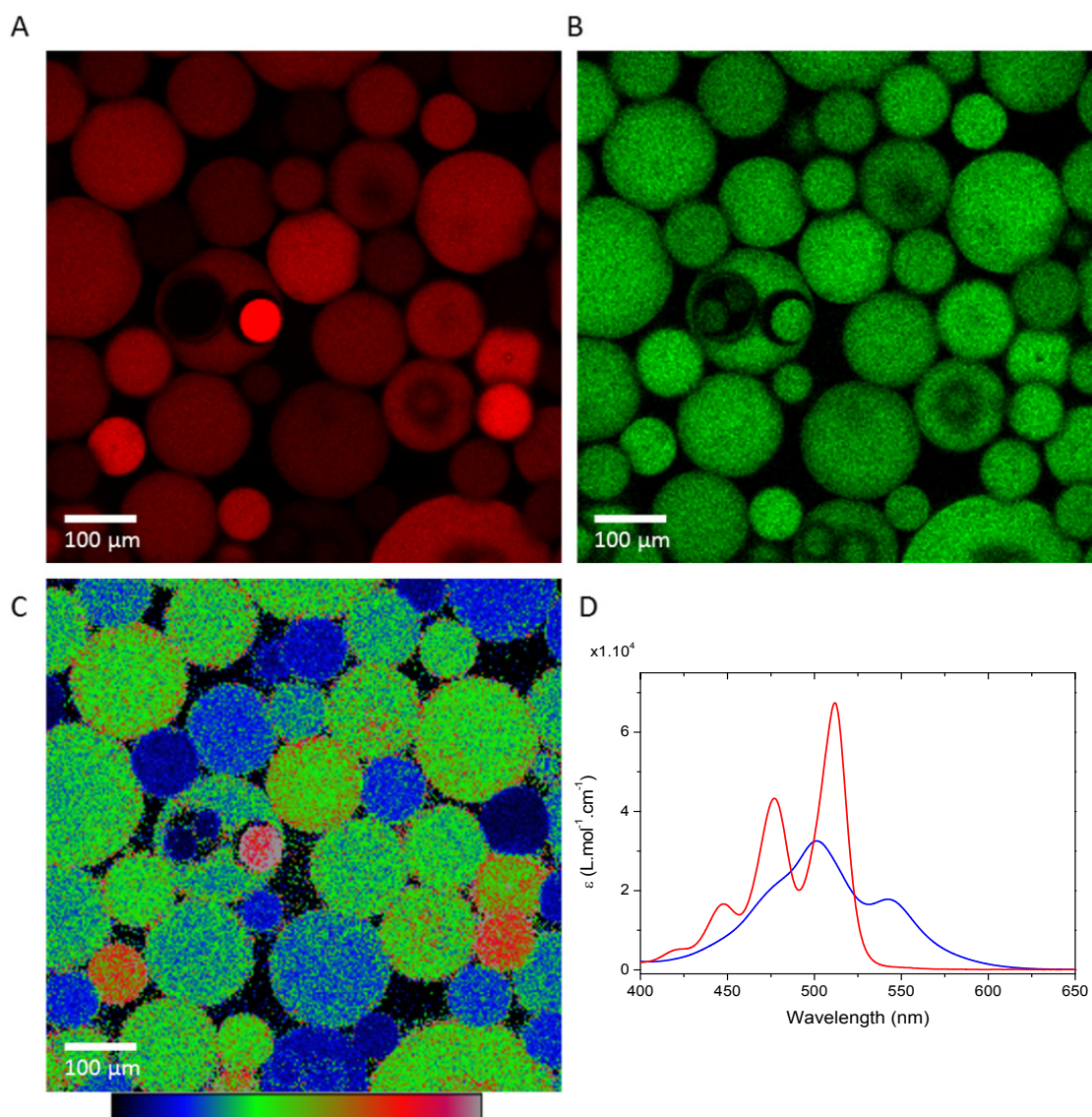
Figure 5.7. Confocal fluorescence microscopy on creamed water/MCH emulsion of **1:3** (c = 5×10^{-5} M), false coloured images (λ_{ex} = 475 nm). A: Fluorescence at λ = 560 nm (monomer). B: Fluorescence at λ = 675 nm (aggregate). C: Ratiometric fluorescence image: I$_{675}$/I$_{475}$, scale bad depicts increasing (blue to red) aggregate to monomer ratio. D: UV–Vis spectra of PBI **1** in the molecularly dissolved state (red line) and aggregated state (blue line).

at λ = 475 nm and the fluorescence was recorded at λ = 560 nm (monomer) and λ = 675 nm (aggregate), respectively. Consistent with the optical microscopy experiments, fluorescent droplets with sizes ranging from 20 to 200 μm are observed, where the fluorescence of both the monomer and the aggregated state is localised in the dispersed phase (Figure 5.8 A and B). Image analysis software is used to construct an image where we divide the aggregate fluorescence intensity by the monomer fluorescence intensity (Figure 5.8 C). In this way, regions that are enriched in

aggregates of perylene **3** can be distinguished. The interface between the dispersed and continuous phase appears enriched in aggregated perylenes as the ratiometric image shows a slightly higher intensity at these boundaries compared to the droplet interior. However, aggregate fluorescence is observed throughout the droplet of the dispersed phase, suggesting a distribution of perylene aggregates at the interface and in the dispersed phase. This is probably related to the fact that the twofold hydrogen bond between **1** and **3** is not selective towards the formation of **1:3** heterodimers and is similar in the formation of **1:1** and **3:3** dimers and subsequent aggregates. Consequently, as the emulsions are prepared by mixing solutions of **1** in water and **3** in MCH, the resulting emulsion contains aggregates of dimers **1:1**, **3:3**, and **1:3** in their respective phase, and fluorescence of aggregated **3:3** can be observed from the dispersed phase. Due to its amphiphilicity, dimer **1:3** is preferentially located at the water/MCH interface, resulting in a higher localised aggregate fluorescence at the water/MCH interface.

To summarise, we have synthesised and characterised supra-amphiphiles by hydrogen bonding for their self-assembly behaviour as amphiphiles in water/MCH emulsions. First, the self-assembly behaviour of tetra(ethyleneoxy) functionalised perylene **1** and triazine **2** was investigated in dilute aqueous solutions and found to be very similar to the self-assembly behaviour of their apolar analogues in MCH solution. Perylene bisimide **1** assembles into aggregates of stacked, hydrogen bonded dimers in aqueous solutions and forms supramolecular hetero-aggregates by hydrogen bonding and π-stacking with triazine **2**. Next, we investigated the formation of supra-amphiphiles based on complementary hydrogen bonding and subsequent π-stacking between perylenes and triazines. We found that supra-amphiphiles based on complementary hydrogen bonding between polar and apolar triazines and perylenes performed as efficient stabilisers of water/MCH emulsions. The hydrogen bonded dimers behave as amphiphiles and aggregate further on the water/MCH interface by π-stacking interactions. The presented approach for the formation of supra-amphiphiles allows a modular methodology towards the synthesis of functional amphiphilic systems. Furthermore, the use of hydrogen bonded dimers of chromophore molecules and their self-assembly at interfaces opens up novel opportunities for the engineering of complex supramolecular architectures with applications such as artificial photosynthetic systems.[28]

5.5 Self-assembly at the water-water interface

In the previous paragraphs we have demonstrated the self-assembly of supra-amphiphiles based on **1 - 4** on the oil/water interface. In this paragraph we turn our attention to water-in-water (all-aqueous) emulsions. The use of traditional oil-in-water emulsions for the formation of functional materials suffers from the use of organic solvents in view of their application as microgel particles[41], liposomes[42], polymersomes[43] and colloidosomes[44] in biological and pharmaceutical systems.[45] Aqueous two-phase systems or water-in-water emulsions offer a promising alternative for the formation of such functional materials.[45,46] The formation of water-in-water emulsions is based on the phenomenon of aqueous two-phase systems in which solutions of two different polymers or surfactants above a critical weight percentage form insoluble phases.[45,47,48] Water-in-water emulsions have been successfully produced by microfluidic techniques,[45,49] though the ease of formation and stability (coagulation) of the emulsions were hampered by the extremely low interfacial tension of aqueous two-phase systems.[49-51] Furthermore, water-in-water emulsions have poor encapsulation efficiencies, limiting their usefulness in applications where the encapsulation of substances in the droplets is required.[45] To alleviate these issues, Shum and Weitz have used both interfacial precipitation and gelation approaches in microfluidics to create a stable interface between the two immiscible water phases.[45] Furthermore, Luk and co-workers investigated the formation of stable droplets of a liquid crystal aqueous solution (sodium cromoglycate) by polyvalent hydrogen bonding of polymers at the water-water interface.[52] In other studies, the adsorption of colloidal or protein particles at the water/water interface proved efficient in stabilising all-aqueous emulsions.[53-55]

To the best of our knowledge, classical molecular or polymeric surfactant-like molecules have not been used for the stabilisation of water-in-water emulsions. Here, we propose the use of small molecule supra-amphiphiles as a methodology to stabilise water-in-water emulsions, with a similar approach as that used for the oil-in-water systems described earlier in this chapter. In the remainder of this chapter we will continue to refer to our supramolecular complexes as supra-amphiphiles, since we attempt to use them as a compatibiliser between two immiscible liquids. We acknowledge the notion that amphiphiles conventionally possess both hydrophilic and lipophilic moieties, which is not the case in our structures. Nevertheless, we feel

that the use of the term supra-amphiphiles is appropriate as the term amphiphile originates from the Greek amphis philia, meaning both love and refers to affinity for two incompatible phases. We aim to prepare supra-amphiphiles for the stabilisation of water-in-water emulsions based on immiscible polymer solutions. Therefore, we adapt the solubilising groups on the periphery of the supra-amphiphiles described earlier in this chapter to make them compatible with the individual polymer phases. The suggested strategy should result in the formation supra-amphiphiles that aggregate on the interface of water-in-water emulsions prepared by microfluidics.

5.6 Molecular design and synthesis

Initial experiments on the stabilisation of water-in-water emulsions were performed by Yang Song in the group of Dr. A.H.C. Shum (The University of Hong Kong). Perylene **1** and triazine **2** were used in an attempt to stabilise an emulsion of a dextran-rich dispersed phase in a polyethylene glycol (PEG)-rich continuous phase, as dextran and PEG are two common polymers that show aqueous phase separation. For this, perylene **1** (0.5 wt%) is dissolved in a PEG solution and triazine **2** (0.5 wt%) is dissolved in a dextran solution. Upon vigorous mixing of the solutions, it is found that hetero-aggregates of **1** and **2** are preferentially solubilised in the PEG-rich aqueous phase instead of stabilising the water/water interface. The supramolecular complex **1:2** does not display a solubilising group for dextran-rich solutions and therefore does not display Janus-character in the dextran/PEG system. For this reason, we design β-D-glucopyranose-functionalised triazine **16**, as complementary hydrogen bonding between perylene **1** and triazine **16** should result in the formation of a supra-amphiphile with the desired Janus-character. For decoration with β-D-glucopyranose moieties, the triazine has the preference over the perylene due to the rather harsh conditions that are required and the solubility issues that are encountered in the perylene synthesis. We selected β-D-glucopyranose **13** as the carbohydrate of choice as it is commercially available and can be conveniently coupled to organic substrates via Sonogashira coupling reactions.

The synthesis of β-D-glucopyranose functionalised triazine **16** is schematically depicted in Scheme 5.2. Commercially available 3,5-dibromobenzoyl chloride **11** was reacted with diphenylbiguanide **10** in a two-step reaction to yield dibromotriazine **12** in moderate yield after column chromatography. Next, commercially available 2-

propynyl-tetra-*O*-acetyl-β-D-glucopyranoside **13** was reacted with **12** under standard Sonogashira coupling conditions to yield triazine **14** in 65% yield and subsequent reduction of the alkyne triple bonds with H_2 over Pd/C catalyst resulted in the formation of **15** in 91% yield. In the last step, the acetyl groups on **15** were removed by treatment with aqueous sodium hydroxide in ethanol to give triazine **16** in a rather low yield of 19**%** after column chromatography. The product was fully characterised by NMR and MALDI-ToF spectroscopy, indicating that **16** was obtained as a highly pure compound.
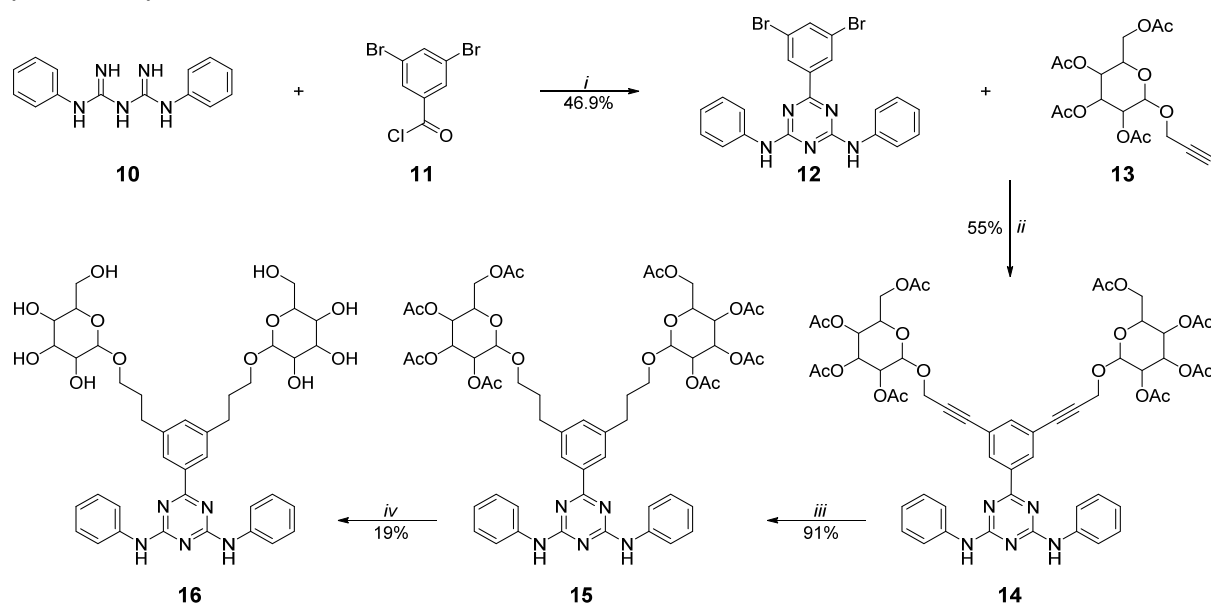
Scheme 5.2. Synthetic scheme towards β-D-glucopyranose-conjugated triazine **16**. Reagents and conditions: i) Et_3N, $CHCl_3$, DMA, 0 °C to 70 °C; ii) $Pd(PPh_3)_2Cl_2$, CuI, Et_3N, DMF, 60 °C; iii) H_2, Pd/C, EtOAc, RT; iv) NaOH, H_2O, ethanol, 80 °C.

5.7 Self-assembly in aqueous solution

The self-assembly of triazine **16** with perylene **1** in aqueous solution was characterised by UV–Vis spectroscopy (Figure 5.9). PBI **1** and triazine **16** were dissolved in H_2O at a concentration of c = $2×10^{-5}$ M and the UV–Vis spectrum was recorded. The UV–Vis spectrum in the perylene absorption region differs greatly for the mixture of perylene **1** and triazine **16** in comparison to perylene **1** only, indicating the presence of heteroaggregates. The spectral features of the hetero-aggregates are similar as observed for **1:2** hetero-aggregates, as the main perylene absorption at λ = 480 nm diminishes in intensity and the absorption in the red-shifter shoulder (λ = 570 nm) becomes more intense, though to a lesser extent as observed for **1:2**. This suggests a somewhat different packing of the PBI chromophores in the π-stacked

heterocomplexes with respect to **1:2**. The slightly altered aggregation behaviour is probably related to the introduction of sterically demanding -glucopyranose groups on the triazine hydrogen-bond moiety but nevertheless, hetero-aggregates **1:16** are formed. Therefore, the resulting hydrogen-bonded supra-amphiphile **1:16** might be an attractive candidate for the stabilisation of all-aqueous emulsions.
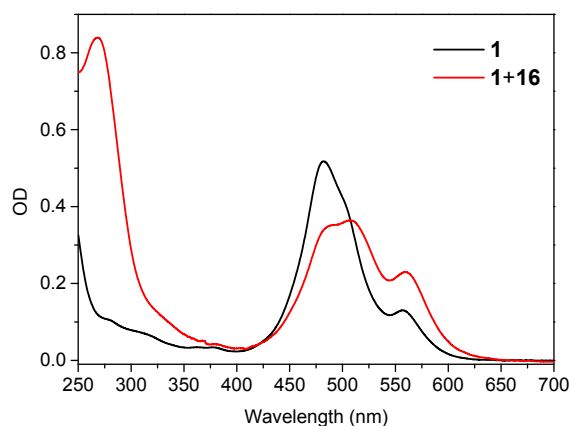
Figure 5.9. UV–Vis spectra of PBI **1** (black line) in H_2O and PBI **1** with triazine **16** (red line) in H_2O (c = 2×10^{-4} M, l = 1 mm, T = 20 °C).

The next step in the formation of supra-amphiphiles by hydrogen bonding and π-stacking interactions is to test perylene **1** and triazine **16** for the stabilisation of water-in-water emulsions. Unfortunately, high weight percent PEG solutions containing perylene **1** (0.5 wt%) were unstable over time and formed insoluble precipitates while solutions of **1** (0.5 wt%) in pure water were stable. Furthermore, when freshly prepared PEG solutions containing PBI **1** (0.5 wt%) are mixed with dextran solutions containing **16** (0.5 wt%), precipitates were also formed instead of stabilised emulsions. Likely, the aggregation of PBI **1** into homo- or heteroaggregates in high weight percentage polymer solutions is too strong for the formation of stable aggregates at the water/water interface. The results suggest that a subtle balance exists between the solution phase affinity of the subunits of supra-amphiphiles by hydrogen bonding and their aggregation strength. Individual subunits should display high affinity for and high solubility in high weight percent aqueous polymer solutions while maintaining sufficient driving force for the formation of supra-amphiphiles and their subsequent aggregation in extended aggregates. In the presented case, perylene **1** could be modified to have increased solubility in PEG solutions by introducing longer oligo(ethyleneoxide) side-chains on the solubilising wedge.

Alternatively, the aggregation strength of perylene **1** could be diminished by the introduction of substituents on the perylene bay position. Furthermore, the aggregation strength of the π-conjugated block can be diminished by using the structurally related naphthalene diimides instead of perylene diimides. Lastly, different complementary hydrogen bonded pairs that possess less aggregation strength might also be used in order to form stable aqueous solutions of supra-amphiphile subunits.

5.8 Conclusion

The synthesis and self-assembly behaviour of supra-amphiphiles based on complementary hydrogen bonding between perylene bisimides and triazines have been investigated. The perylene bisimide and triazine motifs described in Chapter 3 were decorated with hydrophilic tetra(ethyleneoxy) side-chains instead of hydrophobic side-chains to induce solubility in aqueous solutions. The resulting perylene bisimide formed aggregates consisting of π-stacked hydrogen-bonded dimers as evidenced by UV–Vis and FT-IR spectroscopy in a highly similar fashion to the apolar analogue in MCH solution. In presence of the water-soluble triazine, supramolecular heteroaggregates were formed by complementary hydrogen bonding and subsequent π-stacking interactions. Supra-amphiphiles by hydrogen bonding were obtained by mixing perylenes and triazines of different polarity in binary systems of water and MCH. The resulting emulsions were stabilised by the aggregation of supra-amphiphiles on the water/MCH interface and could be visualised by optical and confocal fluorescence microscopy. Next, we investigated the use of supra-amphiphiles in the stabilisation of all-aqueous emulsions. For this, the triazine core was functionalised with glucopyranose moieties to introduce solubility in dextran-rich aqueous solutions, while the tetra(ethyleneoxy) functionalised perylene was used in PEG-rich solutions. Unfortunately, the PEG-solutions of the perylene gave precipitation over time and also in contact with the triazine-dextran solution. A delicate balance appears to exist between the aggregation strength and the solution phase affinity of the individual subunits of the supra-amphiphiles. Tuning of the hydrogen-bond strength and the subsequent aggregation strength of the supra-amphiphiles is of key importance in the formation of emulsions (water/oil or all-aqueous) stabilised by supra-amphiphiles. In the presented system, the performance of the supra-amphiphiles for the all-aqueous system eventually could be

enhanced by increasing the solubility or decreasing the aggregation strength of the perylene subunit in order to prevent undesired precipitation. The presented approach for the formation of supra-amphiphiles allows a modular methodology towards the synthesis of functional amphiphilic systems. Furthermore, the use of hydrogen-bonded dimers of chromophore molecules and their self-assembly at interfaces creates novel opportunities for the engineering of complex supramolecular architectures with applications such as artificial photosynthetic systems.[28]

5.9 Experimental section

Instrumentation, materials and methods

Unless specifically mentioned, reagents and solvents were obtained from commercial suppliers and used without further purification. All solvents were of AR quality. Deuterated chloroform for NMR analyses was provided with TMS as the 0 ppm reference. The methylcyclohexane used in all spectroscopic experiments was of spectroscopic grade. Column chromatography was performed on a Biotage Isolera One using SNAP KP-SNAP columns and solvent gradients. ^{1}H-NMR and ^{13}C-NMR spectra were recorded on a Varian Mercury Vx 400 MHz instrument (100 MHz for ^{13}C) and all chemical shifts are reported in parts per million relative to tetramethylsilane (TMS). MALDI-ToF MS analyses were performed in reflector mode on a PerSeptive Biosystems Voyager-DE Pro using α-cyano-4-hydroxycinnamic acid (CHCA) and 2-[(2E)-3-(4-tert-butylphenyl)-2-methylprop-2-enylidene]malononitrile (DCTB) as matrices. Ultraviolet-visible (UV–Vis) absorbance spectra were recorded on a Jasco V-650 UV–Vis spectrometer with a Jasco ETCR-762 temperature controller. Circular dichroism (CD) spectra were recorded on a JASCO J-815 CD spectrometer with a JASCO PTC-348 temperature controller. Solid state infrared (IR) spectra were recorded on a Perkin Elmer Spectrum One spectrometer equipped with an ATR universal sampler accessory. Fluorescent cell images were acquired with a Leica TCS SP5 AOBS confocal system equipped with an HCX PL APO CS 40x/1.2 NA water immersion lens and a temperature-controlled incubation chamber. Polarisation optical microscopy measurements were performed on a Jenaval polarisation microscope equipped with a Linkam THMS 600 heating device, with crossed polarisers.

Synthesis

3,4,5-Tris(2,5,8,11-tetraoxatridecan-13-yloxy)benzoyl azide (**6**)

3,4,5-Tris(2,5,8,11-tetraoxatridecan-13-yloxy)benzoic acid (**5**) (2.4 g, 3.2 mmol) and triethylamine (1.2 mL, 8.6 mmol) were dissolved in THF (30 mL) and the solution was cooled to 0 °C with an ice-water bath. Ethyl chloroformate (0.8 mL, 8.4 mmol) was dissolved in THF (5 mL) and the resulting solution was dropwise added to the solution of **3** and the mixture was stirred for 1 hour at 0 °C. Sodium azide (3 g, 46 mmol) was dissolved in water (10 mL) and the resulting solution was dropwise added to the above prepared THF solution. The mixture was stirred for 3 hours at room temperature. Afterwards, water (20 mL) was added and the resulting mixture was extracted with DCM (4 x 30 mL). The combined organic fractions were dried over $MgSO_4$. The suspension was filtered and the filtrate was concentrated in vacuo. Vigorous drying over P_2O_5 yielded **6**. The product was used in subsequent steps without further purification. Yield = 2.19 g. η = 89.4%.

3,4,5-Tris(2,5,8,11-tetraoxatridecan-13-yloxy)aniline (**7**)

3,4,5-Tris(2,5,8,11-tetraoxatridecan-13-yloxy)benzoyl azide (**6**) (2.19 g, 2.86 mmol) was dissolved in dioxane (40 mL) and heated at 100 °C for 30 minutes. Afterwards, the solution was cooled down to 70 °C. In a separate flask, tetrabutylammonium hydroxide (3.5 mL, 40 wt% in H_2O) was dissolved in dioxane (30 mL) and heated to 90 °C. The hot dioxane solution of **6** was dropwise added to the tetrabutylammonium hydroxide solution via a cannula, after which the mixture was allowed to stir for 90 minutes at 90 °C. The reaction mixture was concentrated in vacuo and DCM (30 mL) and H_2O (30 mL) were added reaction mixture. The organic layer was isolated and the aqueous phase was extracted with DCM (4 x 30 mL) and the combined organic layers dried over $MgSO_4$. The resulting suspension was filtered and the filtrate was concentrated in vacuo. The crude residue was further purified by column chromatography (gradient 3% to 7% methanol in dichloromethane over 9 column volumes, R_F = 0.2 in 7% methanol in dichloromethane). Yield = 1.7 g. η = 83.5%. ^{1}H-NMR (400 MHz, $CDCl_3$) δ = 5.96 (s, 2H, Ar-H), 4.11 (t, 4H, Ar-O-CH_2), 4.03 (t, 2H, Ar-O-CH_2), 3.81 (t, 6H), 3.66 (m, 30H) 3.54 (m, 6H), 3.38 (s, 9H, CH_3). MALDI-ToF-MS (m/z) calc for $C_{33}H_{61}NO_{15}$ 711.40 found 711.46 $(M^{.})^+$, 734.45 $(M+Na)^+$.

2-(3,4,5-Tris(2,5,8,11-tetraoxatridecan-13-yloxy)phenyl)anthra[2,1,9-def:6,5,10-d'e'f']diisoquinoline-1,3,8,10(2H,9H)-tetraone (**1**)

3,4,5-Tris(2,5,8,11-tetraoxatridecan-13-yloxy)aniline (**7**) (100 mg, 0.26 mmol), perylenetetracarboxylic acid-3,4-anhydride-9,10-imide (182 mg, 0.26 mmol), $Zn(OAc)_2$ and imidazole (5 g) were mixed in a flask at room temperature under an argon atmosphere. The mixture was heated at 140 °C for 6 hours. Afterwards, water (12 mL) and dichloromethane (12 mL) were added to the reaction mixture and the aqueous phase was extracted with dichloromethane (3 x 15 mL). The crude material was purified by column chromatography first using acetone ($R_{F, imidazole}$ = 0.4, $R_{F, perylene\ 1}$ = 0) followed by 5% methanol in dichloromethane. The product was then precipitated from cold ether to give the title compound as a red solid. Yield = 150 mg. η = 47.5%. ^{1}H-NMR (400 MHz, $CDCl_3$) δ = 9.23 (broad, 1H, NH), 8.55 (d, J = 8 Hz, 2H), 8.40 (d, J = 8 Hz, 2H), 8.29 (d, J = 7.6 Hz, 2H), 8.25 (d, J = 7.6 Hz, 2H), 6.73 (s, 2H, aryl), 4.28 (t, J = 4.8 Hz, 2H, Phe-O-CH_2), 4.19 (m, 4H, Phe-O-CH_2), 3.87 (m, 6H), 3.65 (m, 30H), 3.54 (m, 6H), 3.40 (s, 3H, CH_3), 3.35 (s, 6H, CH_3). MALDI-ToF-MS (m/z) calc for $C_{57}H_{68}N_2O_{19}$ 1084.44 found 1107.47 $(M+Na)^+$, 1123.44 $(M+K)^+$.

3,4,5-Tris(2,5,8,11-tetraoxatridecan-13-yloxy)benzoyl chloride (**9**)

3,4,5-Tris(2,5,8,11-tetraoxatridecan-13-yloxy)benzoic acid (**5**) (1.46 g, 1.97 mmol) and a drop of DMF were dissolved in THF (30 mL). Oxalyl chloride (0.9 mL, 10 mmol) in THF (10 mL) was added dropwise to the above solution. The resulting solution was stirred for 90 minutes at room temperature and the reaction was monitored by FT-IR spectroscopy. Afterwards, the solvent was removed in vacuo and the crude product used without further purification.

N^2,N^4-Diphenyl-6-[3,4,5-tris(2,5,8,11-tetraoxatridecan-13-yloxy)phenyl]-1,3,5-triazine-2,4-diamine (**2**)

Diphenylbiguanide **10** (0.52 g, 2.0 mmol) and triethylamine (0.6 mL, 6 mmol) were dissolved in dimethyl acetamide (20 mL). A solution of 3,4,5-tris(2,5,8,11-tetraoxatridecan-13-yloxy)benzoyl chloride **9** (1.58 g, 0.2 mmol) in chloroform (20 mL) was used as prepared and added dropwise to the biguanide solution. The resulting mixture was stirred for 12 hours at room temperature under an argon atmosphere and subsequently heated at 70 °C for 4 hours. The mixture was cooled to room temperature and the solvent removed in vacuo. The product was purified by

column chromatography using 5% methanol in ethyl acetate as eluent. Yield = 1.06 g. η = 53.3%. ^{1}H-NMR (400 MHz, CDCl$_3$) δ = 7.75 (s, 2H, phenyl), 7.68 (d, J = 8 Hz, 4H), 7.37 (t, J = 7.6 Hz, 4H), 7.26 (b, 2H, N-H), 7.12 (t, J = 7.6 Hz, 2H), 4.29 (t, J = 5.2 Hz, 4H), 4.24 (t, J = 4.8 Hz, 2H), 3.91 (t, J = 5.2 Hz, 4H), 3.82 (t, J = 5 Hz, 2H), 3.74 (m, 6H), 3.65 (m, 24H), 3.55 (m, 6H), 3.38 (s, 3H, CH$_3$), 3.37 (s, 6H, CH$_3$). ^{13}C-NMR (100 MHz, CDCl$_3$) δ = 170.8, 164.6, 152.4, 141.7, 138.4, 131.4, 128.8, 123.5, 120.7, 107.8, 72.4, 71.9, 71.9, 70.8, 70.7, 70.7, 70.6, 70.6, 70.6, 70.5, 70.5, 70.5, 69.7, 68.6, 68.0, 59.0, 59.0. MALDI-ToF-MS (m/z) calc for C$_{48}$H$_{71}$N$_5$O$_{15}$ 957.49 found 980.52 (M+Na)$^+$, 996.49 (M+K)$^+$.

6-(3,5-Dibromophenyl)-N^2,N^4-diphenyl-1,3,5-triazine-2,4-diamine (**12**)

Diphenylbiguanide **10** (0.49 g, 1.93 mmol) and triethylamine (0.59 g, 5.8 mmol) were dissolved in chloroform (5 mL) and dimethylacetamide (5 mL) and stirred at 0 °C under and under an argon atmosphere. 3,5-dibromobenzoyl chloride **11** (0.58 g, 1.93 mmol) was dissolved in chloroform (2 mL) and added dropwise to the biguanide solution. The resulting solution was allowed to warm to room temperature and stirred for 60 hours and afterwards heated at 70 °C for 4 hours, resulting in a clear yellow solution. All volatiles were removed by vacuum evaporation and the solid residue was purified by column chromatography (gradient of 30% to 50% dichloromethane in heptane, R$_F$ = 0.4 in 50% DCM in heptane). Yield = 0.45 g. η = 46.9%. ^{1}H NMR (400 MHz, CDCl$_3$) δ = 8.49 (s, 2H, aromatic), 7.82 (s, 1H, aromatic), 7.64 (d, J = 8 Hz, 4H, aromatic), 7.39 (t, J = 8 Hz, 4H), 7.17 (b, 2H, NH), 7.15 (t, 2H, aromatic). ^{13}C-NMR (100 MHz, CDCl$_3$) δ = 164.8, 139.9, 137.9, 136.9, 130.2, 128.9, 123.9, 122.9, 120.8. MALDI-ToF-MS (m/z) calc for C$_{21}$H$_{15}$Br$_2$N$_5$ 496.97 found 497.99 (M+H)$^+$.

6[3,5-Bis(tetra-O-acetyl-β-D-glucopyranosyl-1-O-propargyl)phenyl]-N^2,N^4-diphenyl-1,3,5-triazine-2,4-diamine (**14**)

In a Schlenk tube were subsequently charged 6-(3,5-dibromophenyl)-N^2,N^4-diphenyl-1,3,5-triazine-2,4-diamine **12** (200 mg, 0.402 mmol), CuI (9.2 mg, 0.048 mmol), Pd(PPh$_3$)$_2$Cl$_2$ (17 mg, 0.024 mmol), triethylamine (400 mg, 560 μL, 4.02 mmol) and DMF (20 mL). The Schlenk tube was put under an argon atmosphere, closed and subjugated to four consecutive freeze-pump-thaw cycles. The mixture was heated to 60 °C. 2-Propynyl-tetra-1-O-propargyl-β-D-glucopyranoside **13** (390 mg, 1.0 mmol)

was dissolved in DMF (2 mL) and added to the reaction with a syringe. The mixture was allowed to stir at 60 ^{o}C for 14 hours after which the progress was checked by ^{1}H-NMR in CDCl$_3$. An additional amount of glucopyranoside (150 mg, 0.38 mmol) was added and the mixture was left to stir for an additional 20 hours after which the solvent was removed by vacuum evaporation. The mono- and bis-substituted products were separated with column chromatography (ethyl acetate in heptane). A second column (0.5% to 1.5% ethanol in chloroform) was performed to remove a minor side product. Yield: 245 mg. η = 55%. ^{1}H-NMR (400 MHz, CDCl$_3$) δ = 8.48 and 8.47 (2 x s, 2 x 1H, aromatic), 7.68 (d, J = 8 Hz, 4H, aromatic), 7.64 (s, 1H, aromatic), 7.38 (t, J = 7.6 Hz, 4H, aromatic), 7.14 (t, J = 7.6 Hz, 2H, aromatic), 5.32 (dd, $^{3}J_{2,3}$ = 9.6 Hz, $^{3}J_{3,4}$ = 9.6 Hz, 2H, H-3), 5.15 (dd, $^{3}J_{3,4}$ = 9.6 Hz, $^{3}J_{4,5}$ = 10 Hz, 2H, H-4), 5.08 (dd, $^{3}J_{1,2}$ = 8 Hz, $^{3}J_{2,3}$ = 9.6 Hz, 2H, H-2), 4.9 (d, $^{3}J_{1,2}$ = 8 Hz, 2H, H-1), 4.64 (d, J = 4.4 Hz, 4H, C≡CCH$_2$, diastereotopic), 4.29 (dd, $^{3}J_{5,6a}$ = 4.4 Hz, $^{2}J_{6a,6b}$ = 12.4 Hz, 2H, H-6a), 4.24 (dd, $^{3}J_{5,6b}$ = 2.4 Hz, $^{2}J_{6a,6b}$ = 12.4 Hz, 2H, H-6b), 3.8 (ddd, $^{3}J_{5,6a}$ = 4.4 Hz, $^{3}J_{5,6b}$ = 2.4 Hz, $^{3}J_{4,5}$ = 10 Hz, 2H, H-5), 2.12 (s, 6H, -COCH$_3$), 2.07 (s, 6H, -COCH$_3$), 2.04 (s, 6H, -COCH$_3$), 2.02 (s, 6H, -COCH$_3$). ^{13}C-NMR (100 MHz, CDCl$_3$) δ = 170.4, 169.5, 169.4, 164.7, 138.2, 137.2, 131.9, 128.8, 123.8, 122.8, 120.9, 98.5, 86.0, 84.6, 72.9, 72.0, 71.1, 68.3, 61.9, 56.9, 20.8, 20.8, 20.6, 20.6. MALDI-ToF MS (m/z) calc for C$_{55}$H$_{57}$N$_5$O$_{20}$ 1107.36 found 1108.37 (M+H)$^{+}$, 1130.35 (M+Na)$^{+}$, 1146.32 (M+K)$^{+}$.

6[3,5-Bis(tetra-O-acetyl-β-D-glucopyranosyl-1-O-propyl)phenyl]-N^2,N^4-diphenyl-1,3,5-triazine-2,4-diamine (**15**)

6[3,5-Bis(tetra-O-acetyl-β-D-glucopyranosyl-1-O-propargyl)phenyl]-N^2,N^4-diphenyl-1,3,5-triazine-2,4-diamine (**14**) (245 mg, 0.22 mmol) was dissolved in EtOAc and bubbled with argon for 30 minutes. Pd/C was added and the mixture was subsequently subjected to H$_2$ in a Parr hydrogenation apparatus. After 15 hours, the catalyst was filtered and the solvent removed in vacuo. Yield: 224 mg. η = 91%. ^{1}H-NMR (400 MHz, CDCl$_3$): δ = 8.07 and 8.06 (2 x s, 2 x 1H, aromatic), 7.70 (d, J = 8 Hz, 4H, aromatic), 7.45 (b, 2H, N-H), 7.37 (dd, 7.6 Hz and 8 Hz, 4H, aromatic), 7.15 (s, 1H, aromatic), 7.12 (t, J = 7.6 Hz, 2H aromatic), 5.25 (dd, $^{3}J_{2,3}$ = 9.6 Hz, $^{3}J_{3,4}$ = 9.6 Hz, 2H, H-3), 5.12 (dd, $^{3}J_{3,4}$ = 9.6 Hz and $^{3}J_{4,5}$ = 9.8 Hz, 2H, H-4), 5.06 (dd, $^{3}J_{1,2}$ = 8 Hz, $^{3}J_{2,3}$ = 9.6 Hz, 2H, H-2), 4.56 (d, J = 8 Hz, 2H, H-1), 4.27 (dd, $^{3}J_{5,6a}$ = 4.8 Hz, $^{2}J_{6a,6b}$ = 12.4 Hz, 2H, H-6a), 4.15 (dd, $^{3}J_{5,6b}$ = 2.4 Hz, $^{2}J_{6a,6b}$ = 12.4 Hz, 2H, H-6b), 3.91 (dt, ^{2}J = 6 Hz, ^{3}J = 10 Hz 2H, -COCH$_{2,a}$), 3.7 (ddd, $^{3}J_{5,6b}$ = 2.4 Hz, $^{3}J_{5,6a}$ = 4.8 Hz, $^{3}J_{4,5}$ = 9.8 Hz 2H, H-5), 3.56 (dt, ^{2}J

= 6 Hz, ^3J = 10 Hz, 2H, -COCH$_{2,b}$), 2.73 (m, 4H, CH$_2$), 2.08 (s, 6H, -COCH$_3$), 2.07 (s, 6H, -COCH$_3$), 2.02 (s, 6H, -COCH$_3$), 2.01 (s, 6H, -COCH$_3$), 1.96 (m, 4H, CH$_2$). ^{13}C-NMR (100 MHz, CDCl$_3$) δ = 171.2, 170.4, 170.1, 169.5, 169.4, 164.7, 141.8, 138.5, 132.2, 128.8, 126.2, 123.5, 120.7, 100.7, 72.9, 71.7, 71.5, 69.1, 68.4, 62.0, 60.4, 31.8, 31.0, 20.8, 20.8, 20.7, 20.6 MALDI-ToF MS (m/z) calc for C$_{55}$H$_{65}$N$_5$O$_{20}$ 1115.42 found 1116.43 (M+H)$^+$, 1138.41 (M+Na)$^+$, 1154.38 (M+K)$^+$.

6[3,5-Bis(β-D-glucopyranosyl-1-O-propyl)phenyl]-N^2,N^4-diphenyl-1,3,5-triazine-2,4-diamine (**16**)

6-[3,5-Bis(tetra-*O*-acetyl-β-D-glucopyranosyl-1-*O*-propyl)phenyl)-*N^2*,*N^4*-diphenyl-1,3,5-triazine-2,4-diamine (**15**) (224 mg, 0.2 mmol) was dissolved in ethanol (10 mL). Aqueous NaOH (5 M, 0.8 mL, 4 mmol) was added and the mixture was heated under reflux conditions for 14 hours. Water (15 mL) was added to the reaction mixture and the solution was extracted with chloroform (3 x 20 mL). The combined organic fractions were dried over MgSO$_4$, filtered and concentrated in vacuo. The crude product was purified by reverse phase column chromatography using a gradient of acetonitrile in water as eluent. Yield: 25 mg. η = 16%. ^{1}H-NMR (400 MHz, MeOD) δ = 8.11 (s, 2H, aromatic), 7.76 (d, J = 7.6 Hz, 4H, aromatic), 7.32 (m, 5H, 2 x aromatic), 7.06 (t, J = 7.2 Hz, 2H, aromatic), 4.28 (d, J = 7.6 Hz, 2H), 3.96 (m, 2H), 3.86 (m, 2H), 3.68 (m, 2H), 3.59 (m, 2H), 3.4-3.2 (m, 8H), 2.8 (t, 4H), 2.0 (m, 4H) ^{13}C-NMR.[56] MALDI-ToF MS (m/z) calc for C$_{39}$H$_{49}$N$_5$O$_{12}$ 779.34 found 780.39 (M+H)$^+$, 802.37 (M+Na)$^+$.

5.10 References

[1]   A.V. Kabanov, V.A. Kabanov, *Adv. Drug Deliv. Rev.*, 1998, **30**, 49
[2]   C. Allen, D. Maysinger, A. Eisenberg, *Colloids Surf. B*, 1999, **16**, 3
[3]   G.S. Kwon, K. Kataoka, *Adv. Drug Deliv. Rev.*, 1995, **16**, 295
[4]   A. Rosler, G.W.M. Vandermeulen, H.-A. Klok, *Adv. Drug Deliv. Rev.*, 2001, **53**, 95
[5]   P. Walde, S. Ichikawa, *Biomol. Eng.*, 2001, **18**, 143
[6]   D. M. Vriezema, M.C. Aragonès, J.A.J.W. Welemans, J.J.L.M. Cornelissen, A.W. Rowan, R.J.M. Nolte, *Chem. Rev.*, 2005, **105**, 1445
[7]   D.M. Vriezema, P.M.L. Garcia, N.S. Oltra, N.S. Hatzakis, S.M. Kuiper, R.J.M. Nolte, A.E. Rowan, J.C.M. van Hest, *Angew. Chem. Int. Ed.*, 2007, **46**, 7378
[8]   A. Kishimura, A. Koide, K. Osada, Y. Yamasaki, K. Kataoka, *Angew. Chem. Int. Ed.*, 2007, **46**, 6085
[9]   Y. Wang, H. Xu, N. Ma, Z. Wang, X. Zang, J. Lui, J. Shen, *Langmuir*, 2006, **22**, 5552
[10]   L. Sierra, B. Lopez, H. Gil, J.-L. Guth, *Adv. Mater.*, 1999, **11**, 307

[11]   E. Ruiz-Hitzky, S. Letaïef, V. Préot, *Adv. Mater.*, 2002, **14**, 439

[12]   Q. Zhang, K. Ariga, A. Okabe, T. Aida, *J. Am. Chem. Soc*, 2004, **126**, 988

[13]   M. Hager, F. Currie, K. Holmberg, *Top. Curr. Chem.*, 2003, **227**, 53

[14]   M. Morikawa, M. Yoshihara, T. Endo, N, Kimizuka, *Chem. Eur. J.*, 2005, **11**, 1574

[15]   Y. Kang, K. Liu, X. Zhang, *Langmuir*, 2014, **30**, 5989

[16]   C. Wang, Z. Wang, X. Zhang, *Acc. Chem. Res.*, 2012, **45**, 608

[17]   M.A.C. Broeren, J.G. Linhardt, H. Malda, B.F.M. de Waal, R.M. Versteegen, J.T. Meijer, D.W.P.M. Löwik, J.C.M. van Hest, M.H.P. van Genderen, E.W. Meijer, *J. Polym. Sci., A*, 2005, **43**, 6431

[18]   M.A.C. Broeren, J.L.J. van Dongen, M. Pittelkow, J.B. Christensen, M.H.P. van Genderen, E.W. Meijer, *Angew. Chem. Int. Ed.*, 2004, **43**, 3557

[19]   N. Kimizuka, T. Kawasaki, K. Hirata, T. Kunitake, *J. Am. Chem. Soc.*, 1998, **120**, 4094

[20]   T. Kawasaki, M. Tokuhiro, N. Kimizuka, T. Kunitake, *J. Am. Chem. Soc.*, 2001, **123**, 6793

[21]   N. Kimizuka, T. Kawasaki, T. Kunitake, *J. Am. Chem. Soc.,* 1993, **115**, 4387

[22]   T. Bojinova, Y. Coppel, N.L. Viguerie, A. Milius, I.R. Lattes, A. Lattes, *Langmuir,* 2003, **19**, 5233

[23]   Y.J. Jeon, P.K. Bharadwaj, S.W. Choi, J.W. Lee, K.Kim, *Angew. Chem. Int. Ed.*, 2007, **46**, 2823

[24]   J.F. Gohy, B.G.G. Lohmeijer, U.S. Schubert, *Macromolecules*, 2002, **35**, 4560

[25]   B. Song, G.L. Wu, Z.Q. Wang, X. Zhang, M. Smet, W. Dehaen, *Langmuir*, 2009, **25**, 13306

[26]   A.V. Kabanov, T.K. Bronich, V.A. Kabanov, K. Yu, A. Eisenberg, *J. Am. Chem. Soc.*, 1998, **120**, 9941

[27]   C. Wang, S.C. Yin, H.P. Xu, Z.Q. Wang, X. Zhang, *Angew. Chem. Int. Ed.*, 2008, **47**, 9049

[28]   X. Zhang, Z.J. Chen, F. Würthner, *J. Am. Chem. Soc.*, 2007, **129**, 4886

[29]   H.R. Marsen, A.V. Korobko, E.N.M. van Leeuwen, E.M. Pouget, S.J. Veen, N.A.J.M. Sommerdijk, A. Kros, *J. Am. Chem. Soc.*, 2008, **130**, 9386

[30]   G. Steinberg-Yfrach, P.A. Liddell, S.C. Hung, A.L Moore, D. Gust, T.A. Moore, *Nature*, 1997, **385**, 239

[31]   A.B. Theberge, F. Courtois, Y. Schaerli, M. Fischlechner, C. Abell, F. Hollfelder, W.T.S. Huck, *Angew. Chem. Int. Ed.*, 2010, **49**, 5846

[32]   D. Görl, X. Zhang, F. Würthner, *Angew. Chem. Int. Ed.*, 2012, **51**, 6328

[33]   A. Ustinov, H. Weissman, E. Shirman, I. Pinkas, X. Zuo, B. Rybtchinski, *J. Am. Chem. Soc.,* 2011, **133**, 16211

[33]   F. Wurthner, *Chem. Commun.*, 2004, 1564

[34]   Z. Chen, B. Fimmel, F. Würthner, *Org. Biomol. Chem.*, 2012, **10**, 5845

[35]   P. Jonkheim, M. Fransen, A.P.H.J. Schenning, E.W. Meijer, *J. Chem. Soc., Perkin Trans. 2,* 2001, 1280

[37]   V. Huber, S. Sengupta, F. Würther, *Chem. Eur. J.*, 2008, **14**, 7791

[38]   R. Abbel, R. van der Weegen, E.W. Meijer, A.P.H.J. Schenning, *Chem. Commun.*, 2009, 1697

[39]   H. Langhals, W. Jona, *DE 19709008A1*

[40]   F. Würthner, C. Thalacker, S. Diele, C. Tschierske, *Chem. Eur. J.*, 2001, **7**, 2245

[41]   H. Zhang, E. Tumarkin, R. Peerani, Z. Nie, R.M.A. Sullan, G.C. Walker, E. Kumacheva, *J. Am. Chem. Soc.*, 2006, **128**, 12205

[42]   H.C. Shum, D. Lee, I. Yoon, T. Kodger, D.A. Weitz, *Langmuir*, 2008, **24**, 7651

[43]   H.C. Shum, J.W. Kim, D.A. Weitz, *J. Am. Chem. Soc.*, 2008, **130**, 9543

[44]   R.K. Shah, J.W. Kim, D.A. Weitz, *Langmuir*, 2010, **26**, 1561

[45]   H.C. Shum, J. Varnell, D.A. Weitz, *Biomacromolecules*, **6**, 2012, 012808

[46]   J. Chen, S.K. Spear, J.G. Huddleston, R.D. Rogers, *Green Chem.*, 2005, **7**, 64

[47]   C.R. Mace, O. Akbulut, A.A. Kumar, N.D. Shapiro, R. Derda, M.R. Patton, G.M. Whitesides, *J. Am. Chem. Soc.*, 2012, **134**, 9094

[48]   P.-Å. Albertsson, *Biochim. Biophys. Acta*, 1958, **27**, 378

[49]   I. Ziemecka, V. van Steij, G.J.M. Koper, M. Rosso, A.M. Brizzard, J.H. van Esch, M.T. Kreutzer, *Lab Chip*, 2011, **11** 620

[50]   Y.S. Song, Y.H. Choi, D.H. Kim, *J. Chromatogr. A*, 2007, **180**, 1162

[51]   A.D. Diamond, J.T. Hsu, *AIChE J.*, 1990, **36**, 1070

[52]   K.A. Simon, P. Sejwal, R.B. Gerecht, Y.Y. Luk, *Langmuir*, 2007, **23**, 1453

[53]   A.T. Poortinga, *Langmuir*, 2008, **24**, 1644

[54]   H. Firoozmand, B.S. Murray, E. Dickinson, *Langmuir*, 2009, **25**, 1300

[55]   B.T. Nguyen, T. Nicolai, L. Benyahia, *Langmuir,* 2013, **29**, 10658

[56]   ^{13}C-NMR analysis proved inconclusive as **16** precipitates over time from MeOD and CDCl$_3$

6

Nanoscopic phase-separated architectures based on hydrogen-bonded supramolecular polymers

Abstract

The formation of microphase-separated architectures that show small feature sizes in thin films is investigated by combining concepts from block-copolymer phase separation and supramolecular assembly of small molecules. Complementary hydrogen-bonding motifs are decorated with proposed incompatible side-chains of precise length and investigated for their self-assembly in the solid state. We utilise linear alkyl and oligodimethylsiloxane chains as phase-separating materials, as dimethylsiloxane based polymers are highly incompatible with most other polymers. The formation of aggregates through π-stacking of hydrogen-bonded heterodimers is evidenced by FT-IR and UV–Vis spectroscopy. The heterodimer materials are found to be room temperature liquid crystals displaying columnar hexagonal packing, as evidenced by POM and SAXS measurements. The microphase separation of the supramolecular materials is investigated by AFM. Spin cast films on bare silicon substrates display line patterns with small domain spacings ($\approx$ 4.5 nm), which is consistent with the alignment of columnar aggregates perpendicular to the substrate surface. The results suggest the occurrence of phase separation between the π-conjugated cores and the flexible side-chains, while no additional phase separation occurs between the proposed incompatible side-chains. Interestingly, the AFM phase images are highly reminiscent of conventional block-copolymer phase separation and dissimilar to fibre formation observed in conventional supramolecular polymers. The presented approach demonstrates the generation of feature sizes in thin films that are non-trivially obtainable with block copolymer phase separation, while maintaining long-range order that is generally lacking in supramolecular polymers.

6.1 Introduction

Bottom-up self-assembly processes show great promise to advance the fields of microelectronics, energy storage, optics and biomedicine. In lithographic applications, for example, a continuing demand exists for the miniaturisation of feature sizes. Herein, the microphase-separation behaviour of block copolymers offers an attractive alternative for the preparation of small–feature-size architectures in a high throughput manner.[1-7] The feature sizes obtained in phase-separating block copolymer systems are directly related to the degree of polymerisation (N) and the immiscibility of the blocks, which is reflected by the Flory–Huggins interaction parameter (χ). On the other hand, variation of the molecular weight fractions allows the generation of a variety of thin film morphologies, such as lamellae, cylinders, spheres and gyroid phases.

An appealing approach to address challenges in bottom-up lithography comprises the combination of conventional phase-separating block copolymers with supramolecular interactions.[8-11] The preparation of supramolecular block-copolymers that undergo phase separation on the nanometer-size scale has been demonstrated by functionalising homopolymer subunits with a variety of complementary hydrogen-bonding motifs.[12-16] Although distinct nanoscopic domains are generated, the formation of well-defined architectures over long length scales is only rarely observed.[16-18] A nice example was recently reported by Pitet *et al.*, where self-assembling diblock copolymers were prepared by four-fold complementary hydrogen bonding between ureidoguanosine (UG) functionalised poly(dimethylsiloxane) (PDMS) and 1,7-diamidonaphthyridines (Napy) functionalised poly(DL-lactide) (Figure 6.1).[19] The formation of well-defined lamellar morphologies in thin films was observed by both SAXS and TEM measurements and was comparable to the analogous covalent block copolymers.[20] Typical domain spacings in the order of 20 nm were observed, corresponding to feature sizes in the range of 10 nm. The narrow diffraction peaks observed in the SAXS analysis were attributed to exceptionally sharp domain boundaries and attributed to the supramolecular junction in the polymer material.
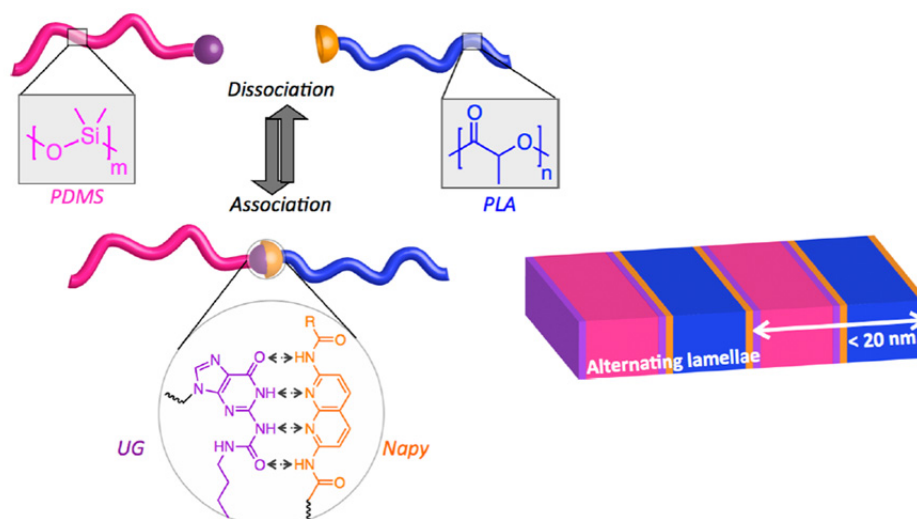
Figure 6.1. Schematic representation of the formation of a supramolecular block copolymer by complementary hydrogen bonding of functional homopolymers. Image adapted from reference 19.

Alternatively, the formation of small molecule based one-dimensional supramolecular polymers is well known. When such architectures are transferred to surfaces, the formation of fibres or fibre bundles is often observed.[26-34] In contrast to block copolymer phase separation, these fibres are often disorganised in thin films and well-defined nanopatterned surfaces with long range order are rarely obtained.

An approach that combines phase separation with small molecule self-assembly was recently described by García-Iglesias *et al.* in our group.[35] Side-chain phase separation of oligodimethylsiloxane (*o*DMS) and alkyl chains was combined with the formation of one-dimensional stacks of benzene-1,3,5-tricarboxamides (BTAs) (Figure 6.2). By balancing the number of alkyl and *o*DMS side-chains in the BTA molecules, the formation of superlattices was observed by XRD measurements. The BTA stacks were proposed to self-assemble into a columnar hexagonal arrangement, after which side-chain phase separation resulted in the formation of hexagonal superlattices. The approach provides opportunities for the generation of nanopatterned silicon surfaces after selective etching.

In an attempt to further miniaturise nanoscale features obtained by microphase separation, we propose to combine concepts from the fields of block-copolymer and small molecule self-assembly. We make use of complementary hydrogen bonding
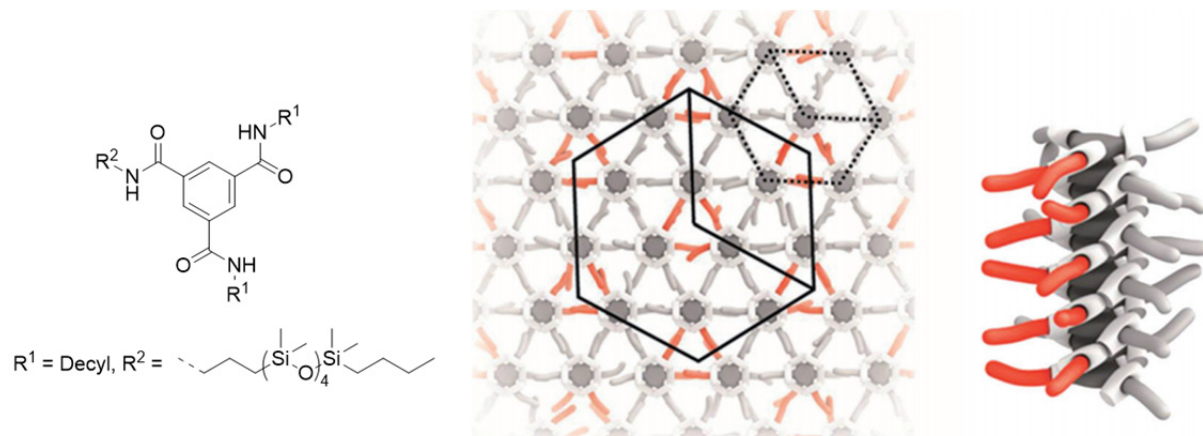
Figure 6.2. Molecular structure of a phase-separating *o*DMS BTA and a schematic representation of the self-assembly into one-dimensional columnar aggregates that show the formation of a superlattice in the columnar hexagonal mesophase. Image adapted from reference 35.

between two motifs that are decorated with side-chains of precise length that would microphase separate in conventional block copolymer systems. Subsequent π-stacking of the hydrogen-bonded heterodimers should amplify the phase separation of the incompatible side-chains mutually and also with the aggregating aromatic core, resulting in sharp domain boundaries. We make use of side-chains of defined length to precisely control the size of the obtained features.

6.2 Molecular design and synthesis

As complementary hydrogen-bonding motifs, we select the *N*-monoarylated perylene bisimide and triazine couple described in earlier in this thesis (Chapter 3) (Figure 6.3). Complementary hydrogen bonding and subsequent π-stacking of heterodimers of these motifs can be conveniently studied with FT-IR and UV–Vis spectroscopy. Furthermore, the gallic-acid-derived solubilising wedge on the triazine is a versatile synthetic building block for the introduction of a variety of solubilising chains. As phase-separating oligomeric side-chains, we select well-defined oligodimethylsiloxane (*o*DMS), because the corresponding polymer (PDMS) shows high incompatibility with most other polymers.[19-22]
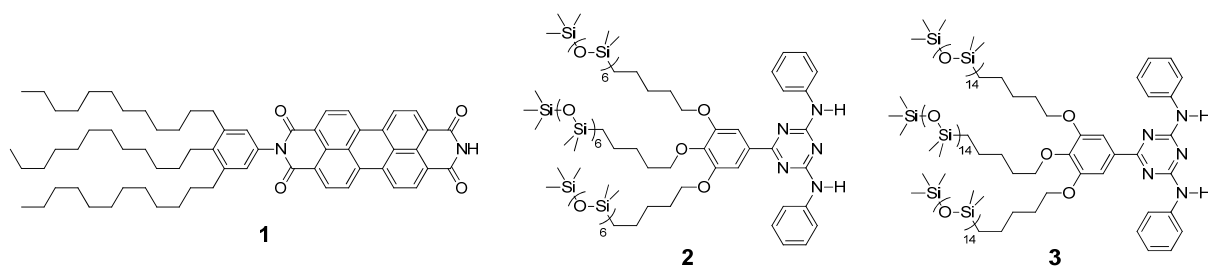
Figure 6.3. Asymmetric perylene bisimide **1** and *o*DMS functionalized triazines **2** and **3**, for the generation of phase-separated nanostructures.

The synthesis of *o*DMS functionalised triazines is outlined in Scheme 6.1. First, methyl 3,4,5-trihydroxybenzoate (**4**) was reacted with 5-bromopent-1-ene in a triple Williamson ether synthesis according to reported procedures to give alkene-functionalised wedge **5** in 95% yield.[23] Subsequently, the methyl ester on **5** was hydrolysed with aqueous sodium hydroxide in ethanol to yield acid **6**. The acid functionality in **6** was converted to the acid chloride derivative **7** by treatment with oxalyl chloride in THF. Diphenylbiguanide **8** was prepared according to reported procedures and reacted with acid chloride **7** to give triazine **9** in 49% yield after column chromatography.[24] The *o*DMS functionalised triazines **2** and **3** were then
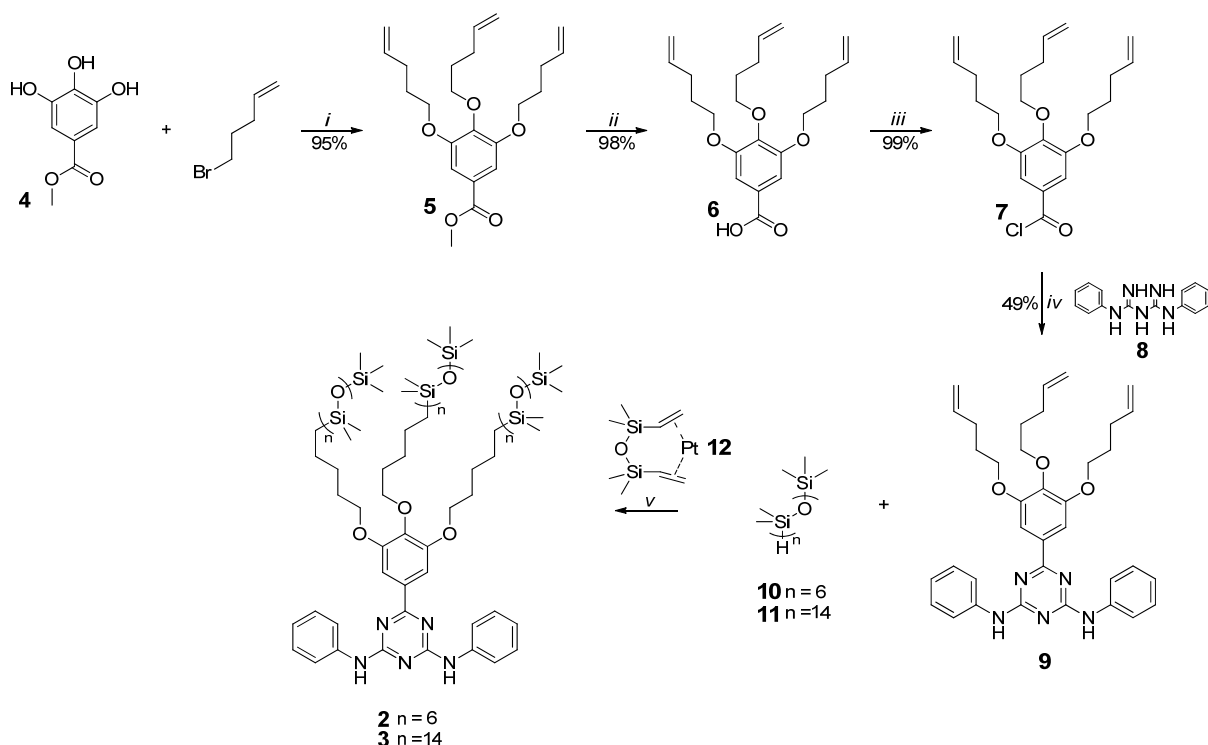
Scheme 6.1. Synthesis of *o*DMS-functionalised triazines **2** and **3**. Reagents and conditions: i) K_2CO_3, acetonitrile, 90 °C; ii) NaOH, EtOH, H_2O, 90 °C; iii) $C_2Cl_2O_2$, DMF, THF, RT; iv) Et_3N, DMA, $CHCl_3$, 0 °C to 80 °C; v) Karstedt's catalyst (**12**), THF, 60 °C.

obtained by reacting alkene-functionalised triazine **9** with well-defined silyl-hydrides **10** and **11** (kindly provided by Bas de Waal)[25] in the presence of Karstedt's catalyst (**12**) in THF. The target triazines were obtained in yields of 49% and 71% after purification by column chromatography. The *o*DMS functionalised triazines **2** and **3** were fully characterised by NMR spectroscopy and MALDI-ToF spectrometry, which indicated **2** and **3** to be of high purity.

6.3 Self-assembly in the solid state by hydrogen bonding and π-stacking

Triazines **2** and **3** are designed to self-assemble with perylene bisimide **1** by threefold complementary hydrogen bonding and subsequent π-stacking interactions. The complementary hydrogen bonding of triazines **2** and **3** with PBI **1** in the solid state was investigated by FT-IR spectroscopy. Drop-cast films were prepared from solutions of **1** with either **2** or **3** from methylcyclohexane (MCH) (c_1 = $c_{2 \text{ or } 3}$ = 1×10^{-4} M). As described in Chapters 2 and 3, the position and shape of the carbonyl vibrations of perylene **1** (1670 and 1705 cm^{-1}) are sensitive to the hydrogen bonds they participate in (Figure 6.4). In thin films of **1:2** and **1:3**, the perylene carbonyl vibrations are dissimilar in shape when compared to thin films of pure perylene **1** (Figure 6.4 B). These observations suggest a different hydrogen-bonding environment of the perylene carbonyl in the heteromixture. Furthermore, the carbonyl vibrations observed in heteromixtures **1:2** and **1:3** are highly similar to the vibrations observed for perylene-triazine heteroaggregates described in Chapter 3. Therefore, we conclude from the FT-IR analysis that hydrogen-bonded heterodimers **1:2** and **1:3** are indeed formed in solid state films drop-cast from MCH solutions.
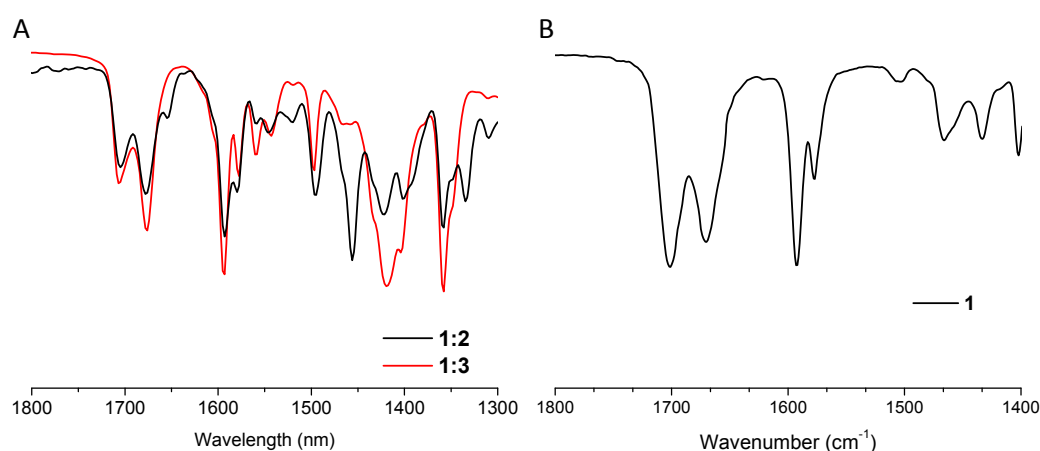

Figure 6.4. FT-IR spectra of heteromixtures **1:2** and **1:3** (A) and pure perylene bisimide **1** (B) in the solid state, drop cast from MCH.

Thin films of **1:2** and **1:3** heteromixtures were spun-cast on glass slides from a dilute solution in MCH (c_1 = $c_{2 \text{ or } 3}$ = 1×10^{-4} M) and evaluated with UV–Vis spectroscopy (Figure 6.5 A). As a reference, the UV–Vis spectrum of PBI **1** as a drop cast film from a dilute solution in MCH (c_1 = 1×10^{-4} M) was also recorded (Figure 6.5 B). The absorption spectrum of PBI **1** in the solid state displays spectral features that are indicative of the formation of face-to-face stacked PBI aggregates. Additionally, the absorption spectra of PBI **1** in the solid state and as a dilute solution in MCH (Chapter 2) are highly similar, suggesting the presence of very similar aggregates in both the solid state and in MCH solutions. For heteromixtures **1:2** and **1:3**, the spectral features of PBI **1** (λ = 400–650 nm) are significantly altered in comparison to those of pure PBI **1** itself, suggesting the presence of π-stacked **1:2** and **1:3** heteroaggregates. The shape and position of the PBI absorption bands is highly reminiscent of the perylene–triazine heteroaggregates studied in Chapter 3, suggesting the formation of similar π-stacked, hydrogen-bonded aggregates for **1:2** and **1:3** in the solid state.
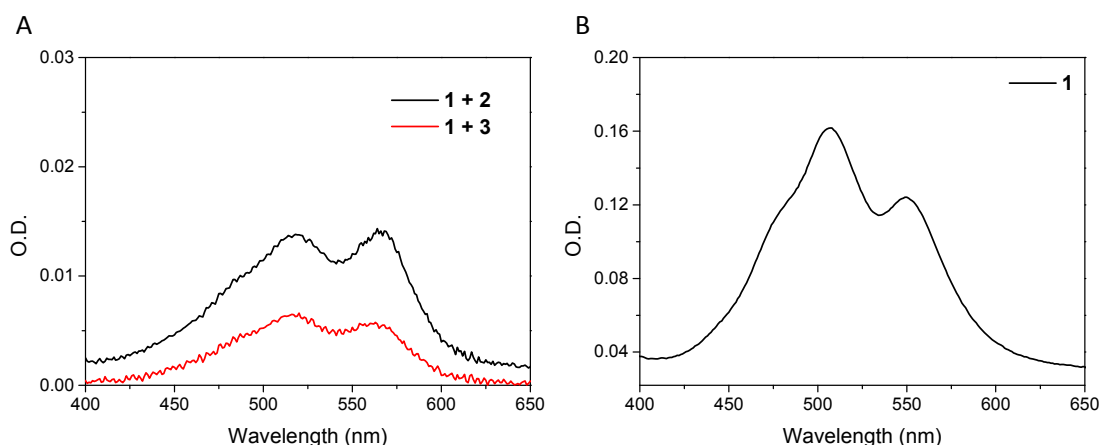
Figure 6.5. UV–Vis absorption spectra of spin-cast films of heteromixtures **1:2** and **1:3** (glass slides, c_1 = $c_{2 \text{ or } 3}$ = 1×10^{-4} M, MCH) (A). UV–Vis absorption spectrum of a drop cast film of PBI **1** (B) (glass slide, c_1 = 1×10^{-4} M, MCH).

Interestingly, the bulk phase material properties of heteroaggregates **1:2** and **1:3** are found to be dramatically different from their individual parent components. Triazines **2** and **3** are viscous liquids at room temperature, while PBI **1** is a brittle solid material. In contrast, bulk-phase heteroaggregates **1:2** and **1:3**, as prepared by evaporation of their respective solutions in MCH, are sticky paste-like materials. Additionally, heteroaggregates **1:3** and **1:3** are found by polarised optical microscopy

to be liquid crystalline at room temperature (Figure 6.6). Bright birefringence is observed from the samples when viewed through crossed polarisers (Figure 6.6 C and D). The materials display shear-induced birefringence and smear out when pressed between glass plates.
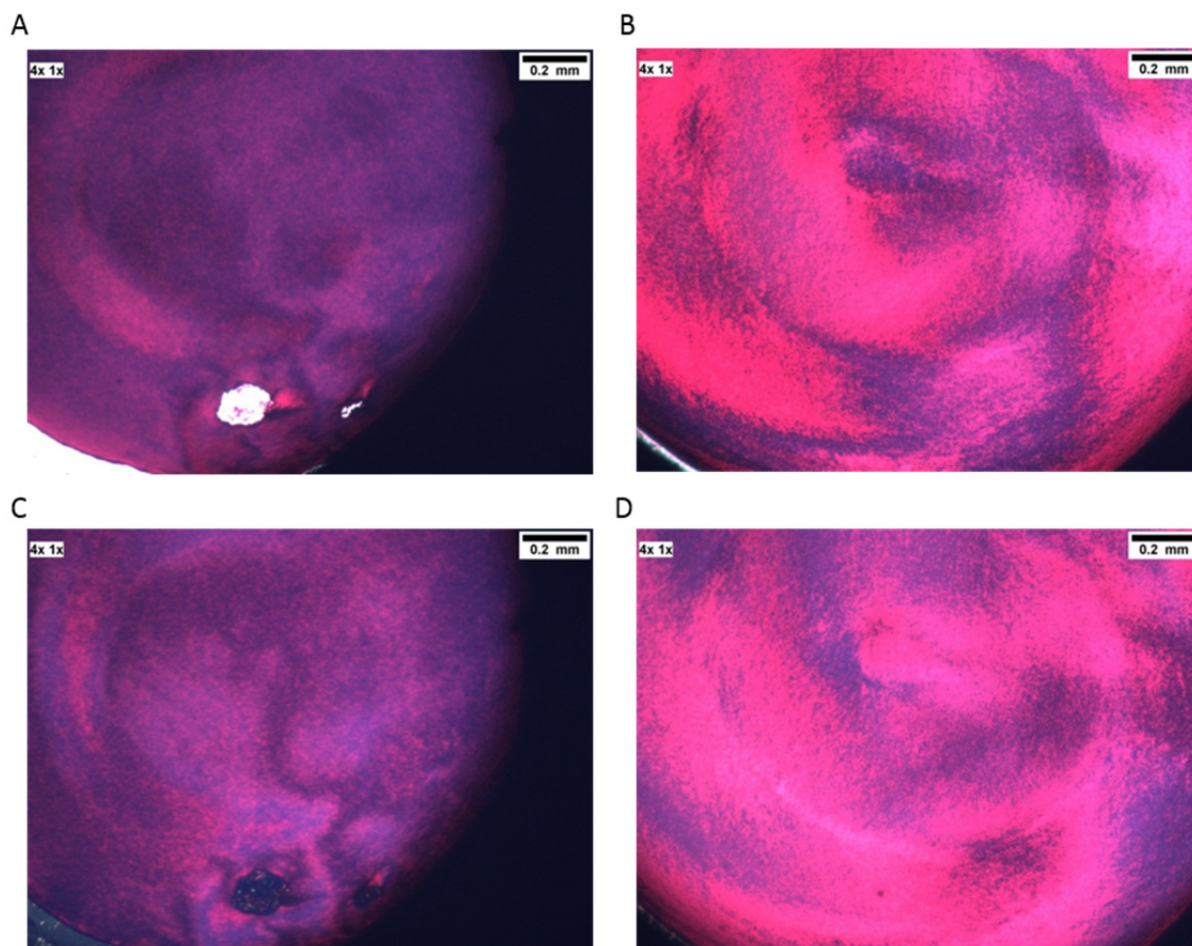
Figure 6.6. Heteromixtures **1:2** and **1:3** as viewed with optical microscopy, with (C, D) and without (A, B) crossed polarisers, respectively.

6.4 Nanostructured morphologies by phase separation

So far we have established that solid state perylene/triazine heteromixtures **1:2** and **1:3** self-assemble into π-stacked aggregates of complementary hydrogen-bonded dimers. To investigate whether microphase separation occurs in these materials, we turn our attention to small-angle X-ray scattering (SAXS) analysis of the bulk phase of **1:2** and **1:3** (Figure 6.7). Remarkably, in the SAXS graphs, both perylene/triazine mixtures show reflections corresponding to a reciprocal ratio of 1 : √3 : 2 : √7, which is consistent with a columnar hexagonally arranged mesophase. In the higher q-part of the graph, two diffuse reflections are observed for both heteromixtures. The first

reflection ($d \approx 0.73$ nm) can be attributed to the short range order of the *o*DMS side-chains on the triazine and increases in intensity for **1:3** compared to **1:2**, consistent with the higher amount of *o*DMS present in **3** compared to **2**. The second halo ($d \approx 0.43$ nm) is typically assigned to the short range order in the alkyl side-chains. In the case of **1:2**, a reflection can additionally be observed at $d \approx 0.35$ nm, which indicates the distance between chromophores in the π-stacked aggregate and is further evidence for the formation of π-stacked heteroaggregates in the bulk state. From the SAXS analyses, intercolumn distances of 4.7 nm and 5.8 nm are extracted for heteromixtures **1:2** and **1:3**, respectively. The slightly larger intercolumnar spacing observed for **1:3** corresponds to the longer *o*DMS fragments in triazine **3** compared to triazine **2**. The results are consistent with the formation of one-dimensional stacks of heterodimers of **1:2** and **1:3**, but, much to our surprise, do not provide evidence for additional phase separation of the *o*DMS side-chains on **2** and **3** from the alkyl side-chains on PBI **1**. On the contrary, the results suggest mixing of the flexible side-chains into a liquid-like matrix around hexagonally packed, one-dimensional columnar aggregates of the rigid, π-conjugated cores of the hydrogen-bonded heterodimers. The formation of a superlattice within the columnar hexagonal structure by phase separation of *o*DMS and alkyl side-chains, like reported by García-Iglesias *et al.* for BTAs, is not observed.[35] Nevertheless, phase-separated architectures with nanoscale feature sizes are obtained.
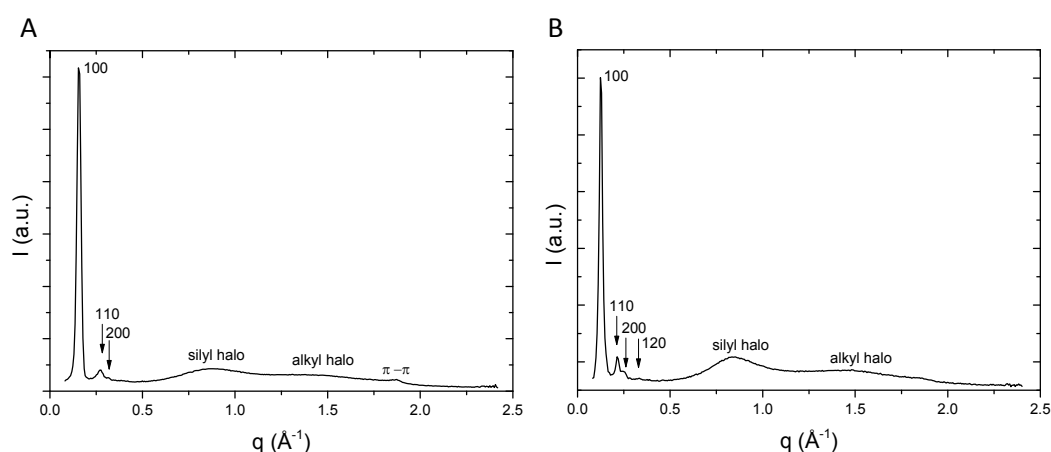
Figure 6.7. Radially averaged scattering patterns of bulk heterostructures **1:2** (A) and **1:3** (B). Arrows indicate expected peak positions for columnar hexagonal packing.

To further characterise the nanoscale phase-separation behaviour of heteromixtures **1:3** and **1:3**, we examined thin films of the supramolecular materials

with atomic force microscopy (AFM). Thin films of **1:3** and **1:3** were prepared from dilute solutions of **1:3** and **1:3** in heptane (c = 1×10^{-4} M) by spin casting (2500 rpm) on bare silicon substrates. When other solvents, such as MCH or chloroform, were used, dewetting of the surface was observed and no homogeneous thin films were obtained. AFM analysis of the spin-coated films of **1:2** and **1:3** reveals the presence of aligned arrays of line patterns in both cases (Figure 6.8) in the phase images. Gratifyingly, the AFM phase images obtained for **1:2** and **1:3** are consistent with the formation of cylindrical nanostructures as determined by SAXS, which orient perpendicular to the substrate surface. By FFT analysis of the AFM phase image and subsequent azimuthal integration of the FFT image, the average domain spacing in
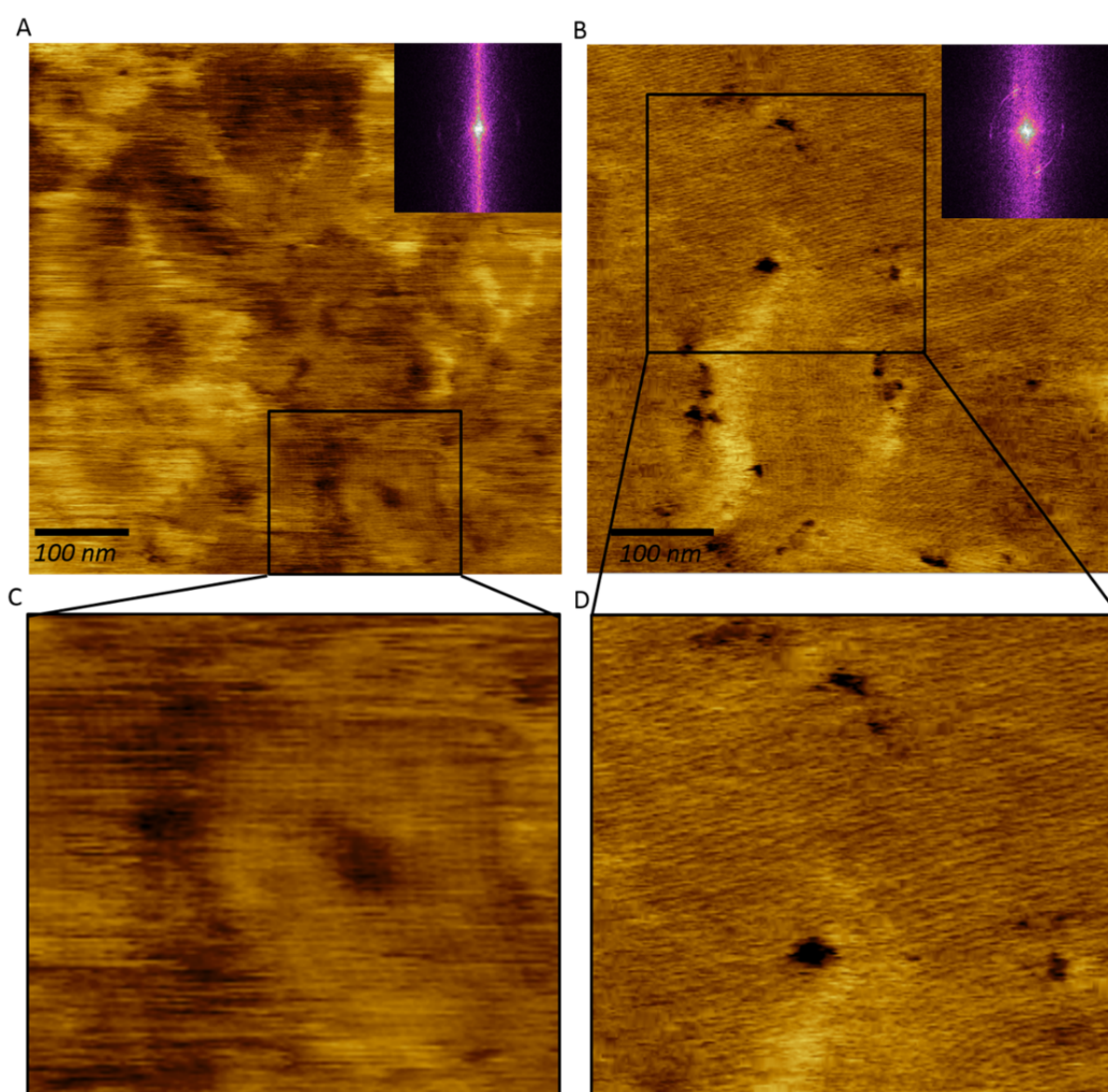
Figure 6.8. AFM phase images of spin-cast films of **1:2** (A, C) and **1:3** (B, D) (as cast) displaying ordered arrays of line patterns. Insets display the FFT of the corresponding AFM images.

the AFM phase image can be determined. For spin-cast films of **1:2** and **1:3**, average domain spacings of 4.2 ± 0.1 nm and 4.7 ± 0.1 nm are obtained, respectively, which correspond to the distance between two adjacent hexagonally packed columns in the thin film. The slightly larger domain spacing observed for **1:3** can be explained by the longer *o*DMS fragments on triazine **3** compared to triazine **2**. The domain spacings obtained from the AFM analysis are slightly smaller in comparison to the intercolumn distance observed in SAXS. This may be due to the fact that the SAXS experiments were performed in the bulk phase while AFM analysis was performed on thin films of the materials. Differences in surface tension of the side-chains and the aromatic cores might result in a slight distortion of the hexagonal columnar packing in the thin films. Nevertheless, extremely small feature sizes in the order of 4 to 5 nm are observed with both experimental techniques and larger domain spacings are observed with triazine **3** that bears longer *o*DMS chains. Additionally, the AFM results provide no evidence for additional phase separation between *o*DMS and alkyl side-chains but are consistent with phase separation of the rigid, π-conjugated cores of the hydrogen-bonded heterodimers from the flexible side-chains.

Intriguingly, when the obtained AFM phase images are compared with conventional phase-separated diblock copolymers[19] and with fibre formation of small molecules by supramolecular polymerisation[26-30], our results closely resemble the former. With heteroaggregates **1:2** and **1:3** topographically flat thin films are obtained (as evidenced by AFM analysis) that display phase-separated architectures on the nanoscale. Thin films of heteroaggregates **1:2** and **1:3** phase-separate into nanoscale hexagonally packed cylinders to form aligned line patterns instead of (intertwined) fibres or fibre bundles commonly observed for small molecules that aggregate into one-dimensional stacks. Most probably, strong phase separation occurs between the flexible side-chains of the hydrogen-bonded heterodimers and the rigid aromatic core, giving rise to one-dimensional π-stacked aggregates in a matrix of *o*DMS and alkyl side-chains.

6.5 Conclusion

We have synthesised triazines that are decorated with oligodimethylsiloxane side-chains of precise length and studied their nanophase-separation behaviour upon complementary hydrogen bonding with an *N*-monoarylated perylene bisimide.

Perylene/triazine threefold complementary hydrogen bonding in the solid state was verified by FT-IR spectroscopy. In addition UV–Vis spectroscopy showed that he resulting heterodimers form π-stacked aggregates in the solid state. Furthermore, the heterodimers are liquid crystalline at room temperature and form a columnar hexagonal mesophase as evidenced by POM and SAXS measurements. Most probably, the rigid aromatic cores assemble into one-dimensional aggregates that are phase-separated from a liquid-like matrix of oDMS and alkyl side-chains. Intercolumn distances of 4.7 and 5.8 nm were obtained, consistent with the size of the hydrogen-bonded heterodimers. Extensive arrays of line patterns were observed in AFM phase images, consistent with hexagonally packed columns in an arrangement perpendicular to the substrate surface. We obtain intercolumn distances of 4.2 and 4.7 nm, with the slightly larger domain spacing for the triazine bearing longer oDMS chains. The intercolumn distances extracted from the AFM phase images are slightly smaller than those from SAXS analyses. In the AFM images, no evidence is found for additional phase-separation between oDMS and alkyl side-chains, confirming the formation of one-dimensional stacks of the rigid aromatic cores in a liquid-like matrix of oDMS and alkyl side-chains. The presented approach allows the generation of architectures with nanoscale feature sizes below 5 nm through a combination of block copolymer-inspired phase-separation and controlled supramolecular aggregation. The proposed absence of side-chain phase-separation is currently being further explored by scanning tunnelling microscopy in a collaborative effort with the group of Steven de Feyter (KU Leuven). Herein, the self-assembly of the heteroaggregates as monolayers on graphite surfaces is investigated. Within such monolayers, the molecules should organise themselves through phase-separation according to side-chain incompatibility. The experiments should provide more insight into phase separation of proposed incompatible oligomers. Presumably in the bulk phase, strong microphase-separation between the π-conjugated cores and the flexible side-chains, combined with strong π-stacking interactions of the PBIs, prevents side-chain phase separation from occurring. To promote side-chain phase separation in the current design, the aggregation strength of the π-conjugated cores may be diminished. Substituents could be introduced on the PBI bay positions or naphthalene diimides could be used instead of PBIs. Furthermore, reducing the number of side-chains on the perylene and triazine moieties may result in the formation of different bulk and thin-film morphologies. The modular synthesis of the

system allows the facile generation of a library of molecules derivatised with different numbers and lengths of incompatible side-chains and the potential generation of a wide variety of (multi)phase-separated nanostructures.

Alternatively, a line of research that is currently being explored in our group is the step-wise synthesis of phase-separating monodisperse block-copolymers of various precise lengths. In this way, very small block-copolymers with precise compositions can be obtained and the theoretical limit for block copolymer microphase-separation (χN > 10.5) can be experimentally tested for high χ polymers. The suggested approach may allow convenient access to a variety of targetable nanophase-separated architectures useful in a multitude of applications. It also provides insights into the potential use of well-defined oligomeric incompatible side-chains as the limits of block-copolymer phase-separation can be investigated.

6.6 Experimental section

Instrumentation, materials and methods

Unless specifically mentioned, reagents and solvents were obtained from commercial suppliers and used without further purification. All solvents were of AR quality. Deuterated chloroform for NMR analyses was provided with TMS as a 0 ppm reference. The methylcyclohexane used in all spectroscopic experiments was of spectroscopic grade. Column chromatography was performed on a Biotage Isolera One using SNAP KP-SNAP columns and solvent gradients. ^{1}H-NMR and ^{13}C-NMR spectra were recorded on a Varian Mercury Vx 400 MHz instrument (100 MHz for ^{13}C) and all chemical shifts are reported in parts per million relative to tetramethylsilane (TMS). MALDI-ToF MS analyses were performed in reflector mode on a PerSeptive Biosystems Voyager-DE Pro using α-cyano-4-hydroxycinnamic acid (CHCA) and 2-[(2E)-3-(4-tert-butylphenyl)-2-methylprop-2-enylidene]malononitrile (DCTB) as matrices. Ultraviolet-visible (UV–Vis) absorbance spectra were recorded on a Jasco V-650 UV–Vis spectrometer with a Jasco ETCR-762 temperature controller. Circular dichroism (CD) spectra were recorded on a JASCO J-815 CD spectrometer with a JASCO PTC-348 temperature controller. Solid state infrared (IR) spectra were recorded on a Perkin Elmer Spectrum One spectrometer equipped with a ATR universal sampler accessory and in dilute solution using 1 mm NaCl cells. X-Ray scattering measurements were performed on a Ganesha lab instrument equipped

with a GeniX-Cu ultra-low divergence source producing X-ray photons with a wavelength of 1.54 Å and a flux of 1 x 10^8 ph/s. Scattering patterns were collected using a Pilatus 300K silicon pixel detector with a 487 x 619 pixel dimension and with 172 μm^2 pixel size at 113 mm and 1513 mm sample to detector distance. The beam centre and the *q* range were calibrated using the diffraction peaks of silver behenate. Conversion of 2D into 1D files (399 linear bins) was accomplished with Saxsgui V2.12.04. Saxsgui automatically uses a beamstop mask, an additional mask was applied to mask out the shadow of the sample holder, corrections for cosmic background radiation and zingers were applied. The peaks were fitted using a Lorentz peak, using a slope to correct for the background slope. Atomic force microscopy (AFM) was performed with an Asylum Research MFP 3D microscope equipped with an anti-vibration table and houses in an insulated chamber. The silicone probes (model AC160TS) were manufactured by Olympus and purchased from Asylum Research. The probes have a 9 nm tip radius and 11 nm tip height and operate with a spring constant k = 26 N/m and with 300 kHz frequency. Measurements were made in AC mode (tapping mode). Images were corrected by employing a flattening procedure with the Asylum Research software package and analysed with the Gwyddion SPM software package. Polarisation optical microscopy measurements were performed on a Jenaval polarisation microscope equipped with a Linkam THMS 600 heating device, with crossed polarisers.

Hydrogen terminated *o*DMS fragments **10** and **11** were kindly provided by Bas de Waal.

Synthesis

Methyl 3,4,5-tris(pent-4-en-1-yloxy)benzoate (**5**)

Methyl 3,4,5-trihydroxybenzoate (5 g, 27.2 mmol) was dissolved in acetonitrile (75 mL) and ground K_2CO_3 (18.8 g, 138 mmol) was added to the mixture. The resulting suspension was flushed with argon for 15 minutes. 5-Bromopent-1-ene was dissolved in acetonitrile (25 mL) and the solution was flushed with argon for 15 minutes after which it was added dropwise to the stirred suspension. The mixture was heated at 90 °C for 15 hours. Upon completion of the reaction, the solvent was removed in vacuo and the residue resuspended in chloroform (100 mL). 1 M HCl was added to neutralise excess K_2CO_3 and the chloroform layer was separated from the aqueous

phase. The aqueous phase was extracted with chloroform (2 x 100 mL) and the combined organic fractions were dried over $MgSO_4$. The suspension was filtered and concentration of the filtrate gave the crude material which was further purified by column chromatography using a gradient of chloroform (75% to 100%) in heptane as eluent. Yield = 10.1 g. η = 95%. ^{1}H-NMR (400 MHz, $CDCl_3$) δ = 7.26 (s, 2H, aromatic) 5.87 (m, 3H, C=CH), 5.03 (m, 6H, C=CH_2), 4.06 (t, J = 6.4 Hz, 2H, OCH_2), 4.04 (t, J = 6.4 Hz, 4H OCH_2), 3,89 (s, 3H, COCH_3), 2.28 (m, 6H, C=CH-CH_2), 1.89 (M, 6H, OCH_2-CH_2).

3,4,5-Tris(pent-4-en-1-yloxy)benzoic acid (**6**)

Methyl 3,4,5-tris(pent-4-en-1-yloxy)benzoate **5** (5 g, 12.9 mmol) was dissolved in ethanol (50 mL) and a solution of NaOH (2.1 g, 50.4 mmol, 10 mL H_2O) was added. The mixture was heated at 90 °C for 15 hours. The solvent was evaporated and the residue partitioned between H_2O and DCM (100 mL each). The organic layer was neutralized with 1 M HCl (50 mL), washed with H_2O (2 x 50 mL) and brine (50 mL) and dried over $MgSO_4$. The solids were filtered off and the solvent was evaporated to yield 3,4,5-tris(pent-4-en-1-yloxy)benzoic acid as a slightly yellow crystalline solid. Yield = 4.76 g. η = 99%. ^{1}H-NMR (400 MHz, $CDCl_3$) δ = 7.33 (s, 2H, aromatic), 5.8 (m, 3H, C=CH), 5.05 (m, 6H, C=CH_2), 4.06 (m, 6H, OCH_2), 2.28 (m, 6H, C=CH-CH_2), 1.9 (m, 6H, OCH_2-CH_2).

3,4,5-Tris(pent-4-en-1-yloxy)benzoyl chloride (**7**)

3,4,5-Tris(pent-4-en-1-yloxy)benzoic acid (1 g, 2.7 mmol) and a drop of DMF were dissolved in THF (20 mL) and oxalyl chloride (1 g, 8 mmol) was slowly added while stirring under an argon atmosphere. The resulting mixture was stirred for 90 minutes at room temperature. The solvent was removed in vacuo and the crude product used without further purification.

N^2,N^4-Diphenyl-6-[3,4,5-tris(pent-4-en-1-yloxy)phenyl]-1,3,5-triazine-2,4-diamine (**9**)

Diphenylbiguanide (**8**) (0.71 g, 2.81 mmol) and triethylamine (0.85 g, 8.43 mmol) were dissolved in a mixture of $CHCl_3$ (20 mL) and DMA (20 mL), cooled to 0 °C and stirred under an argon atmosphere. 3,4,5-Tris(pent-4-en-1-yloxy)benzoyl chloride **7** was dissolved in $CHCl_3$ (5 mL) and added dropwise to the biguanide solution. The resulting solution was stirred for 15 hours at room temperature and afterwards heated at 80 °C for 4 hours. The solvents were removed by vacuum evaporation and

the crude product redissolved in CHCl$_3$ (50 mL). The organic phase was washed 1 M HCl (2 x 50 mL), water (2 x 50 mL) and brine (50 mL) and dried over MgSO$_4$. The suspension was filtered and the solvent removed in vacuo to give the crude material, which was purified by column chromatography (gradient 10% to 20% ethyl acetate in heptane over four column volumes). ^{1}H-NMR (400 MHz, CD$_3$OD) δ = 7.9 (s, 2H), 7.77 (m, 4H), 7.32 (t, J = 7.6 Hz, 4H), 7.06 (t, J = 7.6 Hz, 2H), 5.92 (m, 3H, C=CH), 5.04 (m, 6H, C=CH$_2$), 4.09 (m, 6H, OCH$_2$), 2.31 (m, 6H), 1.91 (m, 6H).

N^2,N^4-Diphenyl-6-{3,4,5-tris[5-(1,1,3,3,5,5,7,7,9,9,11,11,13,13,13-pentadecamethyl heptasiloxanyl)pentyl]oxyphenyl}-1,3,5-triazine-2,4-diamine (**2**)

N^2,N^4-Diphenyl-6-[3,4,5-tris(pent-4-en-1-yloxy)phenyl]-1,3,5-triazine-2,4-diamine (**9**) (100 mg, 0.17 mmol) and 1,1,1,3,3,5,5,7,7,9,9,11,11,13,13-pentadecamethyl heptasiloxane (**10**) (439 mg, 0.845 mmol) were dissolved in THF (5 mL) and put under an argon atmosphere. A drop of Karstedt's catalyst was added and the mixture was stirred at 60 °C for six hours. Upon completion, the solvent was removed in vacuo and the crude product purified by column chromatography using chloroform as eluent. Yield: 176 mg. η = 48.5%. ^{1}H-NMR (400 MHz, CDCl$_3$) δ = 7.68 (s + d, 6H), 7.36 (t, J = 8 Hz, 4H), 7.11 (t + broad s, 4H, aromatic + N-H), 4.1 (t, J = 6.8 Hz, 4H), 4.04 (t, J = 6.8 Hz, 2H), 1.86 (m, 4H), 1.77 (m, 2H), 1.51 (m, 6H), 1.42 (m, 6H), 0.57 (m, 6H), 0.12-0.02 (m, 135H). ^{13}C-NMR (100 MHz, CDCl$_3$) δ = 152.9, 128.8, 123.5, 120.6, 73.5, 69.0, 30.1, 29.8, 29.8, 29.2, 1.8, 1.2, 1.2, 1.2, 1.1, 1.1, 1.0, 1.0, 1.0, 0.3, 0.2, 0.2. MALDI-ToF MS (m/z) calc for C$_{81}$H$_{179}$N$_5$O$_{21}$Si$_{21}$ 2148.82 found 2149.88 (M+H)$^+$, 2171.87 (M+Na)$^+$, 2187.85 (M+K)$^+$.

N^2,N^4-Diphenyl-6-{3,4,5-tris[5-(1,1,1,3,3,5,5,7,7,9,9,11,11,13,13,15,15,17,17,19,19, 21,21,23,23,25,25,27,27,29,29-hentriacontamethylpentadecasiloxanyl)pentyl] oxyphenyl}-1,3,5-triazine-2,4-diamine (**3**)

N^2,N^4-Diphenyl-6-[3,4,5-tris(pent-4-en-1-yloxy)phenyl]-1,3,5-triazine-2,4-diamine (**9**) (50 mg, 0.084 mmol) and 1,1,1,3,3,5,5,7,7,9,9,11,11,13,13,15,15,17,17,19,19,21,21, 23,23,25,25,27,27,29,29-hentriacontamethylpentadecasiloxane (**11**) (470 mg, 0.422 mmol) were dissolved in THF (5 mL) and put under an argon atmosphere. A drop of Karstedt's catalyst (solution in xylene) was added and the mixture was stirred at 60 °C for 18 hours. The resulting yellow solution was concentrated in vacuo. The crude product was purified by column chromatography using CHCl$_3$ as eluent to wash off

excess oligosiloxane followed by ethyl acetate to elute the target compound. Yield = 235 mg. η = 70.8%. ^{1}H-NMR (400 MHz, CDCl$_3$) δ = 7.68 (s + d, 6H), 7.36 (t, J = 8 Hz, 4H), 7.11 (t + broad s, 4H, aromatic + N-H), 4.1 (t, J = 6.8 Hz, 4H), 4.04 (t, J = 6.8 Hz, 2H), 1.86 (m, 4H), 1.77 (m, 2H), 1.51 (m, 6H), 1.42 (m, 6H), 0.57 (m, 6H), 0.12-0.02 (m, 279H). ^{13}C-NMR (100 MHz, CDCl$_3$) δ = 152.9, 128.8, 123.4, 120.6, 73.5, 69.0, 30.1, 29.8, 29.8, 23.2, 23.1, 18.3, 1.7, 1.4, 1.2, 1.2, 1.1, 1.0, 0.7, 0.3, 0.2, 0.2. MALDI-ToF MS (m/z) calc for C$_{129}$H$_{323}$N$_5$O$_{45}$Si$_{45}$ 3927.28 found 3928.37 (M+H)$^+$.

6.7 References

[1]   G. Singh, S. Batra, T. Zhang, H. Yan, K.G. Yager, M. Cakmak, B. Berry, A. Karim, *ACS Nano*, 2013, **7**, 5291

[2]   J. Bang, U. Jeong, D.Y. Ryu, T.P. Russell, C.J. Hawker, *Adv. Mater.*, 2009, **21**, 4769

[3]   J.K. Bosworth, M.Y. Paik, R. Ruiz, E.L. Schwartz, J.Q. Huang, A.W. Ko, D.M. Smiglies, C.T. Black, C.K. Ober, *ACS Nano*, 2008, **2**, 1369

[4]   M. Ramanathan, S.B. Darling, *Prog. Polym. Sci.*, 2011, **36**, 793

[5]   H.C. Kim, S.M. Park, W.D. Hinsberg, *Chem. Rev.*, 2010, **110**, 146

[6]   J.Y. Cheng, C.A. Ross, H.I. Smith, E.L. Thomas, *Adv. Mater.*, 2006, **18**, 2505

[7]   K. Kempe, K.L. Killops, J.E. Poelma, H. Jung, J. Bang, R. Hoogenboom, H. Tran. C.J. Hawker, U.S. Schubert, L. Campos, *ACS Macro Lett.*, 2013, **2**, 677

[8]   M.C. Stuparu, A. Khan, C.J. Hawker, *Polym. Chem.*, 2012, **3**, 3033

[9]   O. Ikkala, G. ten Brinke, *Science*, 2002, **295**, 2407

[10]   G. ten Brinke, J. Ruokolainine, O. Ikkala, *Adv. Polym. Sci.*, 2007, **207**, 113

[11]   S.K. Yang, A.V. Ambade, M. Weck, *Chem. Soc. Rev.*, 2011, **40**, 129

[12]   A. Noro, Y. Nagata, A. Takano, Y. Matsushita, *Biomacromolecules*, 2006, **7**, 1696

[13]   K.E. Feldman, M.J. Kade, T.F.A. de Greef, E.W. Meijer, E.J. Kramer, C.J. Hawker, *Macromolecules*, 2008, **41**, 4696

[14]   W.H. Binder, S. Bernstorff, C. Kluger, L. Petraru, M.J. Kunz, *Adv. Mater.*, 2005, **17**, 2824

[15]   T. Park, S.C. Zimmerman, *J. Am. Chem. Soc.*, 2006, **128**, 13986

[16]   X. Yang, F. Hua, K. Yamamoto, E. Ruckenstein, B. Gong, W. Kim, C.Y. Ryu, *Angew. Chem. Int. Ed.*, 2004, **43**, 6471

[17]   J. Cortese, C. Soulié-Ziakovic, S. Tencé-Girault, L. Leibler, *J. Am. Chem. Soc.*, 2012, **134**, 3671

[18]   J. Cortese, C. Soulié-Ziakovic, M. Cloitre, S. Tencé-Girault, L. Leibler, *J. Am. Chem. Soc.*, 2011, **133**, 19672

[19]   L.M. Pitet, A.H.M. van Loon, E.J. Kramer, C.J. Hawker, E.W. Meijer, *ACS Macro Lett.*, 2013, **2**, 1006

[20]   L.M. Pitet, S.F. Wuister, E. Peeters, E.J. Kramer, C.J. Hawker, E.W. Meijer, *Macromolecules*, 2013, **46**, 8289

[21]   A. Noro, K. Ishihara, Y. Matsushita, *Macromolecules*, 2011, **44**, 6241

[22]   A. Noro, M. Hayashi, A. Ohshika, Y. Matsushita, *Soft Matter*, 2011, **7**, 1667

[23]   J. Guoqian, R. Ponnapati, R. Pernites, M.J. Felipe, R. Advincula, *Macromolecules*, 2010, **43**, 10262

[24]   O. LeBel, T. Maris, H. Duval, J.D. Wuest, *Can. J. Chem.*, 2005, **83**, 615

[25]   The synthesis of monodisperse dimethylsiloxane oligomers used in this chapter will be reported in a separate publication.

[26]   J. Roosma, T. Mes, P. Leclère, A.R.A. Palmans, E.W. Meijer, *J. Am. Chem. Soc.*, 2008, **130**, 1120

[27]   Z. Chen, V. Stepanenko, V. Dehm, P. Prins, L.D.A. Siebbeles, J. Seibt, P. Marquetand, V. Engel, F. Würthner, *Chem. Eur. J.*, 2007, **13**, 436

[28]   F. Helmich, C.C. Lee, M.M.L. Nieuwenhuizen, J.C. Gielen, P.C.M. Christianen, A. Larsen, G. Fytas, P.E.L.G. Leclère, A.P.H.J. Schenning, E.W. Meijer, *Angew. Chem. Int. Ed.*, 2010, **49**, 3939

[29]   P. Jonkheijm, P. van der Schoot, A.P.H.J. Schenning, E.W. Meijer, *Science*, 2006, **313**, 80

[30]   F. Würthner, C. Bauer, V. Stepanenko, S. Yagai, *Adv. Mater.*, 2008, **20**, 1695

[31]   D. González-Rodríguez, A.P.H.J. Schenning, *Chem. Mater.*, 2011, **23**, 310

[32]   Y. Yamamoto, *Sci. Technol. Adv. Mater.*, 2012, **13**, 033001

[33]   F.J.M. Hoeben, P. Jonkheim, E.W. Meijer, A.P.H.J. Schenning, *Chem. Rev.*, 2005, **105**, 1491

[34]   S.S. Babu, V.K. Praveen, A. Ajayaghosh, *Chem. Rev.*, 2014, **114**, 1973

[35]   M. García-Iglesias, B.F.M. de Waal, I. de Feijter, A.R.A. Palmans, E.W. Meijer, *Chem. Eur. J.*, 2015, **21**, 377

Epilogue

The use of multiple components in the formation of supramolecular aggregates allows the generation of more functional and complex structures than supramolecular polymers based on single components. However, the presence of multiple supramolecular interactions and aggregation pathways in these systems may result in less control over the aggregation processes and may lead to the prevalence of undesired aggregates. The principal aim of the work described in this thesis was to provide a detailed study of the preparation and characterisation of multicomponent supramolecular stacks, to gain a better understanding of the mechanisms, interactions and pathway complexity that govern their self-assembly.

We have described the self-assembly of asymmetric perylene bisimides with triazines into one-dimensional aggregates by complementary hydrogen-bonding and subsequent π-stacking in great detail. We have found that homoaggregation pathways of the individual components in multicomponent supramolecular systems greatly influence the formation of the desired supramolecular heteroaggregates.

One of the ideals of the research was to design and synthesise supramolecular donor–acceptor heterostacks of porphyrins and perylenes by complementary hydrogen-bonding of these subunits and subsequent π-stacking of the heterodimers. To achieve this ideal, complementary hydrogen-bonding motifs have to be introduced on the porphyrin and perylene subunits. In Chapters 2 and 3 we have described the design, synthesis and self-assembly of a perylene–triazine complementary hydrogen-bonding couple as a model system. In this relatively simple system we find a delicate interplay between the molecular structure of the triazine hydrogen-bonding motif and the homo- and heteroaggregation pathways present in the system. By blocking of additional hydrogen-bond interactions on the triazines we are able to bias the multicomponent system away from perylene homoaggregation and towards the formation of heteroaggregates. As single component systems, only the perylene subunit shows aggregation by π-stacking in the lateral direction with respect to the hydrogen-bond array. Therefore, in the heteroaggregates, we attribute the lateral π-stacking interactions mainly to the perylene subunit. In the proposed porphyrin–perylene heteroaggregates, both chromophores show the formation of elongated supramolecular structures as homoaggregation pathways, which adds

additional pathway complexity in the self-assembly of the desired supramolecular heterostacks. After the non-trivial synthesis and purification of triazine-functionalised asymmetric porphyrins, we interestingly find that the homoaggregation pathway of the porphyrin derivative is drastically altered with respect to their symmetric counterparts. In fact, we find that small changes in the peripheral solubilising moieties on the porphyrin of symmetric porphyrins greatly influence the self-assembly of porphyrin tetra-amides. Nevertheless, the heteroaggregation of the asymmetric porphyrins with the perylenes was investigated. Regrettably, we find that the homoaggregation pathways in the mixed system dominate over the heteroaggregation pathway. Presumably, there is a mismatch between the strength of the complementary hydrogen-bonding and the strength of the lateral stacking interactions of the individual chromophores. Alternatively, there may be a geometric mismatch in the stacking of the heterodimers in which the stacked chromophores have to adopt a less favourable orientation in comparison to their homoaggregates, thereby favouring the formation of homoaggregates over heteroaggregates. The results clearly show that the design and formation of stacked heteroaggregates based on components that form supramolecular structures themselves is a complex problem in the area of multicomponent supramolecular polymers.

The non-covalent strategy of using complementary hydrogen-bonding and subsequent π-stacking as described above is an attractive approach to bring together molecules of different functionalities. The supramolecular organisation of different functionalities into ordered arrays may result in novel behaviour and properties due to the dynamic nature of the non-covalent interactions in the system. In Chapters 5 and 6 of this thesis we describe two examples where different chemical functionalities are introduced on the perylene–triazine hydrogen-bonding motifs, which should result in the formation of phase-separated supramolecular architectures. In Chapter 5 we focus on the formation of supra-amphiphiles by complementary hydrogen-bonding between subunits that are functionalised with hydrophobic and hydrophilic side-chains. Interestingly, very stable methylcyclohexane/water emulsions are obtained when perylene–triazine based supra-amphiphiles are used. A more scientifically and practically relevant issue is the effective stabilisation of water-in-water emulsions. We have attempted to adapt our supra-amphiphile approach to the stabilisation of water-in-water emulsions by

adjusting the functional groups on the hydrogen-bonding motifs to be compatible with the phase-separating aqueous polymer solutions. Unfortunately, the molecules used in the current design suffer from limited solubility due to strong aggregation in the aqueous polymer solutions and attempts to stabilise water-in-water emulsions with our supra-amphiphile approach were unsuccessful. Nevertheless we feel that the use of hydrogen-bonded heterostacks with different chemical functionalities as compatibilisers between immiscible phases provides opportunities for the formation of functional amphiphilic systems.

In Chapter 6 we describe the study of hydrogen-bonded heterostacks that are functionalised with proposed incompatible side-chains for their self-assembly in the solid state. By combining principles from block-copolymer phase separation and small molecule self-assembly, we aim to obtain phase-separated architectures with feature sizes below the limits of block-copolymer phase separation. Gratifyingly, we obtain cylindrical phase-separated architectures in thin films with intercolumn distances of 4.2 and 4.7 nm. Interestingly, the results suggest the occurrence of phase-separation between the flexible side-chains (dodecyl en oligodimethylsiloxane) and the rigid aromatic core of the hydrogen bonded structures, whereas the targeted phase-separation between the proposed incompatible side-chains is absent. The perylene–triazine heteromixtures display multiple non-covalent interactions of different strengths that govern the behaviour of the system. Ideally, hydrogen-bonding is strong and selective enough to ensure full heterocomplexation in the bulk phase. Next, the phase separation of the side-chains and the π-stacking interactions of the aromatic cores should be balanced to each other in order to achieve both phase-separation of the aromatic cores from the flexible side-chains and between the proposed incompatible side-chains themselves. Presumably, the lateral π-stacking interactions in the system presented in Chapter 6 of this thesis are too strong with respect to side-chain phase separation. The preferred organisation of the chromophores probably enforces the mixing of the side-chains into a single flexible matrix around the π-stacked, aromatic cores.

In review, the formation of multicomponent supramolecular stacks based on π-stacking of hydrogen-bonded heterodimers has been investigated. The non-covalent approach of bringing together structures of different chemical functionality by

hydrogen-bonding and subsequent π-stacking is presented as an attractive route towards functional multicomponent supramolecular systems. In the design of these systems, the competitive homoaggregation pathways of the components should be less favourable than the heteroaggregation processes. To achieve this, the association strength of the hydrogen-bond pair should be sufficiently strong with respect to the lateral aggregation strength of the individual monomers. In the case of phase-separating systems (both in bulk and solution), the lateral aggregation strength of the hydrogen-bonded dimers should be in balance with the driving force for phase separation. If the phase separation is too strong, macrophase separation could dominate the behaviour of the system, while on the other hand if the phase separation is too weak, the lateral organisation of the complexes dictates the aggregate structure and prevents phase-separation.

The results presented in this thesis show the potential to generate complex supramolecular architectures based on multicomponent supramolecular stacks. The insights obtained in this thesis encourage further studies on the design of π-stacked, hydrogen-bonded supramolecular polymers. Careful tuning of the strengths of the individual non-covalent interactions in these systems allows the generation of multicomponent supramolecular stacks for a variety of applications. The molecular design of the individual components can be used as a tool to individually tune each of the non-covalent interactions present in the system. Detailed knowledge about non-covalent interactions, mechanisms and assembly routes in multicomponent supramolecular systems is a necessity in the rational design of complex and functional multicomponent supramolecular structures.

Multicomponent supramolecular systems

The self-assembly of molecular building blocks through well-defined non-covalent interactions is a powerful tool to develop complex and functional supramolecular structures. Single component supramolecular stacks have been described in great detail concerning the type and strength of their non-covalent interactions, self-assembly mechanisms and pathway complexity in self-assembly. Analogous knowledge is less advanced in the formation of multicomponent one-dimensional supramolecular polymers. The individual components used in the formation of such supramolecular stacks may form (metastable) homoaggregates that compete with and therefore complicate the formation of the desired supramolecular heteroaggregates. We deem detailed knowledge of the mechanisms and pathways of formation of one-dimensional multicomponent stacks to be highly beneficial for the generation of functional supramolecular architectures. This thesis addresses the development of multicomponent supramolecular stacks, by π-stacking of hydrogen-bonded complexes, to gain a better understanding of the mechanisms, interactions and pathway complexity that govern their self-assembly.

In Chapter 1, a literature overview on the formation of functional supramolecular architectures based on single components is presented. For the rational design of complex supramolecular architectures, precise knowledge on non-covalent interactions, self-assembly mechanisms and pathways is a necessity. These topics are addressed in relation to one-dimensional supramolecular polymerisation of single components. Furthermore, we present examples of the formation of supramolecular stacks by π-stacking of hydrogen-bonded complexes to highlight the more complex and functional architectures obtained in multicomponent systems.

In Chapter 2, the synthesis and self-assembly of an *N*-monoarylated perylene bisimide is investigated. We find that the perylene bisimide aggregates into supramolecular stacks of hydrogen bonded dimers via a cooperative self-assembly mechanism. We furthermore find that these perylene stacks remain small for a wide concentration range, which is in contrast with conventional cooperative supramolecular polymerisation processes. A growth model is investigated where the association constant in the elongation phase of a nucleation–elongation supramolecular polymerisation model diminishes as a function of aggregate length.

The model correctly describes the experimentally observed cooperative assembly curves as well as the limited size of the aggregates. The results serve as a warning that typical hallmarks of cooperative supramolecular polymerisation do not per se imply the formation of large objects. Furthermore, the steric bulk of solubilising side-chains can be used as a means to control the size of aggregates obtained in cooperative supramolecular polymerisation processes.

In Chapter 3, the formation of heteroaggregates of the *N*-monoarylated perylene bisimide described in Chapter 2 with triazines by complementary hydrogen bonding and subsequent π-stacking is investigated. We find that selective blocking of additional weak non-covalent interaction sites on the triazines results in the more facile formation of perylene–triazine heteroaggregates over homoaggregates of the individual components. However, for all monotriazines, the formation of perylene homoaggregates is shown to precede the formation of perylene–triazine heteroaggregates in the self-assembly processes. To further favour the assembly process towards heteroaggregates, divalent triazines are investigated. Pathway complexity is absent in the assembly of perylene heteroaggregates with divalent triazines, as the stability of the heteroaggregates is increased with respect to the homoaggregates of the individual components. The results indicate that the formation of desired heteroaggregates is sensitive towards competing homoaggregation pathways. Molecular design of the hydrogen-bond couple is shown as a tool to guide the self-assembly process towards the formation of heteroaggregates by limiting the homoaggregation pathways.

In Chapter 4, the pathway complexity in the self-assembly of a library of structurally similar tetra-amidated zinc porphyrins is investigated. Small changes in the solubilizing wedge architecture on the periphery of the porphyrin molecules are shown to have a dramatic effect on the nature of the obtained aggregates. Depending on the wedge architecture, either H- or J-aggregates occur exclusively or coexistence between these species is observed. The aggregated states feature parallel self-assembly pathways from the porphyrin monomers and convert via depolymerisation to the free monomer. The results show that porphyrin supramolecular systems are highly sensitive towards variations in the molecular architecture of the solubilising peripheries. Variations in the peripheral porphyrin

architecture can thus be used as a tool to control the organisation of porphyrins in supramolecular architectures.

In Chapter 5, the formation of supra-amphiphiles by complementary hydrogen bonding and subsequent π-stacking is dealt with. The perylene–triazine system described in Chapter 3 is decorated with tetra(ethyleneoxy) side chains to induce solubility in aqueous media. Mixed systems of hydrophilic and hydrophobic subunits in binary solvent mixtures are found to stabilise emulsions of methylcyclohexane in water by the formation of supra-amphiphiles. This approach is extended towards the stabilisation of water-in-water emulsions. However, limited solubility and strong aggregation of the individual subunits of the supra-amphiphiles in aqueous polymer solutions prevents the successful stabilisation of water-in-water emulsions by these supra-amphiphiles. Nevertheless, the presented approach for the formation of supra-amphiphiles allows a modular methodology towards the formation of functional amphiphilic systems.

In Chapter 6, the formation of nanoscopic phase-separated architectures in thin films is investigated by combining concepts from block-copolymer phase separation and supramolecular assembly of small molecules. The perylene–triazine complementary hydrogen-bond couple described in Chapter 3 is decorated with proposed incompatible side-chains of precise length and investigated for their self-assembly in the solid state. The perylene–triazine mixtures from π-stacked architectures of hydrogen-bonded dimers and are found to be columnar hexagonal liquid crystals at room temperature. SAXS and AFM measurements reveal the formation of nanoscopic phase-separated architectures with extremely small domain spacings (≈ 4.5 nm) and suggest phase separation between the π-conjugated cores and the flexible side-chains. Interestingly, the AFM phase images are highly reminiscent of conventional block-copolymer phase separation and dissimilar to fibre formation observed in conventional supramolecular polymers. The presented approach demonstrates the generation of feature sizes in thin films that are non-trivially obtainable with block copolymer phase separation, while maintaining long-range order that is generally lacking in supramolecular polymers.

Multicomponent supramoleculaire systemen

De zelfassemblage van moleculaire bouwstenen door middel van goed gedefinieerde niet-covalente interacties is een krachtige methode om complexe en functionele supramoleculaire systemen te ontwikkelen. De mechanismen, routes en niet-covalente interacties in supramoleculaire zelfassemblage zijn in groot detail beschreven voor supramoleculaire stapels van enkelvoudige componenten. Analoge kennis op het gebied van multicomponent eendimensionale supramoleculaire polymeren is minder gevorderd. De individuele componenten die in de vorming van zulke supramoleculaire stapels worden gebruikt, kunnen (metastabiele) homoaggregaten vormen die in competitie zijn met de vorming van gewenste supramoleculaire heteroaggregaten. Gedetailleerde kennis over de mechanismen en routes in de zelfassemblage van eendimensionale supramoleculaire polymeren is daarom zeer relevant voor het vormen van functionele supramoleculaire architecturen. Deze thesis beschrijft de ontwikkeling van multicomponent supramoleculaire polymeren, om zodoende een beter begrip te verkrijgen van de mechanismen, routes en interacties die belangrijk zijn in hun zelf-assemblage.

In Hoofdstuk 1 is een overzicht gegeven van de vorming van functionele supramoleculaire polymeren op basis van één component. Voor het rationele ontwerp van complexe supramoleculaire architecturen, is precieze kennis over niet-covalente interacties, zelfassemblage mechanismen en routes noodzakelijk. Er wordt een overzicht gegeven van deze onderwerpen in het licht van eendimensionale supramoleculaire polymerisatie op basis van één component. Om de meer complexe en functionele architecturen van multicomponent systemen aan te tonen, worden enkele voorbeelden gegeven van supramoleculaire polymeren gevormd door middel van π-stapeling van waterstof-gebrugde complexen.

In Hoofdstuk 2 is de synthese en zelf-assemblage van een *N*-monogearyleerde peryleen bisimide onderzocht. De peryleen bisimide aggregeert in stapels van waterstof-gebrugde dimeren door middel van een coöperatief zelfassemblage mechanisme. Deze stapels van peryleen dimeren blijven klein over een groot concentratiebereik, wat in tegenstelling is met conventionele coöperatieve supramoleculaire polymerisaties. Een groeimodel is onderzocht waar de associatieconstante in de elongatiefase van een nucleatie–elongatie supramoleculair

polymerisatiemodel lager wordt als het aggregaat groeit. Het model beschrijft de coöperatieve assemblagecurves en de gelimiteerde grootte van de aggregaten op een correcte manier. De resultaten dienen ter waarschuwing dat typische eigenschappen van coöperatieve supramoleculaire polymerisatie niet met zekerheid de vorming van grote aggregaten impliceert. Verder kan de sterische hindering van oplosbaarheidsgroepen gebruikt worden om het formaat van aggregaten in coöperatieve supramoleculaire polymerisaties te limiteren.

In Hoofdstuk 3 is de vorming van heteroaggregaten van de *N*-monogearyleerde peryleen bisimide uit Hoofdstuk 2 met triazines door middel van complementaire waterstofbruggen en π-stapeling onderzocht. Selectieve uitschakeling van additionele zwakke niet-covalente interactieplaatsen op de triazines resulteert in een gemakkelijkere vorming van peryleen–triazine heteroaggregaten. Echter, voor alle enkelvoudige triazines, vindt in het zelf-assemblage proces de vorming van peryleen zelf-aggregaten plaats voordat de vorming van peryleen–triazine heteroaggregaten wordt geobserveerd. Om de vorming van heteroaggregaten te bevorderen zijn divalente triazines onderzocht. In deze systemen is de routecomplexiteit binnen de zelfassemblage afwezig omdat de stabiliteit van de heteroaggregaten verhoogd is ten opzichte van de homoaggregaten van de individuele componenten. De resultaten tonen aan dat de vorming van gewenste heteroaggregaten gevoelig is voor competitie met zelfassemblage routes richting homoaggregaten. Moleculair ontwerp van het waterstofbrugpaar is een krachtige methode om zelfassemblage processen te sturen richting de vorming van heteroaggregaten door routes naar homoaggregaten te limiteren.

In Hoofdstuk 4, is de routecomplexiteit binnen de zelfassemblage van een serie van op elkaar lijkende tetra-amide zink porfyrines onderzocht. Kleine veranderingen in de oplosbaarheidsgroep aan de buitenkant van de porfyrines hebben een groot effect op het soort aggregaat dat verkregen word. Afhankelijk van de oplosbaarheidsgroep worden exclusief H- of J-aggregaten verkregen of bestaat er co-existentie van deze aggregaten. De aggregaten assembleren via parallelle routes en converteren in elkaar via depolymerisatie naar het vrije monomeer. De resultaten laten zien dat supramoleculaire systemen op basis van porfyrines zeer gevoelig zijn voor variaties in de moleculaire structuur van de oplosbaarheidsgroep. Variaties in de

randarchitectuur van porfyrines kunnen gebruikt worden om controle te verkrijgen over de organisatie van porfyrines in supramoleculaire structuren.

In Hoofdstuk 5 wordt de vorming van supra-amfifielen door middel van waterstofbruggen en π-stapeling beschreven. Het peryleen–triazine systeem beschreven in Hoofdstuk 3 is gefunctionaliseerd met tetra(ethyleenoxy) zijketens om oplosbaarheid te induceren in waterige oplossingen. Gemengde systemen van hydrofobe en hydrofiele eenheden zijn effectief in het stabiliseren van emulsies van methylcyclohexaan in water door de vorming van supra-amfifielen. Deze aanpak is uitgebreid naar de stabilisatie van water-in-water emulsies. Echter blijkt dat de lage oplosbaarheid en sterke aggregatie van de individuele componenten in waterige oplossingen van polymeren de succesvolle stabilisatie van water-in-water emulsies voorkomt. De voorgestelde aanpak voor de vorming van supra-amfifielen biedt een modulaire methodologie voor de vorming van functionele amfifiele systemen.

In Hoofdstuk 6 is de vorming van nanoschaal fase-gescheiden architecturen in dunne lagen onderzocht door concepten uit fasescheidende blokcopolymeren en de supramoleculaire zelfassemblage van kleine moleculen te combineren. Het peryleen– triazine complementaire waterstofbrug koppel uit Hoofdstuk 3 is gefunctionaliseerd met incompatibele zijketens van precieze lengte en onderzocht op zelfassemblage gedrag in de vaste fase. De peryleen–triazine mengsels vormen π-gestapelde structuren van waterstof-gebrugde dimeren en zijn vloeibaar kristallijn op kamertemperatuur met een hexagonale pakking van kolommen. SAXS en AFM metingen laten de vorming van nanoschaal fase-gescheiden architecturen zien met extreem kleine domeinafstanden (≈ 4.5 nm) en suggereren de fasescheiding tussen de π-geconjugeerde gedeelten en de flexibele zijketens van de moleculen. Opmerkelijk is dat de AFM fasebeelden een sterke gelijkenis vertonen met conventionele fasescheidende blokcopolymeren en ongelijk zijn aan fibervorming in supramoleculaire polymeren. De voorgestelde aanpak laat de vorming van structuren met kleine afmetingen zien die niet gemakkelijk te verkrijgen zijn met fasescheidende blokcopolymeren terwijl de orde over lange afstanden die normaalgesproken afwezig is in supramoleculaire polymeren behouden blijft.

Curriculum vitae

Rob van der Weegen was born on June 28th 1987 in Roosendaal and Nispen, the Netherlands. After finishing secondary education at the Gertrudis College in Roosendaal in 2005, he started studying Chemical Engineering and Chemistry at the Eindhoven University of Technology. During his studies, he performed an internship of three months under the supervision of dr. B.A. Helms at the Molecular Foundry, Lawrence Berkeley National Laboratory (Berkeley, USA). His master thesis project was performed in the research group of prof.dr. E.W. Meijer under the supervision of dr.ir. T. Mes and dr.ir. A.R.A. Palmans. After finishing his study *cum laude* in 2010, he started with a PhD project in the laboratory of Macromolecular and Organic Chemistry and the Institute for Complex Molecular Systems (ICMS) under the supervision of prof.dr. E.W. Meijer and dr.ir. A.R.A. Palmans. The most important results of this research are described in this thesis.

Rob van der Weegen werd geboren op 28 juni 1987 te Roosendaal en Nispen, Nederland. Na het behalen van zijn VWO diploma aan het Gertrudis College in Roosendaal begon hij in 2005 aan de studie Scheikundige Technologie aan de Technische Universiteit Eindhoven. Tijdens zijn studie heeft hij drie maanden stage gelopen in de groep van dr. B.A. Helms aan de Molecular Foundry, Lawrence Berkeley National Laboratory (Berkeley, VS). De masterfase van de studie werd afgerond met een afstudeerproject in de groep van prof.dr. E.W. Meijer onder begeleiding van dr.ir. T. Mes en dr.ir. A.R.A. Palmans. Na het *cum laude* afronden van zijn studie in 2010, begon hij met zijn promotieonderzoek in de capaciteitsgroep Macromoleculaire en Organische Chemie en het Instituut voor Complexe Moleculaire Systemen (ICMS), onder begeleiding van prof.dr. E.W. Meijer en dr.ir. A.R.A. Palmans. De belangrijkste resultaten van dit promotieonderzoek staan beschreven in dit proefschrift.

List of publications

Efficient Routes to A₃B-Type meso-(4-Carboxyphenyl) Porphyrin Derivatives
S.I. Presolski, R. van der Weegen, J.J. Wiesfeld, E.W. Meijer, Org. Lett., 2014, **16**, 1864

Small-sized perylene-bisimide assemblies controlled by both cooperative and anti-cooperative assembly processes
R. van der Weegen, P.A. Korevaar, P. Voudouris, I.K. Voets, T.F.A. de Greef, J.A.J.M. Vekemans, E.W. Meijer, *Chem. Commun.*, 2013, **49**, 5532

Plasmonic Chiroptical Response of Silver Nanoparticles with Chiral Supramolecular Assemblies
B.M. Moaz, R. van der Weegen, Z.Y. Fa, A.O. Govorov, G. Ellestad, B. Berova, E.W. Meijer, G. Markovich, *J. Am. Chem. Soc.*, 2012, **134**, 17807

Stealth Rare Earth Oxide Nanodiscs for Magnetic Resonance Imaging
M.J. Bailey, R. van der Weegen, P.J. Klemm, S.L. Baker, B.A. Helms, *Adv. Health. Mater.*, 2012, **1**, 437

Processable Cyclic Peptide Nanotubes with Tunable Interiors
R. Hourani, C. Zhang, R. van der Weegen, L. Ruiz, C.Y. Li, S. Keten, B.A. Helms, T. Xu, *J. Am. Chem. Soc.*, 2011, **133**, 15269

Singe-Chain Polymeric Nanoparticles by Stepwise Folding
T. Mes, R. van der Weegen, A.R.A. Palmans, E.W. Meijer, *Angew. Chem. Int. Ed.*, 2011, **50**, 5085

Multicolour Self-Assembled Fluorene Co-Oligomers: From Molecules to the Solid State via White-Light-Emitting Organogels
R. Abbel, R. van der Weegen, W. Pisula, M. Surin, P. Leclère, R. Lazzaroni, E.W. Meijer, A.P.H.J. Schenning, *Chem. Eur. J.*, 2009, **15**, 9737

Multicolour self-assembled particles of fluorene-based bolaamphiphiles
R.J. Abbel, R. van der Weegen, E.W. Meijer, A.P.H.J. Schenning, *Chem. Commun.*, 2009,1697

Dankwoord / Acknowledgements

Hoe cliché ook: er is een tijd van gaan, er is een tijd van komen en de tijd van gaan is nu gekomen. De afsluitende pagina's van een proefschrift zijn zoals gebruikelijk gereserveerd voor het dankwoord. De afgelopen 8 jaar ben ik achtereenvolgens als Spinoza-student, afstudeerder en promovendus onderdeel geweest van de vakgroep MST. Ter afsluiting van deze mooie en leerzame periode wil ik daarom hier de tijd nemen om een aantal mensen te bedanken.

Als eerste wil ik graag mijn promotor Bert Meijer bedanken. Bert, hartelijk dank dat je mij de mogelijkheid hebt gegeven om mijn promotieonderzoek uit te voeren in jouw groep. De manier waarop je enerzijds kritisch bent op details en anderzijds het onderzoek altijd in een bredere context weet te plaatsen, is zeer inspirerend voor mij. Je toegankelijkheid en professionaliteit hebben er toe geleid dat jouw groep een prachtige omgeving is voor het uitvoeren van fundamenteel onderzoek.

Als tweede wil ik mijn copromotor Anja Palmans bedanken. Hoewel je niet vanaf het begin bij mijn promotieonderzoek betrokken bent geweest en porfyrines, perylenen en triazines natuurlijk heel anders zijn dan je favoriete BTAs, heb ik je adviezen en suggesties altijd enorm gewaardeerd. Jouw suggestie na het vaardigheidsblok Organische Chemie leidde ertoe dat ik als jong studentje binnenkwam bij het Spinoza-instituut en later via een afstudeerproject nu dit proefschrift geschreven heb.

Graag wil ik ook Jef Vekemans bedanken voor de bijdragen aan mijn onderzoek en het plaatsnemen in de promotiecommissie. In mijn eerste jaar als promovendus heb ik genoten van onze samenwerking op het gebied van synthese en analyse van zelf-assemblerende moleculen. Na je pensionering hebben we op de maandagen dat je op de universiteit was nog geregeld gesproken over synthetische problemen en vele andere zaken. Hoewel je vaak aangaf niet meer in het veld te zitten en op de hoogte te zijn van de nieuwste ontwikkelen ging ik toch altijd weer wijzer weg.

Prof. Dr. Steven de Feyter en Prof. Dr. Roeland Nolte wil ik graag bedanken voor het plaatsnemen als externe leden in mijn promotiecommissie. Tevens wil ik Prof. Dr. Rint Sijbesma en Prof. Dr. Albert Schenning graag bedanken als leden van mijn promotiecommissie.

Naast de leden van mijn promotiecommissie wil ik graag alle andere mensen bedanken met wie ik de afgelopen jaren heb samengewerkt of die anderzijds iets voor mijn promotie hebben betekend.

Ik bedank Floris Helmich voor doorgeven van alle ins en outs op het gebied van zelf-assemblage van porfyrines. I would like to thank Stanislav Presolski and Hirohisa Nitta for the collaborations on the asymmetric porphyrin projects and Feng Wang for discussions on the formation of supramolecular complexes by hydrogen bonding. Bas de Waal wil ik graag bedanken voor de synthese van een aantal triazines die beschreven staan in Hoofdstuk 3 en voor de monodisperse siloxanen uit Hoofdstuk 6. Peter Korevaar en Tom de Greef wil ik bedanken voor het modelleerwerk aan de coöperatieve groei van korte stacks van peryleen bisimides. I would like to thank Dr. Ilja Voets and Dr. Panayiotis Voudouris for SAXS and DLS measurements on perylene and perylene-triazine aggregates. I would like to thank Lorenzo Albertazzi for his assistance with measuring confocal microscopy on supra-amphiphiles. I would like to thank Dr. Anderson Shum and Yang Song from the University of Hong Kong for the collaboration regarding the stabilisation of water-in-water emulsions with supramolecular constructs. Although our molecules did not perform as we initially expected, I have very much enjoyed the scientific discussions we have had. I would also like to thank Prof. Dr. Steven de Feyter and Dr. Joan Teyssandier for their STM measurements on phase-separating hydrogen-bonded aggregates. I would like to thank Isja de Feijter and Louis Pitet for their help with SAXS and AFM measurements on the phase-separating hydrogen-bonded aggregates described in Chapter 6. Ik wil Sjef Öllers bedanken voor de nuttige technische feedback op tekst in dit proefschrift.

Gedurende mijn promotieonderzoek heb ik het voorrecht gehad om een aantal studenten in verschillende fasen van hun studie te begeleiden. Als eerste wil ik Bram Teunissen als afstudeerder bedanken. De grote hoeveelheid syntheses en metingen die je uit hebt gevoerd hebben geleid tot een beter begrip van porfyrine zelfassemblage en staan voor een groot deel beschreven in Hoofdstuk 4. Ik wens je veel succes met het voltooien van je eigen promotieonderzoek. Jan Wiesfeld wil ik bedanken voor de optimalisatie van de synthese van peryleen bisimides en triazines. Roy van der Haas wil ik bedanken voor zijn werk aan asymmetrische porfyrines. Lastly I would like to thank Jonathan Cook for his contributions on self-assembly pathways in perylene-triazine supramolecular systems.

Natuurlijk kan ook de ondersteunende staf niet ontbreken in dit dankwoord. Ik wil Ralf Bovee, Xianwen Lou en Joost van Dongen bedanken voor hun hulp bij de analyses. Ik bedank Hans Damen voor de onmisbare aan- en afvoer van chemicaliën en andere benodigdheden. Ik bedank Nora, Martina, Jolanda, Cindy en Carla voor het

werk achter de schermen waardoor de vakgroep zo soepel blijft draaien. Uiteraard mag ook Henk Eding niet ontbreken voor het regelen van koffie en thee, het verzenden van mijn pakketjes en het anderzijds creëren van een gezellige sfeer rondom the koffietafel.

I would like to thank the members of office STO 4.44: Pol, Matt, Patrick, Isja, Luuk, Janus and Thomas for providing scientific and non-scientific contributions as well as a pleasant atmosphere over the past years. I also thank all members of lab 3 for the great atmosphere, the musical warfare and keeping the lab (more or less) clean during my time as lab responsible person. A special note goes to Jolanda Spiering for providing the example on how a lab should be organised and providing assistance in trying to organise lab 3 in the same way. I would also like to thank all the people that have contributed to scientific discussions during the lunch meetings that I have participated in.

Of course the social aspect of life within MST has also contributed a great deal to the pleasant time I have had. I would like to thank Tristan, Floris, Seda, Marko, Martijn, Miguel, Mellany, Isja, Janus, Patrick, Luuk, Pol, Thomas, Stanislav, Elisa, Louis, Matt, Takashi, Paco, Nobu, Yoko, Peter, Daan, Bram, Bram, Bas, Bas, Jolanda, Benjamin, Berry, Olga, Wilco, Lorenzo, Jose, Andreas, Andreas, Neus, Ghislaine, Antonio, Tim, Matthew, Nic, Ronald, Brian, René, Simone, Helen, Feng, Gijs, Gijs, Muge.

Op de voorlaatste plaats wil ik graag mijn familie bedanken voor hun steun en interesse in mijn doen en laten in Eindhoven de afgelopen jaren. In het bijzonder wil ik hierbij mijn ouders noemen. Jullie hebben de basis gelegd voor wat ik bereikt heb door altijd voor me klaar te staan wanneer dat nodig was en mij de mogelijkheid te bieden om mezelf te ontwikkelen. Ook mijn broer Paul wil ik hierbij betrekken. Vaak gaan we op een sportieve manier competitief met elkaar om, maar natuurlijk waardeer ik jou en ons broederschap enorm.

Tot slot wil ik me richten tot jou, Anja. Ik ben ontzettend blij met je en ik wil je bedanken voor alles wat je de afgelopen jaren voor me hebt betekend. Samen gaan we ongetwijfeld een mooie toekomst tegemoet.

Bedankt allemaal!

Rob